Developing Kinetically Facile Routes to Robust B–F Containing Compounds for Bioconjugation and Imaging Applications

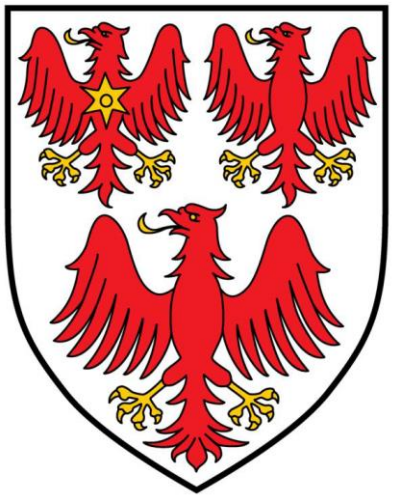

Anna C. Booth

The Queen's College

Thesis submitted for the degree of Doctor of Philosophy

February 2022

Acknowledgements

First and foremost, I'd like to thank my supervisor Prof. Simon Aldridge. From my time as an undergrad, through to the completion this thesis his support, ideas and advice have been invaluable. I thoroughly enjoyed our Monday morning meetings/chats over the course of my DPhil and he has my sincere gratitude for his help and guidance over the years.

Further thanks must also go to my co-supervisors Prof. Stephen Faulkner and Prof. Bart Cornelissen for their additional support and for filling out many doodle polls to find meeting times that suited three very busy schedules! I'd additionally like to thank Steve for allowing me opportunities in his lab since before I was a Part II and for always making time for a chat.

An extra special thanks must go to my fantastic Part II Lewis Wales for his work and commitment. He was a pleasure to work with, even if I couldn't always reach the taps on his line.

Many people generously contributed their time, expertise, and equipment to help me collect data for this thesis. Thanks, therefore, go to the Aldridge group crystallographers Dr. Evgeny Kolychev, Dr. Jamie Hicks, Dr. Maria Ángeles-Fuentes, Andreas Heilmann, and Caitilín McManus for many hours in the CRL basement and solving structures. Dr. Petra Vasko generously imparted some of her vast computation chemistry knowledge onto me and I thank her for her patience with my many questions and problems. Thank you also to Grace McMullon of the Faulkner group for many constructive discussions and collaboration when it came to dealing with Folic Acid and its many idiosyncrasies. Thanks also to: Dr. Nick Rees for his help with all things NMR and for allowing me access to the Venus 400 when covid restrictions limited its use; Dr. Nicky Farrer for allowing me access to her HPLC machine; and Dr. Deborah Sneddon for advice (HPLC based and otherwise).

A big thanks must go to group members, past and present. Whether it be the ritualistic coffee breaks with the daily crossword, the Friday pub trips, or the lab work somewhere in between, they helped make my time around the CRL so enjoyable. A special thanks should "*seriously*" go to Jamie and Petra for helping start me off in the lab so well and to Dr. Huan Do and Dr. Alexa Caise for their additional assistance. I learnt a lot from the four of them and I thank them for their patience with me regularly popping into S12 with a "Can I ask a quick question …?" and the often amusing ensuing discussions. A big thanks should also go to "Double Trouble" Aggy Crumpton and Dr. Matt Roy for making the pandemic S1 lab shifts genuinely enjoyable, with a lot of laughs and *a lot* more coffee. The rest of the S1 Crew, past and present, should also get a mention for putting up with my lab music and my enforcement of the base bath rota – Andrey, Maria, Rob, Haoyu, Ying Kai, Lu, Xiongfei, Simon T, Ili, Matthias, and Kedar. Finally, group pub trips would not have been the same without those already mentioned, as well as Andreas, Caitilín, Lilja and Frank.

Others outside the lab are too many to mention here and I would likely miss important people but a special thanks must go to the ONBI-16 cohort for looking after "the chemist" when it came to all things programming and for helping make the first six months of my PhD so enjoyable.

Finally, a whole-hearted thanks go to my family, not only for their patience in putting up with me while I wrote this "Little Essay" during a pandemic, but for their constant support throughout my time in Oxford and for never failing to show an interest.

Abstract

This thesis reports on investigations into fluoroborate compounds with a view to their application in ^{18}F-PET tracer design. The principle aim was to understand how advances could be made to the functionalisation of fluoroborate compounds for bioconjugation, in addition to improving their hydrolytic stability and optimising synthesis *via* efficient fluoride uptake routes.

Chapter 3 reports on investigations into the synthesis and fluoride binding capabilities of 1,8-bis(boryl)-naphthalene scaffolds featuring boronic acid and ester functional groups. These bidentate "ligands" were investigated for potential thermodynamic enhancement that may be attained by chelating fluoride in such a structure, and the opportunity this offered for hydrolytically robust fluoride complexes. The diboronic acid system is established to be incompatible for this application due to the formation of an exceptionally robust intramolecular anhydride that effectively blocks the binding pocket. An unsymmetrical framework featuring a single boronic ester group is demonstrated to be suitable for chelation, although fluoride binding was subsequently compromised by a thermodynamically driven, functional group rearrangement that positions fluoride in a more labile terminal position, with a B–O–B bridge again being generated.

Chapter 4 explores how highly robust *N*-heterocyclic carbene boron trifluoride adducts may be diversified to facilitate a range of methods for bioconjugation. The modular design of *N*-heterocyclic carbenes is exploited in this endeavour. Thus, a series of adducts has been synthesised featuring systematic variation of the carbene backbone, and the impact on their hydrolytic stability assessed. The preparation of a *N*-alkyne appended NHC-BF_3 derivatives is also described, and their bioconjugation to a folic acid derivative detailed.

Chapter 5 describes the investigation of carbene stabilised boron complexes and their fluoride binding reactions. Three-coordinate carbene-stabilised catecholato-boreniums have been investigated together with related series of four-coordinate complexes featuring either an additional anionic or neutral donor group. Systematic variation of the carbene donor and the leaving group substituent have been used to tune the rate of fluoride binding by these complexes, in addition to their hydrolytic stability. Neutral and cationic boron complexes are thus explored, with the four-coordinate boronium cations being determined to offer the greatest scope for optimising reactivity and stability. Careful choice of the secondary donor (based on pKa) offers a workable compromise between the kinetics of fluoride uptake at 60 °C and the stability of the boronium precursor to hydrolysis. Thus, systematic optimisation allows rapid, promoter-free fluoride binding to be achieved with a bench-stable boronium complex.

Abbreviations

Ar	Aryl
$AMBF_3$	Ammoniomethyl trifluoroborate
br	Broad
calc.	Calculated
Cat	Catecholate; 1,2-$C_6H_4O_2$
CT	Computed Tomography
CuAAC	Copper Catalysed Alkyne Azide Cyclisation
δ	Chemical Shift
d	Days; Doublet
DCM	Dichloromethane
DFT	Density Functional Theory
Dipp	2,6-Diisopropylphenyl
DMAP	4-Dimethylaminopyridine
DMF	Dimethylformamide
DMSO	Dimethylsulfoxide
ESI	Electronspray Ionisation
Et	Ethyl
FA	Folic Acid
FDG	Fluorodeoxyglucose
h	Hours
HMDS	Hexamethyldisilazine
HOMO	Highest Occupied Molecular Orbital
HPLC	High-Performance Liquid Chromatography
ID	Injected Dose
IE	Isotope Exchange
Int	Intermediate
^{i}Pr	Isopropyl
IR	Infrared
J	Coupling Constant
k	Rate Constant
K	Binding Constant; Kelvin
LUMO	Lowest Occupied Molecular Orbital
m	Multiplet
Me	Methyl
meas.	Measured
Mes	2,4,6-Trimethylphenyl
min	Minutes
MRI	Magnetic Resonance Imaging
MS	Mass Spectrometry
n-BuLi	*n*-Butyllithium
Naph	Naphthalene
NCA	No Carrier Added
NHC	*N*-Hetereocyclic Carbene
NMR	Nuclear Magnetic Resonance
PEG	Poly(ethylene glycol)
PET	Positron Emission Tomography
Ph	Phenyl

ppm	Parts Per Million
q	Quartet
quin	Quintet
R	*group*
RCY	Radiochemical Yield
s	Singlet; Seconds
sept.	Septet
SOMO	Singly Occupied Molecular Orbital
SPE	Solid Phase Extraction
SPECT	Single Photon Emission Computed Tomography
t	Triplet
T	Temperature
TAS	Tris(dimethylamino)sulfonium
TASF	Tris(dimethylamino)sulfonium Difluorotrimethylsilicate
TBAF	Tetrabutylammonium Fluoride
Tf	Triflate
THF	Tetrahydrofuran
TS	Transition State

6Mes

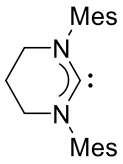

IMes

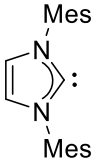

SIMes

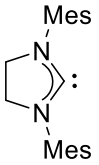

Table of Contents

Chapter 1

Introduction

1.1 PET Imaging

Medical imaging techniques are valuable resources in modern medicine for the non-invasive diagnosis and monitoring of health conditions. Molecular imaging methods such as Positron Emission Tomography (PET) and Single-Photon Emission Computed Tomography (SPECT) supply detailed information on the biochemical processes occurring within the body at the molecular and cellular level.[1] Meanwhile, structural imaging methods such as Magnetic Resonance Imaging (MRI), X-ray, Computed Tomography (CT) and Ultrasound predominantly provide information on anatomical features of the body and may be used to detect structural anomalies. Imaging therefore supplies important information to both clinicians and researchers, aiding in the provision of appropriate treatments, as well as drug discovery for the development of new ones.[2]

PET is a quantitative imaging technique, favoured for its high sensitivity that enables the detection of low concentration (pM) molecular targets and aids in the early diagnosis of disease.[3–5] Image acquisition requires the administration of a radiotracer to produce the signal detected by the scanner. The radiotracer takes the form of a biologically relevant molecule, labelled with a radionuclide capable of decay *via* positron emission. During scanning, the emitted positron will travel a short distance through the tissue before annihilating by collision with an electron (Figure 1.1). The annihilation event produces two gamma-ray photons of 511 keV that travel 180 ° in opposite directions, to be simultaneously detected by the scanner outside the body. The origin of the annihilation event can then be determined using the straight line connecting these coincident photons. The resulting PET

images therefore represent the biodistribution of the radiotracer in the body, with further temporal information on its distribution obtained by continued monitoring of the subject over time. The high sensitivity of PET also means that only a low dosage (10^{-6}-10^{-9} grams) of radiotracer is required, ensuring that dosage remains below the level for inducing undesirable pharmacological effects.[6]

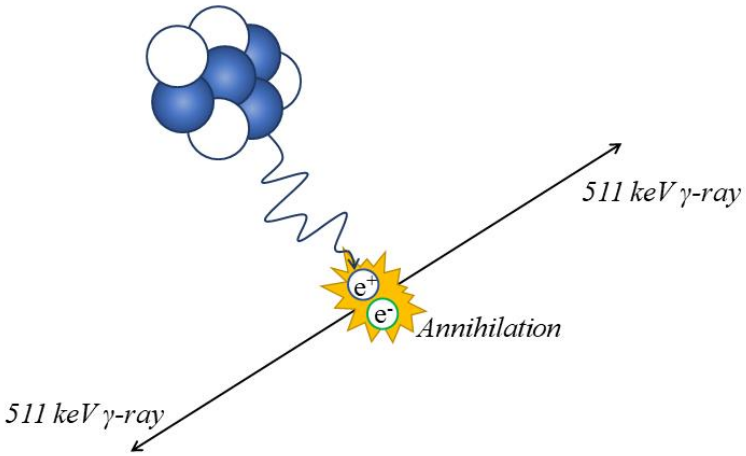

Figure 1.1 – Illustration of positron emission and the subsequent annihilation event that is the foundation for PET imaging.

Considerable efforts have consequently been directed towards the development of radiotracers to enable the imaging of a wide range of ailments. Prospective molecules for labelling can range from drug candidates to biomolecules which exhibit a high affinity for disease biomarkers such as peptides and antibodies. The diversity of molecules has therefore necessitated the development of an extensive and varied range of radiolabelling strategies for incorporating positron emitting isotopes into structures; either directly as part of the molecule or *via* appendage of a prosthetic group.[6–9] To work within the time constraints of the radionuclide decay, synthesis and purification needs to be expeditious, with labelling at a late stage preferred to avoid excessive decay. The product should be obtained in a high purity and, ideally, with a high molar activity, *i.e.* the radioactivity per unit mole (Ci μmol^{-1}). A high molar activity is advantageous for imaging low concentration targets to avoid saturation

of the binding sites with unlabelled ligand, and as such, the addition of the respective stable isotope as a "carrier" should therefore be minimised.

Of the range of positron-emitting isotopes commonly used for PET (Table 1.1) fluorine-18 is generally considered to be the isotope of choice, as holistically its properties fulfil most requirements. The clean isotope decay consists of 97 % positron emission, with the low kinetic energy of the positron also favourable for high image resolution. The half-life of 110 minutes is long enough to be practical for multistep synthesis and studying slower biological processes, but short enough that the radiation exposure of the patient can be limited. The intermediate half-life also enables delivery from an off-site source, so the isotope is readily available to many locations.

Radionuclide	**Half-life, $t_{1/2}$ (min)**	**Percentage of Decay by Positron Emission**	**Maximum Energy (MeV)**	**Decay Product**
^{11}C	20.4	99 %	0.97	^{11}B
^{13}N	9.97	100 %	1.20	^{13}C
^{15}O	2.04	100 %	1.74	^{15}N
^{18}F	110	97 %	0.64	^{18}O
^{64}Cu	762	19 %	0.655	^{64}Ni
^{68}Ga	68.1	89 %	1.90	^{68}Zn

Table 1.1 – Properties of radioisotopes commonly used in PET imaging.[5]

1.2 Inorganic Fluorine-18 Chemistry

A few intrinsic challenges are associated with fluorine-18 radiolabelling. Fluoride anions are highly nucleophilic, however this nucleophilicity is effectively quenched in the presence of water due to the high solvation of the ion. Reactions with [^{18}F]fluoride, which is obtained from the cyclotron in [^{18}O]water, therefore typically require azeotropic drying of the fluoride source before use, introducing additional time-consuming steps. [^{18}F]Fluoride is still generally preferred over the electrophilic [^{18}F]F_2 reagent however since [^{18}F]F_2 has an

inherently lower molar activity from the use of [^{19}F]F_2 in production, and the fact that it is delivered in gaseous form making it more challenging to handle.[10]

Whilst fluorine-18 labelling has traditionally been an organic field of research,[10–13] a selection of other elements, with high E–F bond strengths (Table 1.2), have also become established for incorporating [^{18}F]fluoride into radiotracers. A scattering of reports in the second half of the 20th century detail the radiofluorination of main group and transition metal elements,[14,15] although only [^{18}F]tetrafluoroborate[16–19] and [^{18}F]fluorotrimethylsilane[20] were explored for imaging. The concept subsequently gained momentum in the 2000's, with concurrent reports of boron,[21] silicon[22] and phosphorus[23] labelling (Scheme 1.1). Research has since expanded to also include sulphur,[24] aluminium,[25] gallium[26] and transition metal[27] imaging examples. The amenability of these approaches to late stage labelling, in the presence of water and under mild conditions has led to a flourishing field of research.[28–34]

E–F Bond	**Bond Enthalpy (kJ mol^{-1})**
C–F	460.2 ± 8.4
B–F	732
P–F	≤ 405
Si–F	576.4 ± 17
Al–F	665 ± 12.6
S–F	343.5 ± 6.7
Ga–F	577.4 ± 14.6

Table 1.2 – E–F bond enthalpies of elements used for ^{18}F-fluorination [35]

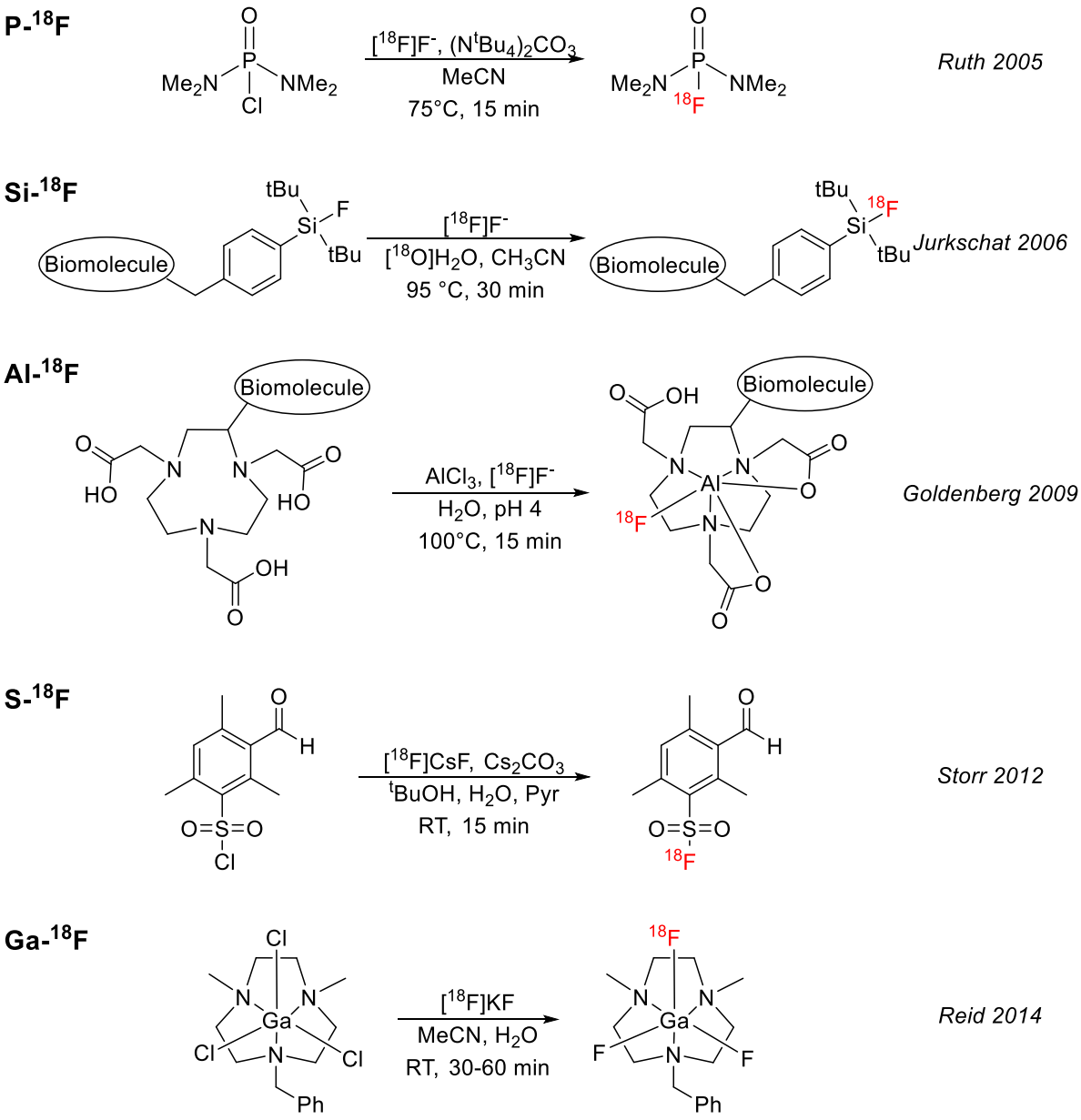

Scheme 1.1 – Inorganic [^{18}F]fluoride complexes and their respective syntheses.

1.3 [^{18}F]Fluoroborates

The simplest example of a B–^{18}F based tracer is the aforementioned [^{18}F]tetrafluoroborate anion. Initially utilised in the 1960's to investigate anion uptake by the thyroid and the imaging of intracranial tumours, the recent rejuvenation of interest in [^{18}F]fluoroborates has also renewed research on the anion.[16–18,36] The comparable size and charge of $[BF_4]^-$ anions with iodide ions facilitates their active transportation into cells by sodium iodide symporters (NIS).[37] The anion has therefore been considered as an attractive

alternative to the gamma emitters [$^{123/131}$I]iodide and [^{99m}Tc]pertechnetate for imaging NIS activity, as a reporter gene or in thyroid diseases, with the superior imaging characteristics provided by ^{18}F-PET. In 2010, Jauregui-Osoro *et al.* reported the labelling of the robust tetrafluoroborate anion in an acid catalysed ^{18}F–^{19}F isotopic exchange reaction, with subsequent imaging demonstrating the expected high uptake in the thyroid.[37] Tetrafluoroborate imaging has since progressed to human trials in both healthy volunteers[38] and thyroid cancer patients.[39–41]

The first system to integrate an [^{18}F]fluoroborate moiety into an organic framework, and thereby demonstrate its potential as a prosthetic group, was reported by Ting *et al.* in 2005.[21] The biotinylated aryltrifluoroborate [^{18}F]**1.1** was synthesised from the respective pinacol boronic ester *via* an aqueous fluoride binding reaction (Scheme 1.2). The mild conditions applied to the synthesis of [^{18}F]**1.1** demonstrated the capacity of these systems to bypass azeotropic drying and conduct labelling at a late-stage. Moreover, the labile substitution of the boronic ester, which was favoured under the acidic conditions, also highlighted the potential of these systems to form compounds of uncommonly high molar activity by accumulating three fluoride ions onto a single boron centre.

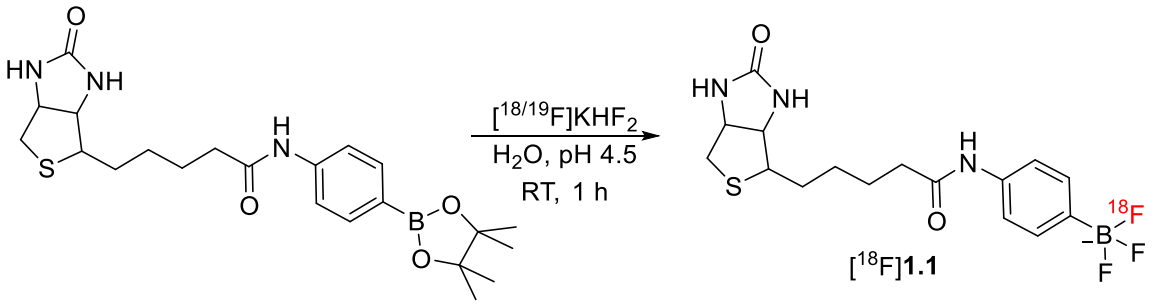

Scheme 1.2 – Radiosynthesis of the biotinylated [^{18}F]trifluoroborate [^{18}F]**1.1**

An inherent challenge in the design of organofluoroborates however, is their instability to hydrolysis. The fluoride ion dissociation that occurs with hydrolysis *in vivo* compromises imaging, as target specificity is lost, and the unbound fluoride ion is taken up by the calcium-rich skeletal system contributing to background. Degradation of the fluoride-containing

compounds in aqueous solution is driven by the high hydration enthalpy of the fluoride ion (*circa* -435 kJ mol^{-1}) which thermodynamically favours hydrolysis to boronic acid species.[42] Furthermore, the commonly accepted series of equilibria for F^-/OH^- exchange at a boron centre (Scheme 1.3) are rendered irreversible in physiological conditions, due to the high dilution and neutral pH, thereby inhibiting fluoride re-binding. The dissociation of the first fluoride ion has been established as the rate determining step of this hydrolysis process, as the mono- and difluoride species are not observed in dilute conditions at pH ≥ 7, consistent with rapid onward degradation.[43,44] The reactions are therefore considered to be pseudo-first order. Consequently, prosthetic group design has sought to disfavour fluoride dissociation, and achieve a complex of high kinetic stability, by endowing the boron centre with high Lewis acidity.

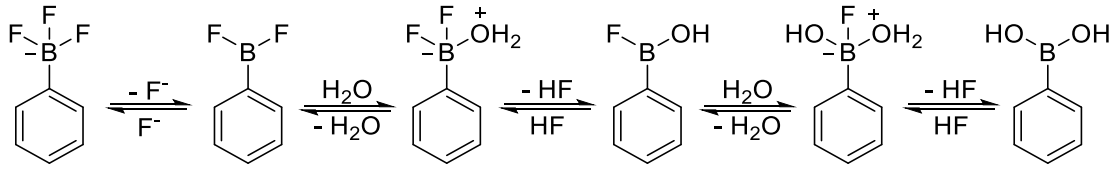

Scheme 1.3 – Hydrolysis of fluoroborates

1.3.1 Anionic Aryltrifluoroborates

The stability of aryltrifluoroborate anions can be controlled through the choice of substituents used to decorate the aromatic ring. The parent system, phenyltrifluoroborate, exhibits rapid fluoride dissociation in phosphate buffered water, with a hydrolysis half-life of two minutes. Electron-withdrawing groups, which are well-established for enhancing the Lewis acidity of arylboranes, were demonstrated by Ting *et al.* to be effective at elongating the half-lives of these systems, by reducing the electron density at boron and increasing its fluoride ion affinity.[43] Meanwhile, electron-donating groups can accelerate hydrolysis; for example, the methoxy group of *para*-anisole trifluoroborate causes it to hydrolyse faster than could be monitored. Accordingly, Hammett analysis established a negative correlation between $\log(k_{obs})$ and the σ values of *para*- and *meta*-substituents ($\rho \approx -1$, $R \approx 0.9$). Notably

however, the *ortho*-anisole trifluoroborate derivative was observed to hydrolyse with a half-life of 14 minutes, *i.e.* markedly slower than phenyltrifluoroborate. This retardation was attributed to steric congestion preventing the stabilisation of the three-coordinate boron intermediate that may occur upon co-planar alignment of the vacant p_π-orbital of boron with the electron rich aromatic π-system.

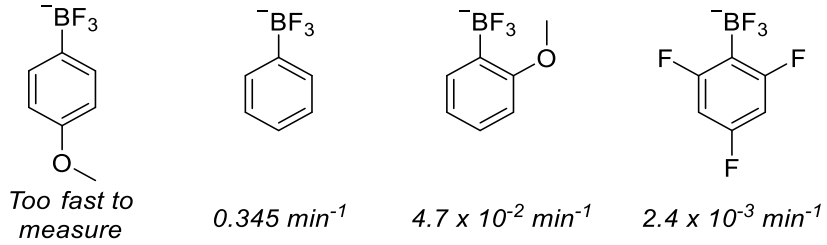

Figure 1.2 – Phenyltrifluoroborate derivatives and their respective rates of hydrolysis in PBS buffered water (~ pH 7).

Electron withdrawing groups have consequently been utilised in the design of robust [^{18}F]aryltrifluoroborates. Following the observation that **1.1** rapidly exchanges fluoride and was thus unlikely to exhibit the required stability *in vivo*, the Perrin group investigated the related systems **1.2** and **1.3** (Figure 1.3).[45,46] In addition to fluorine substituents, carbonyl groups are also employed as electron withdrawing groups, with the additional benefit of providing a handle for conjugation *via* amide bond formation. The loss of fluoride (and hence stability) of [^{18}F]**1.2** and [^{18}F]**1.3** was assessed *via* an isotopic exchange experiment, by taking dilute solutions of the ^{18}F-labelled compounds with a large excess of [^{19}F]fluoride and monitoring the proportion of free [^{18}F]fluoride that evolved over time. The solvolysis half-lives of **1.2** and **1.3** were consequently established to be in excess of 2000 minutes, *i.e.* greatly exceeding the half-life of [^{18}F]fluoride. A related oxime analogue **1.4** has also been reported by Smith and co-workers that is similarly slow to hydrolyse.[47,48] Although no rate constant was established, stability tests showed that less than 5 % of free [^{18}F]fluoride was produced after two hours in cell culture media.

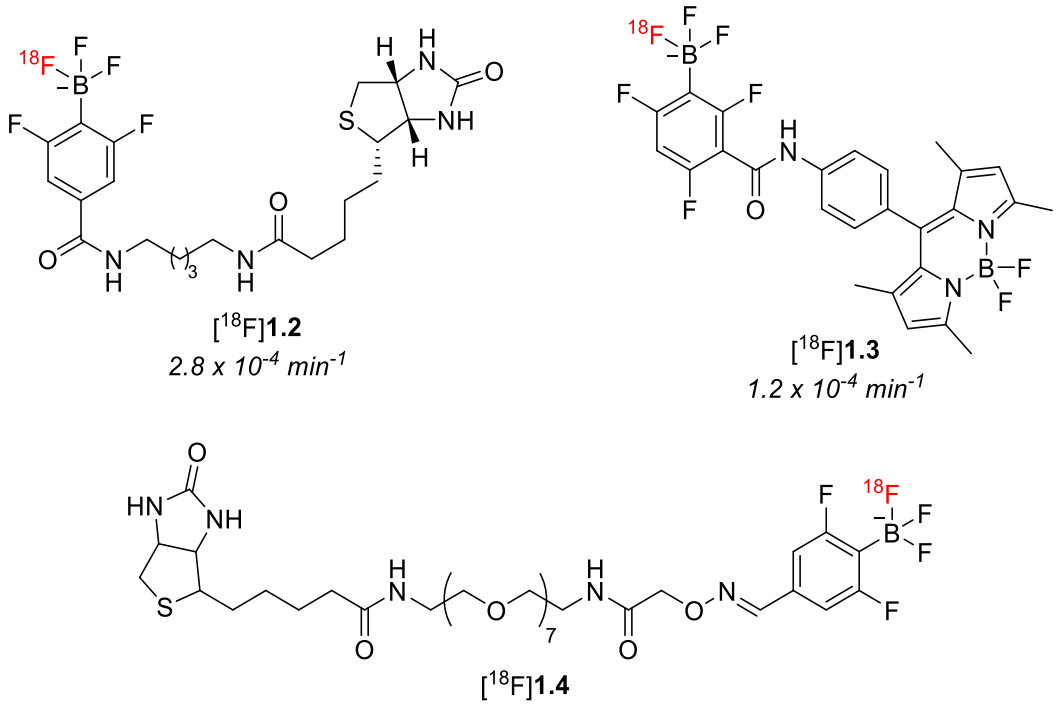

Figure 1.3 – Examples of water resilient [^{18}F]aryltrifluoroborates.

To verify that high aqueous stability for aryltrifluoroborates equates to *in vivo* stability, [^{18}F]**1.6** was prepared from the boronic ester precursor **1.5**.[49] Following the amide coupling of **1.5** with a biotin derivative, the tetraphenylpinacolate boronic ester was radiolabelled using carrier added [^{18}F]KHF_2 under acidic conditions over the course of three hours at room temperature, to produce [^{18}F]**1.6** in 7 % radiochemical yield and with a calculated molar activity of 121 mCi μmol^{-1} (Scheme 1.4). *In vivo* imaging showed no apparent signs of activity uptake by the skeletal system over the course of a 90-minute scan, indicating that no appreciable loss of fluoride had occurred during this period. The ostensible *in vivo* stability of [^{18}F]**1.6** clearly demonstrated that these systems are viable prosthetic groups for imaging. Radiotracers subsequently derived from **1.5** include cyclo-RDG conjugate [^{18}F]**1.7** (Scheme 1.5), in addition to marimastat and LLP2A peptide conjugates.[50–54] All were labelled in the final step, in one hour labelling reactions and with radiochemical yields of up to 15 %.

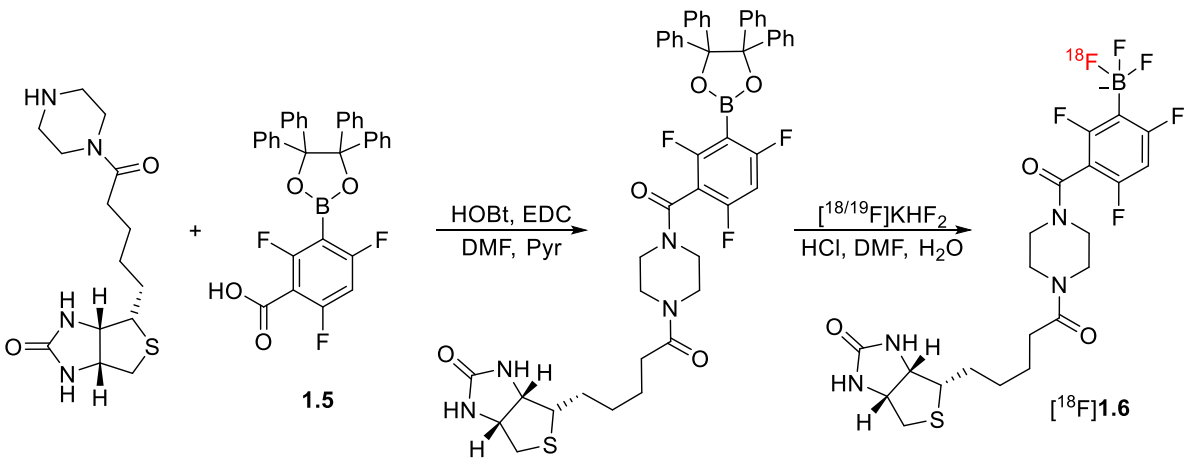

Scheme 1.4 – Bioconjugation and subsequent radiolabelling of radiosynthon **1.5**.

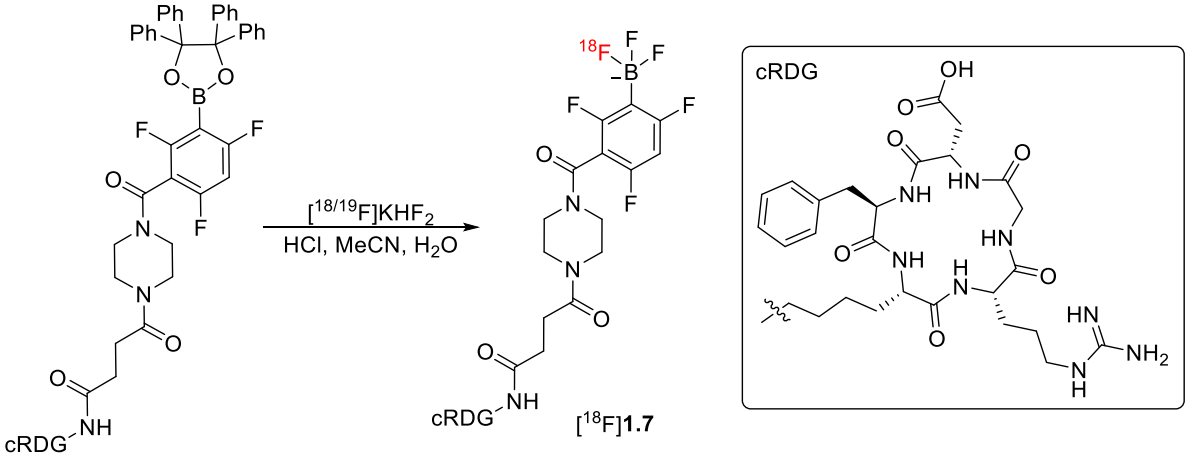

Scheme 1.5 – Radiosynthesis of cyclo-RDG radiotracer, [^{18}F]**1.7**

The cyclo-RDG derivative [^{18}F]**1.10** was also prepared by Perrin and coworkers using an alternative $ArBF_3^-$ precursor **1.8** (Scheme 1.6).[54,55] As a borimidine analogue of **1.5**, **1.8** employs diaminonaphthalene as the boron "leaving group" due to its facile displacement in acidic conditions. The introduction of a pendant alkyne also enables conjugation *via* copper(I) catalysed alkyne azide cycloaddition (CuAAC) reactions. Together, these characteristics facilitate tracer synthesis, in mild conditions, *via* a one-pot-two-step protocol in which the aryltrifluoroborate [^{18}F]**1.9** is formed *in situ* before cycloaddition with the respective azide-appended targeting vector. Hence [^{18}F]**1.10** was prepared in two 15-minute steps with a molar activity of 12 Ci μmol^{-1}.[55] *In vivo* imaging with [^{18}F]**1.10** was noted to lead to improved biodistribution compared to [^{18}F]**1.7** with higher a tumour-to-muscle uptake ratio (7.80 vs. 4.08). Moreover, both tracers demonstrated good *in vivo* stability with bone

uptake noted to be within 0.5 – 1 % ID/g.[54] Similar one-pot-two-step synthetic protocols with **1.8** have also been implemented in the synthesis of agents targeting the $\alpha_4\beta_1$ integrin receptor and the gastrin releasing peptide (GRP) receptor.[52,56]

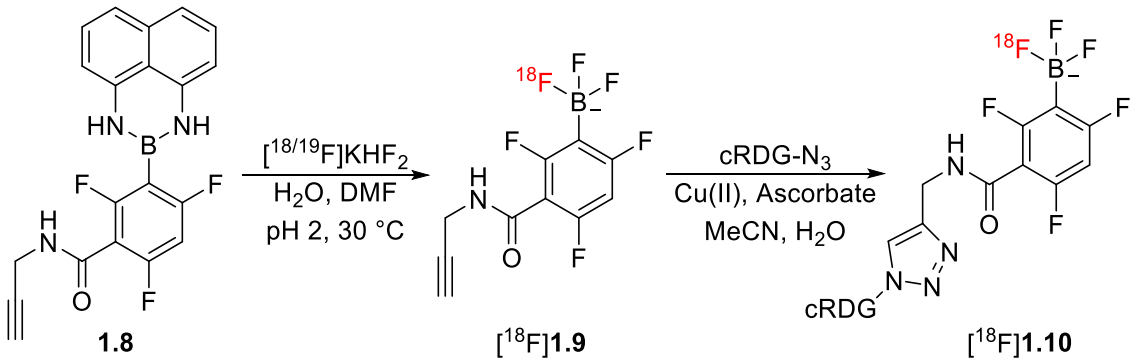

Scheme 1.6 – Two-step-one-pot synthesis of cyclo-RDG conjugate [^{18}F]**1.10** from precursor **1.8**.

The amplification of molar activity that may achieved with these systems, by accumulating three fluorides onto a single boron centre, was experimentally demonstrated by Perrin and co-workers through the 30 minute one-pot-two-step synthesis of [^{18}F]**1.11** (Figure 1.4).[55] An azide-appended rhodamine chromophore was utilised for conjugation, so that an accurate concentration of the [^{18}F]**1.11** product could be determined by HPLC UV methods, and therefore an accurate molar activity value calculated. Thus, [^{18}F]**1.11** was synthesised with a molar activity of 15.5 Ci μmol^{-1} by using a no carrier added source of [^{18}F]fluoride that was separately measured to have a molar activity of 5.3 Ci μmol^{-1} (both decays are corrected to the end of synthesis) thereby validating the tripling effect of boron. A parallel reaction including a small amount of carrier, to increase fluoride concentration, synthesised [^{18}F]**1.11** with a 30 % radiochemical yield (double that of the NCA reaction) and with a high molar activity of 7.4 Ci μmol^{-1}. The carrier added reaction highlights the fact that, due to the "tripling" effect of boron, high molar activities may still be obtained despite the addition of carrier and with the additional advantage of improving yields.

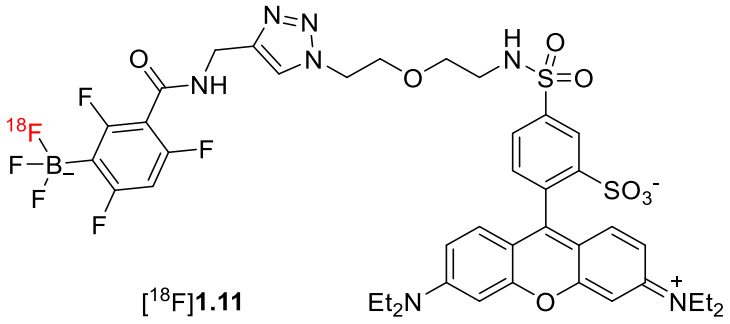

[18F]**1.11**

Figure 1.4 – Radiolabelled rhodamine conjugate [^{18}F]**1.11** derived from **1.8**.

Isotopic exchange has also been employed as an effective method for final stage labelling of aryltrifluoroborates like the cyclo-RDG conjugate **1.7**.[57] Using pre-prepared aliquots for a kit-like labelling protocol, **1.7** was resuspended and heated to 45 °C with aqueous NCA [^{18}F]fluoride at pH 2 for 20 minutes. Following HPLC purification, [^{18}F]**1.7** was obtained in a 65 % radiochemical yield and with a high molar activity of 11.5 Ci μmol^{-1}. Although isotopic exchange is generally favoured for eliminating time-consuming HPLC from radiosynthesis, due to the chemically identical nature of starting material and product, additional purification was required to separate the product from the substantial amount of boronic acid generated by the competing hydrolysis reaction.

In 2014, Liu *et al.* diversified the range of available [^{18}F]ArBF$_3^-$ prosthetic groups by detailing the development of the pyridine-trifluoroborate based **1.13** (Scheme 1.7).[58] The authors employed pyridine-trifluoroborate as the basic scaffold for this work, as it had previously been noted to exhibit aqueous stability exceeding that of phenyl-BF$_3$ (Figure 1.3); the inductive withdrawing effect of the endocyclic nitrogen slows the hydrolysis half-life to 346 minutes.[59] Seeking to further improve the stability of this scaffold, pyridine was functionalised with two electron-withdrawing bromines and an amine group to facilitate conjugation (**1.12**, Scheme 1.7). Assessment of the stability of **1.12** in PBS buffered water confirmed its slow solvolysis. By monitoring the evolution of free fluoride by ^{19}F NMR spectroscopy, the solvolysis half-life was established to be 16,500 minutes, *i.e.* an order of magnitude greater than either **1.2** or **1.3**, indicating **1.12** was a promising candidate for

imaging. The alkyne appended derivative **1.13** was subsequently prepared and conjugated with an azide-appended cyclo-RDG molecule to synthesise **1.14** for stability testing in biological conditions. Labelling of **1.14** by acid-catalysed isotopic exchange with NCA [^{18}F]fluoride at 45 °C for 15 minutes yielded [^{18}F]**1.14** with 16 – 21% radiochemical yield and an effective molar activity of 3.2 Ci μmol^{-1}. [^{18}F]**1.14** demonstrated good plasma stability with less than 1 % free fluoride produced after incubation for 150 minutes, and *in vivo* imaging showed less than 0.5 % was taken up by the skeletal system.

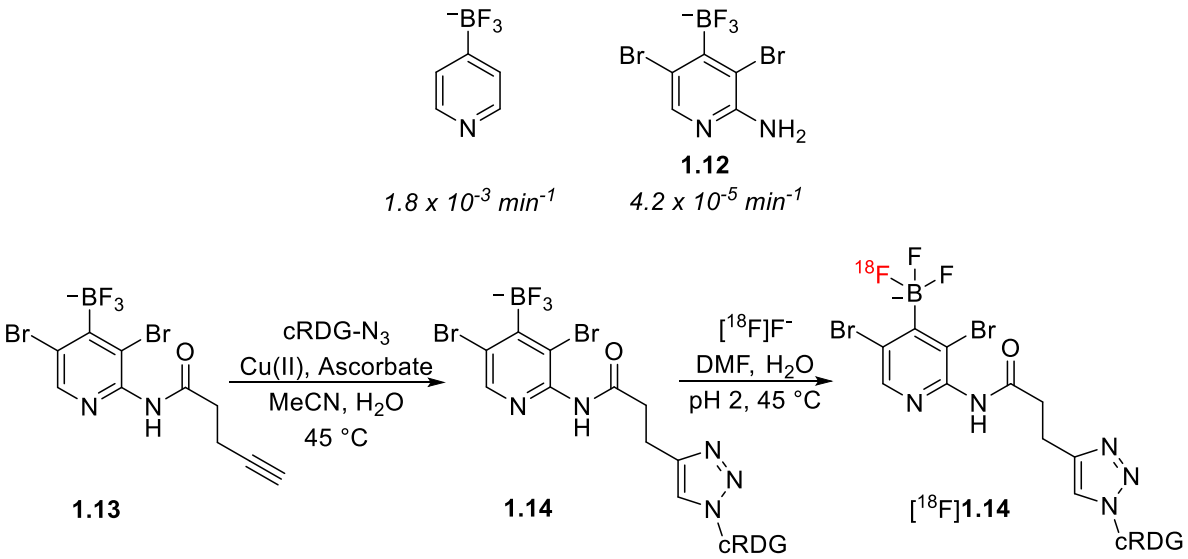

Scheme 1.7 – Top: Pyridinetrifluoroborate and derivative **1.12** with their respective hydrolysis rate constants. Bottom: Synthesis of radiolabelled cyclo-RDG conjugate [^{18}F]**1.14** from precursor **1.13**.

1.3.2 Zwitterionic Trifluoroborates

A significant enhancement in the fluoride ion affinity of boron systems can be achieved by incorporating a cationic group into the structure. The strong negative inductive effects of such a group typically enhance the Lewis acidity of the boron centre, whilst the complementary charges of the cationic substituent and the anionic fluoroborate also introduces a Coulombic component to bonding within the complex. As a result, cationic systems have long been exploited in organoborane sensing chemistry, with examples such as cations **1.15** and **1.16** highlighting the marked increase in the fluoride binding constant that may be attained upon introducing a positive charge (Figure 1.5).[60–64] Whilst the extent of

this increase was immeasurable for the phosphonium system **1.15** under the conditions examined, the sulfonium compound **1.16** was shown to exhibit a fluoride binding constant at least four orders of magnitude greater than that of its neutral equivalent.

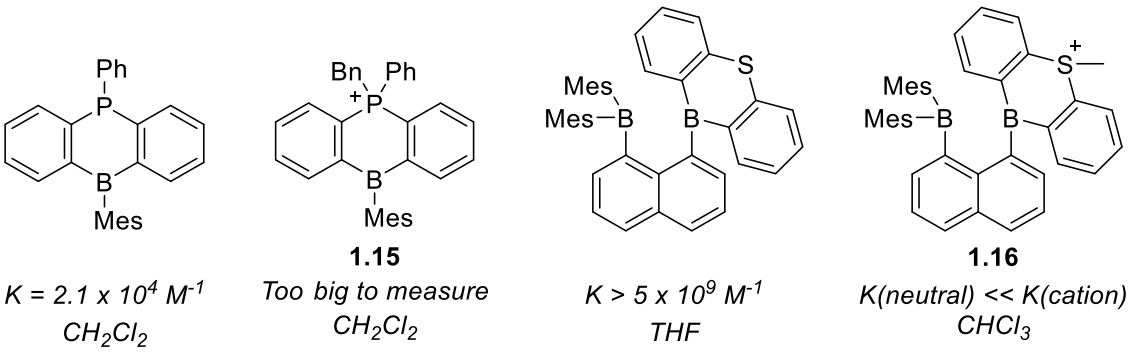

Figure 1.5 – Examples of cationic organoboranes and their respective fluoride binding constants.

1.3.2.1 Zwitterionic Aryltrifluoroborates

Hypothesising that cationic substituents may prove similarly advantageous for PET, the Gabbaï group investigated the rates of hydrolysis of a series of zwitterionic aryltrifluoroborates **1.17** – **1.22** (Figure 1.6).[65,66] These sulfonium, ammonium and phosphonium compounds are analogues of earlier fluoride sensing compounds, reported by the same group, which demonstrate high anion binding affinities.[67–69] Work with the fluoride sensor systems established that the proximal location of the cationic group *ortho*- to the boron centre leads to the greatest enhancement in Lewis acidity, induced primarily by the inductive effects of the substituent.[67] Moreover, the small separation of the charged groups also leads to a strong Coulombic interaction and can facilitate additional donor-acceptor interactions between the substituents.[68]

The observed rates of hydrolysis, monitored by ^{19}F NMR spectroscopy in 8:2 D_2O-CD_3CN, were found to be approximately 200 to 7200 times slower than that of the unadorned phenyltrifluoroborate under the same conditions, establishing the effectiveness of this approach. The differences between **1.17**, **1.18** and **1.19** were primarily attributed to the differing interactions of the cationic substituents with the trifluoroborate group. For example,

the electron density of the sulfonium lone pair is ascribed to have a destabilising effect on the neighbouring anionic trifluoroborate substituent. By contrast, the phosphonium compounds feature a stabilising donor-acceptor interaction with the fluoride lone pair donating electron density into the σ*-orbital of a P–C bond.[68] Notable differences in rate were also observed upon changes to the phosphonium substituents. Iso-propyl substituents led to faster hydrolysis than that observed for the phenyl substituted equivalents, whilst the inclusion of a hydrophilic carboxylic acid was also observed to accelerate degradation. The amino acid-appended zwitterions, **1.23** and **1.24**, described by Bernard *et al.* also fit this trend.[70] The shorter half-lives are therefore suggested to be the result of increased solvation due to the presence of less hydrophobic substituents; an aspect that will also impact the methylated zwitterions **1.17** and **1.18**.

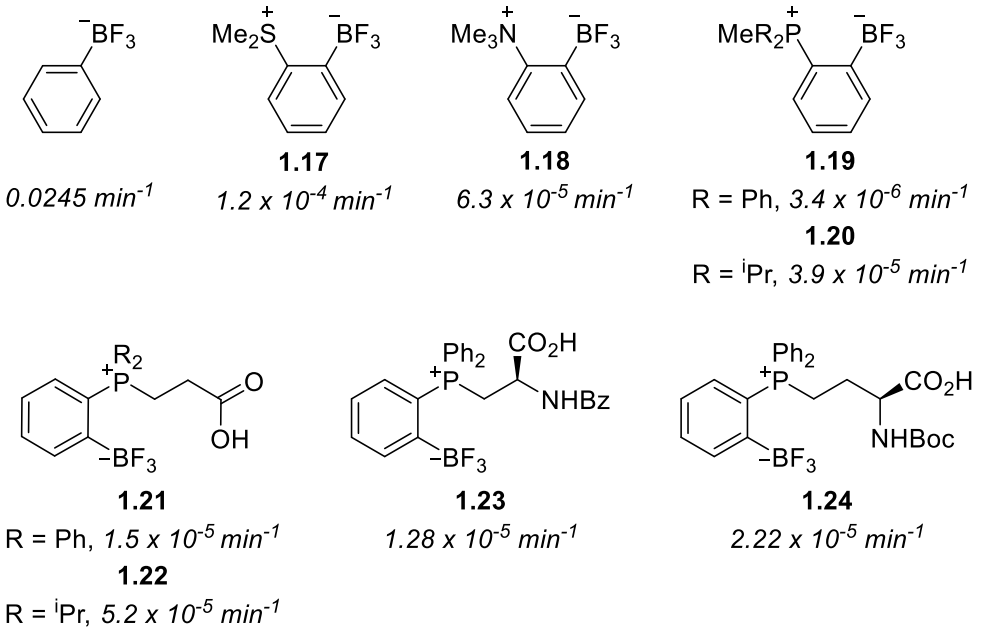

Figure 1.6 - Solvolysis rate constants of zwitterionic aryltrifluoroborates in PBS buffered D_2O/CD_3CN (8:2)

In 2012, Li *et al.* utilised $^{19}F–^{18}F$ isotopic exchange methodology to radiolabel phosphonium zwitterions **1.19** – **1.21**.[66] Time consuming [^{18}F]fluoride preparation was eliminated by using the fluoride directly as sourced from the cyclotron in [^{18}O]water and without addition of further carrier. Thus, labelling was conducted in aqueous acetonitrile at

pH 1.5 over 20 minutes at room temperature to produce all three compounds with excellent radiochemical yields (> 90 %) and molar activities up to 520 mCi μmol^{-1}. The same labelling strategy was later applied to good effect with phosphonium zwitterion conjugates of the cyclooxygenase 2 (COX-2) enzyme targeting drug Indomethacine (**1.25** and **1.26**, Scheme 1.8).[71] [^{18}F]**1.25** and [^{18}F]**1.26** were obtained after a 10 minute acid-catalysed isotopic exchange labelling reaction at 75 °C in radiochemical yields greater than 93 % and molar activities of approximately 50 mCi μmol^{-1}. *In vivo* imaging, to establish the stability of the conjugates, demonstrated promising results for [^{18}F]**1.25**, with negligible bone uptake (0.29 % ID/g) observed after one hour. However, the lower stability of the iso-propyl phosphonium species was again apparent with [^{18}F]**1.26** exhibiting a high bone uptake (3.4 % ID/g), indicating that appreciable defluorination had occurred. Further impacts of the phosphonium substituents on biodistribution were also noted with the localisation of [^{18}F]**1.25** in the liver and intestinal system due the lipophilic character of the phenyl substituents.

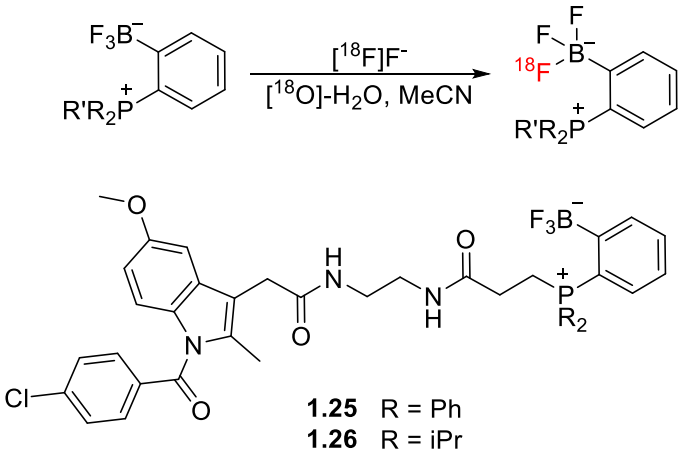

Scheme 1.8 – Isotopic exchange labelling of phosphonium aryltrifluoroborates and Indomethacine conjugates **1.25** and **1.26**.

Zwitterionic [^{18}F]aryltrifluoroborates have also taken the form of an *N*-alkyl pyridinium trifluoroborate prosthetic group, **1.27**.[72,73] During their earlier work with the pyridine-trifluoroborate scaffold, Perrin and coworkers had observed that methylation of the

endocyclic nitrogen slowed the rate of solvolysis in PBS buffered water by an order of magnitude to 1.1 x 10^{-4} min^{-1}.[59] Realising this system was therefore likely to demonstrate the requisite *in vivo* stability for a prosthetic group, the same group recently reported the preparation of the alkyne appended pyridinium **1.27**, and its CuAAC mediated conjugation to peptides targeting either the $\alpha_4\beta_1$ integrin receptor or the prostate-specific membrane antigen (PSMA).[72,73] The peptide conjugates were readily radiolabelled by isotopic exchange with NCA [^{18}F]fluoride under acidic aqueous conditions at 80 °C to yield the respective radiotracers in respectable yields and molar activities. Imaging with the PSMA targeting radiotracers demonstrated negligible bone uptake, confirming the *in vivo* stability of this prosthetic group. Moreover, although a high bone uptake (3.7 % ID/g) was observed with the integrin targeting radiotracer, blocking studies confirmed this was the result of normal expression of the $\alpha_4\beta_1$ integrin receptor in the bone marrow rather than defluorination.

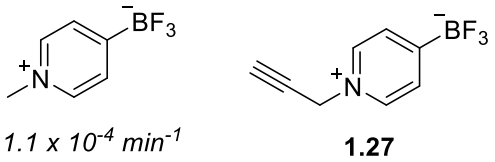

1.1 x 10^{-4} min^{-1} **1.27**

Figure 1.7 – *N*-alkyl pyridinium trifluoroborate complexes.

Alternative systems, which can also be considered to feature a delocalised positive charge, are the imidazolium trifluoroborates **1.28** and **1.29** (Scheme 1.9).[74] These compounds can also be described as *N*-heterocyclic carbene boron trifluoride adducts. Upon assessment of their rates of hydrolysis in PBS buffered 8:2 D_2O-CD_3CN both **1.28** and **1.29** were found to be exceptionally slow at releasing fluoride. Indeed, **1.29** evolved no free fluoride after a week in solution, leading the authors to describe it as "essentially immortal". The tightly bound nature of the fluoride necessitates the addition of a Lewis acid promoter to the ^{19}F–^{18}F isotopic exchange reactions to enable sufficient exchange to occur. Tin(IV) chloride was used for this purpose as it had previously been demonstrated, with BODIPY systems (*vide infra*), to be effective at labilising B–F bonds for isotopic exchange.[75] Hence,

the radiosynthesis of the maleimide functionalised [^{18}F]**1.29** was achieved using NCA [^{18}F]TBAF and an excess of $SnCl_4$ in azeotropically dry conditions heated to 60 °C for 10 minutes (Scheme 1.9). Following solid phase extraction (SPE) purification [^{18}F]**1.29** was isolated in 54 % radiochemical yield and moderate molar activity (51.3 mCi μmol^{-1}) before conjugation with a model peptide *via* a thiol-Michael addition. Final stage labelling was also conducted with tumour targeting peptide conjugates of **1.29** under similar conditions.[76] This shortened labelling procedure produced the [^{18}F]**1.29** peptide conjugates in sufficient molar activities for imaging, however, the presence of $SnCl_4$ did cause some minor degradation of the attached peptides, leading to lower radiochemical yields (21.4 – 29.6 %) and necessitating HPLC purification. *In vivo* imaging studies with the cyclo-RDG and neurotensin peptide tracers demonstrated good tumour contrast and negligible bone uptake verifying the potential of the *N*-heterocyclic carbene boron trifluoride prosthetic group.

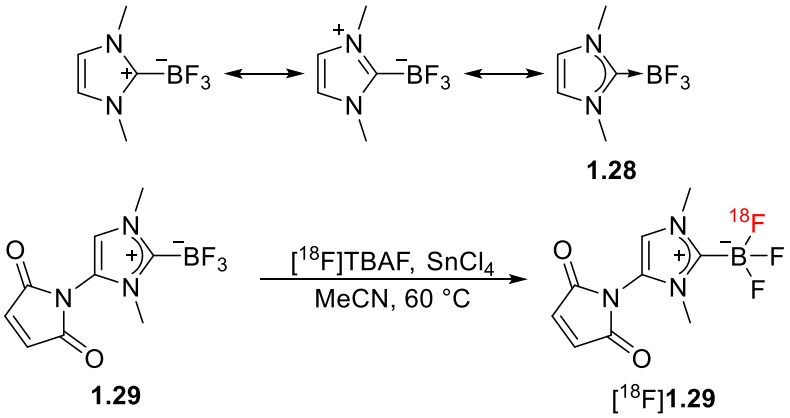

Scheme 1.9 – Resonance forms of *N*-Heterocyclic carbene boron trifluoride adducts and isotopic exchange labelling of the maleimide functionalised adduct **1.29**.

1.3.2.2 Zwitterionic Alkyltrifluoroborates

Cationic substituents have also been employed to slow the hydrolysis of alkyl trifluoroborate systems to make them compatible with imaging applications. In screening a range of candidates Liu *et al*. observed the zwitterionic candidates **1.30** – **1.32** to be some of the most robust of the alkyl systems investigated, with half-lives extending from seven days to several months.[77] The short linker utilised to connect the charged groups in **1.30** – **1.32**

ensures both high inductive effects and through-space Coulombic attraction. The authors also established a general correlation between the (negative log of the) rate of hydrolysis of alkyl trifluoroborates and the pKa of the respective alkyl carboxylic acid equivalent and predicted that this may form a useful guide for future development in the field.

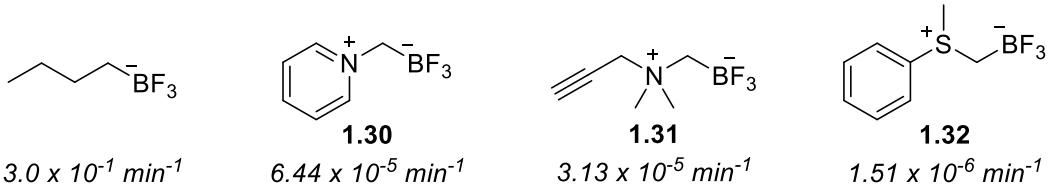

Figure 1.8 – Alkyl trifluoroborates and their respective rates of hydrolysis in PBS buffered water (~ pH 7).

The alkyne functionalised ammoniomethyl trifluoroborate ($AMBF_3$) **1.31** has been used as a prosthetic group suitable for final stage labelling. A kit-like isotopic exchange labelling protocol has been developed which combines the CuAAC conjugated derivatives of **1.31** with a no carrier added source of [^{18}F]fluoride in a DMF-water mixture buffered with pyridazine-HCl (pH ~2).[78] The reaction mixtures were heated at 80 °C for 10-20 minutes before quenching and purification by either HPLC or solid phase extraction (SPE) depending upon the sample. Additionally, preparation of the fluoride source is limited to a concentration step, to aid efficiency, by trapping on an anion exchange resin and eluting with saline. The high activities that may be achieved with an $AMBF_3$ prosthetic group were verified with a rhodamine dye conjugate.[79] Prepared in 25 minutes and purified by an SPE cartridge, the ^{18}F-product was isolated with a 25 % radiochemical yield. HPLC confirmed the high purity of the product and the molar activity was established to be 3-4 Ci μmol^{-1}.

An octreotate derivative was conjugated with **1.31** ($AMBF_3$-TATE, **1.33,** Figure 1.9) with the resulting system showing favourable results *in vivo*.[79,80] Interest in the octreotate peptide stems from its affinity for the somatostatin type 2 receptor (sstr2) which is overexpressed in neuroendocrine tumours. Using the aforementioned protocol, $AMBF_3$-

TATE was radiolabelled and purified by SPE cartridge to produce [^{18}F]**1.33** at 3 Ci μmol^{-1} and a 20-25 % radiochemical yield in 25 minutes. Imaging confirmed the *in vivo* stability of the $AMBF_3$ prosthetic group with negligible bone uptake after an hour (0.46 % ID/g). Moreover, the radiotracer demonstrated high tumour uptake and tumour-to-background ratios exceeding that of the ^{68}Ga-DOTATATE clinical standard. Consequently, research into the clinical translation of [^{18}F]**1.33** is ongoing.[81,82] Further peptide conjugates with **1.31** have been investigated for the targeted imaging of a range of other receptors including: the GRP receptor,[83] the bradykinin B1 receptor,[84] the $\alpha_4\beta_1$ integrin receptor,[72,85] the melanocortin 1 receptor (MC1R),[86,87] PSMA[73] and the CXC chemokine receptor 4 (CXCR4).[88]

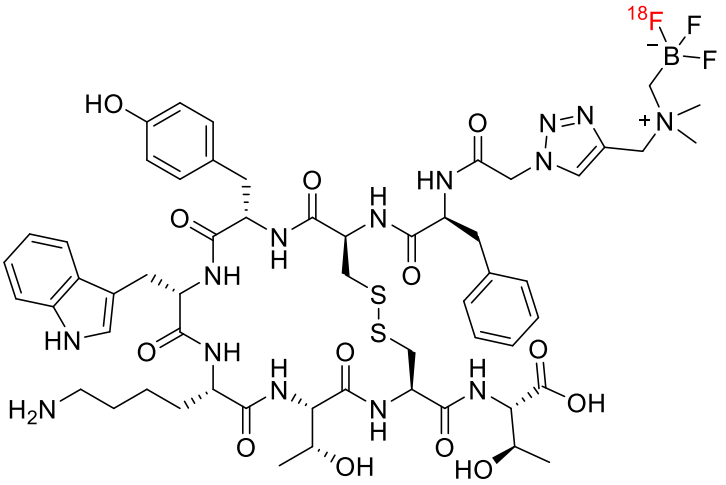

[^{18}F]**1.33**

Figure 1.9 – [^{18}F]$AMBF_3$-TATE radiotracer

The utility of the $AMBF_3$ motif has led to its incorporation into a range of frameworks that widen the scope of its applications. This is readily achieved by the facile synthesis of these systems through alkylation of the respective amine with iodomethylboronylpinacolate, ICH_2Bpin, followed by acid mediated ^{19}F-fluorination (Scheme 1.10). Prosthetic groups obtained by this method comprise the azide-appended **1.34**, as an alternative CuAAC click reagent, and the carboxylic acid appended system **1.35** (Figure 1.10).[79,88–91] The trimeric

species **1.36** has likewise been prepared.[79] The pendant alkynes of this prosthetic group have been utilised for conjugation with three identical targeting vectors or several different groups, such as in **1.37** which combines the peptide cyclo-RDG and a rhodamine dye into a multimodal PET-fluorescence tracer.[79,92,93]

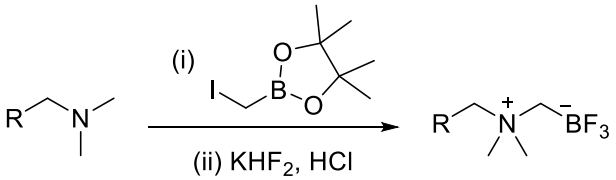

Scheme 1.10 - General synthesis of $AMBF_3$ compounds

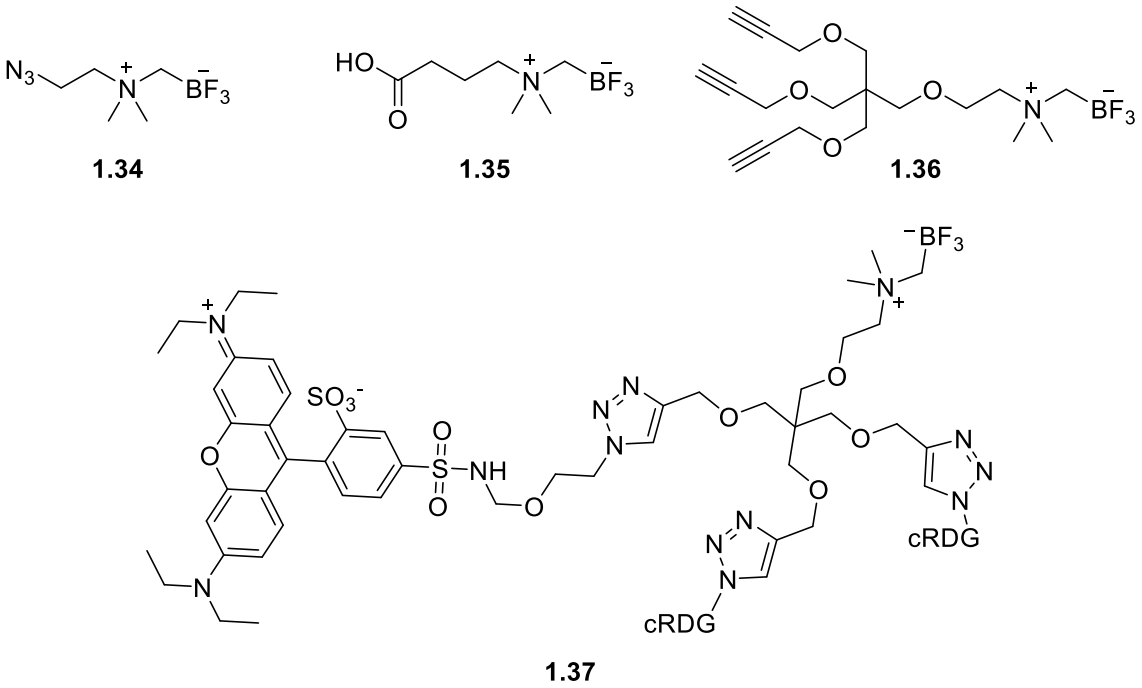

Figure 1.10 – Examples of $AMBF_3$ prosthetic groups (**1.34** – **1.36**) and multimodal tracer **1.37**

Quaternary ammoniomethyl trifluoroborate examples also extend to small molecule tracers (Figure 1.11). Ergo, the $AMBF_3$ group has been directly incorporated into compounds such as the phosphonium **1.38** and the nitroimidazole derivative **1.39**, which were investigated for imaging myocardial perfusion and hypoxia respectively.[94,95] Furthermore, Ting and coworkers have also recently exploited an existing tertiary amine centre in the brain cancer drug Dasatinib to directly install an ammonium methyl trifluoroborate functional group (**1.40**).[96] Affixed onto the piperazine group of the drug scaffold, the small prosthetic

group exhibits the same high stability as $AMBF_3$ derivatives and was labelled using the same final stage protocol, enabling the brain distribution of Dasatinib derivatives to be monitored *via* PET.

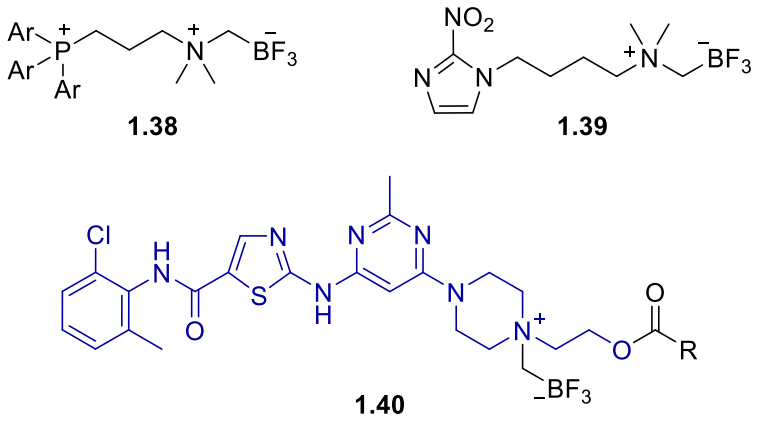

Figure 1.11 – Small molecule tracers **1.38** and **1.39** featuring the $AMBF_3$ group. Dasatinib drug derivative **1.40** with original drug structure highlighted in blue.

In 2015, Liu and coworkers described the synthesis of a set of [^{18}F]fluoroborate amino acid mimics.[97] These so-called boramino acids (BAAs) are analogues of natural amino acids whereupon the carboxylic acid functional group has been replaced by the isosteric trifluoroborate functional group. As zwitterions at physiological pH, the proximal ammonium centre generally confers a high aqueous stability on the trifluoroborate group. These [^{18}F]BAAs, labelled by isotopic exchange, display amino acid transporter mediated cell uptake comparable to their equivalent amino acids. Moreover *in vivo* imaging with the phenylalanine BAA analogue **1.41** revealed high tumour uptake and minimal background, further demonstrating the promise of these compounds.

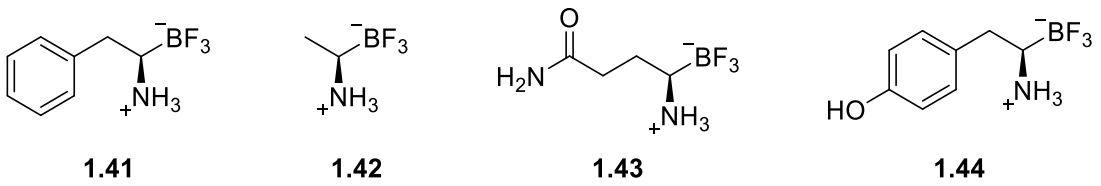

Figure 1.12 – Boramino acids of naturally occurring amino acids.

The Liu group has subsequently reported further examples of BAAs, however, these feature some variation in aqueous and *in vivo* stability.[98–102] Defluorination was especially prevalent with the glutamine BAA analogue **1.43**, both in aqueous and in *in vivo* conditions; bone uptake *in vivo* was as high as 8.88 % ID/g.[100] The authors established that intramolecular cyclisation reactions were compromising compound stability and therefore increased the chain length within the structure, to inhibit these reactions and successfully increase stability.[101] Meanwhile, the alanine BAA analogue **1.42** also shows signs of *in vivo* defluorination, despite exhibiting reasonable stability in PBS.[99] The activity uptake by the skeletal system was therefore attributed to alanine metabolism pathways deaminating the zwitterionic tracer, to leave an anionic trifluoroborate product that is more susceptible to defluorination. In contrast, the tyrosine BAA analogue **1.44** was found to be robust and has progressed to human trials, with additional interest in exploring its application in boron neutron capture therapy.[102,103] Finally, a recent innovation by Liu and co-workers elegantly exploits the high tumour uptake and slow fluoride release by phenylalanine derivative **1.41** as part of a desilylation-based release mechanism for targeted drug delivery.[104]

1.3.3 Difluoroborate systems

Dipyrrometheneboron difluoride, also known as BODIPY, forms the core of a family of BODIPY dyes widely used in fluorescence imaging in the biological sciences, as well as forming the basis for a variety of fluorescent chemical sensors.[105,106] The widespread use of BODIPY dyes stems from their favourable photophysical properties and readily modifiable structures, in addition to their high photochemical and chemical stability. The B–F bonds of BODIPY therefore presented an appealing radiofluorination target for researchers to obtain a multimodal PET-fluorescence prosthetic group.

The first example of a [^{18}F]BODIPY derivative, [^{18}F]**1.46**, was reported by Li *et al.* in 2011.[107] Two alternative substitution strategies were described to obtain the tracer from the

respective boronic acid cation **1.45** (Scheme 1.11). Hydroxide substitution in aqueous media was carried out with carrier added [^{18}F]KHF_2 and was facilitated by the acidic conditions (pH 2-3), yielding [^{18}F]**1.46** in 22 % radiochemical yield and with a molar activity of 25 mCi μmol^{-1}. Activation of the B–OH bond was also achieved using Me_3SiOTf, however this approach requires azeotropically dry conditions. Hence **1.45** was pretreated with an excess of Me_3SiOTf before addition of no carrier added [^{18}F]TBAF and heating at 60 °C for 5 minutes. This second pathway produces [^{18}F]**1.46** in greater yields (61 %) and a molar activity exceeding 1.4 Ci μmol^{-1}. PET imaging with [^{18}F]**1.46** confirmed its *in vivo* stability with no bone uptake observed after four hours. Ensuing *ex vivo* examination of a selection of organs by optical and PET imaging methods also demonstrated concordant results for the biodistribution of [^{18}F]**1.46**, verifying the multimodal potential of BODIPY-based compounds.

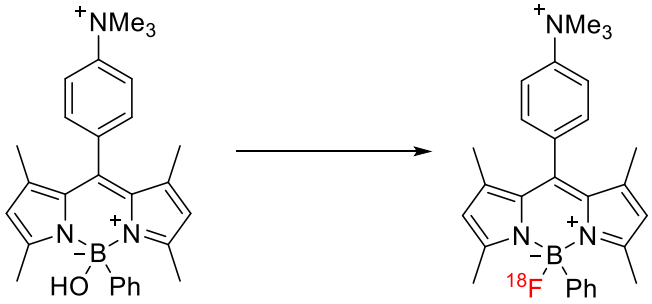

1.45 [^{18}F]**1.46**

Scheme 1.11 – Radiosynthesis of cation [^{18}F]**1.46** *via* hydroxide substitution.
Method 1: Carrier added [^{18}F]KHF_2, MeOH, [^{18}O]H_2O, pH 2-3, Room temperature
Method 2: [^{18}F]TBAF, xs Me_3SiOTf, 60 °C

In 2012, Hendricks *et al.* investigated the known DMAP boronium complex **1.48** (Scheme 1.12) as an alternative precursor for accessing [^{18}F]BODIPY systems.[108] The iodide salt of the **1.48** boronium cation had originally been reported by Hudnall and Gabbaï as a fluoride sensing fluorophore with a turn-on fluorescence response.[109] In order to achieve efficient fluoride uptake for radiolabelling, Hendricks *et al*. used microwave heating to warm [**1.48**][OTf] and NCA [^{18}F]fluoride to 100 °C for 10 minutes to produce [^{18}F]**1.47**

with a 67.7 % radiochemical yield. However, the relatively harsh conditions required to synthesise and radiolabel the DMAP complex were anticipated to be incompatible with many functional groups used to functionalise more sophisticated BODIPY derivatives.

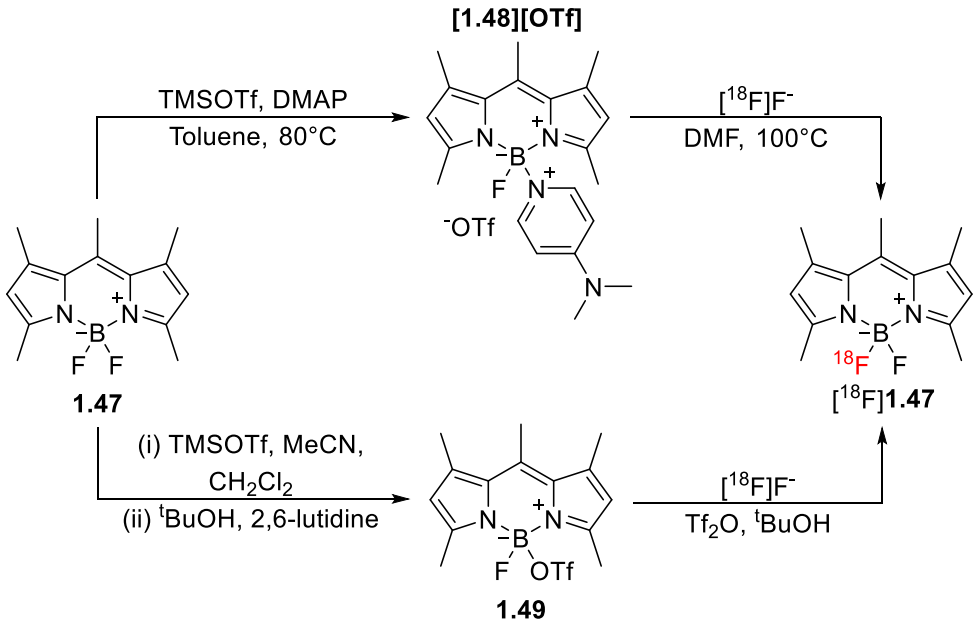

Scheme 1.12 – Two synthetic routes to [^{18}F]**1.47**

Consequently, Hendricks *et al.* described a milder one-pot-two-step isotopic exchange protocol for the synthesis of [^{18}F]**1.47**.[108] As for the synthesis of the **1.48** cation, fluoride is abstracted using Me_3SiOTf, leading to the *in situ* formation of the activated triflate intermediate **1.49**. After quenching residual Me_3SiOTf with *tert*-butanol, to prevent undesirable fluoride sequestration by the silane, **1.49** was combined with an acidic source of NCA [^{18}F]fluoride to generate [^{18}F]**1.47** in 67 % radiochemical yield and with a molar activity of 0.96 Ci μmol^{-1}. The labile nature of the triflate group enables rapid substitution so the radiofluorination step is complete within one minute. Dry conditions are also required throughout the reaction, hence triflic anhydride is used to pre-treat the fluoride source to remove residual water. Excess triflic anhydride is subsequently quenched with *tert*-butanol, generating triflic acid and thereby provide the acidic conditions required for efficient triflate substitution. The wider applicability of this synthetic route was demonstrated by the

successful labelling of a *N*-hydroxysuccinimide ester functionalised BODIPY structure in 73 % radiochemical yield before conjugation with a Trastuzumab antibody.

The combination of triflic anhydride and *tert*-butanol was subsequently demonstrated to directly facilitate isotopic exchange labelling of BODIPY derivatives, obviating the need for the Me_3SiOTf activation step.[110] The two reagents independently do not promote exchange, with both reagents required to instead generate triflic acid for the acid catalysed isotopic exchange. Furthermore, the *in situ* generation of triflic acid was noted to be preferable to direct addition of the acid, which caused degradation. Thus functionalised [^{18}F]BODIPY derivatives, such as [^{18}F]**1.50**, were obtained by heating triflic anhydride and *tert*-butanol with azeotropically dry [^{18}F]fluoride and the respective ^{19}F-fluorinated BODIPY precursor to 50 °C for 30 minutes (Scheme 1.13). The reaction conditions were tolerant of the *N*-hydroxysuccinimide ester and maleimide groups within the BOPIDY compounds examined, although the radiochemical yields varied greatly from 16.2 – 86.2 %.

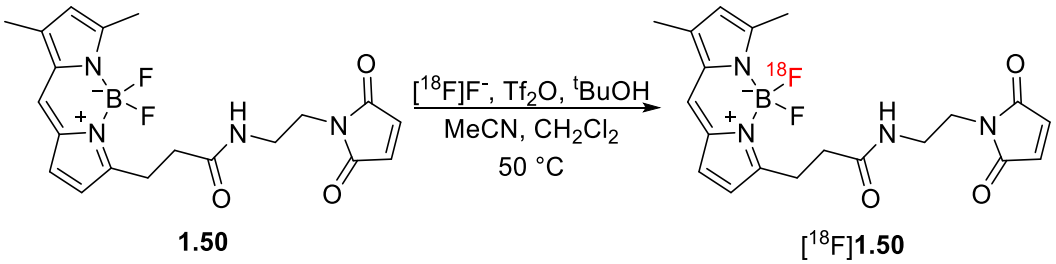

Scheme 1.13 – Acid catalysed isotopic exchange

An alternative strategy for promoting ^{19}F–^{18}F isotopic exchange with fluoroborate compounds utilises a Lewis acid to labilise the B–F bond. Following poorly yielding attempts to synthesise [^{18}F]**1.51** *via* isotopic exchange in acidified water (pH 2), Conti and coworkers screened a selection of Lewis acids (Scheme 1.14).[75] Using azeotropically dry conditions, quantitative yields were obtained after 10 minutes at room temperature with an 8-fold excess of $ZnCl_2$, $SnCl_4$ or $TiCl_4$. Under the same conditions $AlCl_3$ and AlF_3 produced negligible yields, likely a result of the high Al–F bond strength leading to fluoride

sequestration. The most favourable results were obtained with $SnCl_4$ which produced [^{18}F]**1.51** with a radiochemical yield exceeding 95 %. $SnCl_4$ was therefore utilised to synthesise [^{18}F]**1.51** and a range of analogues for myocardial perfusion imaging studies with variation in the ammonium substituents used to modify the *in vivo* biodistribution.[111,112]

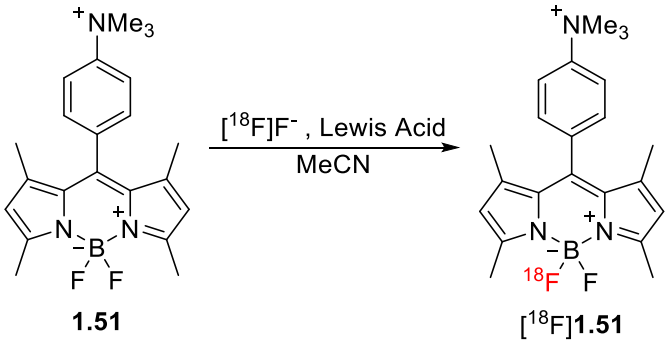

Scheme 1.14 – Lewis acid promoted isotopic exchange labelling

Tin(IV) chloride has subsequently become the Lewis acid of choice for promoting isotopic exchange with a range of BODIPY based PET-fluorescence tracers, examples of which were recently reviewed by Kwon, Byun and Kim.[113] A noteworthy exception however is the synthesis of cyclo-RDG conjugate [^{18}F]**1.52** (Scheme 1.15).[114] $SnCl_4$ promoted isotopic exchange with **1.52** was relatively low yielding (35.3 %) with the Lewis acid suggested to have caused degradation of the peptide conjugate. This led Li and co-workers to investigate $SnCl_2$ as an alternative, obtaining improved yields of 82.2 % at room temperature.

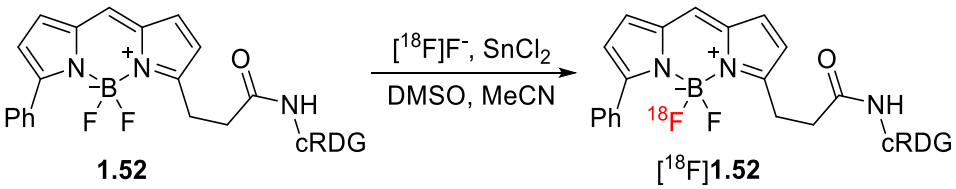

Scheme 1.15 – Lewis acid promoted isotopic exchange

An *et al.* have recently expanded the known [^{18}F]difluoroborate systems to include [^{18}F]difluoro-dioxaborinin examples (Figure 1.13).[115] In addition to tuning the fluorescence properties, the ligand backbone was found to have a considerable impact on the stability of

the compound to hydrolysis. Advantageously for imaging, compounds with extended π-systems featuring electron donor substituents, such as **1.53** and **1.54**, exhibited the slowest solvolysis in the presence of water, and fluorescence emission close to the near-IR region. Radiolabelling was achieved *via* isotopic exchange in a 10 minute, room temperature reaction using dry [^{18}F]fluoride and 2 % tin(IV) chloride, yielding the products in high radiochemical yields (≥ 75 %). [^{18}F]**1.55** was subsequently investigated for the multi-modal imaging of sentinel lymph nodes, with the target specific uptake of the radiotracer established using both PET and fluorescence imaging.

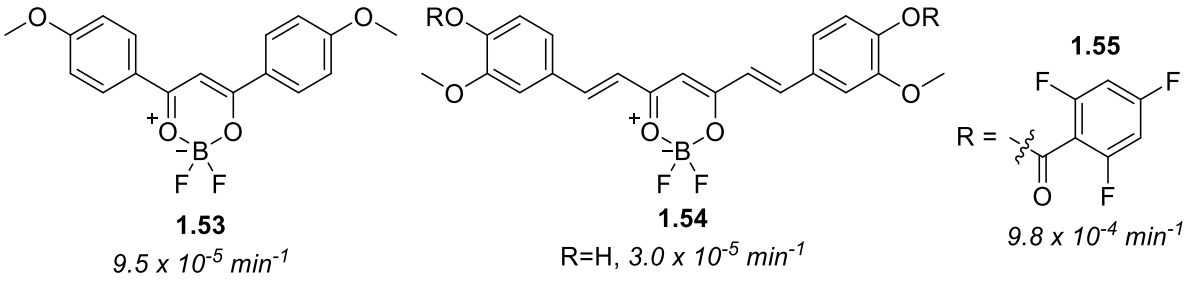

Figure 1.13 – Difluoro-dioxaborinin systems explored for PET-fluorescence imaging. Rate constants for hydrolysis determined in 10 % water 90 % DMSO.

1.4 Research Proposal

The compelling advantages of the B–^{18}F approach, for forming prosthetic groups with a high molar activity, at a late stage, using mild conditions warrants the development of further suitable systems. The broad aim of this DPhil project is therefore to further the expansion and diversification of the available catalogue of fluoroborate compounds which can be utilised for PET imaging. Hence over the course of this project we will endeavour to systematically approach the design of these systems, to explore how advances can be made with respect to three fundamental design features:

i. ***Robustness***. The slow solvolysis of the fluoroborate group is essential for ensuring *in vivo* stability. A high fluoride binding affinity is required to disfavour dissociation of the first fluoride, *i.e.* the rate determining step of the solvolysis reaction.

ii. ***Rapid, efficient fluoride binding***. To work within the time constraints imposed by the fluorine-18 decay, and to maximise possible molar activity, precursors ought to rapidly take up fluoride in a carrier-free reaction. Ideally the reaction is water compatible and does not require promoter reagents that can cause degradation.

iii. ***Versatility***. Structures should offer a point of attachment suitable for a variety of bioconjugation handles, to allow for efficient and varied bioconjugation strategies. A modular design would benefit this.

These design features will form the central objectives for the molecules investigated over the course of this project.

1.5 References

[1] D. A. Mankoff, *J. Nucl. Med.* **2007**, *48*.

[2] H. Son, K. Jang, H. Lee, S. E. Kim, K. W. Kang, H. Lee, *Nucl. Med. Mol. Imaging (2010).* **2019**, *53*, 208–215.

[3] M. E. Phelps, *Proc. Natl. Acad. Sci. U. S. A.* **2000**, *97*, 9226–33.

[4] A. M. J. Paans, A. Van Waarde, P. H. Elsinga, A. T. M. Willemsen, W. Vaalburg, *Methods* **2002**, *27*, 195–207.

[5] S. M. Ametamey, M. Honer, P. A. Schubiger, *Chem. Rev.* **2008**, *108*, 1501–1516.

[6] X. Deng, J. Rong, L. Wang, N. Vasdev, L. Zhang, L. Josephson, S. H. Liang, *Angew. Chemie - Int. Ed.* **2019**, *58*, 2580–2605.

[7] P. W. Miller, N. J. Long, R. Vilar, A. D. Gee, *Angew. Chemie - Int. Ed.* **2008**, *47*, 8998–9033.

[8] T. J. Wadas, E. H. Wong, G. R. Weisman, C. J. Anderson, *Chem. Rev.* **2010**, *110*, 2858–2902.

[9] R. Schirrmacher, B. Wängler, J. Bailey, V. Bernard-Gauthier, E. Schirrmacher, C. Wängler, *Semin. Nucl. Med.* **2017**, *47*, 474–492.

[10] S. Preshlock, M. Tredwell, V. Gouverneur, *Chem. Rev.* **2016**, *116*, 719–766.

[11] L. Cai, S. Lu, V. W. Pike, *European J. Org. Chem.* **2008**, *2008*, 2853–2873.

[12] A. F. Brooks, J. J. Topczewski, N. Ichiishi, M. S. Sanford, P. J. H. Scott, *Chem. Sci.* **2014**, *5*, 4545–4553.

[13] D. Van Der Born, A. Pees, A. J. Poot, R. V. A. Orru, A. D. Windhorst, D. J. Vugts, *Chem. Soc. Rev.* **2017**, *46*, 4709–4773.

[14] J. M. Winfield, *J. Fluor. Chem.* **1980**, *16*, 1–17.

[15] M. F. Ghorab, J. M. Winfield, *J. Fluor. Chem.* **1990**, *49*, 367–383.

[16] M. Anbar, S. Guttmann, Z. Lewitus, *Endocrinology* **1960**, *66*, 888–890.

[17] H. M. Askenasy, M. Anbar, Y. Laor, Z. Lewitus, I. Z. Kosary, S. Guttmann, *Am. J. Roentgenol. Radium Ther. Nucl. Med.* **1962**, *88*, 350–354.

[18] W. Entzian, S. Aronow, A. H. Soloway, W. H. Sweet, *J. Nucl. Med.* **1964**, *5*, 542–50.

[19] C. M. E. Matthews, *Nature* **1967**, *214*, 933–935.

[20] M. S. Rosenthal, A. L. Bosch, R. J. Nickles, S. J. Gatley, *Int. J. Appl. Radiat. Isot.* **1985**, *36*, 318–319.
[21] R. Ting, M. J. Adam, T. J. Ruth, D. M. Perrin, *J. Am. Chem. Soc.* **2005**, *127*, 13094–13095.
[22] R. Schirrmacher, G. Bradtmöller, E. Schirrmacher, O. Thews, J. Tillmanns, T. Siessmeier, H. G. Buchholz, P. Bartenstein, B. Wängler, C. M. Niemeyer, K. Jurkschat, *Angew. Chemie - Int. Ed.* **2006**, *45*, 6047–6050.
[23] A. R. Studenov, M. J. Adam, J. S. Wilson, T. J. Ruth, *J. Label. Compd. Radiopharm.* **2005**, *48*, 497–500.
[24] J. A. H. Inkster, K. Liu, S. Ait-Mohand, P. Schaffer, B. Guérin, T. J. Ruth, T. Storr, *Chem. – A Eur. J.* **2012**, *18*, 11079–11087.
[25] W. J. McBride, R. M. Sharkey, H. Karacay, C. A. D'Souza, E. A. Rossi, P. Laverman, C. H. Chang, O. C. Boerman, D. M. Goldenberg, *J. Nucl. Med.* **2009**, *50*, 991–998.
[26] R. Bhalla, C. Darby, W. Levason, S. K. Luthra, G. McRobbie, G. Reid, G. Sanderson, W. Zhang, *Chem. Sci.* **2014**, *5*, 381–391.
[27] P. J. Blower, W. Levason, S. K. Luthra, G. McRobbie, F. M. Monzittu, T. O. Mules, G. Reid, M. N. Subhan, *Dalt. Trans.* **2019**, *48*, 6767–6776.
[28] V. Bernard-Gauthier, J. J. Bailey, Z. Liu, B. Wängler, C. Wängler, K. Jurkschat, D. M. Perrin, R. Schirrmacher, *Bioconjug. Chem.* **2016**, *27*, 267–279.
[29] G. E. Smith, H. L. Sladen, S. C. G. Biagini, P. J. Blower, *Dalt. Trans.* **2011**, *40*, 6196–6205.
[30] K. Chansaenpak, B. Vabre, F. P. Gabbaï, *Chem. Soc. Rev.* **2016**, *45*, 954–971.
[31] C. Fersing, A. Bouhlel, C. Cantelli, P. Garrigue, V. Lisowski, B. Guillet, *Molecules* **2019**, *24*, 2866.
[32] R. Schirrmacher, V. Bernard-Gauthier, E. Schirrmacher, J. J. Bailey, K. Jurkschat, C. Wängler, B. Wängler, in *Fluor. Life Sci. Pharm. Med. Diagnostics, Agrochem. Prog. Fluor. Sci. Ser.*, Academic Press, **2018**, pp. 551–574.
[33] G. Pascali, L. Matesic, B. Zhang, A. T. King, A. J. Robinson, A. T. Ung, B. H. Fraser, *EJNMMI Radiopharm. Chem.* **2017**, *2*, 1–18.
[34] Q. Zheng, H. Xu, H. Wang, W. G. H. Du, N. Wang, H. Xiong, Y. Gu, L. Noodleman, K. B. Sharpless, G. Yang, P. Wu, *J. Am. Chem. Soc.* **2021**, *143*, 3753–3763.
[35] Y.-R. Luo, *Comprehensive Handbook of Chemical Bond Energies*, CRC Press, Boca Raton ; London, **2007**.
[36] M. Anbar, S. Guttmann, Z. Lewitus, *Nature* **1959**, *183*, 1517–1518.
[37] M. Jauregui-Osoro, K. Sunassee, A. J. Weeks, D. J. Berry, R. L. Paul, M. Cleij, J. P. Banga, M. J. O'Doherty, P. K. Marsden, S. E. M. Clarke, J. R. Ballinger, I. Szanda, S. Y. Cheng, P. J. Blower, *Eur. J. Nucl. Med. Mol. Imaging* **2010**, *37*, 2108–2116.
[38] H. Jiang, N. R. Schmit, A. R. Koenen, A. Bansal, M. K. Pandey, R. B. Glynn, B. J. Kemp, K. L. Delaney, A. Dispenzieri, J. N. Bakkum-Gamez, K. W. Peng, S. J. Russell, T. M. Gunderson, V. J. Lowe, T. R. DeGrado, *EJNMMI Res.* **2017**, *7*, 1–9.
[39] J. O'Doherty, M. Jauregui-Osoro, T. Brothwood, T. Szyszko, P. K. Marsden, M. J. O'Doherty, G. J. R. Cook, P. J. Blower, V. Lewington, *J. Nucl. Med.* **2017**, *58*, 1666–1671.
[40] S. Samnick, E. Al-Momani, J. S. Schmid, A. Mottok, A. K. Buck, C. Lapa, *Clin. Nucl. Med.* **2018**, *43*, 162–167.
[41] M. Dittmann, J. M. Gonzalez Carvalho, K. Rahbar, M. Schäfers, M. Claesener, B. Riemann, R. Seifert, *Eur. J. Nucl. Med. Mol. Imaging* **2020**, *47*, 2639–2646.
[42] C. G. Zhan, D. A. Dixon, *J. Phys. Chem. A* **2004**, *108*, 2020–2029.
[43] R. Ting, C. W. Harwig, J. Lo, Y. Li, M. J. Adam, T. J. Ruth, D. M. Perrin, *J. Org. Chem.* **2008**, *73*, 4662–4670.

[44] A. J. J. Lennox, G. C. Lloyd-Jones, *J. Am. Chem. Soc.* **2012**, *134*, 7431–7441.
[45] R. Ting, J. Lo, M. J. Adam, T. J. Ruth, D. M. Perrin, *J. Fluor. Chem.* **2008**, *129*, 349–358.
[46] C. W. Harwig, R. Ting, M. J. Adam, T. J. Ruth, D. M. Perrin, *Tetrahedron Lett.* **2008**, *49*, 3152–3156.
[47] L. Trembleau, M. Simpson, R. W. Cheyne, I. Escofet, M. V. C. A. L. Appleyard, K. Murray, S. Sharp, A. M. Thompson, T. A. D. Smith, *New J. Chem.* **2011**, *35*, 2496–2502.
[48] T. A. D. Smith, M. Simpson, R. Cheyne, L. Trembleau, *Appl. Radiat. Isot.* **2011**, *69*, 1395–1400.
[49] R. Ting, C. Harwig, U. Auf Dem Keller, S. McCormick, P. Austin, C. M. Overall, M. J. Adam, T. J. Ruth, D. M. Perrin, *J. Am. Chem. Soc.* **2008**, *130*, 12045–12055.
[50] U. auf dem Keller, C. L. Bellac, Y. Li, Y. Lou, P. F. Lange, R. Ting, C. Harwig, R. Kappelhoff, S. Dedhar, M. J. Adam, T. J. Ruth, F. Bénard, D. M. Perrin, C. M. Overall, *Cancer Res.* **2010**, *70*, 7562–7569.
[51] Y. Li, R. Ting, C. W. Harwig, U. Auf Dem Keller, C. L. Bellac, P. F. Lange, J. A. H. Inkster, P. Schaffer, M. J. Adam, T. J. Ruth, C. M. Overall, D. M. Perrin, *Medchemcomm* **2011**, *2*, 942–949.
[52] D. Walker, Y. Li, Á. Roxin, P. Schaffer, M. J. Adam, D. M. Perrin, *Bioorg. Med. Chem. Lett.* **2016**, *26*, 5126–5131.
[53] Y. Li, Z. Liu, J. Lozada, M. Q. Wong, K. S. Lin, D. Yapp, D. M. Perrin, *Nucl. Med. Biol.* **2013**, *40*, 959–966.
[54] Y. Li, J. Guo, S. Tang, L. Lang, X. Chen, D. M. Perrin, *Am. J. Nucl. Med. Mol. Imaging* **2013**, *3*, 44–56.
[55] Z. Liu, Y. Li, J. Lozada, P. Schaffer, M. J. Adam, T. J. Ruth, D. M. Perrin, *Angew. Chemie - Int. Ed.* **2013**, *52*, 2303–2307.
[56] Y. Li, Z. Liu, C. W. Harwig, M. Pourghiasian, J. Lau, K.-S. Lin, P. Schaffer, F. Benard, D. M. Perrin, *Am. J. Nucl. Med. Mol. Imaging* **2013**, *3*, 57–70.
[57] Z. Liu, Y. Li, J. Lozada, M. Q. Wong, J. Greene, K. S. Lin, D. Yapp, D. M. Perrin, *Nucl. Med. Biol.* **2013**, *40*, 841–849.
[58] Z. Liu, N. Hundal-Jabal, M. Wong, D. Yapp, K. S. Lin, F. Bénard, D. M. Perrin, *Medchemcomm* **2014**, *5*, 171–179.
[59] Y. Li, A. Asadi, D. M. Perrin, *J. Fluor. Chem.* **2009**, *130*, 377–382.
[60] C. R. Wade, A. E. J. Broomsgrove, S. Aldridge, F. P. Gabbaï, *Chem. Rev.* **2010**, *110*, 3958–3984.
[61] H. Zhao, L. A. Leamer, F. P. Gabbaï, *Dalt. Trans.* **2013**, *42*, 8164–8178.
[62] T. Agou, J. Kobayashi, T. Kawashima, *Inorg. Chem.* **2006**, *45*, 9137–9144.
[63] H. Zhao, F. P. Gabbaï, *Organometallics* **2012**, *31*, 2327–2335.
[64] J. D. Hoefelmeyer, S. Solé, F. P. Gabbaï, *Dalt. Trans.* **2004**, *4*, 1254–1258.
[65] C. R. Wade, H. Zhao, F. P. Gabbaï, *Chem. Commun.* **2010**, *46*, 6380.
[66] Z. Li, K. Chansaenpak, S. Liu, C. R. Wade, P. S. Conti, F. P. Gabbaï, *Medchemcomm* **2012**, *3*, 1305.
[67] T. W. Hudnall, F. P. Gabbaï, *J. Am. Chem. Soc.* **2007**, *129*, 11978–11986.
[68] T. W. Hudnall, Y. M. Kim, M. W. P. Bebbington, D. Bourissou, F. P. Gabbaï, *J. Am. Chem. Soc.* **2008**, *130*, 10890–10891.
[69] Y. Kim, H. Zhao, F. P. Gabbai, *Angew. Chemie - Int. Ed.* **2009**, *48*, 4957–4960.
[70] J. Bernard, R. Malacea-Kabbara, G. S. Clemente, B. P. Burke, M.-J. Eymin, S. J. Archibald, S. Jugé, *J. Org. Chem.* **2015**, *80*, 4289–4298.
[71] K. Chansaenpak, M. Wang, S. Liu, Z. Wu, H. Yuan, P. S. Conti, Z. Li, F. P. Gabbaï, *RSC Adv.* **2016**, *6*, 23126–23133.

[72] Á. Roxin, C. Zhang, S. Huh, M. L. Lepage, Z. Zhang, K.-S. Lin, F. Bénard, D. M. Perrin, *Nucl. Med. Biol.* **2018**, *61*, 11–20.
[73] H.-T. Kuo, M. L. Lepage, K.-S. Lin, J. Pan, Z. Zhang, Z. Liu, A. Pryyma, C. Zhang, H. Merkens, A. Roxin, D. M. Perrin, F. Bénard, *J. Nucl. Med.* **2019**, *60*, 1160–1166.
[74] K. Chansaenpak, M. Wang, Z. Wu, R. Zaman, Z. Li, F. P. Gabbaï, *Chem. Commun.* **2015**, *51*, 12439–12442.
[75] S. Liu, T. P. Lin, D. Li, L. Leamer, H. Shan, Z. Li, F. P. Gabbaï, P. S. Conti, *Theranostics* **2013**, *3*, 181–189.
[76] K. Chansaenpak, M. Wang, H. Wang, B. C. Giglio, F. P. Gabbaï, Z. Wu, Z. Li, *RSC Adv.* **2017**, *7*, 17748–17751.
[77] Z. Liu, D. Chao, Y. Li, R. Ting, J. Oh, D. M. Perrin, *Chem. - A Eur. J.* **2015**, *21*, 3924–3928.
[78] Z. Liu, K. S. Lin, F. Bénard, M. Pourghiasian, D. O. Kiesewetter, D. M. Perrin, X. Chen, *Nat. Protoc.* **2015**, *10*, 1423–1432.
[79] Z. Liu, M. Pourghiasian, M. A. Radtke, J. Lau, J. Pan, G. M. Dias, D. Yapp, K. S. Lin, F. Bénard, D. M. Perrin, *Angew. Chemie - Int. Ed.* **2014**, *53*, 11876–11880.
[80] Z. Liu, M. Pourghiasian, F. Bénard, J. Pan, K. S. Lin, D. M. Perrin, *J. Nucl. Med.* **2014**, *55*, 1499–1505.
[81] K. Lisova, M. Sergeev, S. Evans-Axelsson, A. D. Stuparu, S. Beykan, J. Collins, J. Jones, M. Lassmann, K. Herrmann, D. Perrin, J. T. Lee, R. Slavik, R. M. van Dam, *Nucl. Med. Biol.* **2018**, *61*, 36–44.
[82] J. Lau, J. Pan, E. Rousseau, C. F. Uribe, S. R. Seelam, B. W. Sutherland, D. M. Perrin, K. S. Lin, F. Bénard, *EJNMMI Res.* **2020**, *10*, 1–10.
[83] M. Pourghiasian, Z. Liu, J. Pan, Z. Zhang, N. Colpo, K. S. Lin, D. M. Perrin, F. Bénard, *Bioorganic Med. Chem.* **2015**, *23*, 1500–1506.
[84] Z. Liu, G. Amouroux, Z. Zhang, J. Pan, N. Hundal-Jabal, N. Colpo, J. Lau, D. M. Perrin, F. Bénard, K. S. Lin, *Mol. Pharm.* **2015**, *12*, 974–982.
[85] Á. Roxin, C. Zhang, S. Huh, M. Lepage, Z. Zhang, K. S. Lin, F. Bénard, D. M. Perrin, *Bioconjug. Chem.* **2019**, *30*, 1210–1219.
[86] C. Zhang, Z. Zhang, K.-S. Lin, J. Lau, J. Zeisler, N. Colpo, D. M. Perrin, F. Bénard, *Mol. Pharm.* **2018**, *15*, 2116–2122.
[87] C. Zhang, Z. Zhang, H. Merkens, J. Zeisler, N. Colpo, N. Hundal-Jabal, D. M. Perrin, K. S. Lin, F. Bénard, *Sci. Rep.* **2019**, *9*, 1–10.
[88] D. Kwon, J. Lozada, Z. Zhang, J. Zeisler, R. Poon, C. Zhang, Á. Roxin, K. S. Lin, D. M. Perrin, F. Benard, *Mol. Pharm.* **2021**, *18*, 187–197.
[89] Y. Wang, J. Weng, J. Lin, D. Ye, Y. Zhang, *J. Am. Chem. Soc.* **2020**, *142*, 2787–2794.
[90] A. Kirby, M. Suchý, A. Brouwer, A. Shuhendler, *Chem. Commun.* **2019**, *55*, 5371–5374.
[91] S. Ye, S. Wang, D. Gao, K. Li, Q. Liu, B. Feng, L. Qiu, J. Lin, *Bioconjug. Chem.* **2020**, *31*, 174–181.
[92] J. Lau, Z. Liu, K.-S. Lin, J. Pan, Z. Zhang, D. Vullo, C. T. Supuran, D. M. Perrin, F. Bénard, *J. Nucl. Med.* **2015**, *56*, 1434–1440.
[93] Z. Liu, M. A. Radtke, M. Q. Wong, K. S. Lin, D. T. Yapp, D. M. Perrin, *Bioconjug. Chem.* **2014**, *25*, 1951–1962.
[94] Z. Zhang, S. Jenni, C. Zhang, H. Merkens, J. Lau, Z. Liu, D. M. Perrin, F. Bénard, K. S. Lin, *Bioorg. Med. Chem. Lett.* **2016**, *26*, 1675–1679.
[95] P. S. G. Nunes, Z. Zhang, H.-T. Kuo, C. Zhang, J. Rousseau, E. Rousseau, J. Lau, D. Kwon, I. Carvalho, F. Bénard, K.-S. Lin, *J. Label. Compd. Radiopharm.* **2018**, *61*, 370–379.
[96] U. Tosi, H. Kommidi, V. Bellat, C. S. Marnell, H. Guo, O. Adeuyan, M. E.

Schweitzer, N. Chen, T. Su, G. Zhang, U. B. Maachani, D. J. Pisapia, B. Law, M. M. Souweidane, R. Ting, *ACS Chem. Neurosci.* **2019**, *10*, 2287–2298.
[97] Z. Liu, H. Chen, K. Chen, Y. Shao, D. O. Kiesewetter, G. Niu, X. Chen, *Sci. Adv.* **2015**, *1*, e1500694.
[98] X. Yang, Z. Liu, H. Zhang, Z. Li, J. P. Munasinghe, G. Niu, G. Teng, X. Chen, *Eur. J. Nucl. Med. Mol. Imaging* **2018**, *45*, 585–592.
[99] H. Liu, Y. Han, J. Li, M. Qin, Q. Fu, C. Wang, Z. Liu, *Mol. Pharm.* **2018**, *15*, 947–954.
[100] C. Li, H. Liu, D. Duan, Z. Zhou, Z. Liu, *Nucl. Med. Biol.* **2018**, *64–65*, 34–40.
[101] J. Chen, C. Li, H. Hong, H. Liu, C. Wang, M. Xu, Y. Han, Z. Liu, *Mol. Pharm.* **2019**, *16*, 5035–5041.
[102] J. Li, Y. Shi, Z. Zhang, H. Liu, L. Lang, T. Liu, X. Chen, Z. Liu, *Bioconjug. Chem.* **2019**, *30*, 2870–2878.
[103] Z. Li, Z. Kong, J. Chen, J. Li, N. Li, Z. Yang, Y. Wang, Z. Liu, *Eur. J. Nucl. Med. Mol. Imaging* **2021**, 1–9.
[104] Q. Wang, Y. Wang, J. Ding, C. Wang, X. Zhou, W. Gao, H. Huang, F. Shao, Z. Liu, *Nature* **2020**, *579*, 421–426.
[105] A. Loudet, K. Burgess, *Chem. Rev.* **2007**, *107*, 4891–4932.
[106] N. Boens, V. Leen, W. Dehaen, *Chem. Soc. Rev.* **2012**, *41*, 1130–1172.
[107] Z. Li, T.-P. Lin, S. Liu, C.-W. Huang, T. W. Hudnall, F. P. Gabbaï, P. S. Conti, *Chem. Commun.* **2011**, *47*, 9324.
[108] J. A. Hendricks, E. J. Keliher, D. Wan, S. A. Hilderbrand, R. Weissleder, R. Mazitschek, *Angew. Chemie - Int. Ed.* **2012**, *51*, 4603–4606.
[109] T. W. Hudnall, F. P. Gabbaï, *Chem. Commun.* **2008**, 4596–4597.
[110] E. J. Keliher, J. A. Klubnick, T. Reiner, R. Mazitschek, R. Weissleder, *ChemMedChem* **2014**, *9*, 1368–1373.
[111] S. Liu, D. Li, H. Shan, F. P. Gabbaï, Z. Li, P. S. Conti, *Nucl. Med. Biol.* **2014**, *41*, 120–126.
[112] K. Chansaenpak, H. Wang, M. Wang, B. Giglio, X. Ma, H. Yuan, S. Hu, Z. Wu, Z. Li, *Chem. - A Eur. J.* **2016**, *22*, 12122–12129.
[113] Y. Do Kwon, Y. Byun, H. K. Kim, *Nucl. Med. Biol.* **2021**, *93*, 22–36.
[114] S. Liu, D. Li, Z. Zhang, G. K. Surya Prakash, P. S. Conti, Z. Li, *Chem. Commun.* **2014**, *50*, 7371–7373.
[115] F. An, F. Nurili, H. Sayman, Z. Ozer, H. Cakiroglu, O. Aras, R. Ting, *J. Med. Chem.* **2020**, *63*, 12693–12706.

Chapter 2

Experimental Methods

2.1 Manipulation of Air-Sensitive Compounds

Some of the compounds featured in this thesis are highly air- and moisture-sensitive and thus required the use of a dual manifold Schlenk line for solution-phase manipulations and a glovebox for the manipulation of solids. These techniques enabled the storage and handling of the sensitive compounds under an inert atmosphere of argon or nitrogen.[1,2]

Schlenk line techniques are an efficient and effective way to minimise the risk of decomposition by oxidation or hydrolysis.[3] The Schlenk line consists of two Pyrex manifolds linked by a series of two-way taps. One manifold was connected to a high vacuum pump, *via* a liquid nitrogen cooled cold trap, and was typically maintained at a pressure of *ca.* 10^{-3} mbar. The vacuum manifold pressure was monitored with a Pirani gauge attached to a digital gauge controller. The second manifold was attached to a source of purified argon gas and vented through a mercury bubbler, allowing a positive pressure slightly above atmospheric to be maintained. A dry and oxygen free environment was obtained in reaction vessels by connecting the vessel to the taps of the line and undertaking a sequence of "pump and purge" cycles. A cycle was completed by evacuating the vessel to *ca.* 10^{-2} mbar before backfilling with argon gas, in a process that was repeated at least three times. Glassware was thoroughly dried before use by storing in the oven overnight or by "flaming out" with a Bunsen burner during the first vacuum cycle. Ground glass joints were lubricated using high vacuum grease to produce an air-tight seal. Liquids were transferred between vessels *via* cannulae or syringe to minimise exposure to air.

A glovebox, maintained under a nitrogen atmosphere, was used for the manipulation and storage of air- and moisture-sensitive solids. The atmosphere was purified by passage through an activated copper catalyst and molecular sieves, to remove oxygen and moisture, respectively. Compounds entered the box *via* an antechamber, which was subjected to three 'pump and purge' cycles.

2.2 Spectroscopic Techniques

2.2.1 NMR Spectroscopy

NMR spectra were measured on a 400MHz Bruker Avance III HD nanobay NMR spectrometer equipped with a 9.4 T magnet, a 500MHz Bruker Avance III NMR spectrometer equipped with a 11.75 T magnet or a 500MHz Bruker Avance NMR spectrometer equipped with a 11.75 T magnet with a ^{13}C detect cryoprobe. Chemical shifts are quoted in ppm and coupling constants in Hz. ^{1}H and ^{13}C NMR spectra were internally referenced to residual protio-solvent and solvent signals respectively. ^{11}B and ^{19}F spectra were externally referenced against $BF_3{\bullet}OEt_2$ and $CFCl_3$ respectively. Air and moisture sensitive samples were prepared under inert atmosphere in 5 mm Wilmad 507-PP tubes fitted with J. Youngs valves. Dry deuterated solvents were obtained by stirring over CaH_2 before distillation under reduced pressure and degassing with three freeze-pump-thaw cycles.

2.2.2 Mass Spectrometry

ESI-MS measurements were carried out by Dr Victor Mikhailov, University of Oxford. Samples were prepared as dilute solutions in acetonitrile.

2.2.3 X-Ray Crystallography

Crystallographic structure determinations were carried out by Dr Evgeny Kolychev, Dr Jamie Hicks, Dr Maria Angeles-Fuentes, Andreas Heilmann or Caitilin McManus of the Aldridge Group. X-ray quality crystals were selected under Paratone-N oil, mounted on

Micromount loops and quench-cooled using an Oxford Cryosystems open-flow N_2 cooling device.[4] Single-crystal X-ray diffraction data were collected using an Oxford Diffraction Supernova dual-source diffractometer equipped with a 135 mm Atlas CCD area detector. Data was reduced using DENZO/SCALEPACK[5] or the CrysAlisPro package, including unit cell parameter refinement and inter-frame scaling (carried out using SCALE3 ABSPACK with CrysAlisPro).[6] Equivalent reflections were merged and diffraction patterns processed with the CrysAlisPro programme. The structures were solved using SIR92,[7] Superflip,[8] or SHELXT-2014, and refined with full-matrix least-squares within CRYSTALS[9,10] or SHELXL 2014 package.[11–14]

2.2.4 Elemental Analysis

Elemental analyses were either carried out by London Metropolitan University or Elemental Microanalysis, Devon, UK. Air and moisture sensitive samples were packed in a sealed glass capillary under argon or in a vial sealed with Parafilm M under nitrogen.

2.2.5 DFT Calculations

DFT calculations were undertaken by the author in conjunction with Dr Petra Vasko using the Gaussian 09 (Revision D.01) program.[15] Geometry optimisations were performed with the PBE1PBE hybrid exchange-correlation functional[16–19] using the Def2-TZVP basis set[20] and with Grimme's empirical dispersion correction (GD3BJ).[21,22] All calculations employed the Polarizable Continuum Model (PCM) for a simulated solvent model (acetonitrile).[23] To confirm the nature of the stationary points found (minima with no imaginary frequencies or a saddle point for transition states), full frequency calculations were performed for optimised geometries. Graphics were created with the program GaussView.[24] The xyz-coordinates for each of the optimised geometries are included in the Appendix.

2.3 Preparation of Starting Materials

2.3.1 Purification of Solvents and Reagents

Commercially available materials used in chemical reactions described in this thesis are listed in the Appendix, which also includes details of the commercial supplier, the purity of the material supplied and whether any further purification was required before use. Liquids for air- and/or moisture-sensitive chemistry were stored under an inert atmosphere in glass ampoules. Dry solvents were obtained by passing through a column of the appropriate drying agent using a commercially available MBRAUN Solvent Purification System (SPS) and were degassed by sparging with argon.

2.3.2 Starting Materials

The following compounds were prepared according to literature procedures: lithium dimesityl(1,8-naphthalenediyl)borate tetrakis(tetrahydrofuran),[25] chlorocatecholborane,[26] methoxycatecholborane,[27] 1,3,4-triphenyl-1,2,4-triazolium iodide,[28] 1-mesityl-1*H*-imidazole,[29] (1-mesityl-3-propargyl)imidazolium bromide,[30] (1-methyl-3-propargyl)imidazolium bromide,[31] and H_2N-$(PEG)_n$-N_3.[32] The [(NHC)H]Br salts used as precursors to saturated backbone carbenes were themselves synthesised according to the procedure described by Iglesias *et al*.[33] using bis-aryl-formadines prepared according to the procedure described by Kolychev *et al*.[34] Anion exchange to obtain [(NHC)H][BF_4] salts was conducted using the procedure described by Iglesias *et al.* unless otherwise stated.[33] Compounds which were prepared by modified literature procedures are described below.

1,8-Diiodonaphthalene

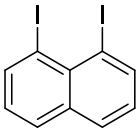

The method reported by Campbell *et al.* was employed with minor modifications.[35] 1,8-diaminonaphthalene (2.0 g, 12.7 mmol) was suspended in 6.9 M sulfuric acid (30 mL) in a 500 mL round bottom flask and cooled to -20 °C. Sodium nitrite (2.6 g, 38.1 mmol) was dissolved in 10 mL water and added dropwise to the reaction, which was maintained between -15 and -20 °C at all times. After addition was complete, a solution of potassium iodide (12.6 g, 76.2 mmol) in water (14 mL) was added dropwise to the reaction mixture with vigorous stirring over 2 h. The reaction mixture was then heated to 80 °C, with the excess iodine evolving as a gas. After cooling to room temperature, the reaction mixture was basified with sodium hydroxide and the black precipitate filtered. The product was extracted from the resulting solid with several portions of boiling diethyl ether (3 x 100 mL). The ether extracts were washed with 10 % hydrochloric acid (2 x 50 mL), a saturated solution of sodium sulfite (2 x 50 mL) and a dilute solution of sodium hydroxide (2 x 50 mL). The organic layer was dried with $MgSO_4$ and the solvent removed *in vacuo*. The resulting solid was recrystallised from hot hexane with the insoluble black precipitate removed by filtration. The product was isolated as dark brown crystals. Yield: 2.05 g, 43 %. The ^{1}H NMR data is consistent with literature reports.[35]

Fluorodimesitylborane

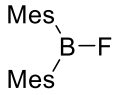

The synthesis of Mes_2BF was based upon that described by Chisholm *et al.*.[36] A flame dried two-neck flask, fitted with a reflux condenser, was charged with magnesium (1.0 g, 41.2 mmol). In a separate flask bromomesitylene (6 mL, 39.2 mmol) was diluted with dry THF

(40 mL). One third of the bromomesitylene solution was added to the magnesium turnings and the mixture activated by heating, before dropwise addition of the remaining arene reagent. The reaction was refluxed for 3 h before cooling completely to room temperature. A separate reflux apparatus was prepared containing BF_3 OEt_2 (2 mL, 15.7 mmol) and diethyl ether (20 mL). The cooled Grignard solution was added by filter cannula over the course of 1 h and the resulting reaction mixture was refluxed for 3 h. The reaction mixture was cooled to room temperature, before filtering and removal of the solvent *in vacuo*. The residue was purified by sublimation at 100 °C under dynamic vacuum (*ca*. 10^{-2} mbar) to yield a spectroscopically pure white solid. Yield: 2.43 g, 58 %. The ^{1}H, ^{11}B and ^{19}F NMR data are consistent with literature reports.[37]

Bromocatecholborane

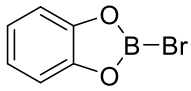

The preparation of bromocatecholborane was modified slightly from that described by Wang *et al*.[38] A flame dried Schlenk tube was charged with catechol (16 g, 0.145 mmol) and the solid suspended in dry dichloromethane (50 mL) and cooled to 0 °C. In a separate Schlenk tube, BBr_3 (14.5 mL, 0.153 mmol) was diluted with dichloromethane (25 mL) before slow, dropwise addition to the catechol suspension *via* cannula. During addition of the boron tribromide, the reaction flask was vented through a NaOH solution (~5 M). The reaction mixture was stirred at 0 °C for one hour, with continued venting, for 1 h following complete addition of the borane, before the vessel was closed off, warmed to room temperature and stirred for a further 2 h. Volatiles were removed *in vacuo* and the white residue sublimed (45 °C, 10^{-1} mbar) to yield a spectroscopically pure product. Yield: 25 g, 87 %. The ^{1}H NMR and ^{11}B NMR data are consistent with those reported in the literature.

General procedure for generation of free carbene

The method employed is based on that reported by Iglesias et al.[33] A flame dried Schlenk tube was charged with the [(NHC)H][BF_4] salt (10 mmol) and the salt suspended in THF (40 mL) before addition of a solution of K[N($SiMe_3$)$_2$] (11 mmol) in THF (20 mL) *via* cannula. The reaction was stirred for 30 min before the suspension was filtered and the volatiles removed in vacuo from the filtrate. The free carbene was then extracted from the residue using diethyl ether (3 x 15 mL). Crystalline product was subsequently obtained from the diethyl ether solution by concentrating under reduced pressure before and storage at -25 °C. The ^{1}H NMR data in each case was consistent with literature reports.[33]

2.4 References

[1] R. E. Dodd, P. L. Robinson, *Experimental Inorganic Chemistry : A Guide To Laboratory Practice*, Elsevier, Amsterdam ; London, **1963**.

[2] R. J. Errington, *Advanced Practical Inorganic and Metalorganic Chemistry*, Blackie Academic & Professional, London, **1997**.

[3] D. F. Shriver, M. A. Drezdzon, *The Manipulation of Air-Sensitive Compounds*, Wiley, New York, **1986**.

[4] B. J. Cosier, A. M. Glazer, *J. Appl. Crystallogr.* **1986**, *19*, 105–107.

[5] Z. Otwinowski, W. Minor, *Methods Enzymol.* **1997**, *276*, 307–326.

[6] CrysAlisPro, *V.1.171.35.8 Agilent Technologies*, **2011**.

[7] A. Altomare, G. Cascarano, C. Giacovazzo, A. Guagliardi, *J. Appl. Crystallogr.* **1993**, *26*, 343–350.

[8] L. Palatinus, G. Chapuis, *J. Appl. Crystallogr.* **2007**, *40*, 786–790.

[9] R. I. Cooper, A. L. Thompson, D. J. Watkin, *J. Appl. Crystallogr.* **2010**, *43*, 1100–1107.

[10] A. L. Thompson, D. J. Watkin, *J. Appl. Crystallogr.* **2011**, *44*, 1017–1022.

[11] G. M. Sheldrick, *Acta Crystallogr. Sect. A Found. Crystallogr.* **2008**, *64*, 112–122.

[12] G. M. Sheldrick, *SHELX-2014*, **2014**.

[13] O. V. Dolomanov, L. J. Bourhis, R. J. Gildea, J. A. K. Howard, H. Puschmann, *J. Appl. Crystallogr.* **2009**, *42*, 339–341.

[14] L. J. Barbour, *J. Supramol. Chem.* **2001**, *1*, 189–191.

[15] M. J. Frisch, G. W. Trucks, H. B. Schlegel, G. E. Scuseria, M. A. Robb, J. R. Cheeseman, G. Scalmani, V. Barone, B. Mennucci, G. A. Petersson, H. Nakatsuji, M. Caricato, X. Li, H. P. Hratchian, A. F. Izmaylov, J. Bloino, G. Zheng, J. L. Sonnenberg, M. Hada, M. Ehara, K. Toyota, R. Fukuda, J. Hasegawa, M. Ishida, T. Nakajima, Y. Honda, O. Kitao, H. Nakai, T. Vreven, J. A. Montgomery Jr., J. E. Peralta, F. Ogliaro, M. Bearpark, J. J. Heyd, E. Brothers, K. N. Kudin, V. N. Staroverov, R. Kobayashi, J. Normand, K. Raghavachari, A. Rendell, J. C. Burant, S. S. Iyengar, J. Tomasi, M. Cossi, N. Rega, J. M. Millam, M. Klene, J. E. Knox, J. B. Cross, V. Bakken, C. Adamo, J. Jaramillo, R. Gomperts, R. E. Stratmann, O. Yazyev,

A. J. Austin, R. Cammi, C. Pomelli, J. W. Ochterski, R. L. Martin, K. Morokuma, V. G. Zakrzewski, G. A. Voth, P. Salvador, J. J. Dannenberg, S. Dapprich, A. D. Daniels, Ö. Farkas, J. B. Foresman, J. V. Ortiz, J. Cioslowski, D. J. Fox, *Gaussian 09, Revision D.01*, Gaussian, Inc., Wallingford, CT, **2009**.

[16] J. P. Perdew, K. Burke, M. Ernzerhof, *Phys. Rev. Lett.* **1996**, *77*, 3865.

[17] J. P. Perdew, K. Burke, M. Ernzerhof, *Phys. Rev. Lett.* **1997**, *78*, 1396.

[18] J. P. Perdew, M. Ernzerhof, K. Burke, *J. Chem. Phys.* **1996**, *105*, 9982–9985.

[19] C. Adamo, V. Barone, *J. Chem. Phys.* **1999**, *110*, 6158.

[20] F. Weigend, R. Ahlrichs, *Phys. Chem. Chem. Phys.* **2005**, *7*, 3297–3305.

[21] S. Grimme, J. Antony, S. Ehrlich, H. Krieg, *J. Chem. Phys.* **2010**, *132*, 154104.

[22] S. Grimme, S. Ehrlich, L. Goerigk, *J. Comput. Chem.* **2011**, *32*, 1456–1465.

[23] J. Tomasi, B. Mennucci, R. Cammi, *Chem. Rev.* **2005**, *105*, 2999–3093.

[24] R. D. Dennington, T. A. Keith, J. M. Millam, *GaussView 6.0.16*, Semichem, Inc., **2016**.

[25] J. D. Hoefelmeyer, F. P. Gabbaï, *Organometallics* **2002**, *21*, 982–985.

[26] W. B. Reid, J. J. Spillane, S. B. Krause, D. A. Watson, *J. Am. Chem. Soc.* **2016**, *138*, 5539–5542.

[27] G. Povie, G. Villa, L. Ford, D. Pozzi, C. H. Schiesser, P. Renaud, *Chem. Commun.* **2010**, *46*, 803–805.

[28] T. Strassner, Y. Unger, D. Meyer, O. Molt, I. Münster, G. Wagenblast, *Inorg. Chem. Commun.* **2013**, *30*, 39–41.

[29] J. Liu, J. Chen, J. Zhao, Y. Zhao, L. Li, H. Zhang, *Synthesis (Stuttg).* **2003**, *2003*, 2661–2666.

[30] S. Warsink, R. M. Drost, M. Lutz, A. L. Spek, C. J. Elsevier, *Organometallics* **2010**, *29*, 3109–3116.

[31] S. Ravula, N. E. Larm, Y. Liu, J. L. Atwood, S. N. Baker, G. A. Baker, *New J. Chem.* **2018**, *42*, 1979–1986.

[32] L. N. Goswami, Z. H. Houston, S. J. Sarma, S. S. Jalisatgi, M. F. Hawthorne, *Org. Biomol. Chem.* **2013**, *11*, 1116–1126.

[33] M. Iglesias, D. J. Beetstra, J. C. Knight, L. L. Ooi, A. Stasch, S. Coles, L. Male, M. B. Hursthouse, K. J. Cavell, A. Dervisi, I. A. Fallis, *Organometallics* **2008**, *27*, 3279–3289.

[34] E. L. Kolychev, I. A. Portnyagin, V. V. Shuntikov, V. N. Khrustalev, M. S. Nechaev, *J. Organomet. Chem.* **2009**, *694*, 2454–2462.

[35] H. O. House, D. G. Koepsell, W. J. Campbell, *J. Org. Chem.* **1972**, *37*, 1003–1011.

[36] M. H. Chisholm, K. Folting, S. T. Haubrich, J. D. Martin, *Inorganica Chim. Acta* **1993**, *213*, 17–24.

[37] É. Dorkó, E. Varga, T. Gáti, T. Holczbauer, I. Pápai, H. Mehdi, T. Soós, *Synlett* **2014**, *25*, 1525–1528.

[38] Y. F. Wang, C. X. Zhang, H. Wu, A. Zhang, J. C. Wang, S. F. Zhang, J. L. Pu, *Soft Matter* **2015**, *11*, 712–718.

Chapter 3

Bidentate 1,8-Diboryl-Naphthalenes for Fluoride Chelation

3.1 Introduction

In 1966, seminal work by Shriver and Biallas described the one to one binding of a methoxide anion by the diborane $F_2BCH_2CH_2BF_2$.[1][2] This complex was notable as the first example of anion chelation by a multidentate Lewis acid, with chelation previously only being demonstrated in cation coordination chemistry. The enhanced thermodynamic stability that may be attained upon chelation of an anion has been demonstrated by examples such as bis(dimethylboryl)naphthalene **3.i** which out-competes its monodentate equivalent **3.ii** to complex fluoride and hydride (Scheme 3.1).[3,4] This thermodynamic advantage and the ability to tune the strength and selectivity of chelation through the electronic, spatial and steric properties of multidentate Lewis acids has led to their application as anion sensors[5] and anion transporters[6,7] in addition to roles in catalysis.[8–11] A wide range of Lewis acidic elements have therefore been incorporated into multidentate frameworks, however, for the purposes of this thesis this introduction will focus solely on examples featuring Lewis acidic boron centres.[11–21]

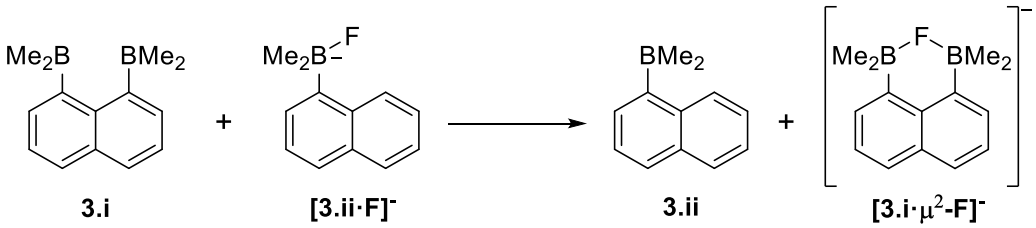

Scheme 3.1 – Competitive fluoride binding reaction of 1,8-bis(dimethylboryl)-naphthalene, **3.i** and 1-(dimethylboryl)-naphthalene, **3.ii**.

Anion chelating bisboranes have commonly employed rigid backbone frameworks. In addition to enhancing the binding affinity of the molecule *via* preorganisation, the defined separation of the boron centres can be used to control selectivity for different anions. The distances between the boron centres of *ortho*-phenylene diboranes (3.06 – 3.35 Å) and *peri*-naphthalene diboranes (3.00 – 3.39 Å), such as those shown in Figure 3.1, are ideal for chelating small anions.[22–25] This is exemplified by the fluoride bound complexes of receptors **3.iii** and **3.iv**, in which the anions are positioned relatively centrally between the boron groups, and exhibit B–F bonds that are longer than those typically found in $[Ar_3BF]^-$ complexes (*ca.* 1.47 Å): 1.600(5) Å and 1.606(5) Å for **[3.iv·μ$_2$-F]$^-$** and a range of 1.59 – 1.62 Å for **[3.iii·μ$_2$-F]$^-$**.[26,27] The marginally wider boron-boron separation of 3.684 Å observed in association with the five membered ring of ferrocene derivative **3.v** however, is too large to be bridged by fluoride, with coordination instead occurring at a single boron centre (1.471(5) Å) and leaving fluoride well separated from the second boron atom.[28] Similarly, for polycyclic backbones such as biphenylene or anthracene, **3.vi**, where the boron separations are in excess of 4.5 Å, no B–F–B chelation can occur.[29,30] These large binding pockets have instead been shown to be suitable for μ(1,2) chelation of linear anions such as cyanide and neutral dibasic species such as hydrazine.[31–33]

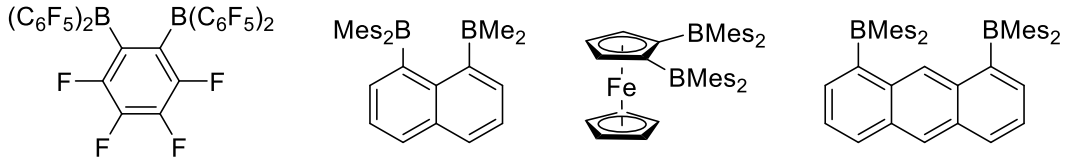

3.138(2) Å **3.iii** | 3.204 Å **3.iv** | 3.684 Å **3.v** | 5.576(4) Å **3.vi**

Figure 3.1 – Examples of diboryl substituted aromatics capable of binding fluoride with their respective boron-boron separation distances.[22,28,29,34]

Piers and co-workers have extensively explored anion chelates of *ortho*-diboryl-perfluorobenzene as weakly coordinating anions in catalysis, demonstrating that these receptors bind fluoride, hydroxide, methoxide, azide and chloride with varying

affinities.[24,35–38] The electron-deficient boron centres of these highly fluorinated structures are strongly Lewis acidic, so much so that the fluoride complex of **3.iii** can be synthesised by abstracting fluoride from a $[BF_4]^-$ anion.[35] Although the diboronic acid **3.vii** was isolated as a useful intermediate in the synthetic pathway to the -BAr_2 derivatives, it demonstrates interesting fluoride binding properties in its own right. Over the course of half an hour, **3.vii** undergoes full fluoride substitution in aqueous conditions to the air- and moisture-stable fluoroborates **3.viii** and **3.ix**.[24] Structural characterisation of chelate complex **3.ix** reveals the bridging B–F bonds are extended (1.487(4) Å) compared to those of the terminal B–F bonds (1.405(4) Å and 1.427(4) Å). The chelate structure **3.ix** also exists in equilibrium with **3.viii**, with the position of the equilibrium between the two species noted to be dependent upon the amount of water present. Although the direction of this equilibrium shift was not explicitly stated by Chase *et al.*, it may be surmised that the high hydration enthalpy of fluoride causes fluoride release from **3.viii**, favouring chelate **3.ix** as the water content increases. Boron trifluoride was noted to abstract fluoride from both **3.viii** and **3.ix** to produce a neutral bis -BF_2 species that was water sensitive.

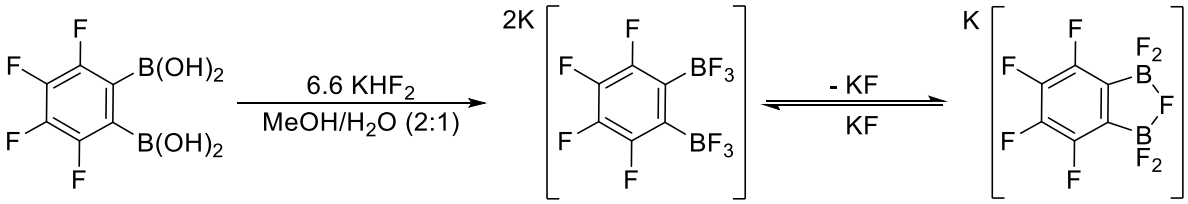

3.vii **3.viii** **3.ix**

Scheme 3.2 – Fluoride substitution of *ortho*-diboronic acid perfluorophenylene

In 1985, Katz first demonstrated the suitability of rigid 1,8-diboryl-naphthalenes for chelating small hard anions with 1,8-bis(dimethylboryl)naphthalene, **3.i**.[3,4] Also known as "hydride sponge", **3.i** is the Lewis acidic inverse of the basic 1,8-bis(dimethylamino)-naphthalene "proton sponge", and is a strong chelator of hydride, fluoride and hydroxide.[3] In a similar fashion to the nitrogen lone pairs in the proton sponge, sterics force the vacant boron *p*-orbitals out of conjugation with the naphthalene plane and towards one another. This

orbital preorganisation, which is advantageous for chelation, was further exploited by Hoefelmeyer and Gabbaï in the reduction of 1,8-bis(diphenylboryl)-naphthalene to give a B–B one electron sigma bond.[22]

Further work by the Gabbaï group has led to the synthesis of a library of unsymmetrical 1,8-diboryl-naphthalenes and evaluation of their chelation properties for fluoride sensing.[26,39–42] The receptors in Figure 3.2 exhibit fluoride binding constants three to four orders of magnitude greater than monodentate triarylboranes such as trimesitylborane. This dominance is exemplified by the fact that one equivalent of **3.xi** outcompeted twelve equivalents of trimesitylborane to form complex **[3.xi·μ$_2$-F]$^-$** in quantitative amounts.[39] Moreover, the cationic derivative **3.xii** gives rise to a fluoride binding affinity that is estimated to be four orders of magnitude greater than that observed for the neutral equivalent **3.xi**, an observation that was attributed to the additional Coulombic attraction in the binding.[41] The greater thermodynamic stability of these chelate complexes, compared to their monodentate equivalents, indicates that although the chelated B–F bonds are much longer (1.54 - 1.82 Å), and likely individually weaker than terminal B–F bonds, overall the chelating interaction is stronger. The thermodynamic stability of complexes **[3.xi·μ$_2$-F]$^-$** and **3.xii·μ$_2$-F** is further highlighted by their retention of fluoride in the presence of water.[39,41]

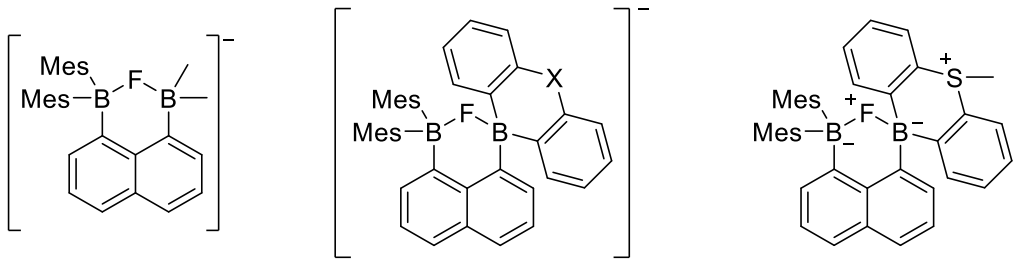

[3.iv·μ_2-F]$^-$

K = 5.0 (± 0.2) x 10^5 M^{-1}
$CHCl_3$

X = O **[3.x·μ_2-F]$^-$**
X = S **[3.xi·μ_2-F]$^-$**

*K(**3.xi**) > 5 x 10^9 M^{-1}*
THF

3.xii·μ_2-F

*K(**3.xii**) >> K(**3.xi**)*
$CHCl_3$

Figure 3.2 – Fluoride chelation by examples of unsymmetrical 1,8-diboryl-naphthalenes with their respective binding constants.

Inherent steric strain in these ligand frameworks also has a two-fold impact on the binding properties of these species. The ^{1}H NMR spectra of the free receptors typically show broad signals for the mesityl groups, indicative of hindered rotation and therefore a high degree of steric crowding around the binding site. This bulk around the binding pocket inhibits large anions from coordinating, contributing to the high fluoride selectivity of these systems.[39,40] Steric strain is also apparent in the structural data of these receptors, with the boryl groups typically distorting away from one another and out of the plane of the naphthalene backbone. However, upon fluoride coordination the borons are pyramidalised and there is a noticeable reduction in the steric strain of the ligand framework. The ^{1}H NMR spectra of the fluoride adducts typically imply that the mesityl groups attain free rotation, whilst the solid state structures show relaxation of the boron-boron separation. Gabbaï *et al.* therefore suggested that the relief of steric strain upon complexation has a stabilising effect on the system, greatly favouring binding.[40]

3.2 Aims

The work reported in this chapter will investigate the synthesis and fluoride uptake of 1,8-diboryl-naphthalene systems featuring at least one boronic acid or ester functional group, to explore their potential as prosthetic group precursors for ^{18}F-PET. It is anticipated that the

enhanced thermodynamic stability which may be attained by the chelation of fluoride in such a scaffold will disfavour fluoride dissociation in aqueous solution and thereby address our first project objective of robustness. Furthermore, by utilising substituents with B–O bonds, the compound may be expected to demonstrate a degree of water tolerance whilst the labile nature of the bonds could also enable fluoride uptake akin to that observed with the related phenylene diboronic acid **3.iv**.[24] Incorporating two of these functional groups, moreover, offers the attractive possibility of a penta-fluorinated system with potential for an uncommonly high molar activity (Scheme 3.3). With this in mind, synthesis of 1,8-naphthalene diboronic acid was the initial starting point for this research.

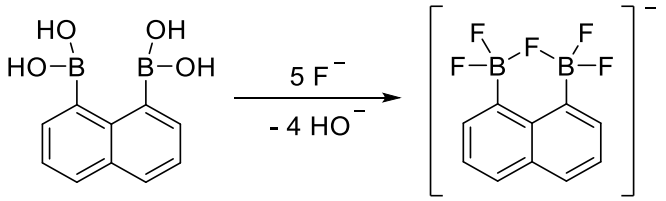

Scheme 3.3 – Potential fluoride substitution reaction of 1,8-naphthalene diboronic acid

3.3 1,8-Naphthalene Diboronic Acid

3.3.1 Synthesis and Characterisation

The synthesis of 1,8-naphthalene diboronic acid was based on previous literature.[43,44] Thus, 1,8-diiodonaphthalene was subject to halogen-lithium exchange with *n*-butyllithium at low temperatures before electrophilic quenching with trimethyl borate. After stirring overnight, the reaction was hydrolysed with dilute aqueous acid to yield a spectroscopically pure product. The ^{1}H and ^{11}B NMR spectra show that a single symmetrical product is present in solution with the ^{11}B NMR signal at 30 ppm indicating the formation of three co-ordinate boron centres.

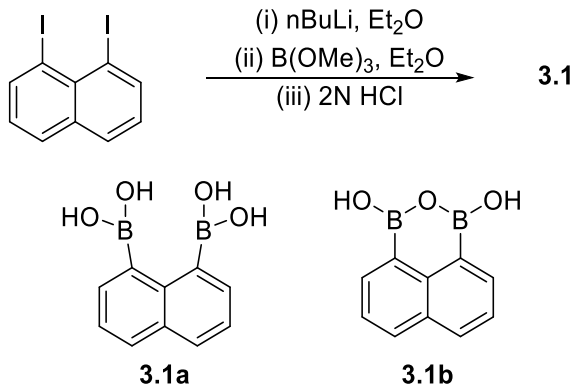

Scheme 3.4 – Synthesis of **3.1** from the 1,8-diiodonaphthalene with the two potential structures of **3.1**: the fully hydrated 1,8-naphthalene diboronic acid **3.1a** and the partially hydrated 1,8-naphthalene diboronic acid anhydride, **3.1b**.

Previous literature presented contrasting suggestions as to the structure of the product, featuring either the hydrated acid form (**3.1a**)[43,45] or the partially hydrated anhydride form (**3.1b**).[46,47] These two species would be virtually indistinguishable *via* NMR spectroscopy, due to the broad nature of OH signals in ^{1}H NMR spectra and the intrinsically broad resonances for three coordinate borons in ^{11}B NMR spectra. Whilst no characterisation data is given in the reports featuring the hydrated acid forms, IR characterisation of the anhydride by Letsinger *et al.* notes an absorption band at 676 cm^{-1} which is attributed to the B–O–B anhydride bridge.[46] Additionally, Katz favoured the anhydride form based upon elemental analysis.[47] Recrystallisation of **3.1** from boiling water yielded pale yellow needles suitable for X-ray diffraction, allowing structural characterisation of the product for the first time. Diffraction data revealed that compound **3.1** in the solid state exists as the partial anhydride, **3.1b** (Figure 3.3) in accord with the characterisation of Katz and Letsinger *et al*. A subsequently reported solid state structure of **3.1** is also noted to have taken the anhydride form.[48] The prevalent self-condensation to the anhydride structure is perhaps unsurprising given the well-established self-assembly properties of boronic acids and the preorganisation provided by the naphthalene backbone.[49] The anhydride exhibits a planar geometry with the six membered heterocyclic ring taking ideal bond angles of *ca.* 120 °. The bridging oxygen is

symmetrically bound between the two borons with B–O bond lengths (O1–B2 1.390(2) Å, O1–B7 1.398(2) Å) slightly elongated compared to the terminal bonds (B2–O3 1.335(2) Å, B7–O8 1.338(2) Å).

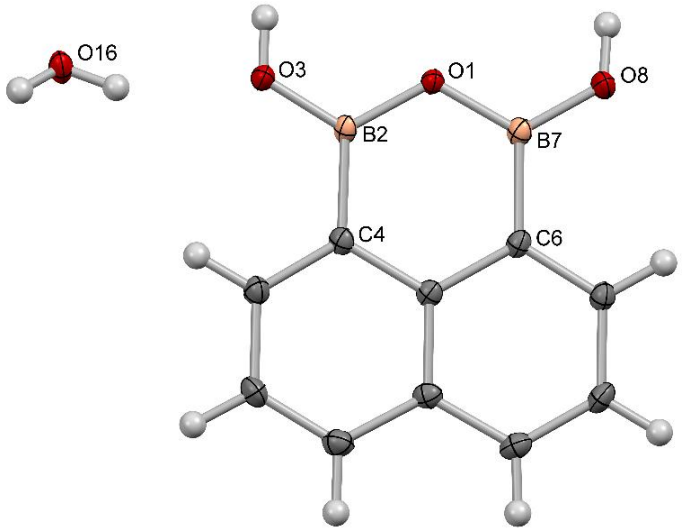

Figure 3.3 – Structure of 1,8-naphthalene diboronic acid anhydride, **3.1b**; thermal ellipsoids set at 40 % probability level. Selected bond lengths (Å) and angles (°): B2–C4 1.559(2), B7–C6 1.568(2), B2–B7 2.434(3), B2–O1–B7 121.7(1), O1–B2–O3 119.7(1), O1–B2–C4 120.3(1), O3–B2–C4 119.9(1), B2–C4–C5 119.0(1), B7–C6–C5 119.4(1), C4–C5–C6 120.20(14), B7–C6–C5–C4 -0.5(2), O1–B7–C6–C5 0.6(2).

3.3.2 Reactivity

Previous reactivity studies with the 1,8-naphthalene diboronic acid anhydride species by Katz in 1985, found the B–O–B linkage to be exceptionally robust.[47] Reactions with methanol, PCl_5 and Grignard reagents simply substituted both terminal hydroxide groups with methoxide, chloride and methanide respectively, whilst leaving the anhydride bridge intact. Alternative attempts to displace the central oxygen by thiolation or amination were likewise unsuccessful.

Despite concerns that the highly robust B–O–B linkage was likely to interfere with fluoride chelation, fluoride binding studies were undertaken with **3.1**. Combining **3.1** with an excess of potassium fluoride and one equivalent of 18-crown-6 in acetonitrile leads to a loss in symmetry in the ^{1}H NMR spectrum and to the emergence of two distinct signals in the ^{11}B

NMR spectrum at 28 ppm and 4 ppm, consistent with three-coordinate and four-coordinate boron centres respectively. The upfield shifted ^{11}B NMR signal is resolved as triplet ($^{1}J_{BF}$ = 43.6 Hz) with the ^{19}F NMR spectrum featuring a corresponding 1:1:1:1 quartet at -113.5 ppm, thus indicating that a -BF_2 moiety is present. Crystallographic study of crystals grown from acetonitrile confirmed this to be the case, with the structure **[K(18-crown-6)][3.2]** illustrated in Figure 3.4.

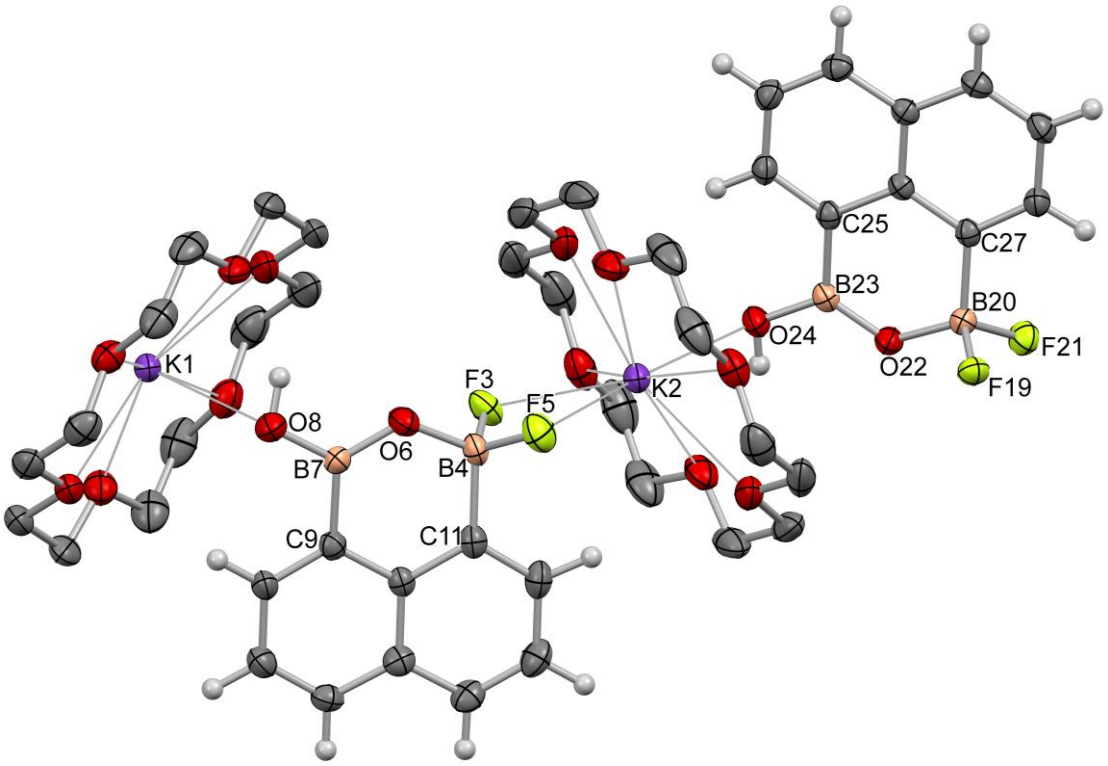

Figure 3.4 – Molecular structure of **[K(18-crown-6)][3.2]**. Solvent and most hydrogens have been omitted for clarity. Thermal ellipsoids are set to 40 %. Selected bond lengths (Å) and angles (°): B4–B7 2.488(4), B20–B28 2.478(4), B4–F3 1.448(3), B4–F5 1.416(3), B20–F19 1.443(3), B20–F21 1.4261(3), B7–O8 1.326(3), B7–O6 1.345(3), B4–O6 1.458(3), B28–O24 1.369(3), B28–O22 1.342(3), B20–O22 1.464(3), B4–C11 1.638(4), B7–C9 1.576(4), K1–O8 2.849(2), K2–F3 2.691(2), K2–F5 2.936(2), B7–O6–B4 125.1(2), B20–O22–B28 124.1(2).

As anticipated, the B–O–B linkage proved robust to cleavage in the presence of fluoride, with substitution instead occurring at the more labile B–O bond of the terminal position. Unlike the symmetrical substitution at both boron centres observed by Katz, fluoride uptake occurs at a single boron centre to form the **3.2** anion.[47] The difluorination

observed at B4 may be attributed to the high Lewis acidity of the fluoroborane group after initial substitution, leading to coordination of a second fluoride ion, in preference to nucleophilic attack at the B7 boronic acid group. Further substitution is then disfavoured by the electrostatic repulsion between the negatively charged **3.2** anion with further fluoride ions. The disparate coordination of the difluoroborate and boronic acid groups is also reflected in the position of the bridging oxygen which shows a marked shift towards the three coordinate boron centre: B4–O6 1.458(3), B7–O6 1.345(3).

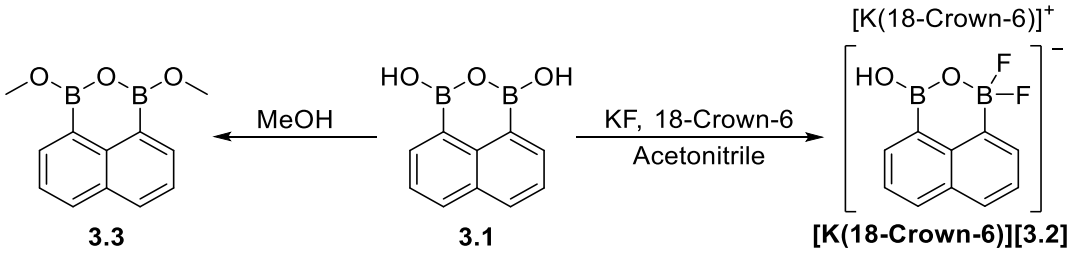

Scheme 3.5 – Fluoride and methanol substitution of **3.1**.

Having established fluoride is incapable of displacing oxygen from the binding pocket, attention was directed to our own attempts at breaking the anhydride bridge. Refluxing **3.1** in neutral and acidic water yielded no change to the characterisation data, whilst attempts to trap out the hydrated form as an ester by heating **3.1** to reflux with methanol only succeeded in substituting the terminal B–O bonds (**3.3**, Figure 3.5). Similarly, refluxing **3.1** with chelating diols such as pinacol and catechol, and utilising molecular sieves or a Dean-Stark apparatus to remove water also failed to conclusively synthesise the doubly substituted form; a multitude of unidentified species are observed in the ^{11}B and ^{1}H NMR spectra. It was speculated that rather than breaking the anhydride link, the diols bridge between naphthalene units, leading to dimerization or macrocycles similar to those synthesised by Tanaka *et al.* with 1,8-naphthalene diboronic acid and aliphatic diols.[50]

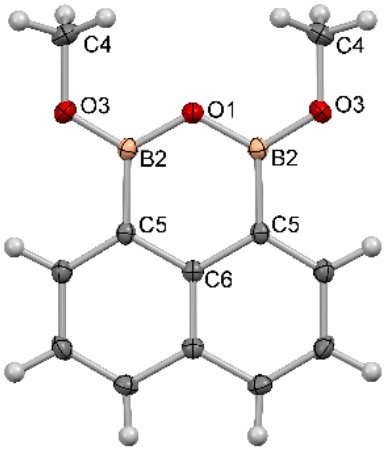

Figure 3.5 – Structure **3.3** is illustrated with thermal ellipsoids set to 40%. Selected bond lengths (Å) and angles (°) of structure 3.3: O1–B2 1.3801(14), B2–O3 1.3523(16), O3–C4 1.4325(16), B2–C5 1.5611(19), B2–B2 2.413(2), B2–O1–B2 121.93(15), O1–B2–C5 120.33(10), C5–C6–C5 120.49(15).

Given the apparent futility of endeavours to break the robust B–O–B bridge, efforts were made to avoid the linkage altogether by synthesising 1,8-naphthalene diboronic esters directly from the di-lithiated naphthalene. Attempts were made to isolate 1,8-bis(dimethoxyboryl)-naphthalene using trimethyl borate and di-lithiated naphthalene, however in our hands the compound could not be cleanly isolated. Moreover, addition of boranes such as chlorocatecholborane or boron trifluoride etherate to low temperature solutions of the di-lithiated naphthalene species in diethyl ether also did not progress cleanly to yield identifiable products.

3.4 1-(Dimesitylboryl)-8-(catecholatoboryl) naphthalene

3.4.1 Synthesis and Characterisation

Consequently, our attention instead turned towards creating an unsymmetrical 1,8-diboryl-naphthalene unit containing a single boronic ester group. Previous work by Hoefelmeyer and Gabbaï developed a convenient intermediate suited for this purpose: an anionic boron-bridged naphthalene species (Scheme 3.6) that readily reacts with electrophilic reagents in a ring opening reaction to yield 1,8-disubstituted naphthalene products.[42]

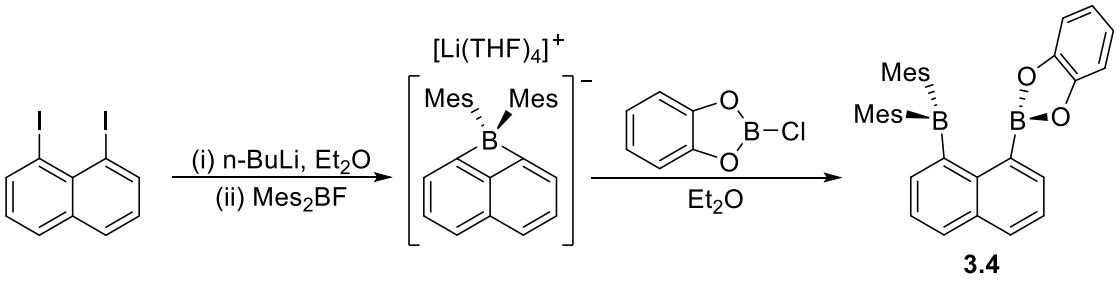

Scheme 3.6 – Reaction pathway to **3.4** *via* the dimesityl-1,8-naphthalenediylborate anion

Accordingly, 1-(dimesitylboryl)-8-(catecholatoboryl) naphthalene, **3.4** (Scheme 3.6) was synthesised by combining ether solutions of lithium dimesityl-1,8-naphthalenediylborate and chlorocatecholborane at -10 °C before stirring at room temperature overnight. The product was purified by recrystallisation from hot acetonitrile to give **3.4** in 73 % yield. The presence of an unsymmetrical structure was confirmed by NMR spectroscopy with the ^{11}B NMR spectrum showing two broad resonances at 77 ppm and 33 ppm corresponding to the -$BMes_2$ and -BCat functions respectively. Meanwhile, the ^{1}H NMR spectrum features a pattern of four broad C–H signals in the aromatic region and six broad methyl signals in the aliphatic region, indicating that the mesityl groups are inequivalent and experience significantly hindered rotation consistent with related systems such as **3.x** – **3.xii**.[39–42] Crystallographic studies of **3.4** (Figure 3.6) confirm that no anhydride bridge forms under these conditions and reveals significant steric strain in the structure, with the boron groups distorted away from one another, beyond the ideal 120 ° angle (B1–C1–C2 126.91(11) °, B2–C3–C2 126.53(12) °, C1–C2–C3 123.60(12) °), and out of the plane of the naphthalene ring (B1–C1–C2–C3 22.6(2) °, B2–C3–C2–C1 17.3(2) °). The resulting distance between the boron centres of 3.189(2) Å is shorter than for previously reported 1-(dimesitylboryl)-8-boryl-naphthalene systems in which the boron-boron separation invariably exceeds 3.2 Å, a testament to the limited steric bulk of the planar catecholborane group.[5]

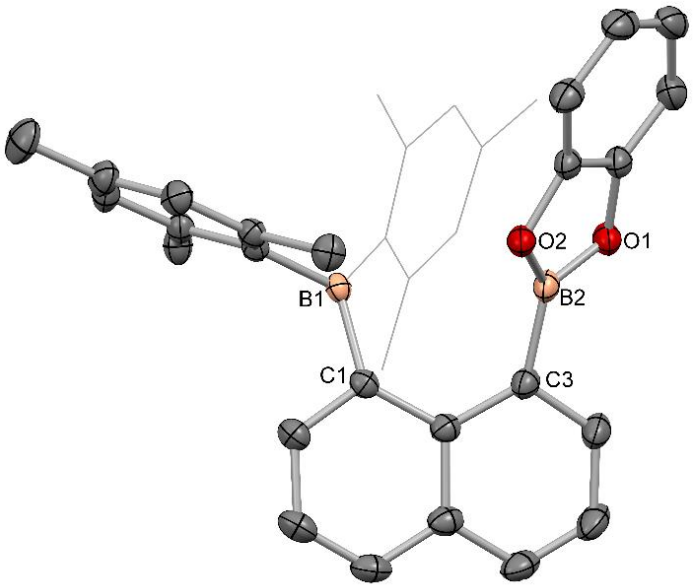

Figure 3.6 – Molecular structure of 1-(dimesitylboryl)-8-(catecholatoboryl) naphthalene, **3.4.** For clarity, a mesityl group is shown in wireframe and the hydrogens and solvent have been omitted. Thermal ellipsoids are set to 40 %. Selected additional bond lengths (Å) and angles (°): B1–C1 1.573(2), B2–C3 1.551(2), B2–O1 1.3881(19), B2–O2 1.3919(17), B2–C20 2.890(2), B1–B2 3.189(2), O1–B2–O2 111.2(1), O1–B2–C3 122.3(1), O2–B2–C3 125.5(1).

The structure of **3.4** was also optimised computationally. Calculations were carried out at the PBE1PBE/Def2-TZVP level of theory with acetonitrile solvation included using the SCRF Polarizable Continuum Model. Dispersion forces were also accounted for using the GD3BJ empirical dispersion model. The geometry of the optimised structure is in good agreement with the experimental data, with a few minor differences: the boron-boron separation shortens to 3.100 Å and the B–C–C–C torsion angles (16.760 ° and 14.305 °) are several degrees smaller than those observed experimentally.

The form of the LUMO (and energetically proximal anti-bonding orbitals) indicates that the -$BMes_2$ group is the more electrophilic of the two Lewis acidic centres. As illustrated in Figure 3.7, the vacant *p*-orbital of the dimesityl boron fragment contributes to the LUMO and the LUMO+1 whilst the vacant *p*-orbital of the catecholborane contributes to the LUMO+1 and the LUMO+3. The catecholborane group is stabilised by π-donation from the catechol-oxygens into the vacant *p*-orbital of boron, reducing the electrophilicity of the

boron centre compared to the diarylborane. Indeed, the higher electron density at the catecholborane is also reflected in the ^{11}B NMR spectrum in which the catecholborane signal is well up-field of the -$BMes_2$ group.

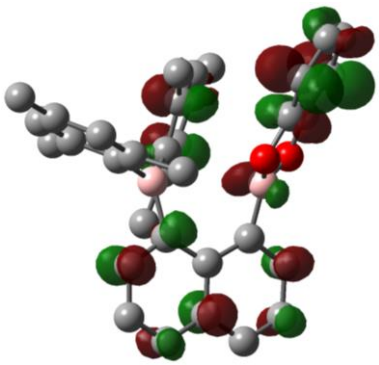

LUMO+3 (-54.3 kJ mol^{-1})

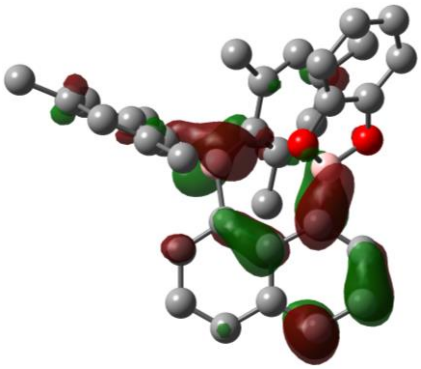

LUMO+1 (-120.6 kJ mol^{-1})

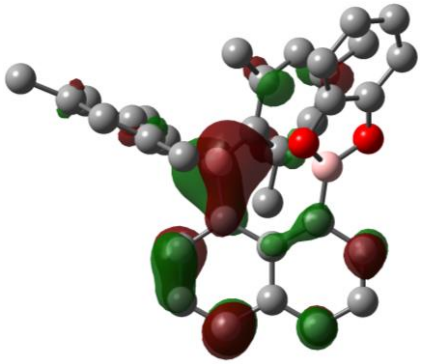

LUMO (-199.9 kJ mol^{-1})

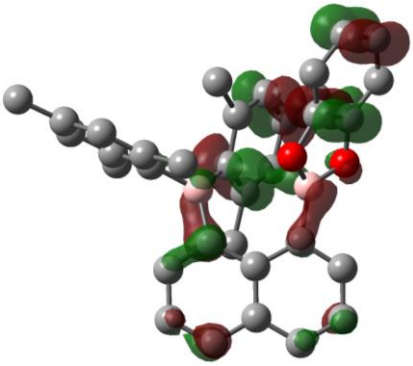

HOMO-5 (-698.4 kJ mol^{-1})

Figure 3.7 – Selection of molecular orbitals of **3.4** set at the iso-surface value of 0.04.

Whilst the naphthalene-based HOMO of **3.4** is unremarkable, the HOMO-5 features a notable interaction between one of the mesityl-*ipso*-carbons and the boron centre of the catecholborane unit. This weak π-interaction with the Lewis acidic boron centre has previously been noted by Gabbaï and co-workers in experimental structures such as **3.x**, which feature a shortened separation between the respective boron and carbon atoms, in addition to a slight pyramidalization of the trigonal planar geometry at boron.[23,40] Indeed, inspection of the experimental (B2–C20 2.890(2) Å and Σ = 359.0 °) and optimised (2.824 Å and 358.1 °) structures of **3.4** also shows these structural traits.

3.4.2 Fluoride Binding

Fluoride binding by **3.4** was assessed with a selection of anhydrous fluoride sources. Unexpectedly, two distinctly different systems were crystallographically characterised as the fluoride-bound products of **3.4** under different conditions (Scheme 3.7). The **[TAS][3.5]** salt in Figure 3.8 features the μ_2-fluoride bridged structure for the anion that was initially targeted. This chelated compound was synthesised by stirring ligand **3.4** with tris(dimethylamino)sulfonium difluorotrimethylsilicate (TASF) overnight in THF at room temperature before recrystallization from a concentrated acetonitrile solution at -25 °C. By contrast, **[K(18-crown-6)][3.6]** in Figure 3.9 features an isomeric anion which has undergone significant rearrangement to place a catechol-derived oxygen in the binding pocket and the fluoride ion in a terminal position. **[K(18-crown-6)][3.6]** was obtained by stirring **3.4** with an excess of potassium fluoride and one equivalent of 18-crown-6 at room temperature overnight in THF, before removal of the solvent and extraction into acetonitrile. Subsequent slow evaporation of the acetonitrile solution at room temperature over several weeks produced X-ray quality crystals that were used for characterisation. Key structural data for both fluoride bound products are listed in Table 3.1 with the respective data for the free receptor **3.4** also included for comparison.

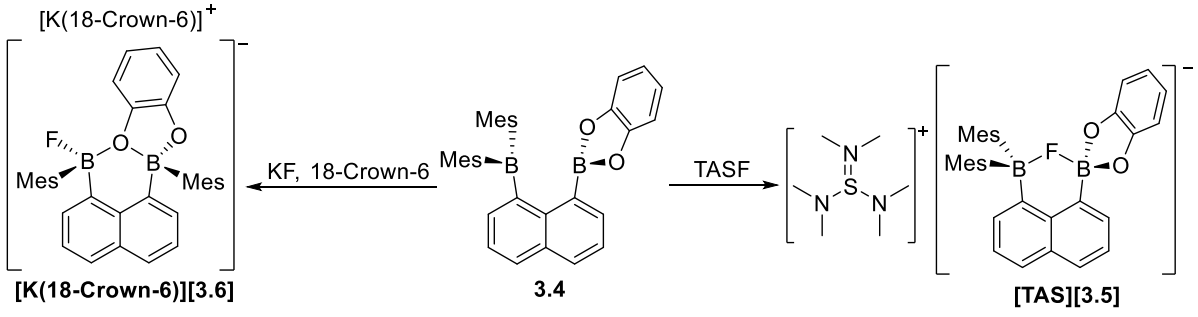

Scheme 3.7 – Fluoride binding reactions of ligand **3.4** used to synthesise fluoride chelated structure **[TAS][3.5]** and the fluoride bound rearranged structure **[K(18-crown-6)][3.6]**.

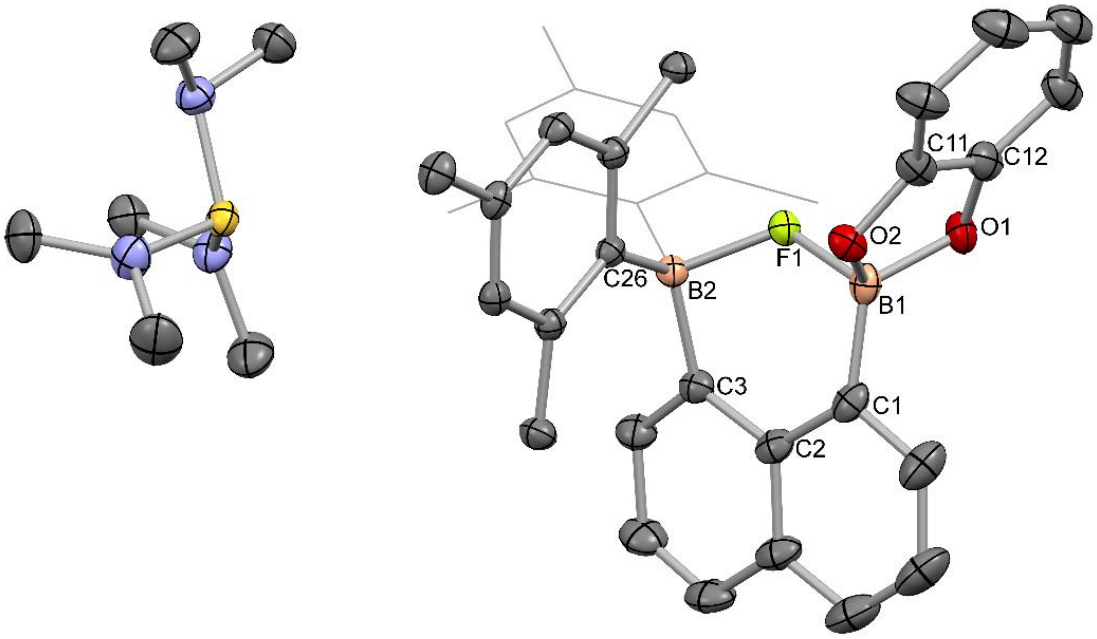

Figure 3.8 – Molecular structure of **[TAS][3.5]** The mesityl group is shown in wireframe format and hydrogens are omitted for clarity. Thermal ellipsoids are set at the 40 % probability level. Selected distances (Å) and angles (°): O1–C11 1.37(1), O2–C12 1.37(2), O1–B1–O2 103.6(6), F1–B1–C1–C2 0.0(2), F1–B2–C3–C2 34.7(2).

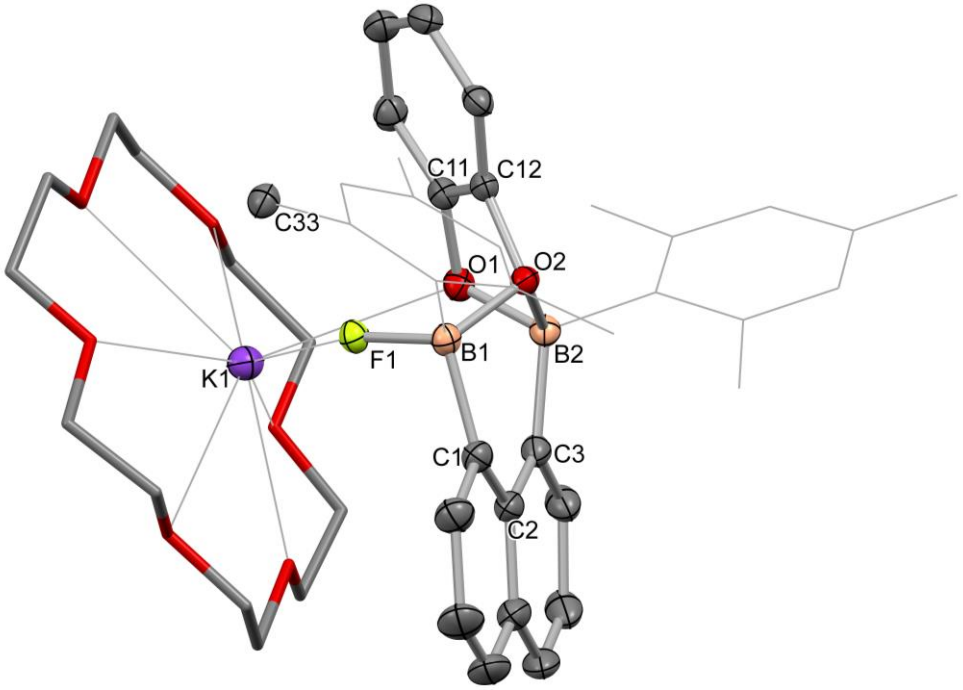

Figure 3.9 – Molecular structure of **[K(18-crown-6)][3.6].** The mesityl groups are shown in wireframe format and hydrogens are omitted for clarity. Thermal ellipsoids are set at the 40 % probability level. Selected distances (Å) and angles (°): O1–C11 1.356(2), O2–C12 1.416(2), K1–F1 2.6650(8), K1–O1 3.040(1), C33–F1 2.681(2), C12–O2–B1 109.84(9), C12–O2–B2 100.57(9), O1–B2–O2 98.9(1), O2–B1–C1–C2 -41.2(2), O2–B2–C3–C2 3.1(2).

	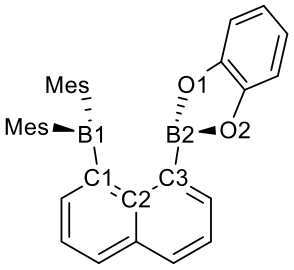	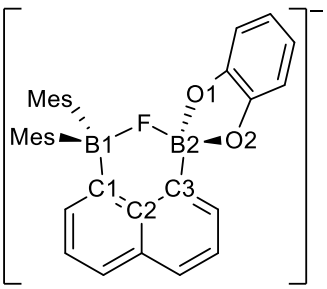	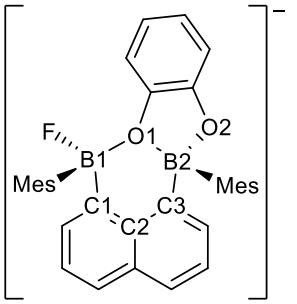
d(B1---B2)	3.189(2)	2.836(3)	2.758(2)
d(B1–C1)	1.573(2)	1.614(2)	1.615(2)
d(B2–C3)	1.551(2)	1.587(3)	1.601(2)
d(B–F)	–	1.633(2) [B1] 1.549(2) [B2]	1.4283(16)
d(B–O)	1.388(2) 1.392(2)	1.497(9) 1.46(1)	1.6157(17) [B1-O1] 1.6409(17) [B2-O1] 1.5007(17) [B2-O2]
∠(B1–X–B2)	–	126.05(11)	115.75(9)
∠(B1–C1–C2)	126.9(1)	122.90(14)	120.56(12)
∠(B2–C3–C2)	126.5(1)	124.44(15)	125.06(12)
∠(C1–C2–C3)	123.6(1)	122.01(15)	121.19(13)
∠(B1-C1-C2-C3)	22.6(2)	-13.9(2)	14.6(2)
∠(B2-C3-C2-C1)	17.3(2)	-7.1(2)	6.2(2)

Table 3.1 – Key bond lengths (Å) and angles (°) of structures **3.4**, **[TAS][3.5]** and **[K(18-crown-6)][3.6]**. Atom labelling corresponds only to the chemdraws in the header.

The crystal structure of [**TAS][3.5]** reveals that the chelated fluoride is not symmetrically bound between the two boron centres, but more closely associates with the catecholborane unit: the B1–F1 and B2–F1 separations are 1.549(2) Å and 1.6331(19) Å, respectively. This unsymmetrical association is also evident in the ^{11}B NMR spectrum which shows two well-separated signals at 24 ppm and 13 ppm, with the upfield signal attributed to the catecholborane functional group. In the ^{19}F NMR spectrum the chelated fluoride appears as a broad signal at -141.8 ppm. The discernibly higher fluoride affinity, and therefore Lewis acidity, of the catecholborane compared to the more electrophilic dimesitylborane centre

may primarily be attributed to the differing steric profiles of the two boron centres. The catecholborane readily undergoes pyramidalisation (Σ_{B1} = 342.0 °) whilst the bulky dimesitylborane, retains a greater degree of planarity (Σ_{B2} = 346.2 °) due to the significant back-strain generated by the mesityl groups upon pyramidalisation. Additionally, the inductive withdrawing ability of the catecholborane oxygens can more effectively stabilise the increased electron density at the four-coordinate boron formed upon fluoride coordination. The coordination of fluoride also disrupts the stabilising π-donation of the catechol oxygens resulting in the elongation of the B–O bond lengths from 1.388(2) Å and 1.392(2) Å in **3.4** to 1.497(9) Å and 1.46(1) Å in anion **3.5**.

The chelation of fluoride also has a significant impact on reducing the steric strain of the backbone, compared to the unbound parent receptor. This is evident in the ^{1}H NMR spectrum in which the mesityl groups are now characterised by a single aromatic singlet and two methyl singlets, indicating they are equivalent and in unhindered free rotation. The relaxation of strain is also apparent in the X-ray crystal structure, in which the boron-boron separation has decreased from 3.189(2) Å to 2.836(3) Å and the central angles B1–C1–C2 (124.44(15) °), B2–C3–C2 (122.90(14) °) and C1–C2–C3 (122.01(15) °) are all closer to the ideal value of 120 °. Finally, the distortion of the boryl groups out of the plane of the naphthalene backbone has considerably decreased with torsion angles of B1–C1–C2–C3 -7.1(2) ° and B2–C3–C2–C1 -13.9(2) °.

The ‘rearranged’ anion in **[K(18-crown-6)][3.6]** experiences a similar reduction in steric strain compared to the receptor ligand, **3.4**. As with [**TAS][3.5]**, the B–C–C and C1–C2–C3 bond angles all decrease closer to the ideal value of 120 ° and the distortions of the boron groups out of the plane of the naphthalene ring likewise decrease. The shortening of the boron-boron separation to 2.758(2) Å is also more pronounced than that observed in [**TAS][3.5]**.

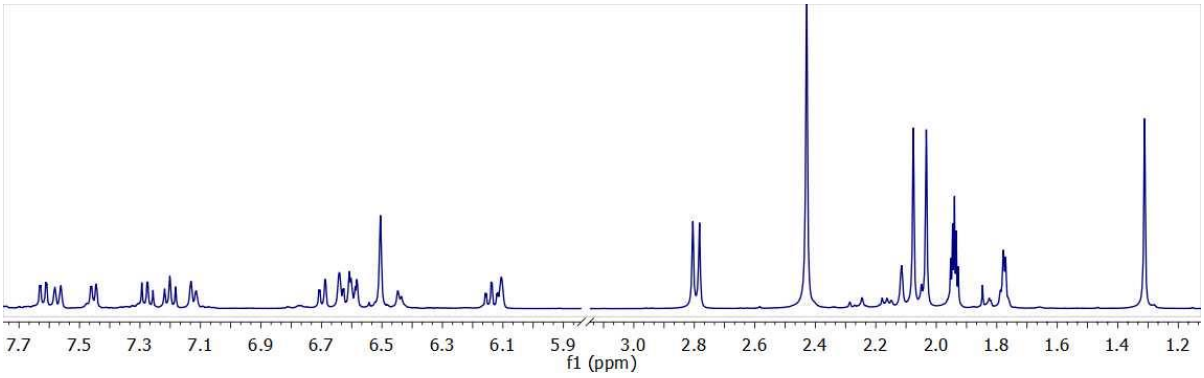

Figure 3.10 – ^{1}H NMR spectrum of **[K(18-crown-6)][3.6]** in d_3-acetonitrile. The central region of the spectrum (including the signal for 18-crown-6) has been cropped for clarity.

NMR characterisation of **[K(18-crown-6)][3.6]** reveals that some steric crowding still remains. The aromatic region of the ^{1}H NMR in Figure 3.10 features two broad singlet proton signals at 6.1 ppm and 6.63 ppm, in addition to a sharp two proton singlet at 6.5 ppm, suggesting that only one of the mesityl groups is in free rotation. Inspection of the solid-state structure in Figure 3.9 reveals that the rotation of the mesityl group attached to the fluoroborane moiety is likely to be restricted by its proximity to the catechol group. This hindered mobility is also made further apparent by through-space ^{1}H-^{19}F coupling between the fluoride and the protons of the proximal C33 *ortho*-methyl group: a three-proton doublet at 2.80 ppm (J_{HF} = 8.8 Hz) in the ^{1}H NMR spectrum is resolved into a broad singlet in the ^{19}F-decoupled spectrum. Resolution of the corresponding splitting in the ^{19}F NMR spectrum, in which the resonance appears at -130.5 ppm, is however hindered by broadening due to the quadrupolar nature of the connected boron atom (^{11}B, I = 3/2). The B–F bond is also significantly shorter with the fluoride is bound in a terminal position, and at 1.4283(16) Å, falls within the conventional range of fluoroborate bonds.

The rearrangement of the functional groups in **[K(18-crown-6)][3.6]** leads oxygen O2 to take up a bridging position and a three-coordinate pyramidal geometry (Σ_{O2} = 326.17 °). O2 is positioned relatively centrally between the boron centres with bond lengths to B1 and B2 of 1.6157(17) Å and 1.6409(17) Å respectively, *i.e.* markedly longer than the bridging

B–O bonds of **3.1** and **3.2** that fell in the range 1.34 – 1.46 Å. The similar coordination environment at both boron centres is also reflected in the ^{11}B NMR spectrum in which both signals fall in the four-coordinate range at 15 ppm and 12 ppm. As a result, anion **3.6** may be described as a combination of the three adduct resonance forms shown in Scheme 3.8, thereby distributing the negative charge.

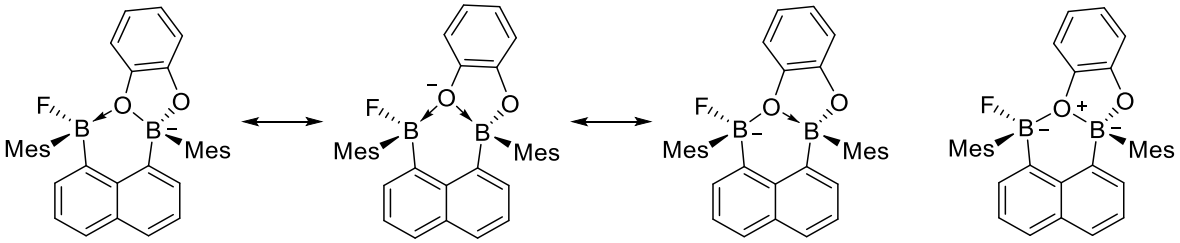

Scheme 3.8 – Resonance structures of anion **3.6**

Interestingly, whilst **3.6** has four possible stereoisomers only the enantiomeric pair with the mesityl groups on the same face of the naphthalene ring are present in the unit cell of **[K(18-crown-6)][3.6]**, as illustrated in Figure 3.11. These *cis*-type enantiomers exist in a racemic mixture in the unit cell. This apparent geometric selectivity may be the result of the mechanism of rearrangement to **[K(18-crown-6)][3.6]**. The arrangement of the non-bridging oxygen and fluoride on the same face of the anion in **[K(18-crown-6)][3.6]** is also noted to favour coordination with the potassium crown ether cation. Coordination of the K(18-crown-6) cation may therefore play an active role in the functional group rearrangement and confer some stereoselectivity to the mechanism.

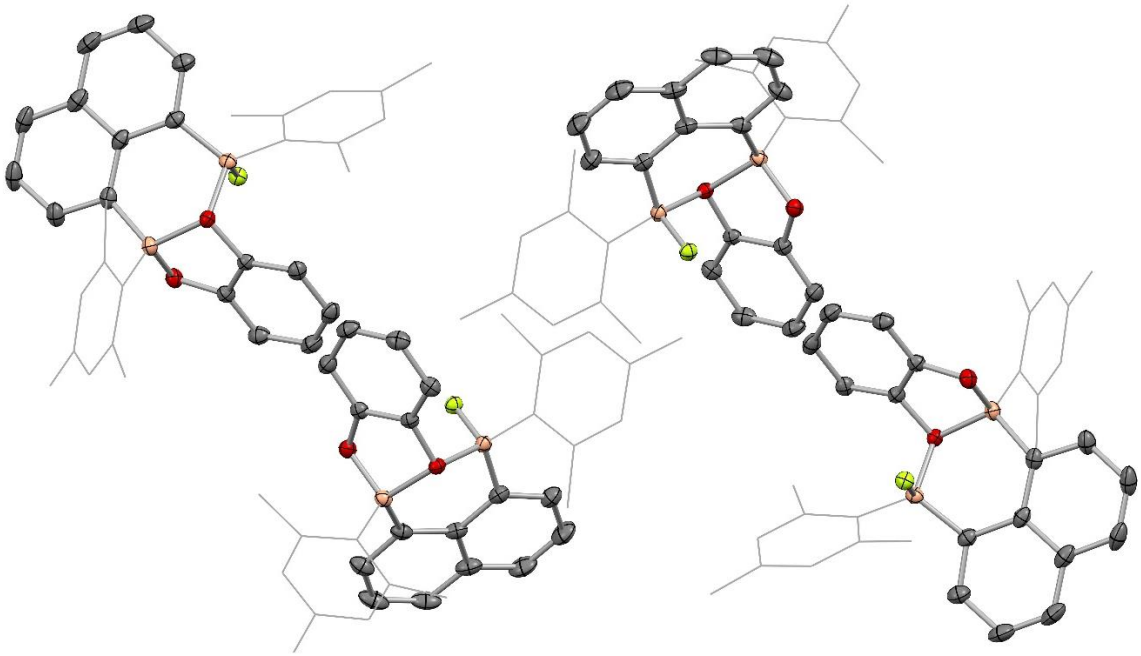

Figure 3.11 – Unit cell packing of **[K(18-crown-6)][3.6]** where the top two molecules exhibit R,R isomerism and the bottom two are the S,S isomers. K(18-crown-6) counter cations, solvent molecules and hydrogens are omitted and mesityl groups are wireframe for clarity. Ellipsoids are set to 40 % thermal probability.

3.5 Rearrangement Study

3.5.1 Solution Phase

Monitoring a solution of **[TAS][3.5]** by *in situ* ^{1}H NMR measurements over several days in CD_3CN, a new set of signals for a naphthalene species was observed to be slowly growing in (Figure 3.12). In particular, the new signals appearing at 6.14 ppm, 6.11 ppm and 2.44 ppm are in accord with the isomer **3.6** anion, implying that the anion **3.6** forms *via* the rearrangement of **3.5**. Indeed, given the close match of the new species to the NMR spectrum of the isolated species **[K(18-crown-6)][3.6]**, it can therefore be inferred that only the *cis* isomer is again being formed, and that the conversion is therefore highly selective. Moreover, this conversion indicates that the rearrangement occurs even in the presence of a strongly Lewis acidic cation such as $[K(18\text{-crown-6})]^{+}$. This conversion additionally suggests that while anion **3.5** is the kinetic product of the reaction of **3.4** with fluoride ions, anion **3.6**

is the thermodynamic product. This further highlights the prevalence of the B–O–B bridge as a thermodynamic sink in these systems.

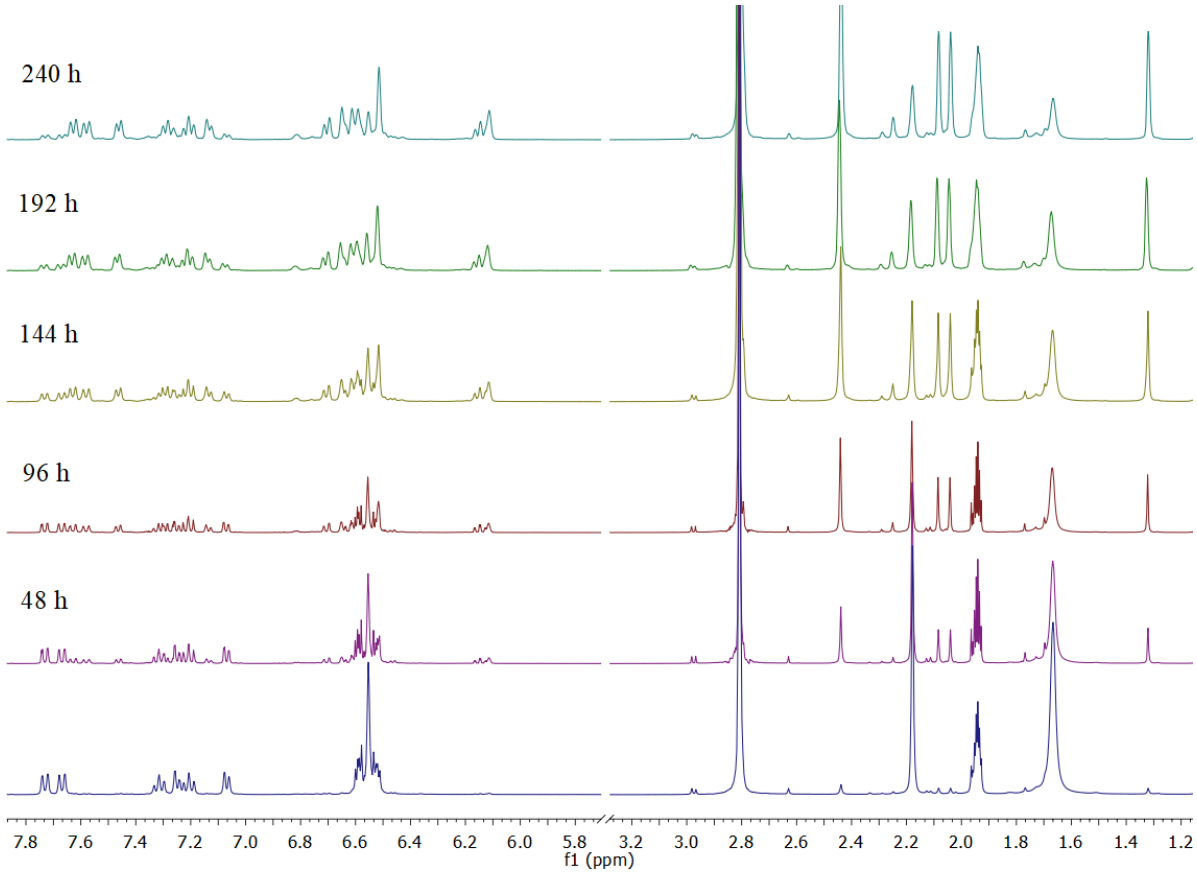

Figure 3.12 – Selected ^{1}H NMR spectra illustrating the conversion of **[TAS][3.5]** to **[TAS][3.6]** in d_3-acetonitrile. The counter cation, $[TAS]^+$, features as a singlet at 2.8 ppm. The central region of the spectrum has been cropped for clarity.

To quantify the conversion of **[TAS][3.5]** to **[TAS][3.6]**, 16 mg of **[TAS][3.5]** was dissolved in 0.4 mL of dry MeCN-d_3 and the solution monitored by ^{1}H NMR spectroscopy. The tris(dimethylamino)sulfonium cation (2.8 ppm) provided a convenient internal standard signal, whilst the single proton naphthalene signals of anion **3.5** at 7.07 ppm and anion **3.6** at 7.46 ppm were used to monitor the concentrations of the respective compounds. After 11 days at room temperature, the reaction had not reached full conversion but had progressed cleanly, producing anion **3.6** in *ca.* 70 % yield, (Figure 3.13). A plot of the natural log of the concentration of anion **3.5** against time in Figure 3.14 gives a straight line, demonstrating

first order kinetics for the conversion and a half-life for **[TAS][3.5]** in acetonitrile solution of 157 h (k_{obs} = 1.77 x 10^{-6} s^{-1}).

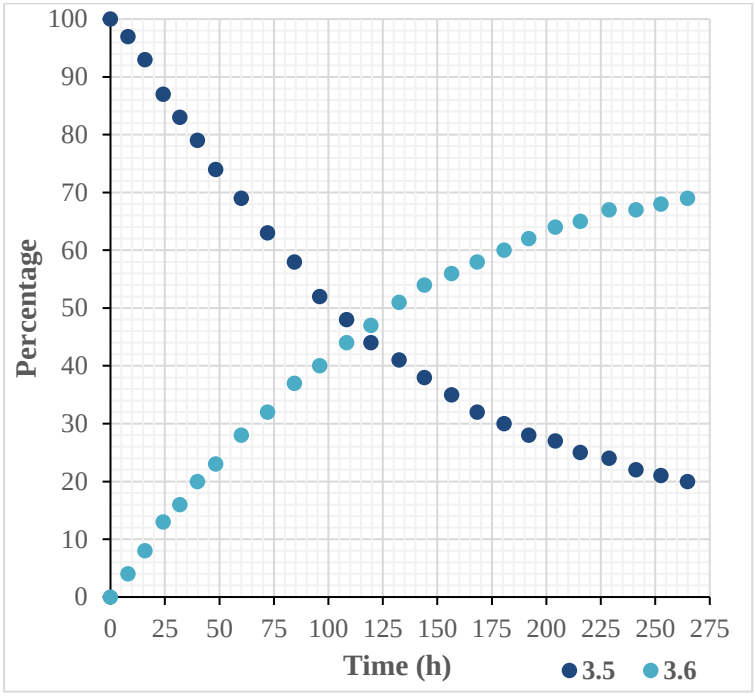

Figure 3.13 – Plot of the intensities of single proton resonances of anions **3.5** and **3.6** relative to the TASF signal in ^{1}H NMR monitoring.

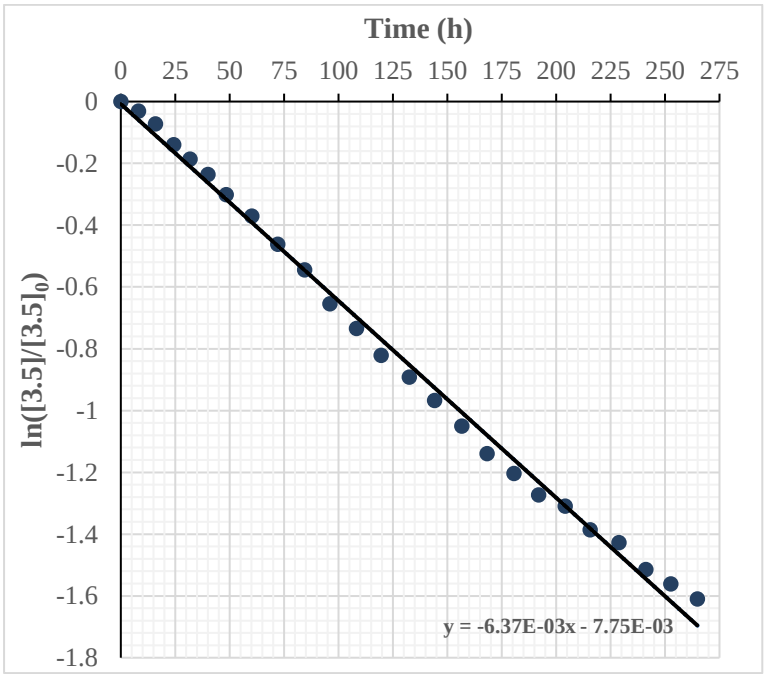

Figure 3.14 – First order plot of ln([**3.5**]/[**3.5**]$_0$) vs time (hours). R^2 = 0.9949.

3.5.2 DFT Studies

DFT calculations were conducted to shed light on why anion **3.5** undergoes selective rearrangement, and the mechanism by which this may proceed. Calculations were carried out using the same method discussed earlier in this chapter, *i.e.* at the PBE1PBE/Def2-TZVP level of theory with empirical dispersion and acetonitrile solvent included. Given that the rearrangement was noted to occur irrespective of the countercation, calculations were performed solely on the anionic component. The geometry optimisations of anions **3.5** and **3.6** produced structures whose geometries correlate well with the experimental data. The rearrangement from **3.5** to **3.6** was noted to be energetically favoured by only 3 kJ mol^{-1} (Figure 3.15). Although the energy difference between the structures is very small, it does point towards an increased thermodynamic stability in the oxygen bridged structure, consistent with the experimental observations.

The structural rearrangement is proposed to proceed *via* the mechanism outlined in Figure 3.15. In order to facilitate the migration of the mesityl group between the boron centres, a rotation occurs around the B–C(naphth) bond of the -B(F)Mes_2 moiety in **3.5**. The rotation removes fluoride from the binding pocket, breaking the chelate bridge and bringing one of the mesityl groups into close proximity with the -BCat Lewis acidic centre. Mesityl migration then occurs between the boron centres *via* the transition state **TS** to form intermediate **Int**. A subsequent rotation of the -B(Mes)Cat moiety of the intermediate, leads to coordination of the proximal oxygen to the three-coordinate -B(F)Mes centre, thereby forming **3.6**. This mechanism is consistent with the geometric selectivity of the experimental reaction, exclusively producing the *cis*-isomer. The possibility of scrambling at the intermediate **Int**, by 180 ° rotation of the -B(F)Mes group, is highly disfavoured by the high steric bulk of the adjacent four coordinate -B(Mes)Cat group, especially when compared to the effectively unimpeded pathway for catechol-oxygen coordination to form **3.6**.

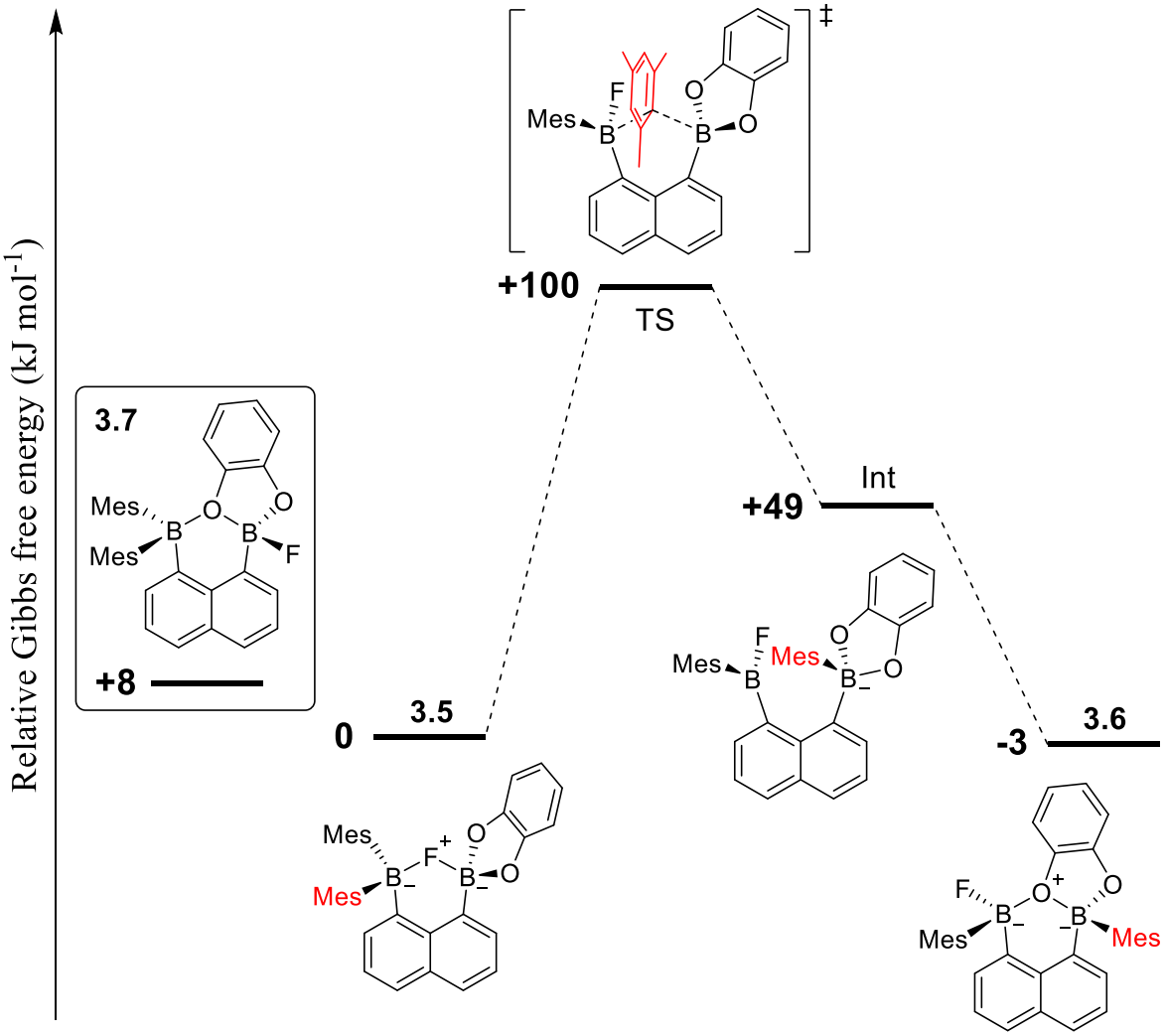

Figure 3.15 – Energy profile for the rearrangement mechanism of anion **3.5** to anion **3.6.** The undetected isomeric anion **3.7** is also included in the box.

Interestingly, the alternative scenario whereupon the -B(F)Cat moiety of **3.5** rotates around its B–C(naphth) bond is thermodynamically disfavoured. This pathway, which would also break the μ_2-fluoride chelate bridge and directly position the catechol-oxygen in the bridging position, leads to a product **3.7** (Figure 3.15) that is destabilised compared to the starting material and 11 kJ mol^{-1} higher in energy than the observed rearranged anion **3.6**. The higher energy of this undetected product suggests that the thermodynamic favourability of the **3.6** anion may in part be derived from the fact that the bulky mesityl groups are bound to different boron centres. Whilst this alternative isomer is undetected, it is likely to be energetically accessible, with a lower energy barrier to formation than that for the mesityl

migration. However, the energy barrier for reversion to **3.5** will likely be similarly low, leading to an equilibrium between the isomers that is weighted towards the more thermodynamically favourable anion **3.5**.

The energetic barrier of the mesityl migration step, at 100 kJ mol^{-1}, is consistent with the experimental observation of the reaction occurring at room temperature, albeit slowly. It is interesting to note that this migration step bears a marked resemblance to the stabilising π-interaction in ligand **3.4** where an *ipso*-carbon of the mesityl group donates electron density to the vacant *p*-orbital of the -BCat group (*vide supra* HOMO-5 in Figure 3.7). It can therefore be inferred that a similar interaction occurring here would lead to the mesityl migration, induced by the increased electron density at the four-coordinate dimesitylborate unit.

3.6 Conclusions

1,8-Naphthalene-diboronic acid anhydride was synthesised and structurally characterised. Although it was hoped the fully hydrated diboronic acid may be accessible, the preorganisation of the structure highly favours self-condensation to the partially hydrated anhydride. The B–O–B anhydride bridge was confirmed to be exceptionally robust, suggesting the anhydride form is a thermodynamic sink for the system. With the oxygen bridge effectively blocking any chelation of fluoride between the boron centres, substitution solely occurs at the more labile terminal boronic acid bonds. It is interesting to note however that since this work was undertaken, Wagner and co-workers reported the successful breakdown of the anhydride bridge *via* reduction of **3.1b** with the (admittedly highly reactive) lithium aluminium hydride to produce the corresponding hydride bridged borane.[51]

The mono-ester, 1-dimesitylboryl-8-catecholboryl-naphthalene **3.4** was synthesised to circumvent the anhydride problem. Fluoride was successfully chelated into the binding pocket of **3.4** to yield the μ_2-fluoride bridged anion **3.5**. Over the course of several weeks in solution at room temperature the **3.5** anion undergoes rearrangement to form a new fluoroborate species, anion **3.6**, where fluoride resides in a terminal position. The rearrangement is proposed to break the μ_2-fluoride chelate bridge and migrate a mesityl group between the boron centres, before once again placing oxygen in the boron bridging position. Experimental and DFT observations established anion **3.5** to be the kinetic product from the fluoride binding reaction of **3.4**, whilst anion **3.6** is the thermodynamic product.

Studies of the water stability of the μ_2-fluoride chelated anion **3.5** were inhibited by the rearrangement removing fluoride from the chelating position. Although this rearrangement is slow compared to the timescale of fluorine-18 decay, it does present a serious limitation on the system by moving fluoride to a more labile terminal position. The preference to position oxygen in the binding pocket, either directly or *via* rearrangement of substituents, suggests 1,8-diborylnaphthalenes featuring boronic acid or ester groups do not readily lend themselves to our desired application. With this in mind, alternative strategies were explored with systems less likely to reorganise and compromise B–F bonding. These studies are described in Chapters 4 and 5.

3.7 Experimental

3.1 - 1,8-naphthalene diboronic acid anhydride

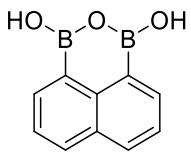

Based on the preparation of Sanjayan *et al*.[43] 1,8-diiodonaphthalene (5 g, 13.16 mmol) was dissolved in dry diethyl ether (80 mL) and cooled to -78 °C. A solution of *n*-butyllithium in

hexane (19.7 mL of a 1.6 M solution, 31.58 mmol) was added dropwise to the reaction mixture, which was allowed to warm to room temperature and stirred for 2 h before re-cooling to -78°C. A dilute solution of excess trimethyl borate (5 mL, 44.85 mmol) in diethyl ether (80 mL) was subsequently added dropwise, and the stirred at room temperature overnight. 2 M HCl (150 mL) was used to quench the reaction and the ether layer separated. The product was subsequently extracted from the ether layer using 1 M NaOH (2 x 150 mL) and the alkaline solution acidified with 2 M HCl. The resulting white precipitate was filtered and recrystallised from water/ethanol to yield pale brown crystals (2.02 g, 78%). Crystals suitable for X-ray diffraction were obtained from a concentrated solution in boiling water that was slowly cooled to room temperature.

Spectroscopic Data: **^{1}H NMR** (500.3 MHz, CD_3CN, 298 K): δ_H 8.16 (dd, $^{3}J_{HH}$ = 6.8 Hz, $^{4}J_{HH}$ = 1.1 Hz, 2H, Naph C*H*), 8.07 (dd, $^{3}J_{HH}$ = 8.3 Hz, $^{4}J_{HH}$ = 1.1 Hz, 2H, Naph C*H*), 7.60 (dd, $^{3}J_{HH}$ = 6.8 Hz, $^{3}J_{HH}$ = 8.2 Hz, 2H, Naph 3,6-C*H*), 6.74 (2H, s, BO*H*). **^{11}B{^{1}H} NMR** (128.4 MHz, CD_3CN, 298 K): δ_B 30 (br s). **^{13}C{^{1}H} NMR** (125.8 MHz, CD_3CN, 298 K): δ_C 142.5 (Naph *C*), 135.0 (Naph *C*H), 132.7, 128.6 (br s, Naph *C*B) 126.5 (Naph *C*H). **Elemental Microanalysis**: calc. for $C_{10}H_8B_2O_3 \cdot 0.5(H_2O)$: C 58.08 %, H 4.39 %; meas. C 57.74 %, H 4.47 %.

[K(18-crown-6)][3.2]

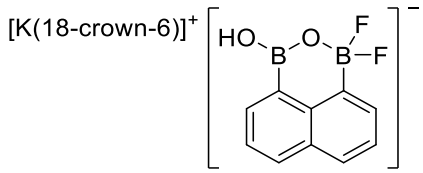

3.1 (50 mg, 0.253 mmol) was dissolved in acetonitrile (10 mL) and stirred with potassium fluoride (80 mg, 1.39 mmol) and 18-crown-6 (61 mg, 0.232 mmol) for 6 h. The solution was concentrated and stored at -25 °C yielding colourless crystals suitable for X-ray diffraction.

Spectroscopic Data: **^{1}H NMR** (500.3 MHz, CD_3CN, 298 K): δ_H 7.89 (dd, $^{3}J_{HH}$ = 6.6 Hz, $^{4}J_{HH}$ = 1.0 Hz, 1H, Naph C*H*), 7.84 (dd, $^{3}J_{HH}$ = 8.1 Hz, $^{4}J_{HH}$ = 1.1 Hz, 1H, Naph C*H*), 7.64 (d, $^{3}J_{HH}$ = 8.2 Hz, 1H, Naph C*H*), 7.61 (d, $^{3}J_{HH}$ = 6.6 Hz, 1H, Naph C*H*), 7.41 – 7.35 (overlapping m, 2H, Naph C*H*), 5.50 (br s, 1H, BO*H*), 3.53 (s, 48H, crown). **^{11}B{^{1}H} NMR** (128.4 MHz, CD_3CN, 298 K): δ_B 28 (br s, *B*OH), 4 (t, $^{1}J_{BF}$ = 43.6 Hz, -*B*F_2). **^{19}F{^{1}H} NMR** (376.5 MHz, CD_3CN, 298 K): δ_F -133.6 (q, $^{1}J_{BF}$ = 42.0 Hz, -B*F*$_2$). **^{13}C{^{1}H} NMR** (125.8 MHz, CD_3CN, 298 K): δ_C 141.6, 132.7, 131.6, 130.7, 129.5, 126.4, 125.7, 70.9 (crown).

3.3 – 1,8-naphthalene-di(methylboronate) anhydride

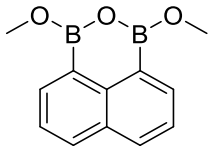

In a procedure similar to that described by Katz,[47] a flask was charged with solid **3.1** and a minimal volume of methanol added. The reaction was heated to reflux and more methanol added until the solid just dissolved. The solution was allowed to slowly cooled to room temperature. Colourless crystals of the product were subsequently isolated in good yield.

Spectroscopic Data: **^{1}H NMR** (400.2 MHz, C_6D_6, 298 K): δ_H 8.38 (dd, $^{3}J_{HH}$ = 6.7 Hz, $^{4}J_{HH}$ = 1.2 Hz, 2H, Napth C*H*), 7.72 (dd, $^{3}J_{HH}$ = 8.3 Hz, $^{4}J_{HH}$ = 1.2 Hz, 2H, Napth C*H*), 7.35 (dd, $^{3}J_{HH}$ = 8.2 Hz, $^{3}J_{HH}$ = 6.7 Hz, 2H, *3,6*-Napth-C*H*), 3.64 (s, 6H, OC*H*$_3$). **^{11}B{^{1}H} NMR** (128.4 MHz, C_6D_6, 298 K): δ_B 29 (br s, *B*OMe). **^{13}C{^{1}H} NMR** (100.6 MHz, C_6D_6, 298 K): δ_C 142.3 (Naph *C*), 134.5 (Naph *C*H), 132.3 (Naph *C*), 132.1 (Naph *C*H), 125.9 (3,6-Naph *C*H), 50.5 (O*C*H$_3$). **Elemental Microanalysis**: calc. for $C_{12}H_{12}B_2O_3$: C 63.82 %, H 5.36 %; meas. C 63.73 %, H 5.22 %.

3.4 – 1-(dimesitylboryl)-8-(catecholatoboryl) naphthalene

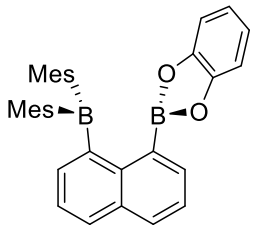

Freshly isolated lithium dimesityl-1,8-naphthalenediylborate (210 mg, 0.313 mmol) was suspended in diethyl ether (10 mL) and cooled to -10 °C. A solution of chlorocatecholborane (58 mg, 0.376 mmol) in diethyl ether (5 mL) was added to the cooled reaction mixture. After stirring for 15 min it was warmed to room temperature and stirred overnight. After filtration and removal of volatiles *in vacuo*, the resulting yellow powder was recrystallised from acetonitrile to yield crystals suitable for X-ray crystallography. Yield: 113 mg, 73 %.

Spectroscopic Data: **^{1}H NMR** (400.2 Hz, C_6D_6, 298 K): δ_H 7.99 (dd, $^{3}J_{HH}$ = 7.0 Hz, $^{4}J_{HH}$ = 1.5 Hz, 1H, Naph C*H*), 7.78 (dd, $^{3}J_{HH}$ = 6.9 Hz, $^{4}J_{HH}$ = 1.5 Hz, 1H, Naph C*H*), 7.66 (td, $^{3}J_{HH}$ = 7.9 Hz, $^{4}J_{HH}$ = 1.5 Hz, 2H, Naph C*H*), 7.20 – 7.14 (overlapping m, 3H, Naph C*H*, C_6D_6), 7.05 (br s, 1H, Mes *m*-C*H*), 6.93 (m, 2H, Cat C*H*), 6.81 (m, 2H, Cat C*H*), 6.75 (br s, 1H, Mes *m*-C*H*), 6.57 (br s, 1H, Mes *m*-C*H*), 6.13 (br s, 1H, Mes *m*-C*H*), 2.90 (br s, 3H, Mes CH_3), 2.26 (br s, 3H, Mes CH_3), 2.05 (br s, 3H, Mes CH_3), 1.94 (br s, 3H, Mes CH_3), 1.69 (br s, 3H, Mes CH_3), 1.20 (br s, 3H, Mes CH_3). **^{11}B{^{1}H} NMR** (128.4 Hz, C_6D_6, 298 K): δ_B 76 (br s, *B*Mes$_2$), 33 (br s, *B*Cat). **^{13}C{^{1}H} NMR** (125.8 Hz, C_6D_6, 298 K): δ_C 149.2 (Cat *C*O), 148.3 (br s, Mes), 145.3 (br s, Mes *C*B), 143.8 (br s, Mes), 142.3 (br s, Mes), 141.5 (br s, Mes), 140.8 (br s, Mes), 140.6, 140.4 (br s, Mes), 139.1 (br s, Mes *C*B), 138.6, 136.3, 134.2, 134.1, 132.8, 130.3 (br s, Mes), 130.1 (br s, Mes), 129.6 (br s, Mes), 126.4, 125.3, 122.4 (Cat *C*H), 112.8 (Cat *C*H), 25.5 (br s, Mes *o*-*C*H$_3$), 24.6 (br s, Mes *o*-*C*H$_3$), 23.3 (br s, Mes *o*-*C*H$_3$), 22.8 (br s, Mes *o*-*C*H$_3$), 21.3 (Mes *p*-*C*H$_3$). **Elemental microanalysis**: calc. for $C_{34}H_{32}B_2O_2$: C 82.63 %, H 6.53 %; meas. C 82.54 %, H 6.64 %.

[TAS][3.5]

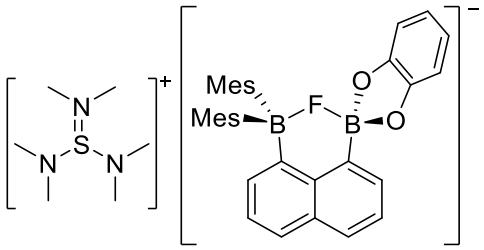

3.4 (95 mg, 0.192 mmol) and TASF (58 mg, 0.211 mmol) were dissolved in THF (15 mL) and the reaction mixture stirred at room temperature for 2 h. Volatiles were removed *in vacuo* and the product extracted into minimal acetonitrile. The solution was then concentrated and stored at -25 °C to yield colourless crystals suitable for X-ray diffraction. Yield: 35 mg, 27 %.

Spectroscopic Data: **^{1}H NMR** (400.2 MHz, CD_3CN, 298 K): δ_H 7.72 (d, $^{3}J_{HH}$ = 8.0 Hz, 1H, Naph C*H*), 7.66 (d, $^{3}J_{HH}$ = 8.0 Hz, 1H, Naph C*H*), 7.30 (t, $^{3}J_{HH}$ = 7.4 Hz, 1H, Naph C*H*), 7.23 (d, $^{3}J_{HH}$ = 6.8 Hz, 1H, Naph C*H*), 7.19 (t, $^{3}J_{HH}$ = 7.4 Hz, 1H, Naph C*H*), 7.05 (d, $^{3}J_{HH}$ = 6.8 Hz, 1H, Naph C*H*), 6.60 – 6.56 (overlapping m, 2H, Cat C*H*), 6.54 (s, 4H, Mes *m*-C*H*), 6.53 – 6.49 (overlapping m, 2H, Cat C*H*), 2.84 (s, 18H, NCH_3), 2.17 (s, 6H, Mes *p*-CH_3), 1.65 (br s, 12H, Mes *o*-CH_3). **^{11}B{^{1}H} NMR** (128.4 MHz, CD_3CN, 298 K): δ_B 25 (br s, *B*Mes_2), 13 (br s, *B*Cat). **^{19}F{^{1}H} NMR** (376.5 MHz, CD_3CN, 298 K): δ_F -141.8 (br s). **^{13}C{^{1}H} NMR** (100.6 MHz, CD_3CN, 298 K): δ_C 153.3, 142.9, 140.0, 134.9, 133.4, 131.1 (d, J_{CF} = 7.5 Hz, Ar), 130.3 (d, J_{CF} = 6.8 Hz, Ar), 129.5, 128.3, 127.1, 125.6, 125.2, 119.0, 109.5, 38.8 (N*C*H_3), 24.9 (Mes *C*H_3), 20.95 (Mes *C*H_3). **Elemental Microanalysis**: calc. for $C_{40}H_{50}B_2FN_3O_2S$: C 70.91 %, H 7.44 %, N 6.20 %; meas. C 70.78 %, H 7.25 %, N 6.29 %.

[K(18-crown-6)][3.6]

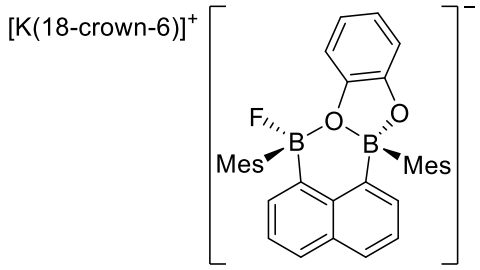

A Schlenk tube was charged with potassium fluoride (88 mg, 1.52 mmol) and 18-crown-6 (54 mg, 0.202 mmol) and THF (8 mL) added to form a suspension. In a separate Schlenk tube, **3.4** was dissolved in THF (8 mL) before addition to the stirred suspension. The reaction was stirred at room temperature for 6 weeks then volatiles were removed *in vacuo*. The product was extracted in acetonitrile (2 x 5 mL) and the solvent removed *in vacuo* to yield a spectroscopically pure product. Yield: 88 mg, 71 %. Crystals suitable for X-ray diffraction were grown by slow evaporation of an acetonitrile solution.

Spectroscopic Data: **^{1}H NMR** (400.2 MHz, CD_3CN, 298 K): δ_H 7.61 (d, $^{3}J_{HH}$ = 8.1 Hz, 1H, Naph C*H*), 7.56 (d, $^{3}J_{HH}$ = 8.0 Hz, 1H, Naph C*H*), 7.45 (d, $^{3}J_{HH}$ = 6.7 Hz, 1H, Naph C*H*), 7.27 (t, $^{3}J_{HH}$ = 7.4 Hz, 1H, Naph C*H*), 7.19 (t, $^{3}J_{HH}$ = 7.3 Hz, 1H, Naph C*H*), 7.12 (d, $^{3}J_{HH}$ = 6.6 Hz, 1H, Naph C*H*), 6.69 (dd, $^{3}J_{HH}$ = 7.7 Hz, $^{4}J_{HH}$ = 1.3 Hz, 1H, Cat C*H*), 6.63 (br s, 1H, Mes *m*-C*H*), 6.60 (m, 2H, Cat C*H*), 6.50 (s, 2H, Mes *m*-C*H*), 6.13 (td, $^{3}J_{HH}$ = 7.7 Hz, $^{4}J_{HH}$ = 1.4 Hz, 1H, Cat C*H*), 6.10 (br s, 1H, Mes *m*-C*H*), 3.57 (s, 24H, OCH_2), 2.79 (d, J_{HF} = 8.8 Hz, 3H, Mes CH_3), 2.42 (s, 6H, Mes *o*-CH_3), 2.07 (s, 3H, Mes CH_3), 2.03 (s, 3H, Mes CH_3), 1.30 (s, 3H, Mes CH_3). **^{11}B{^{1}H} NMR** (128.4 MHz, CD_3CN, 298 K): δ_B 15 (br s), 12 (br s). **^{19}F{^{1}H} NMR** (376.5 MHz, CD_3CN, 298 K): δ_F -130.5 (br s). **^{13}C{^{1}H} NMR** (100.6 MHz, CD_3CN, 298 K): δ_C 143.5, 135.2, 134.8, 132.7, 130.6, 129.7, 129.5, 129.0, 127.1, 126.4, 125.2, 125.0, 123.5, 117.0, 116.0, 112.0, 70.9 (crown), 25.1 (d, J_{CF} = 4.3 Hz, Mes *o*-*C*H_3), 23.4 (Mes *C*H_3), 20.8 (Mes *C*H_3).

3.8 References

[1] M. J. Biallas, D. F. Shriver, *J. Am. Chem. Soc.* **1966**, *88*, 375–376.
[2] D. F. Shriver, M. J. Biallas, *J. Am. Chem. Soc.* **1967**, *89*, 1078–1081.
[3] H. E. Katz, *J. Org. Chem.* **1985**, *50*, 5027–5032.
[4] H. E. Katz, *J. Am. Chem. Soc.* **1985**, *107*, 1421–1423.
[5] C. R. Wade, A. E. J. Broomsgrove, S. Aldridge, F. P. Gabbaï, *Chem. Rev.* **2010**, *110*, 3958–3984.
[6] M. E. Jung, H. Xia, *Tetrahedron Lett.* **1988**, *29*, 297–300.
[7] S. Aoyagi, K. Tanaka, Y. Takeuchi, *J. Chem. Soc. Perkin Trans. 2* **1994**, 1549.
[8] C. Jiang, O. Blacque, H. Berke, *Chem. Commun.* **2009**, 5518–5520.
[9] M. Reilly, T. Oh, *Tetrahedron Lett.* **1995**, *36*, 221–224.
[10] L. Schweighauser, H. A. Wegner, *Chem. - A Eur. J.* **2016**, *22*, 14094–14103.
[11] R. Panisch, M. Bolte, T. Müller, *J. Am. Chem. Soc.* **2006**, *128*, 9676–9682.
[12] K. Tamao, T. Hayashi, Y. Ito, M. Shiro, *J. Am. Chem. Soc.* **1990**, *112*, 2422–2424.
[13] X. Yang, Z. Zheng, C. B. Knobler, M. F. Hawthorne, *J. Am. Chem. Soc.* **1993**, *115*, 193–195.
[14] K. Tamao, T. Hayashi, Y. Ito, *J. Organomet. Chem.* **1996**, *506*, 85–91.
[15] R. Altmann, K. Jurkschat, M. Schürmann, D. Dakternieks, A. Duthie, *Organometallics* **1998**, *17*, 5858–5866.
[16] A. S. Wendji, C. Dietz, S. Kühn, M. Lutter, D. Schollmeyer, W. Hiller, K. Jurkschat, *Chem. - A Eur. J.* **2016**, *22*, 404–416.
[17] M. Newcomb, J. H. Horner, M. T. Blanda, P. J. Squattrito, *J. Am. Chem. Soc.* **1989**, *111*, 6294–6301.
[18] W. Uhl, F. Hannemann, *J. Organomet. Chem.* **1999**, *579*, 18–23.
[19] M. Hirai, F. P. Gabbaï, *Angew. Chemie - Int. Ed.* **2015**, *54*, 1205–1209.
[20] C.-H. Chen, F. P. Gabbaï, *Angew. Chemie Int. Ed.* **2017**, *56*, 1799–1804.
[21] M. J. Bayer, S. S. Jalisatgi, B. Smart, A. Herzog, C. B. Knobler, M. F. Hawthorne, *Angew. Chemie Int. Ed.* **2004**, *43*, 1854–1857.
[22] J. D. Hoefelmeyer, F. P. Gabbaï, *J. Am. Chem. Soc.* **2000**, *122*, 9054–9055.
[23] J. D. Hoefelmeyer, S. Solé, F. P. Gabbaï, *Dalt. Trans.* **2004**, *4*, 1254–1258.
[24] P. A. Chase, L. D. Henderson, W. E. Piers, M. Parvez, W. Clegg, M. R. J. Elsegood, *Organometallics* **2006**, *25*, 349–357.
[25] K. Durka, S. Luliński, J. Serwatowski, K. Woźniak, *Organometallics* **2014**, *33*, 1608–1616.
[26] C. L. Dorsey, P. Jewula, T. W. Hudnall, J. D. Hoefelmeyer, T. J. Taylor, N. R. Honesty, C. W. Chiu, M. Schulte, F. P. Gabbaï, *Dalt. Trans.* **2008**, 4442–4450.
[27] W. Clegg, *CCDC 1501846: Experimental Crystal Structure Determination*, **2016**.
[28] M. J. Kelly, A. E. J. Broomsgrove, I. R. Morgan, I. Siewert, P. Fitzpatrick, J. Smart, D. Vidovic, S. Aldridge, *Organometallics* **2013**, *32*, 2674–2684.
[29] R. Teerasarunyanon, L. C. Wilkins, G. Park, F. P. Gabbaï, *Dalt. Trans.* **2019**, *48*, 14777–14782.
[30] C. H. Chen, F. P. Gabbaï, *Angew. Chemie - Int. Ed.* **2018**, *57*, 521–525.
[31] H. E. Katz, *J. Org. Chem.* **1989**, *54*, 2179–2183.
[32] C. H. Chen, F. P. Gabbaï, *Chem. Sci.* **2018**, *9*, 6210–6218.
[33] P. Niermeier, S. Blomeyer, Y. K. J. Bejaoui, J. L. Beckmann, B. Neumann, H. G. Stammler, N. W. Mitzel, *Angew. Chemie - Int. Ed.* **2019**, *58*, 1965–1969.
[34] V. C. Williams, W. E. Piers, W. Clegg, M. R. J. Elsegood, S. Collins, T. B. Marder, *J. Am. Chem. Soc.* **1999**, *121*, 3244–3245.
[35] V. C. Williams, G. J. Irvine, W. E. Piers, Z. Li, S. Collins, W. Clegg, M. R. J.

Elsegood, T. B. Marder, *Organometallics* **2000**, *19*, 1619–1621.
[36] J. Chai, S. P. Lewis, S. Collins, T. J. J. Sciarone, L. D. Henderson, P. A. Chase, G. J. Irvine, W. E. Piers, M. R. J. Elsegood, W. Clegg, *Organometallics* **2007**, *26*, 5667–5679.
[37] S. P. Lewis, N. J. Taylor, W. E. Piers, S. Collins, *J. Am. Chem. Soc.* **2003**, *125*, 14686–14687.
[38] S. P. Lewis, L. D. Henderson, B. D. Chandler, M. Parvez, W. E. Piers, S. Collins, *J. Am. Chem. Soc.* **2005**, *127*, 46–47.
[39] S. Solé, F. P. Gabbaï, *Chem. Commun.* **2004**, *21*, 1284–1285.
[40] M. Melaïmi, S. Solé, C. W. Chiu, H. Wang, F. P. Gabbaï, *Inorg. Chem.* **2006**, *45*, 8136–8143.
[41] H. Zhao, F. P. Gabbaï, *Organometallics* **2012**, *31*, 2327–2335.
[42] J. D. Hoefelmeyer, F. P. Gabbaï, *Organometallics* **2002**, *21*, 982–985.
[43] P. Prabhakaran, V. G. Puranik, J. N. Chandran, P. R. Rajamohanan, H.-J. Hofmann, G. J. Sanjayan, *Chem. Commun.* **2009**, *124*, 3446.
[44] H. O. House, D. G. Koepsell, W. J. Campbell, *J. Org. Chem.* **1972**, *37*, 1003–1011.
[45] H. Wang, G. Kehr, R. Fröhlich, G. Erker, *Angew. Chemie Int. Ed.* **2007**, *46*, 4905–4908.
[46] R. L. Letsinger, J. M. Smith, J. Gilpin, D. B. MacLean, *J. Org. Chem.* **1965**, *30*, 807–812.
[47] H. E. Katz, *J. Org. Chem.* **1985**, *50*, 2575–2576.
[48] A. L. Rheingold, P. Iovine, *CCDC 1906117: Experimental Crystal Structure Determination*, **2019**.
[49] D. G. Hall, in *Boronic Acids Prep. Appl. Org. Synth. Med. Mater.* (Ed.: D.G. Hall), Wiley-VCH Verlag GmbH & Co. KGaA, Weinheim, FRG., Weinheim, Germany, **2011**, pp. 1–133.
[50] J. Tanaka, H. Tagawa, S. Kanemasa, "Synthesis and conformational analysis of macrocyclic esters of 1,8-naphthalenediboronic anhydride," **1996**.
[51] A. S. Scholz, J. G. Massoth, M. Bursch, J. M. Mewes, T. Hetzke, B. Wolf, M. Bolte, H. W. Lerner, S. Grimme, M. Wagner, *J. Am. Chem. Soc.* **2020**, *142*, 11072–11083.

Chapter 4

N-Heterocyclic Carbene Boron Trifluoride Adducts: Functionalisation for Bio-Conjugation

4.1 Introduction

4.1.1 *N*-Heterocyclic Carbenes Background

In the 30 years since the isolation of the first "bottleable" carbene by Arduengo *et al.*, *N*-heterocyclic carbenes (NHCs) have become ubiquitous ligands.[1] These versatile compounds, which feature a divalent carbon with six valence electrons, are highly favoured for their strong σ-donor properties, and have consequently been utilised to stabilise compounds featuring elements from across the Periodic Table.[2–6] Their modular design facilitates the tuning of their electronic and steric properties to suit their application and has led to an ever-growing catalogue of NHCs and a plethora of complexes.[7] Stable carbene design and donor characteristics have been extensively reviewed over the years,[8–10] so for the purposes of this thesis only a brief overview is given here, and primarily with a focus on Arduengo-type systems.

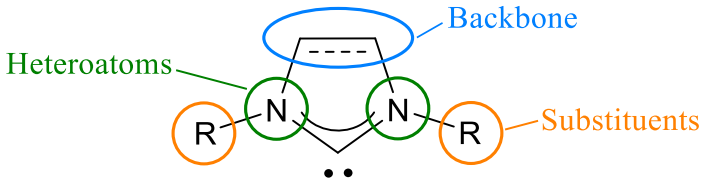

Figure 4.1 – Components in the modular design of *N*-heterocylic carbenes.

The non-bonding electrons of carbenic centres may exist in one of two possible spin ground states, depending upon the structure. A linear carbene may adopt a triplet ground state with the spin aligned electrons residing in a pair of degenerate *p*-orbitals. A singlet ground state can be favoured when bending breaks the degeneracy of the two *p*-orbitals. The

in-plane *p*-orbital is stabilised in the bent structure, mixing with the bonding *sp*-orbitals to generate a σ-orbital of approximate sp^2 type hybridisation, whilst the vacant *p*-orbital is p_π in character (Figure 4.2). Calculations indicate the singlet state is favoured when an energy gap of at least 2 eV separates these orbitals, while an energy gap of less than 1.5 eV favours the triplet state.[11]

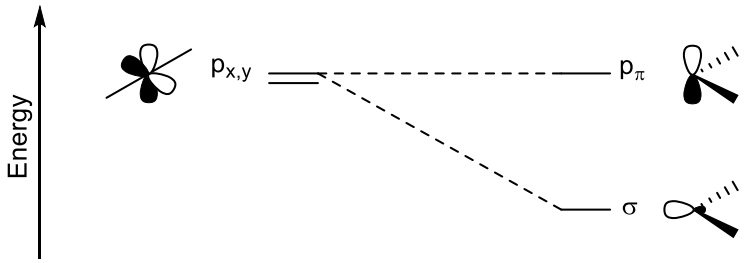

Figure 4.2 – Molecular orbital diagram depicting the orbitals of linear and bent carbenes.

N-heterocyclic carbenes incorporate at least one nitrogen adjacent to the carbene centre favouring the singlet state through both inductive and mesomeric effects. The nitrogens have a negative inductive effect, withdrawing electron density from the carbene and lowering the energy of the σ-orbital. Concurrently, the nitrogen lone pairs interact with the empty p_π-orbital of the carbene, donating electron density and destabilising the orbital to further increase the HOMO-LUMO gap and favour the singlet state. The carbene donor characteristics can be modified by varying the number and identity of the heteroatoms to change the inductive and mesomeric effects experienced by the carbene centre.[12–14]

The cyclic framework can also be used to tune the electronic properties of the NHC systems, affecting their σ-donor strength and overall stability. For example, the size of the heterocyclic ring can control the degree of non-linearity of the carbene centre, and therefore the degree of mixing between the in-plane *p*-orbital and the bonding *sp*-orbitals.[15] Hence, six-membered ring carbenes will typically be stronger σ-donors than in the saturated five-membered ring equivalents; the larger ring size allows for a more linear carbene centre, which results in less mixing and a σ-orbital of higher energy and *p*-character. Changes to the

backbone saturation of five-membered ring carbenes can also have a two-fold impact on the electronic properties. The shorter double bond leads to a narrower N–C–N angle at the carbene centre, increasing the *s*-character and stabilising the σ-orbital. An unsaturated backbone also increases delocalisation of the π-electrons, with imidazolylidenes exhibiting partial aromaticity and being calculated to be 25 kcal mol^{-1} more stabilised than the saturated imidazolinylidenes.[16,17] This superior stabilisation is highlighted by the free carbene IMe remaining persistent in solution whilst the saturated analogue exists as a dimer (Figure 4.3).[18,19]

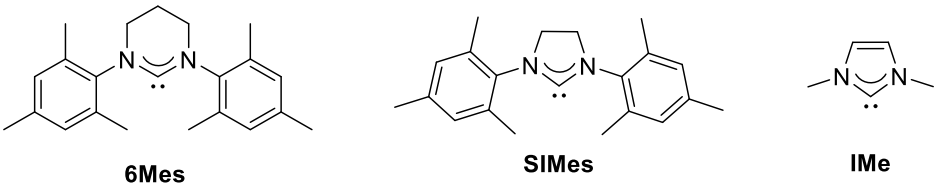

Figure 4.3 – Common examples of kinetically stable NHCs of differing ring size and backbone saturation.

The *N*-substituents are another point of modification of the modular design of NHCs and can play an important steric role.[20] In particular, bulky *N*-substituents can be used to confer kinetic stability to carbene structures, enabling isolation of frameworks such as imidazolinylidenes which otherwise dimerise with less sterically encumbering groups.[19,21] Moreover, control of the steric profile flanking the carbene centre has also been shown to be important in the utilisation of NHCs for the stabilisation of low valent species or in asymmetric catalysis.[2,6,22,23]

Finally, although π-interactions were originally considered to be negligible for *N*-heterocyclic carbenes as ligands, computational and experimental studies have demonstrated π-acid and π-base contributions to carbene coordination are not insignificant.[24–28] Thus, in addition to the variation in their σ-donor properties, NHCs offer differing π-properties. Recent heteronuclear NMR studies have consequently evaluated the

π-acceptor properties of a wide range of NHCs using phosphinidene and selenium adducts.[29–31] The most well-established example of this variation in π-properties is the lower π-acidity of unsaturated imidazolylidenes, compared to the saturated imidazolinylidenes, due to the additional anti-bonding interaction with the backbone π-bond leading to destabilisation of the LUMO.[27]

4.1.2 *N*-Heterocyclic Carbene Boron Trifluoride Adducts

Of the numerous examples of carbene boron complexes,[2] carbene stabilised trifluoroboranes have been noted for their exceptional stability. In 2000, Arduengo *et al.* synthesised the *N*-heterocyclic carbene-boron trifluoride adduct **4.i** (NHC-BF_3, Scheme 4.1) *via* a facile synthesis using the free carbene and boron trifluoride etherate.[32] Then in 2012, Tian *et al.* noted that a related adduct **4.ii**, could be synthesised by vigorously heating the respective imidazolium tetrafluoroborate salt under vacuum. This system was also reported to be both air- and moisture-stable and could be recrystallised from boiling water without any noticeable hydrolysis.[33]

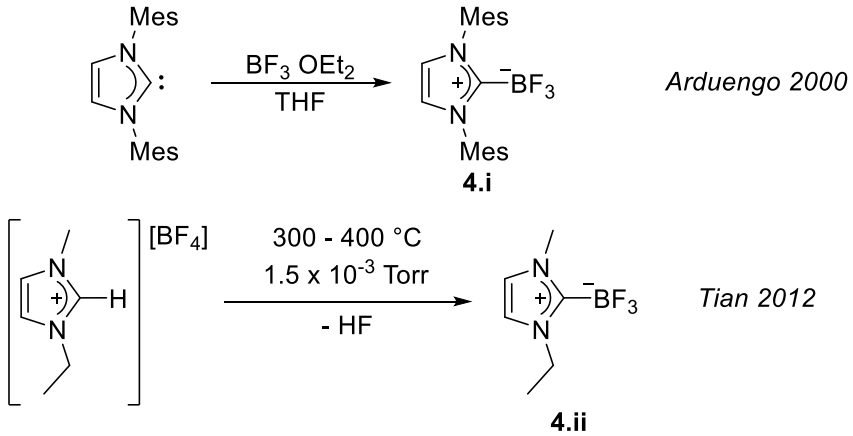

Scheme 4.1 – NHC-BF_3 synthesise

The apparent stability of NHC-BF_3 adducts inspired Gabbaï and co-workers to investigate their application for PET imaging.[34,35] In 2015, Chansaenpak *et al.* described the synthesis of the nitro functionalised adduct **4.iv**, from the respective silver(I) iodide salt, and its conversion into the maleimide derivative **4.vi** (Scheme 4.2).[34] Assessment of the water

stability of the series **4.iii – 4.vi**, in phosphate buffered 8:2 D_2O/CD_3CN (pH 7.5), revealed exceptionally high stability throughout. In particular, **4.iv** and **4.vi** were described as "essentially immortal" with ^{19}F NMR monitoring showing no signs of free fluoride after a week. **4.iii** and **4.v** showed traces of free fluoride, and therefore hydrolysis, over the same time-period with rates of hydrolysis subsequently calculated to be 1.1 – 1.2 x 10^{-6} min^{-1}. The higher resilience of **4.iv** and **4.vi** was attributed to the electron withdrawing substituents attached to the carbene backbone, leading to increased Lewis acidity at the boron centre. The highly robust nature of these NHC-BF_3 adducts was further corroborated with bioconjugates of [^{18}F]**4.iv**, that were labelled *via* $SnCl_4$ promoted isotopic exchange, and which demonstrated negligible uptake of free fluoride by the skeletal system *in vivo*.[34,35]

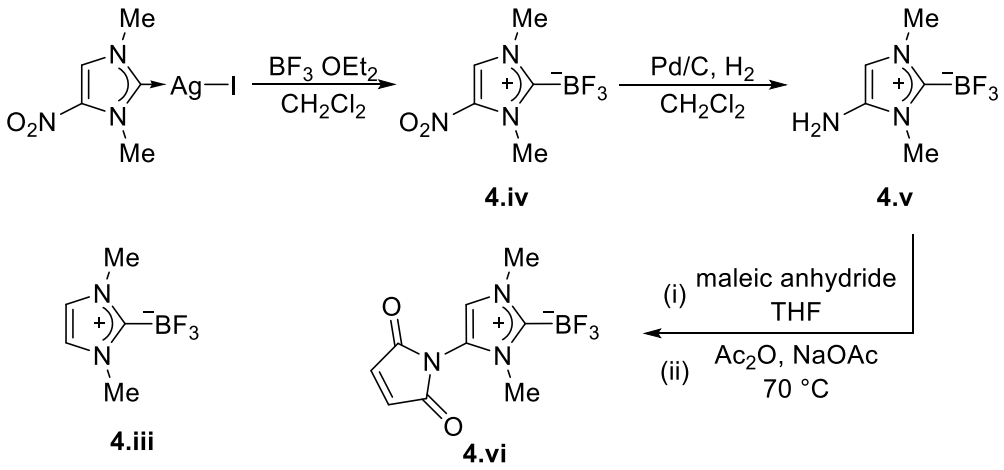

Scheme 4.2 – Synthetic route to maleimide functionalised NHC-BF_3 **4.vi**

4.2 Aims

Chansaenpak *et al.* demonstrated the ability of NHC-BF_3 systems to form attractive prosthetic groups for ^{18}F-PET imaging with labelling at a late stage and exceptional *in vivo* stability. To fully exploit the utility of these systems, additional bioconjugation strategies are sought to enable the labelling of a greater range of biologically relevant molecules. The modular design of NHCs lend themselves to this purpose, with the interchangeable nature of the carbene backbone and nitrogen substituents providing numerous opportunities for

functionalisation. Therefore, in line with our third project objective, the work in this chapter will explore how greater versatility may be achieved with NHC-BF_3 systems by variation of the NHC donor and the introduction of groups for bioconjugation.

Changes to the NHC backbone were noted by Chansaenpak *et al.* to impact the stability of the NHC-BF_3 compounds. Consequently, this chapter will first explore the hydrolytic stability of a series of NHC-BF_3 compounds utilising carbene donors that could form the basis of future functionalised systems. By making systematic changes to the carbene ring size and saturation, the stability of these systems will be probed and thereby indicate whether a carbene other than imidazolylidene can be employed without compromising adduct robustness.

This chapter will also explore functionalisation *via* the nitrogen substituents of the NHC-BF_3 systems. *N*-substituted imidazoles are an accessible building block for this endeavour, with the nucleophilic nitrogen providing a convenient point onto which a pendant functional group maybe tethered. Hence work will seek to incorporate an alkyne functional group at this position and explore its utility for copper catalysed click chemistry for bioconjugation.

4.3 Simple Carbene Boron Trifluoride Adducts

4.3.1 Synthesis and Characterisation

The series of carbene-BF_3 adducts **4.1** depicted in Scheme 4.3 was synthesised *via* simple coordination reactions of the free carbenes with boron trifluoride etherate in diethyl ether. The known IMes derivative **4.i**, was also synthesised as an imidazolylidene-based comparison.[32] Adduct formation was confirmed by the observable B–F coupling in the heteronuclear NMR spectra: a 1:3:3:1 quartet in the ^{11}B NMR spectrum at *ca.* 0 ppm and a

1:1:1:1 quartet in the ^{19}F NMR spectrum with coupling constants $^{1}J_{BF}$ in the range 31 – 38 Hz (Table 4.1).

The molecular structures of **4.1^{6Mes}** and **4.1^{7Dipp}** were obtained from X-ray crystallography using crystals grown from THF and hot methanol respectively. The structures feature some disorder, with the positions of the fluorine atoms rotationally disordered around the boron centre, and disorder of the carbene backbones being modelled by two components. The B–C bond of **4.1^{7Dipp}** at 1.698(5) Å is slightly longer than that observed in previously reported imidazolylidene NHC-BF_3 adducts (1.63 – 1.66 Å, Table 4.1). This elongation may be attributed to the less bent carbene centre in 7Dipp giving rise to a donor orbital with a higher *p*-character.

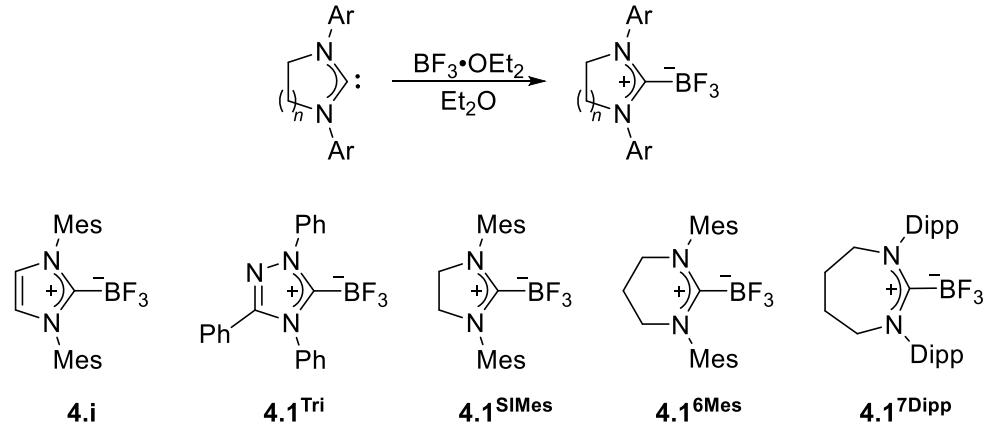

Scheme 4.3 – The NHC-BF_3 **4.1** series and their synthetic procedure.

	^{19}F NMR (ppm)	$^{1}J_{BF}$ (Hz)	d(C–B) (Å)
4.i [32]	-143.7	34.2	1.6346
4.iii [34]	-139.2	37.0	1.637(5), 1.641(3)
4.vi [34]	-138.5	35.6	1.656(9)
4.1^{Tri}	-136.8	31.5	–
4.1^{SIMes}	-143.8	35.5	–
4.1^{6Mes}	-141.8	37.3	1.657(8)
4.1^{7Dipp}	-135.7	36.9	1.698(5)

Table 4.1 – NMR and structural information for NHC-BF_3 compounds.

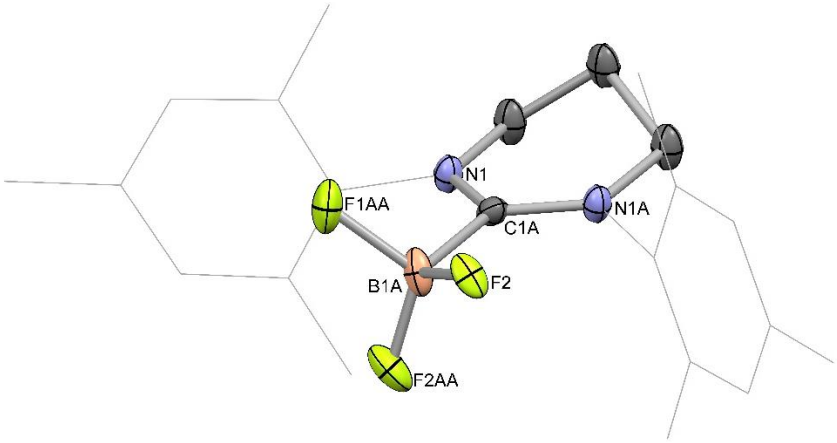

Figure 4.4 – Molecular structure of **4.1**^{6Mes} with thermal ellipsoids set at the 40 % probability level. Mesityl groups are represented as wireframe and hydrogens and second disorder component are omitted for clarity. Selected bond length (Å) and angles (°): B1A–F2 1.47(1), B1A–F1AA 1.439(9), B1A–F2AA 1.33(1), C1A–N1 1.335(7), C1A–N1A 1.336(7), N1–C1A–N1A 109.0(4).

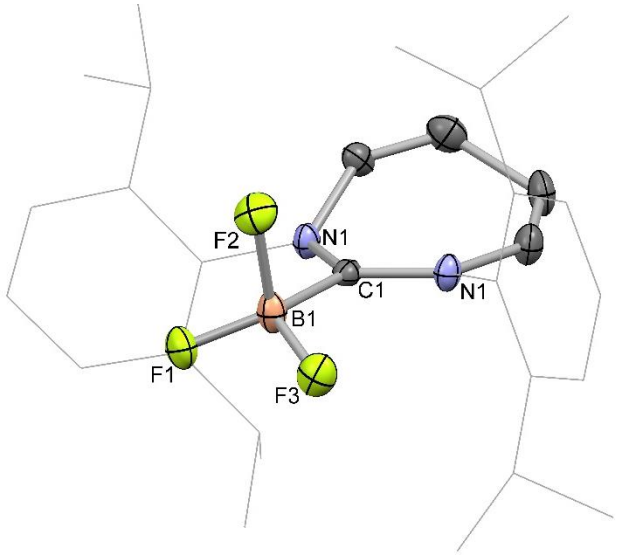

Figure 4.5 – Molecular structure of **4.1**^{7Dipp} with thermal ellipsoids set at the 40 % probability level. Dipp groups are represented as wireframe and hydrogens and second disorder component are omitted for clarity. Selected bond length (Å) and angles (°): B1–F1 1.35(2), B1–F2 1.529(16), B1–F3 1.326(11), C1–N1 1.338(2), N1–C1–N1 119.4(3).

4.3.2 Stability

Water stability studies with compounds of the type **4.1** were conducted in 9:1 DMF-water on solutions of 5 mM concentration. The samples were monitored *via* ^{19}F NMR over the course of several weeks, with samples stored in polypropylene tubes to limit fluoride sequestration by glass over this period. With the exception of **4.1**^{Tri}, all samples remain

unchanged over a period of five weeks with no sign of free fluoride or other degradation products detected. The low percentage of water used in these experiments precludes comparisons with other trifluoroborates that were tested in predominantly aqueous solutions, given that higher percentage of water have been demonstrated to increase the rates of trifluoroborate hydrolysis.[36] Unfortunately, the choice of conditions was greatly restricted by the poor solubility of the adducts, especially **4.1**$^{\mathbf{SIMes}}$, in water and water miscible solvents. Whilst the conditions did not allow any changes in adduct stability with differing donor characteristics to be discerned, these experiments did confirm that NHCs with hydrocarbon backbones collectively yield boron trifluoride adducts that are highly resistant to hydrolysis in the presence of water.

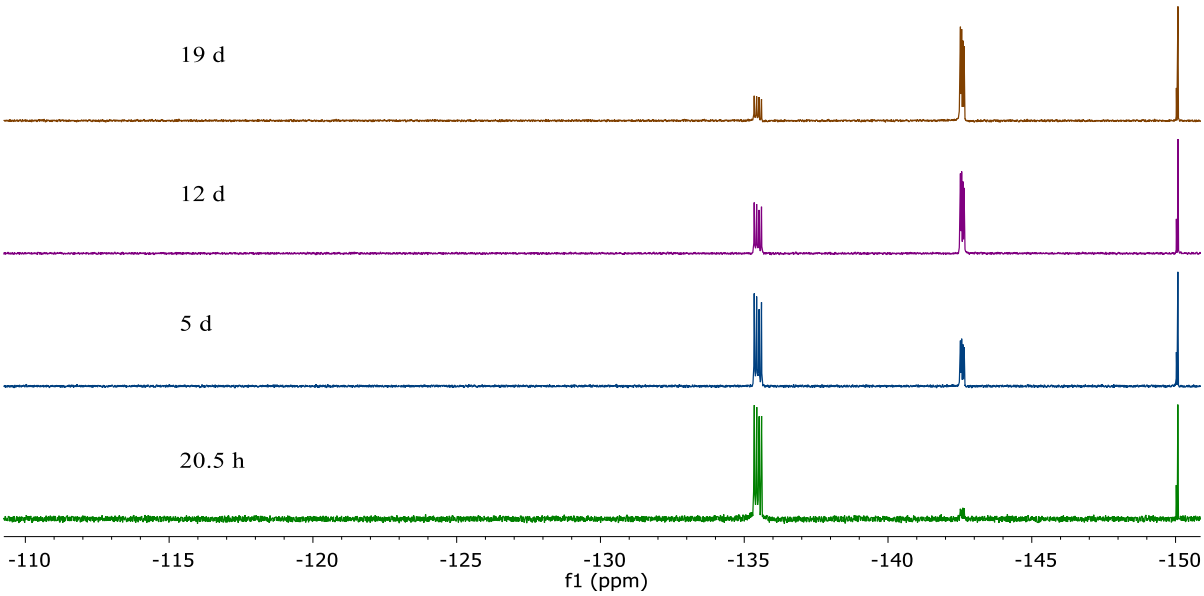

Figure 4.6 – ^{19}F NMR spectra of the hydrolysis reaction of **4.1**$^{\mathbf{Tri}}$ over time.

The outlier of the series, **4.1**$^{\mathbf{Tri}}$, was however observed to degrade over three weeks forming a new fluoroborane compound. The new species appears in the ^{19}F NMR as a quartet at -142.6 ppm ($^{1}J_{BF}$ = 16.1 Hz, Figure 4.6) with a corresponding quartet observed in the ^{11}B NMR spectrum at 1 ppm, indicating the new species involves a -BF_3 group. It is therefore suggested that the new species is the $[BF_3(OH)]^-$ anion, resulting from a proto-deboronation reaction between water and **4.1**$^{\mathbf{Tri}}$ that also generates the protonated carbene.

Proto-deboronation may occur either by protonation of the carbenic carbon, followed by B–C bond cleavage or by the concerted addition of an O–H bond across the B–C bond. The occurrence of this unexpected degradation pathway, rather than the typical trifluoroborane hydrolysis involving fluoride dissociation and boronic acid formation, may be the consequence of two effects. Firstly, the zwitterionic compound highly disfavours the initial fluoride dissociation that is the rate determining step of the "usual" hydrolysis pathway. Secondly, carbene donation may be affected by interactions occurring at the backbone nitrogen that consequently favour protodeboronation. The weakly basic lone pair of the backbone nitrogen likely participates in hydrogen bonding with water, increasing the degree to which the compound is hydrated and favouring decomposition. Moreover, donation from the backbone nitrogen would lower the electron density at the carbene, weakening the donation of the carbene to the boron centre and making the B–C bond increasingly labile.

4.4 Alkyne Appended NHC-BF_3 Adducts

4.4.1 Imidazolium Salts: Synthesis and Characterisation

Known *N*-prop-2-ynyl appended imidazolium salts were considered an ideal starting point for introducing a pendent alkyne group into the *N*-heterocyclic carbene framework. **[4.2^{Mes}]Br** and **[4.2^{CH3}]Br** were prepared according to literature procedure by combining the relevant *N*-substituted imidazole with propargyl bromide and either stirring at room temperature or refluxing for several days as described by Warsink *et al.*[37] and Ravula *et al.*[38] respectively (Scheme 4.4). Noteworthy characteristic ^{1}H NMR signals of these compounds are those attributed to the prop-2-ynyl functional group: a two-proton doublet between 5 and 6 ppm for the bridging methylene group and a single-proton triplet in the 2 – 3 ppm range for the terminal methine group. Exchange of the bromide counterion for tetrafluoroborate (brought about by stirring the **[4.2]Br** salts with sodium tetrafluoroborate in methanol/water) also facilitated the crystallographic characterisation of cation **4.2^{Mes}** (Figure

4.7). Slow evaporation from a chloroform solution of **[4.2^{Mes}][BF$_4$]** yielded crystals from which the structure shown in Figure 4.7 could be obtained. This imidazolium structure features a terminal alkyne triple bond (1.180(2) Å) and a C–C single bond linking the pendant alkyne to the heterocycle (C4–C5 1.460(2) Å).

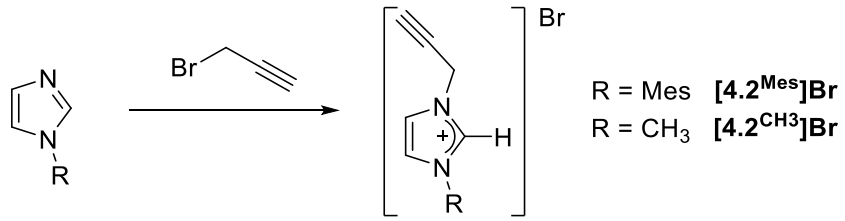

Scheme 4.4 – Synthesis of alkyne appended imidazolium bromide salts [**4.2**]**Br**
Conditions for R = Mes: MeCN, 82 °C. Conditions for R = CH_3: Toluene, room temperature.

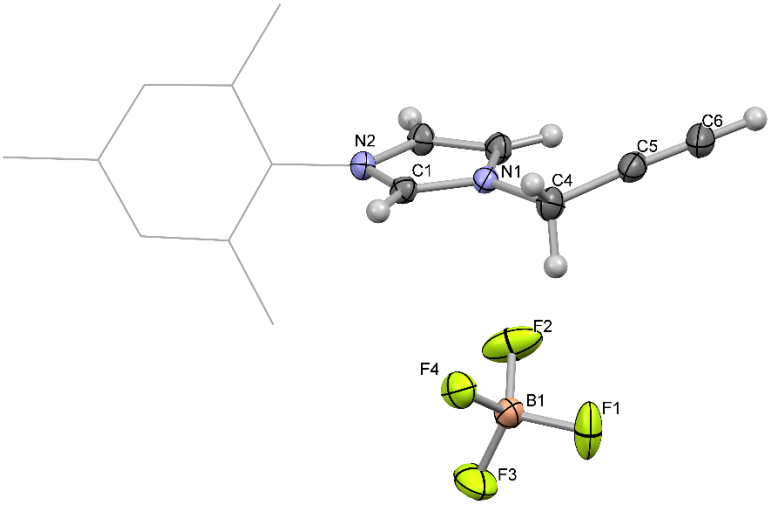

Figure 4.7 – Solid state structure of **[4.2^{Mes}][BF$_4$]**. Thermal ellipsoids are set at 40 % probability level. The mesityl group is represented in wireframe and some hydrogens are omitted for clarity. Key bond lengths (Å): C4–C5 1.460(2), C5–C6 1.180(2), N1–C4 1.478(2), N1–C1 1.327(1), N2–C1 1.334(2).

An allene derivative, **[4.3][BPh$_4$]**, was also unexpectedly isolated from another anion exchange reaction when **[4.2^{Mes}]Br** was combined with sodium tetraphenylborate in ethanol and acetonitrile and stirred overnight before work up. The ^{1}H NMR spectrum revealed that the expected doublet and highfield triplet signals of the propargyl group, had shifted to 5.90 ppm and 7.24 ppm respectively, with $^4J_{HH}$ = 6.5 Hz coupling. Crystallographic characterisation of the salt **[4.3][BPh$_4$]** (Figure 4.8) reveals that the C–C bonds of the

pendant arm are also of comparable length and consistent with two double bonds (1.294(3) Å and 1.287(3) Å). The isomerisation of the structure was attributed to a base catalysed rearrangement with the ^{1}H NMR shifts of the methylene groups in cations **4.2^{Mes}** and **4.2^{CH3}** (*ca.* 5.2 ppm) signalling that these protons are relatively acidic, and therefore susceptible to migration.[39] Use of an alternative source of sodium tetraphenylborate and a shorter reaction time of 40 minutes did subsequently yield **[4.2^{Mes}][BPh$_4$]** without the accompanying alkyne to allene rearrangement.

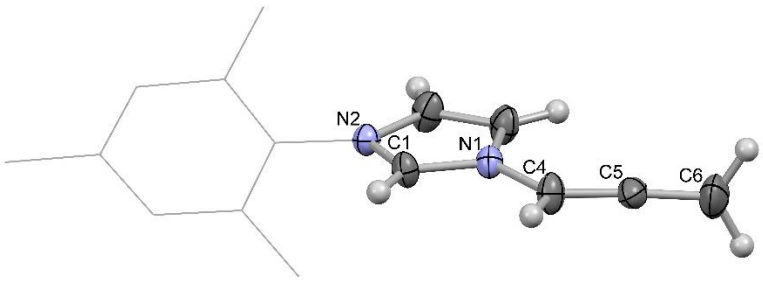

Figure 4.8 – Molecular structure of allene derivative **[4.3][BPh$_4$]**. Thermal ellipsoids are set at 40 % probability level. Mesityl group is represented in wireframe and some hydrogens are omitted for clarity. Selected bond lengths (Å): N1–C4 1.427(2), C4–C5 1.294(3), C5–C6 1.287(3), N1–C1 1.332(2), N2–C1 1.326(2).

The triazole appended imidazolium salt **[4.4][BF$_4$]** was also synthesised *via* a CuAAC reaction with **[4.2^{Mes}][BF$_4$]** (Scheme 4.5). Hence the respective alkyne-appended imidazolium salt was combined with 2,6-diisopropylphenylazide (DippN$_3$), stoichiometric copper(II) sulfate and sodium ascorbate and heated to 60 °C to synthesise **[4.4][BF$_4$]** in an adaption of the method described by Warsink *et al.*.[37] NMR characterising data for **[4.4][BF$_4$]** is comparable to that previously reported for the related bromide salt, with the ^{1}H NMR spectrum featuring a characteristic low field triazole singlet at 8.30 ppm and the bridging methylene group now represented by a singlet at 5.87 ppm. Slow evaporation of a chloroform solution of **[4.4][BF$_4$]** produced crystals suitable for X-ray diffraction allowing crystallographic characterisation of the **[4.4]$^{+}$** cation for the first time.

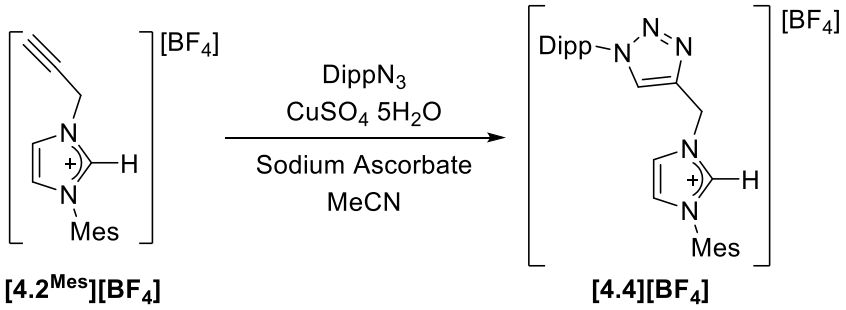

Scheme 4.5 – CuAAC synthesis of the triazole appended imidazolium salt **[4.4][BF$_4$]**.

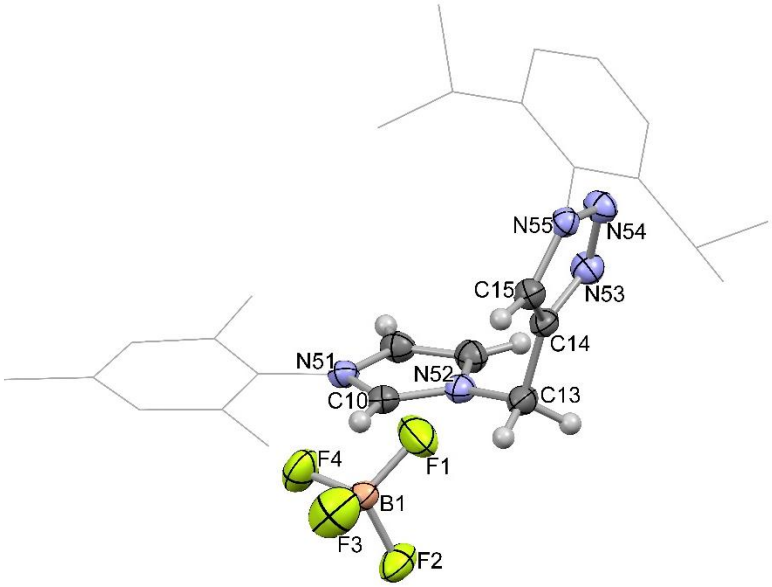

Figure 4.9 – Solid state structure of **[4.4][BF$_4$]** as determined by X-ray crystallography. Thermal ellipsoids are set at 40 % probability level. Mesityl and Dipp groups are wireframe and some hydrogens have been omitted for clarity. Selected bond lengths (Å): C13–C14 1.501(4), C14–C15 1.363(4), C10–N51 1.333(3), C10–N52 1.331(4), N52–C13 1.475(4).

4.4.2 NHC-BF$_3$ Synthesis *via* a Silver Transfer Reagent

Initial endeavours to synthesise the boron trifluoride adducts of the alkyne-appended imidazolium salt **[4.2^{Mes}]Br** proceeded *via* a silver transfer reagent. The silver salt of **[4.2^{Mes}]Br** in Scheme 4.6 was prepared according to the report of Warsink *et al.* using silver oxide.[37] The bis-carbene silver(I) complex was then reacted with boron trifluoride etherate in dichloromethane over the course of five days yielding the desired adduct **4.5^{Mes}**, as confirmed by the diagnostic quartets in the ^{11}B NMR and ^{19}F NMR spectra. However, poor yields for the adduct formation step (< 15 %) and the low-yielding transfer agent synthesis

limited further investigation of the click chemistry of these systems. A more efficient route to these functionalised NHC-BF_3 adducts was therefore sought.

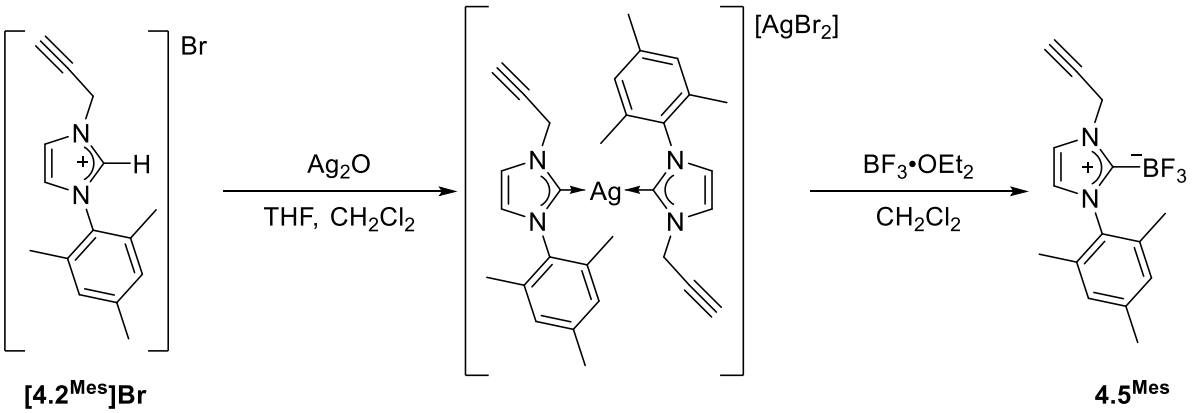

[4.2^{Mes}]Br **4.5^{Mes}**

Scheme 4.6 - Synthesis of boron trifluoride adduct **4.5^{Mes}** from **[4.2^{Mes}]Br** *via* a silver transfer salt.

4.4.3 NHC-BF_3 Synthesis *via* Imidazolium Salt Deprotonation

A range of conditions and bases were applied to both **[4.2^{Mes}][BF_4]** and **[4.4][BF_4]** in efforts to isolate the respective NHC-BF_3 systems *via* deprotonation routes. The tetrafluoroborate salts were used for these reactions as the bromide salts are known to be more susceptible to degradation in carbene synthesis.[40] K[N($SiMe_3$)$_2$] proved to be an unsuitable choice of base for both imidazolium salts. Reaction mixtures at room temperature or at -78 °C in THF rapidly turned black and produced intractable mixtures of unidentifiable products. The absence of signals for the acidic imidazolium protons, in the ^{1}H NMR spectra of the products, did however indicate that deprotonation had occurred. The mixture of products was therefore tentatively attributed to the reactions of the generated carbene with other reactive functional groups present in the molecule. For example NHCs have been demonstrated to cyclise with alkynes to form cyclopropenes.[41]

On the other hand, reacting **[4.4][BF_4]** with lithium bis(trimethylsilyl)amide, in THF at -78 °C, does cleanly yield a single product **4.6**, albeit as a brown oily solid. **4.6** can be warmed to room temperature without immediate decomposition but was observed to subsequently degrade over several days. ^{1}H NMR characterisation of the freshly isolated product, depicted in Figure 4.10, clearly shows a loss of the characteristic low field

imidazolium proton, along with minor broadening of the methylene and triazole signals and retention of some THF. The ^{13}C NMR spectrum also features a weak broad signal at 199 ppm which is shifted marginally upfield compared to that usually observed for free carbenes (*ca.* 210 ppm). The small shift in the carbene signal is however consistent with previously reported lithium carbene adducts which have reported signals between 186.3 ppm and 206.5 ppm.[42–44] The formation of a lithium complex has also previously been noted to help inhibit degradation with similar carbene compounds.[37,42,43] The moderate stability of the complex is likely due to chelation involving the pendant triazole function and, to a lesser extent, coordination by THF (Figure 4.10).

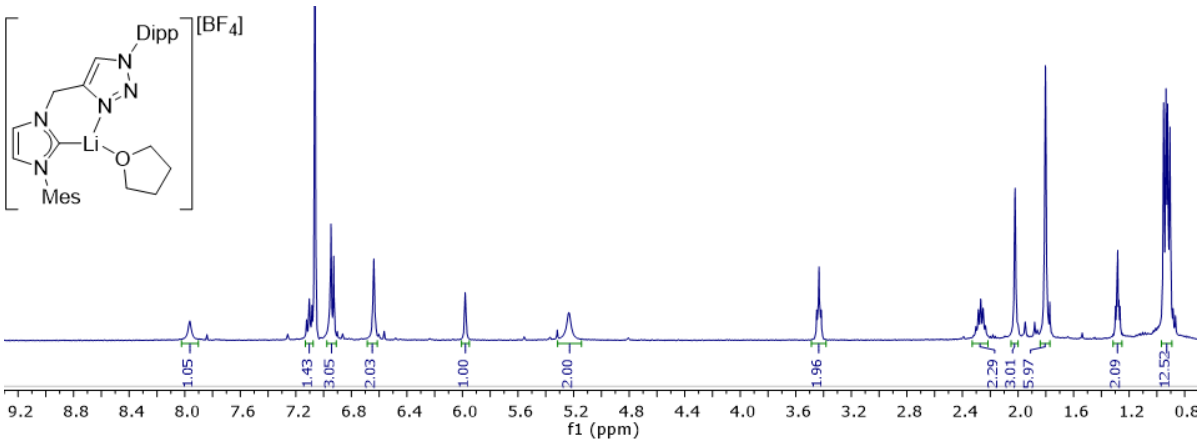

Figure 4.10 – Proposed structure of **4.6** and ^{1}H NMR (C_6D_6) of the product from the reaction of LiHMDS and **[4.4][BF$_4$]**

Combining **4.6** with an excess of boron trifluoride etherate produces the desired NHC-BF_3 adduct **4.7**, as confirmed by heteronuclear NMR (Scheme 4.7). The characteristic ^{19}F NMR quartet for the adduct appears at -140.6 ppm ($^{1}J_{BF}$ = 34.7 Hz) with the corresponding ^{11}B NMR quartet being found at 0 ppm. **4.7** was subsequently synthesised in greater purity by generating the lithium complex *in situ* at -78 °C and maintaining low temperature until the boron trifluoride etherate had been added, thereby minimising degradation of the intermediate, and producing the clean product in a quantitative yield. Slow evaporation of a toluene solution of **4.7** also yielded crystals suitable for X-ray crystallography. The resulting structure, depicted in Figure 4.11, features a carbene unit that

is essentially unchanged from the imidazolium salt and features a C12–B1 bond length of 1.67(1) Å, similar to previous imidazolylidene boron trifluoride adducts (Table 4.1).

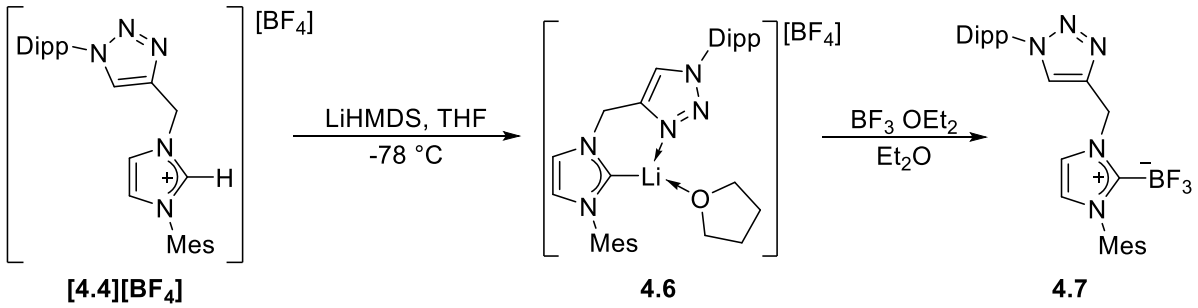

Scheme 4.7 – Synthesis of lithium complex **4.6** and NHC-BF_3 adduct **4.7**

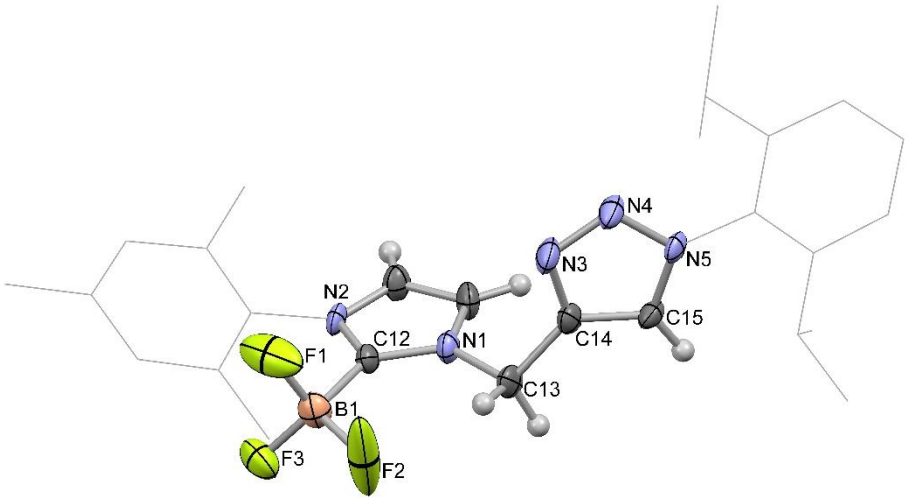

Figure 4.11 – Molecular structure of **4.7**. Thermal ellipsoids are set to 40 % probability level. The Mesityl and Dipp groups are wireframe and some hydrogens have been omitted for clarity. Selected bond lengths (Å): C12–B1 1.67(1), B1–F1 1.36(1), B1–F2 1.33(1), B1–F3 1.37(1).

Lithium bis(trimethylsilyl)amide was also successfully utilised for *in situ* deprotonations of the alkyne-appended imidazolium salts. The imidazolium salts were stirred with 1.1 equivalents of the lithium base at -78 °C in THF and the reaction mixture in each case maintained at low temperature until excess boron trifluoride etherate had been added. This procedure produces both **4.5^{Mes}** and **4.5^{CH3}** in yields greater than 75 %, *i.e.* markedly better than that achieved with the silver transfer agent. The diagnostic heteronuclear quartets are observed at 0 ppm in the ^{11}B NMR spectra and at -141.8 ppm ($^1J_{BF}$ = 34.7 Hz) and -139.8 ppm ($^1J_{BF}$ = 35.7 ppm) in the ^{19}F NMR spectra for **4.5^{Mes}** and **4.5^{CH3}** respectively. The ^{1}H NMR spectrum also shows clean conversion has occurred, with retention of the alkyne

functional groups confirmed by the characteristic doublet and high-field triplet. The absence of the problematic degradation that was observed with the potassium base upon deprotonation, suggests a lithium carbene complex again forms as an intermediate. Attempts to isolate the product of the lithium bis(trimethylsilyl)amide deprotonation however were hindered by low thermal stability, as indicated by a rapid colour change from near colourless to dark brown upon warming to room temperature from -78 °C. It is anticipated that without a pendant donor group, such as the triazole in **4.6**, to provide additional coordination, any complexation of lithium is likely to be relatively weak. Additional attempts to stabilise the complex by including TMEDA in the reaction as a lithium chelator were also unsuccessful.

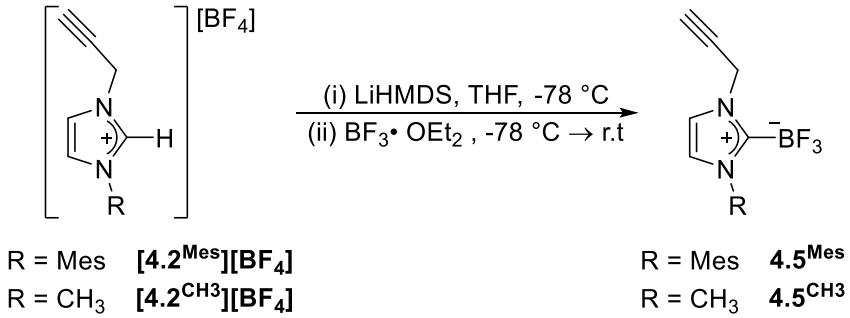

Scheme 4.8 – Synthesis of the alkyne appended NHC-BF_3 adducts

Crystals of **4.5^{Mes}** suitable for X-ray crystallography were obtained from a concentrated THF solution. The resulting asymmetric unit contains two similar molecules of **4.5^{Mes}**, one of which is depicted in Figure 4.12. The B–C bond lengths (1.648(6) Å and 1.651(6) Å) are directly comparable to that of previous imidazolylidene boron trifluoride adducts (Table 4.1). The B–F bonds average to 1.377 Å, *i.e.* similar to previous structures. Additionally, the carbene unit shows no significant changes compared to the imidazolium salt present in **[4.2^{Mes}][BF$_4$]** with the terminal triple bonds averaging to 1.173 Å and the propargyl single bonds averaging to 1.463 Å.

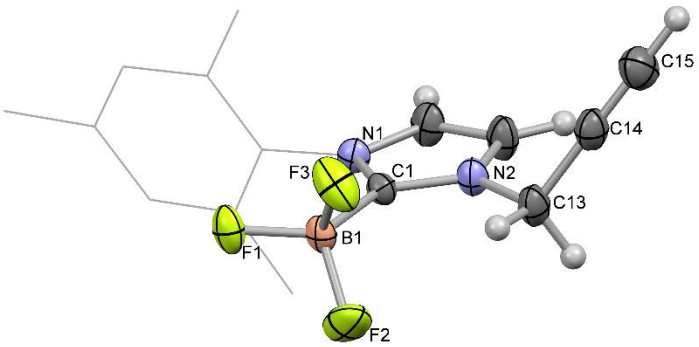

Figure 4.12 – Molecular structure of **4.5^{Mes}**; showing one of two molecules in the asymmetric unit. Thermal ellipsoids are set to 40 % probability level. The mesityl group is wireframe and some hydrogens have been omitted for clarity. Selected bond lengths (Å): C1–B1 1.648(6), C13–C14 1.464(6), C14–C15 1.178(7), B1–F1 1.388(6), B1–F2 1.373(6), B1–F3 1.389(6), C16–B2 1.651(6), C28–C29 1.462(6), C29–C30 1.168(7).

4.4.4 Water Stability

The water stability of both compounds of type **4.5** was assessed in a 4:6 acetonitrile-PBS (0.01 M, pH 7.5) solvent mixture, with solutions made up to 10 mM concentration and sonicated for 30 s to ensure solubility. The reactions were monitored over a period of ten days by ^{19}F NMR, whereupon trace quantities of free fluoride were observed at -119.6 ppm. Hydrolysis is exceptionally slow however, with 98.7 % of **4.5^{Mes}** and 97.4 % of **4.5^{CH3}** remaining after 10 days in solution; based upon the proportion of the free fluoride and NHC-BF_3 signals in the ^{19}F NMR spectra. The greater resilience of **4.5^{Mes}** to solvolysis may stem from the compound experiencing a lower degree of hydration than the **4.5^{CH3}** analogue, due to the lipophilic character of the mesityl group.

4.4.5 Click Reactions

With compounds of the type **4.5** in hand, the click chemistry of the pendant alkyne function could be explored. As for the synthesis of **[4.4][BF_4]**, stoichiometric quantities of copper (II) sulfate pentahydrate and sodium ascorbate were warmed to 60 °C in acetonitrile before **4.5^{Mes}** and diisopropylphenylazide were added (Scheme 4.9). The reaction was monitored *via* ^{19}F NMR, with the quartet for **4.7** arising at -138.9 ppm, marginally downfield

shifted with respect to **4.5^{Mes}** at -139.5 ppm. Additionally, no signs of degradation products were observed, confirming the NHC-BF_3 group is robust to these reaction conditions. The product was subsequently isolated and confirmed to be **4.7** by ^{1}H NMR spectroscopy, with the characteristic triazole singlet appearing at 8.06 ppm and methylene singlet being found at 5.82 ppm. Additionally, the product is identified in positive mode ESI-MS by the $[M+Na]^+$ molecular ion at *m/z* 518.2672. The pure product was obtained in a 45 % yield, thereby establishing that the click reaction is a more efficient route to **4.7** than that involving the deprotonation of the respective imidazolium salt. Moreover, unlike the harsh, basic conditions required for deprotonation and adduct formation, the comparatively mild conditions of the click reaction should be compatible with more sophisticated, biologically relevant molecules.

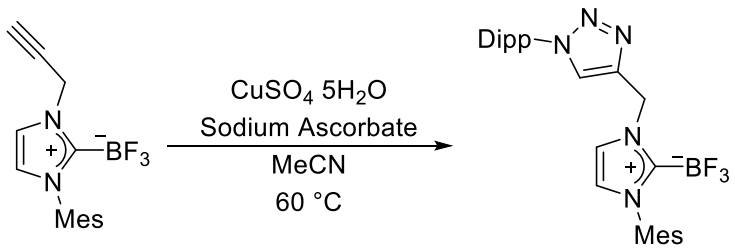

4.5^{Mes} **4.7**

Scheme 4.9 – CuAAC click reaction with alkyne appended NHC-BF_3 **4.5^{Mes}**.

4.5 Folic Acid Conjugation

Folate receptors (FR) are biomarkers of interest in clinical and research medicine as both an imaging and a therapeutic target. Of the four known receptor isoforms, the membrane bound FR-α and FR-β isoforms are of primary interest as medical targets.[45–47] FR-α is the most widely expressed of the isoforms, and is of particular interest in oncology with 100 – 300 times greater expression on tumour cells than healthy cells.[48,49] Meanwhile, the expression of the FR-β isoform, on activated macrophages and other hematopoietic cells

with myeloid lineage, has made it a point of investigation for inflammatory diseases such as rheumatoid arthritis.[47,50,51]

The high binding affinity of these folate receptors for folic acid (K_D ~ 1 nM) has been exploited in the design of therapeutic and imaging agents targeting the receptors.[49,52,53] One of a family of folate molecules, folic acid is a non-immunogenic compound comprised of pteroic acid and glutamic acid moieties (Figure 4.13). Folic acid can be internalised into cells by receptor mediated endocytosis with folate receptor binding interactions occurring *via* the pteroate moiety of the structure.[54] The exposed glutamate moiety can therefore be functionalised at either the α- or γ- carboxylic acid groups without impacting the binding affinity.[54,55] Groups appended in this manner include therapeutics attached with a releasable linker, and molecules for imaging such as fluorophores for optical imaging and metal chelates for SPECT and PET.[52,53,56,57]

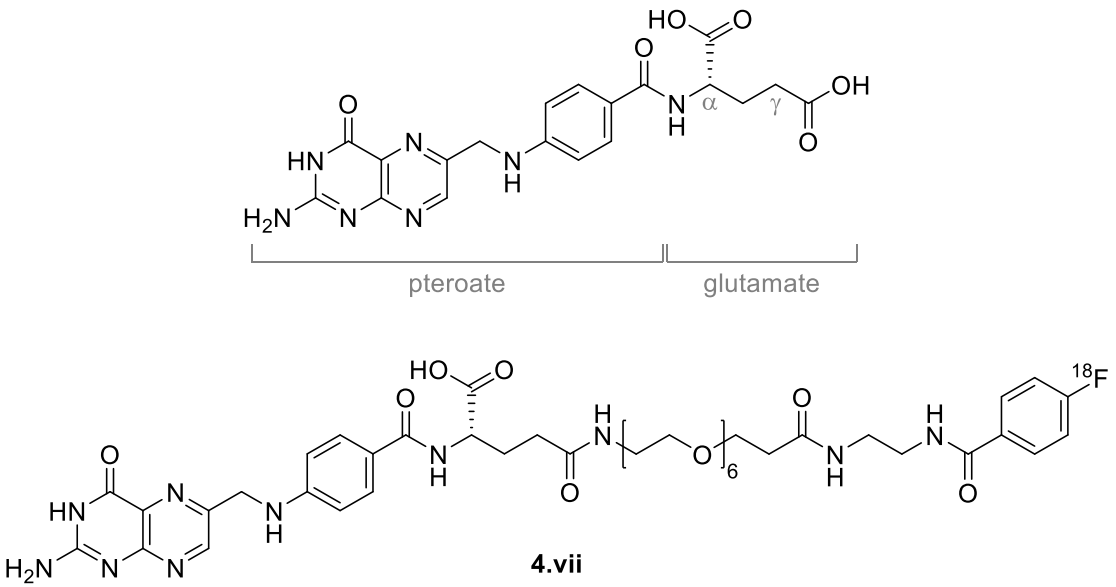

Figure 4.13 – Folic acid (top) and the derivative [^{18}F]fluoro-PEG-folate (**4.vii**) which is used to image rheumatoid arthritis.

Folic acid conjugated PET tracers have also included [^{18}F]fluoride labelled examples; these were recently reviewed by Boss and Ametamey in 2020.[52] Briefly, radiolabelling has been achieved by two methods: directly fluorinating the folic acid molecule[58,59] or by

conjugation of a radiolabelled prosthetic group to the glutamate moiety.[55,60–66] Indeed, the appended example [^{18}F]fluoro-PEG-folate (**4.vii**, Figure 4.13) has recently demonstrated promising first-in-human results for imaging rheumatoid arthritis by targeting the FR-β unit on macrophages.[67] However, [^{18}F]folate conjugates often involve multistep radiosynthesis, low radiochemical yields or unfavourable biodistributions with high uptake by the abdomen, liver or kidneys leading to poor signal-to-noise ratios. Efforts to overcome unfavourable biodistributions have involved reducing the lipophilicity, to lower uptake by the gastrointestinal system, and the utilisation of linkers which help increase circulation time.[61–64] Meanwhile, approaches to simplify radiosynthesis and improve labelling efficiency have included the use of prosthetic groups suited to late-stage labelling, such as an Al–^{18}F NOTA complex.[65,66] A folic acid conjugate of our alkyne-appended NHC-BF_3 systems was thus targeted. In addition to providing an opportunity to verify the application of our compounds of the type **4.5**, it was anticipated the late-stage, isotopic exchange labelling offered by NHC-BF_3 adducts could prove advantageous for addressing the synthetic challenges of folate.

4.5.1 Folic Acid-PEG-Azide: Synthesis and Characterisation

To enable click chemistry with the alkyne functionalised NHC-BF_3 molecules, an azide group was appended onto the folic acid core. A poly-ethylene glycol (PEG) chain was used as the linker to achieve this, as it exhibits properties beneficial to the pharmacokinetics of the target compound, and should help increase the hydrophilicity of the folic acid which has a notoriously low solubility in water.[68,69] The previously reported folic acid-PEG-azide conjugate **4.8^{2}** was consequently prepared, along with a longer PEG chain derivative **4.8^{5}** *via* an adaptation of the synthesis described by Ke *et al.* (Scheme 4.10).[70] Accordingly, the required amine-PEG-azide chains were first synthesised, based on literature procedure, from the respective polyethylene glycols, before DCC-mediated coupling to the folic acid

carboxylic acid groups was achieved.[71] Additional purification was accomplished by column chromatography to remove minor quantities of unreacted starting material and bis-substituted folic acid, in addition to some product cleaved of the pterin moiety. The new compound, **4.8^5** was characterised by its protonated molecular ion in positive mode electron spray mass spectrometry at *m/z* 730.3262.

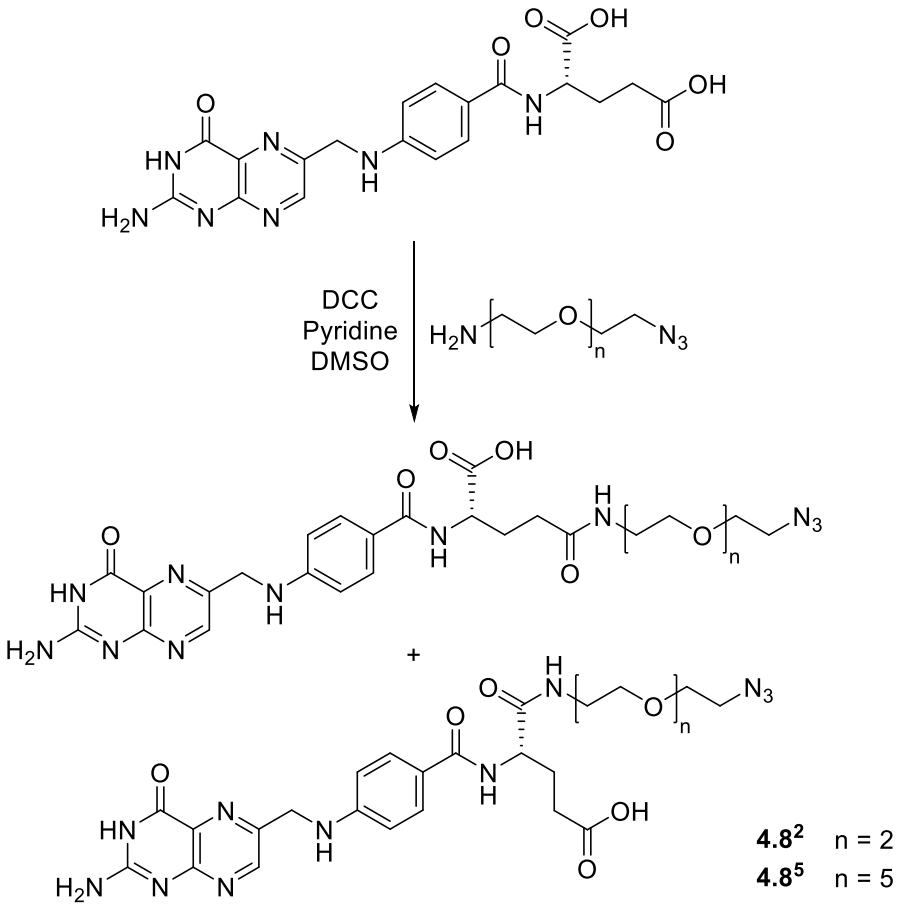

Scheme 4.10 – Synthesis of azide conjugated folic acid compounds **4.8**.

This synthetic route to the folic acid-PEG-azide conjugates is non-selective, producing a mixture of the α- and γ- coupled products (Scheme 4.10). In our hands, the two regioisomers could not be resolved by HPLC, however it is generally accepted that reactions at the α-position are disfavoured on steric grounds and the γ-substituted product should dominate.[60,70] For the purposes of this study, a mixture of regioisomers was acceptable as the substitution position has previously been demonstrated to have no impact on the binding affinity with the folate receptors.[55] It is worth noting however that in a comparative study of

α- and γ-functionalised systems, the *in vivo* biodistribution did vary slightly with differing background uptake, attributed to the presence of other folate transporting structures in the body.[55]

4.5.2 Click Chemistry

The generally low solubility of the folic acid derivatives in solvents other than DMSO initially challenged the scale and purification of the click reaction. However, with its combination of acidic and basic groups, folic acid is responsive to changes in solution pH and can exist in a number of different ionic forms which are noted for their differing solubilities.[69] Solubility issues were thus mitigated upon basifying the reactions to pH 9, above the pKa of the cyclic amide group (pKa ~ 8.4), to produce an anionic form of folic acid that exhibits a marked increase in water solubility and overall solvent compatibility.[72] Additionally, subsequent acidification of basic aqueous solutions of the folic acid derivatives to pH 2 leads to precipitation, aiding purification from the water-soluble salts involved in the click reaction. With the limited solubility of folic acid compounds in mind, the longer PEG chain derivative **4.8^{5}** was prioritised for conjugation, to maximise the aqueous solubility of the target product. Similarly, the water-soluble methylated derivative **4.5^{CH3}** was also prioritised to help limit the lipophilicity of the target product.

Effective CuAAC reaction conditions were subsequently identified, employing methanol and a 0.1 M sodium hydroxide solution as the reaction medium. The reactions were also established to be amenable to lower copper percentages than the stoichiometric quantities previously applied in section 4.4.5. Hence, **4.9** was synthesised by combining **4.5^{CH3}** with 0.25 equivalents of copper (II) sulfate and 0.75 equivalents of sodium ascorbate in methanol before addition of the azide **4.8^{5}** as a basic aqueous solution (Scheme 4.11). The reaction may be monitored by ^{19}F NMR spectroscopy where the product signal appears at -137.4 ppm, slightly downfield shifted from **4.5^{CH3}** at -138.2 ppm. After stirring at room

temperature for two hours, the product was then isolated in high yield by precipitation with 0.1 M hydrochloric acid and centrifugation. The product is discernible in positive ion ESI-MS at *m/z* 918.3997, successful cycloaddition was also indicated in the ^{1}H NMR spectra with the characteristic triazole singlet appearing at 8.02 ppm. Finally, although the reaction was carried out over a period of two hours, monitoring by ^{19}F NMR spectroscopy suggests the end point may be reached within 10 minutes, with no further changes observed after this period. This observation could offer synthetic flexibility for future radiolabelling studies with ^{18}F-labelling potentially occurring pre- or post- click.

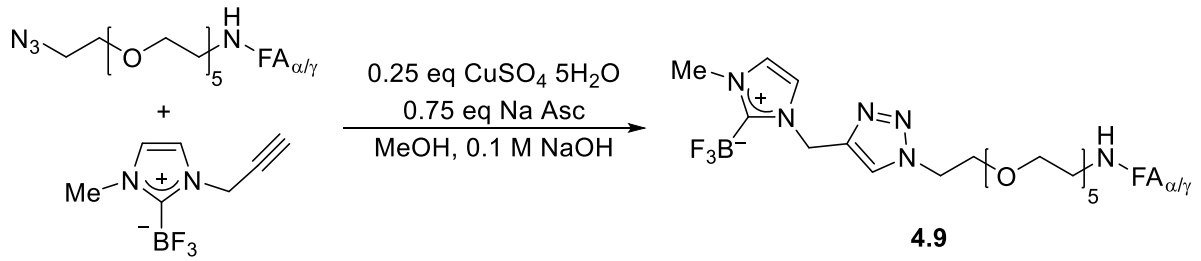

Scheme 4.11 – CuAAC reaction of **4.8**^{5} and **4.5**^{CH3} to synthesis **4.9**.

4.6 Conclusions

A new series of NHC-BF_3 compounds have been synthesised. Water stability studies confirmed that these adducts are highly resistant to hydrolysis when the carbene donor features a hydrocarbon backbone. However, the incorporation of a nitrogen within the Ender's carbene backbone was revealed to compromise the stability of the NHC-BF_3 framework. The degradation of **4.1**^{Tri} *via* a proto-deboronation reaction was attributed to interactions between water and the backbone nitrogen promoting C–B bond cleavage.

An effective synthetic route was developed for the synthesis of nitrogen functionalised NHC-BF_3 systems from readily available imidazoles. A lithium base was used for *in situ* carbene generation, with the functional group tolerance of this method attributed to the formation of carbene-lithium complexes as the intermediates. It is anticipated future work could utilise this route to synthesise a diverse range of NHC-BF_3 systems functionalised for

bioconjugation, thereby expanding the versatility of the NHC-BF_3 approach. Carboxylic acid and amine functionalised imidazolium salts such as those in Figure 4.14, for example, could be particularly suited to this route as the pendant functional groups would also serve to stabilise the lithium complex intermediate.

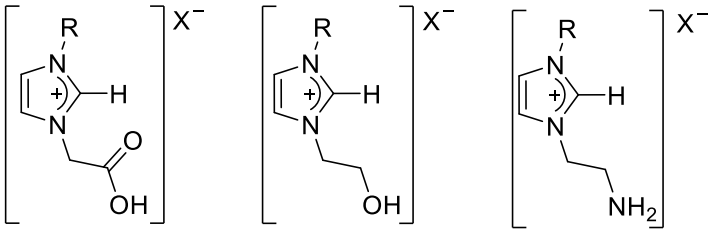

Figure 4.14 – Imidazolium salts functionalised with useful groups for bioconjugation.

The alkyne appended NHC-BF_3 compounds were readily attached to either an aryl azide or a folic acid-PEG-azide conjugate *via* CuAAC click chemistry. The trifluoroborane adducts were robust to the range of conditions applied for the CuAAC reactions and the respective products were produced in good yields. Future work would explore the isotopic exchange radiolabelling of both **4.5** and the folic acid conjugated **4.9** to verify their applicability for PET imaging.

4.7 Experimental

General procedure for the synthesis of NHC-BF_3 adducts 4.1

The free carbene was taken into *ca.* 20 mL diethyl ether and 1.1 equivalents of boron trifluoride etherate added dropwise to the stirred reaction mixture leading to the formation of a white precipitate. After stirring for 1 h, the reaction mixture was filtered, and the solid dried *in vacuo* for 30 min to produce the product in a quantitative yield.

4.1^{SIMes}

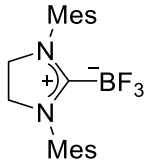

Scale: SIMes (500 mg, 1.63 mmol), BF_3-OEt_2 (0.22 mL, 1.79 mmol), 20 mL diethyl ether. Yield: 575 mg, 94 %. The product can be recrystallised from hot acetonitrile.

^{1}H NMR (400.2 MHz, CD_3CN, 298 K): δ_H 6.98 (s, 4H, Mes *m*-C*H*), 4.05 (s, 4H, NCH_2), 2.29 (s, 18H, Mes CH_3). **^{11}B{^{1}H} NMR** (128.4 MHz, CD_3CN, 298 K): δ_B -1 (q, $^{1}J_{BF}$ = 35.5 Hz). **^{19}F{^{1}H} NMR** (376.5 MHz, CD_3CN, 298 K): δ_F -143.8 (q, $^{1}J_{BF}$ = 35.5 Hz). **^{13}C{^{1}H} NMR** (100.6 MHz, CD_3CN, 298 K): δ_C 139.6 (Mes), 136.7 (Mes), 135.3 (Mes), 130.0 (Mes *m*-*C*H), 51.7 (N*C*H_2), 21.1 (Mes *p*-*C*H_3), 17.7 (Mes *o*-*C*H_3). **Elemental Microanalysis:** calc. for $C_{21}H_{26}N_2BF_3$: C 67.40, H 7.00, N 7.49; meas. C 68.29, H 7.01, N 7.60 **MS (ESI):** *m/z* calc. for $C_{21}H_{26}N_2BF_3Na$ ($[M+Na]^+$) 397.2034, meas. 397.2038 (100 %).

4.1^{6Mes}

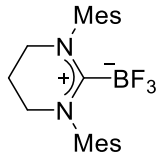

Scale: 6Mes (260 mg, 0.811 mmol), BF_3-OEt_2 (0.12 mL, 0.974 mmol), 15 mL diethyl ether. Yield: 140 mg, 44 %. Crystals suitable for X-ray crystallography were obtained from a concentrated THF solution.

^{1}H NMR (400.2 MHz, $CDCl_3$, 278 K): δ_H 6.91 (s, 4H, Mes *m*-C*H*), 3.49 (t, $^{3}J_{HH}$ = 5.9 Hz, 4H, NCH_2CH$_2$), 2.35 (quin, $^{3}J_{HH}$ = 5.9 Hz, 2H, NCH$_2$CH_2), 2.31 (s, 12H, Mes *o*-CH_3), 2.27 (s, 6H, Mes *p*-CH_3). **^{11}B{^{1}H} NMR** (128.4 MHz, $CDCl_3$, 298 K): δ_B -1 (q, $^{1}J_{BF}$ = 37.3 Hz). **^{19}F{^{1}H} NMR** (376.5 MHz, $CDCl_3$, 298 K): δ_F -141.8 (q, $^{1}J_{BF}$ = 37.3 Hz). **^{13}C{^{1}H} NMR** (100.6 MHz, $CDCl_3$, 298 K): δ_C 140.9 (Mes *C*N), 137.9 (Mes *p*-*C*CH$_3$), 134.2 (Mes *o*-

CCH_3), 129.4 (Mes *m*-*C*H), 48.4 (N*C*$H_2$$CH_2$), 21.2 (Mes *p*-*C*$H_3$), 20.8 (N$CH_2$*C*$H_2$), 17.9 (Mes *o*-*C*$H_3$). **Elemental Microanalysis:** calc. for $C_{22}H_{28}N_2BF_3$ C 68.05, H 7.27, N 7.21; meas. C 67.94, H 7.36, N 7.17. **MS (ESI):** *m/z* calc. for $C_{22}H_{28}N_2BF_3Na$ ($[M+Na]^+$) 411.2191, meas. 411.2195 (100 %).

4.1^{7Dipp}

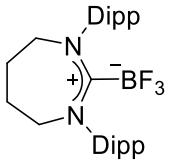

Scale: 7Dipp (750 mg, 1.79 mmol), BF_3-OEt_2 (0.24 mL, 1.97 mmol), 30 mL diethyl ether. Yield: 603 mg, 69 %. Crystals suitable for X-ray crystallography were obtained from a concentrated methanol solution cooled to -25 °C.

^{1}H NMR (400.2 MHz, $CDCl_3$, 298 K): δ_H 7.30 (t, $^3J_{HH}$ = 7.7 Hz, 2H, Dipp *p*-C*H*), 7.18 (d, $^3J_{HH}$ = 7.7 Hz, 4H, Dipp *m*-C*H*), 4.04 (br m, 4H, NC*H*$_2$$CH_2$), 3.16 (sept, $^3J_{HH}$ = 6.8 Hz, 4H, C*H*(CH_3)$_2$), 2.31 (br m, 4H, NCH_2C*H*$_2$), 1.36 (d, $^3J_{HH}$ = 6.8 Hz, 12H, CH(C*H*$_3$)$_2$), 1.33 (d, $^3J_{HH}$ = 6.8 Hz, 12H, CH(C*H*$_3$)$_2$). **^{11}B{^{1}H} NMR** (128.4 MHz, $CDCl_3$, 298 K): δ_B -1 (q, $^1J_{BF}$ = 36.9 Hz). **^{19}F{^{1}H} NMR** (376.5 MHz, $CDCl_3$, 298 K): δ_F -135.7 (q, $^1J_{BF}$ = 36.9 Hz). **^{13}C{^{1}H} NMR** (100.6 MHz, $CDCl_3$, 298 K): δ_C 144.58 (Dipp), 142.58 (Dipp), 128.55 (Dipp *p*-*C*H), 124.23 (Dipp *m*-*C*H), 58.07 (N*C*$H_2$$CH_2$), 29.25 (Dipp *C*H($CH_3$)$_2$), 25.74 (Dipp CH(*C*$H_3$)$_2$), 24.00, 23.82 (br q, J_{CF} = 1.8 Hz). **Elemental Microanalysis:** calc. for $C_{29}H_{42}N_2BF_3$: C 71.60, H 8.70, N 5.76; meas. C 71.29, H 8.58, N 5.75. **MS (ESI):** *m/z* calc. for $C_{29}H_{42}N_2BF_3Na$ ($[M+Na]^+$) 509.3288, meas. 509.3287 (100 %).

4.1^{Tri}

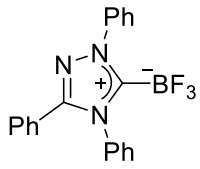

Yields for **4.1^{Tri}** were improved by using a slightly modified procedure. The free carbene (325 mg, 1.09 mmol) was dissolved in THF (30 mL) and boron trifluoride etherate (0.27 mL, 2.19 mmol) added dropwise. After stirring at room temperature for 20 min, the volatiles were removed *in vacuo*. The resulting residue was washed with diethyl ether (3 x 8 mL) before drying *in vacuo* for 1 h. Yield: 270 mg, 68 %.

^{1}H NMR (400.2 MHz, CD_3CN, 298 K): δ_H 7.79 (m, 2H, Ar*H*), 7.63 (m, 3H, Ar*H*), 7.59 – 7.46 (overlapping m, 6H, Ar*H*), 7.43 – 7.35 (overlapping m, 4H, Ar*H*). **^{11}B{^{1}H} NMR** (128.4 MHz, CD_3CN, 298 K): δ_B -1 (q, $^{1}J_{BF}$ = 31.5 Hz). **^{19}F{^{1}H} NMR** (376.5 MHz, CD_3CN, 298 K): δ_F -136.8 (q, $^{1}J_{BF}$ = 31.5 Hz). **^{13}C{^{1}H} NMR** (100.6 MHz, CD_3CN, 298 K): δ_C 154.2 (*C*BF_3), 138.7 (NN*C*N), 135.0, 131.9, 130.9, 130.8, 130.1, 129.7, 129.3, 128.3, 126.3, 124.5.

[4.2^{Mes}][BF_4]

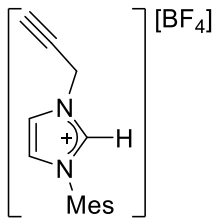

A solution of **[4.2^{Mes}]Br** (3 g, 9.83 mmol) in methanol (100 mL) was combined with a solution of sodium tetrafluoroborate (3.3 g, 28 mmol) in water (40 mL) and the mixture stirred for 30 min at room temperature. The methanol was removed *in vacuo* and the residue extracted into dichloromethane (3 x 30 mL) and the organic phase dried over $MgSO_4$. The resulting solution was concentrated (to approx. 20 mL) and diethyl ether (50 mL) added leading to the formation of a white precipitate. The suspension was filtered, and the residue

dried *in vacuo*. The product was obtained as a white solid (2.44 g, 79.5 % yield). Crystals suitable for X-ray crystallography were obtained by slow evaporation of a $CHCl_3$ solution.

^{1}H NMR (500.3 MHz, $CDCl_3$, 298 K): δ_H 8.84 (s, 1H, NC*H*N), 7.74 (d, $^3J_{HH}$ = 2.0 Hz, 1H, C*H*N), 7.15 (d, $^3J_{HH}$ = 2.0 Hz, 1H, C*H*N), 6.95 (s, 2H, Mes *m*-C*H*), 5.26 (d, $^4J_{HH}$ = 2.6 Hz, 2H, NCH_2), 2.65 (t, $^4J_{HH}$ = 2.6 Hz, 1H, CC*H*), 2.28 (s, 3H, Mes *p*-CH_3), 1.99 (s, 6H, Mes *o*-CH_3). **^{13}C{^{1}H} NMR** (125.8 MHz, $CDCl_3$, 298K): δ_C 141.5, 136.7 (N*C*HN), 134.4, 130.7, 130.0 (Mes *m*-*C*H), 123.7 (N*C*H), 123.1 (N*C*H), 77.9 (C*C*H), 74.2 (CH_2*C*CH), 40.0 (NCH_2), 21.0 (Mes *p*-*C*H_3), 17.3 (Mes *o*-*C*H_3). **Elemental Microanalysis:** calc. for $C_{15}H_{17}BF_4N_2$: C 57.72 %, H 5.49 %, N 8.98 %, found: C 57.54 %, H 5.65 %, N 8.86 %.

[4.2^{CH3}][BF$_4$]

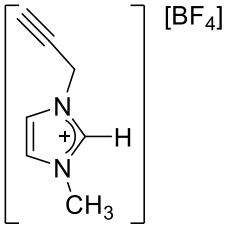

A mixture of **[4.2^{CH3}]Br** (7g, 34.8 mmol) and sodium tetrafluoroborate (5 g, 45.5 mmol) was taken into methanol (40 mL) and the reaction mixture stirred for 20 min. Volatiles were then removed *in vacuo* and the oily residue taken into acetonitrile (20 mL) and filtered through celite to remove the inorganic salts. The acetonitrile solution was then dried with $MgSO_4$ and filtered before the solvent was removed *in vacuo*. The residue was taken into minimal methanol and titurated with diethyl ether with vigorous stirring. The brown solid was filtered and dried *in vacuo* for 3 h. Yield: 5.79 g, 80 %.

^{1}H NMR (400.2 MHz, D_2O, 298 K): δ_H 8.90 (s, 1H, Im C*H*), 7.63 (s, 1H, Im C*H*), 7.52 (s, 1H, Im C*H*), 5.12 (d, $^4J_{HH}$ = 2.6 Hz, 2H, NCH_2C), 3.96 (s, 3H, NCH_3), 3.13 (t, $^4J_{HH}$ = 2.6 Hz, 1H, CC*H*). **^{11}B{^{1}H} NMR** (128.4 MHz, D_2O, 298 K): δ_B -1 (s, BF_4). **^{19}F{^{1}H} NMR** (376.5 MHz, D_2O, 298 K): δ_F -150.5 (s, BF_4).

[4.3^{Mes}][BPh$_4$]

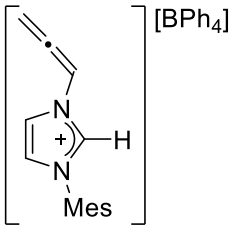

3-Mesityl-1-propynyl-1*H*-imidazolium bromide (2.0 g, 6.55 mmol) and sodium tetraphenylborate (3.0 g, 8.77 mmol) were dissolved in a mixture of ethanol (100 mL) and acetonitrile (80 mL). The reaction mixture was stirred overnight before volatiles were removed *in vacuo*. The white residue was dissolved in dichloromethane (80 mL) and washed with water (80 mL) three times. The organic phase was dried over $MgSO_4$ before concentrating to a minimum (*ca.* 15 mL) and the product precipitated with excess diethyl ether (*ca*. 50 mL). The resulting white solid was dried *in vacuo* (3.15 g, 88 %).

^{1}H NMR (400.2 MHz, CD_3CN, 298 K): δ_H 8.56 (t, $^4J_{HH}$ = 1.67 Hz, 1H, Im NC*H*N), 7.63 (t, $^3J_{HH}$ = 1.90 Hz, 1H, Im NC*H*), 7.43 (t, $^3J_{HH}$ = 1.86 Hz, 1H, Im NC*H*), 7.28 (br m, 8H, Ph *o*-C*H*), 7.24 (t, $^4J_{HH}$ = 6.52 Hz, 1H, NC*H*C), 7.12 (s, 2H, Mes *m*-C*H*), 6.99 (t, J_{HH} = 7.38 Hz, 8H, Ph *m*-C*H*), 6.84 (t, J_{HH} = 7.21 Hz, 4H, Ph *p*-C*H*), 5.90 (d, $^4J_{HH}$ = 6.46 Hz, 2H, CC*H*$_2$), 2.36 (s, 3H, Mes *p*-C*H*$_3$), 2.03 (s, 6H, Mes *o*-C*H*$_3$). **^{11}B{^{1}H} NMR** (128.4 MHz, CD_3CN, 298 K): δ_B -7 (s, BPh_4). **^{13}C{^{1}H} NMR** (125.8 MHz, CD_3CN, 298 K): δ_C 203.3 (CH*C*CH$_2$), 165.5 (Ph *i*-*C*), 165.0 (Ph *i*-*C*), 164.5 (Ph *i*-*C*), 164.0 (Ph *i*-*C*), 142.4 (Mes *i*-*C*), 136.7 (Ph *o*-*C*H), 136.7 (Ph *o*-*C*H), 136.7 (Ph *o*-*C*H), 136.7 (Ph *o*-*C*H), 135.9 (Mes), 135.7 (Mes), 130.5 (Mes), 126.6 (Ph *m*-*C*H), 126.6 (Ph *m*-*C*H), 126.6 (Ph *m*-*C*H), 126.5 (Ph *m*-*C*H), 125.7 (Im N*C*H), 122.8 (Ph *p*-*C*H), 122.2 (Im N*C*H), 97.5 (N*C*HC), 92.2 (C*C*H$_2$), 21.1 (Mes *p*-*C*H$_3$), 17.5 (Mes *o*-*C*H$_3$).

[4.4][BF$_4$]

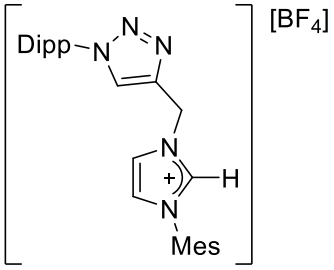

An adaption of the synthesis by Warsink *et al.* was followed.[37] In a Schlenk tube, copper sulphate (3.2 g, 12.82 mmol) and sodium ascorbate (3.81 g, 19.22 mmol) were combined and made up to a combined 0.1 M solution with acetonitrile (320 mL). The reaction mixture was stirred at 60 °C for 20 min, yielding a yellow solution and an undissolved blue solid. [**4.3][BF$_4$]** (4.0 g, 12.82 mmol) was then added, and the reaction mixture stirred at 60 °C for a further 1 h, producing an orange solution and a white solid. To this mixture was added 1-azido-2,6-diisopropylbenzene (2.61 g, 12.82 mmol), and the reaction stirred at 60 °C for a further 2 d, resulting in a brown solution with a green solid. The reaction mixture was cooled to room temperature and filtered before volatiles were removed *in vacuo*. The residue was then extracted into chloroform (400 mL) and washed with water (3 x 150 mL). The organic layer was dried over $MgSO_4$ before removing the volatiles *in vacuo*, yielding a yellow solid (5.65 g, 85.6 % yield). Crystals suitable for X-ray crystallography were obtained by the slow evaporation of a $CHCl_3$ solution.

^{1}H NMR (500.3 MHz, $CDCl_3$, 298 K): δ_H 9.06 (s, 1H, NC*H*N), 8.30 (s, 1H, CC*H*NDipp), 7.95 (s, 1H, NC*H*), 7.48 (t, $^3J_{HH}$ = 7.8 Hz, Dipp *p*-C*H*), 7.26 (d, $^3J_{HH}$ = 7.8 Hz, Dipp *m*-C*H*), 7.19 (s, 1H, NC*H*), 6.99 (s, 2H, Mes *m*-C*H*), 5.87 (s, 2H, NCH_2), 2.33 (s, 3H, Mes *p*-CH_3), 2.11 (sept, $^3J_{HH}$ = 6.8 Hz, 2H, Dipp C*H*(CH_3)$_2$), 2.00 (s, 6H, Mes *o*-CH_3), 1.08 (overlapping m, 12H, Dipp CH(CH_3)$_2$). **^{13}C{^{1}H} NMR** (125.8 MHz, $CDCl_3$, 298 K): δ_C 145.9, 141.6, 140.3, 137.2 (N*C*HN), 134.4, 132.9, 131.1 (Dipp *p*-*C*H), 130.7, 130.0 (Mes *m*-*C*H), 128.3 (C*C*HNDipp), 124.0 (Dipp *m*-*C*H), 123.6(N*C*H), 123.5 (N*C*H), 44.8 (N*C*H_2), 28.6 (Dipp

*C*H(CH_3)$_2$), 24.1 (Dipp CH(*C*H_3)$_2$), 24.0 (Dipp CH(*C*H_3)$_2$), 21.2 (Mes *p*-*C*H_3), 17.2 (Mes *o*-*C*H_3). **Elemental Microanalysis:** calc. for $C_{27}H_{34}N_5BF_4$: C 62.92 %, H 6.65 %, N 13.59 %, found: C 62.77 %, H 6.73 %, N 13.58 %.

4.5^{Mes}

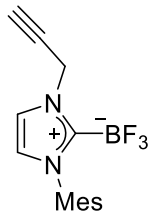

[4.2^{Mes}][BF_4] (1 g, 3.2 mmol) was suspended in tetrahydrofuran (20 mL) and cooled to -78 °C. In a separate Schlenk tube, lithium bis(trimethylsilyl)amide (0.64 g, 3.84 mmol) was dissolved in tetrahydrofuran (20 mL) and transferred dropwise into the cooled reaction *via* cannula. The reaction mixture was stirred at -78 °C for 3 h, with the grey suspension becoming a light brown solution. Boron trifluoride diethyl etherate (0.79 mL, 6.4 mmol) was then added to the reaction mixture, which was stirred at -78 °C for a further 2 h before warming slowly to room temperature and stirring overnight. Volatiles were then removed *in vacuo*. The solid residue was dissolved in 50 mL of ethyl acetate and washed with water (3 x 30 mL). The organic phase was dried with $MgSO_4$ and the solvent removed *in vacuo*. The product was obtained as an off-white solid (0.73 g, 78 % yield). Crystals suitable for X-ray crystallography were obtained from a concentrated THF solution.

^{1}H NMR (400.2 MHz, $CDCl_3$, 298 K): δ_H 7.54 (d, $^3J_{HH}$ = 1.8 Hz, 1H, NC*H*), 6.97 (s, 2H, Mes *m*-C*H*), 6.91 (d, $^3J_{HH}$ = 1.8 Hz, 1H, NC*H*), 5.26 (d, $^4J_{HH}$ = 2.64 Hz, 2H, NCH_2C), 2.65 (t, $^4J_{HH}$ = 2.64 Hz, 1H, CC*H*), 2.23 (s, 3H, Mes *p*-CH_3), 2.01 (s, 6H, Mes *o*-CH_3). **^{11}B{^{1}H} NMR** (128.4 MHz, $CDCl_3$, 298 K): δ_B 0 (q, $^1J_{BF}$ = 34.3 Hz). **^{19}F{^{1}H} NMR** (376.5 MHz, $CDCl_3$, 298 K): δ_F -140.4 (q, $^1J_{BF}$ = 34.1 Hz). **^{13}C{^{1}H} NMR** (100.6 MHz, CD_3CN, 298K): δ_C 140.5, 135.9, 135.0, 129.5 (Mes *m*-*C*H), 123.9 (N*C*H), 122.7 (N*C*H), 77.6 (*C*CH), 76.4

(C*C*H), 39.5 (q, J_{CF} = 3.62 Hz, N*C*H$_2$C), 21.1 (Mes *p*-*C*H$_3$), 17.3 (Mes *o*-*C*H$_3$). **Elemental Microanalysis:** calc. for $C_{15}H_{16}N_2BF_3$: C 61.68 %, H 5.52 %, N 9.59 %, found: C 60.71 %, H 5.62 %, N 9.37 %. **MS (ESI):** *m/z* calc. for $C_{15}H_{16}N_2BF_3Na$ ([M+Na]$^+$) 315.1251, meas. 315.1251 (100 %).

4.5^{CH3}

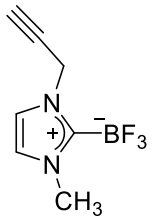

A flame-dried Schlenk tube was charged with **[4.2^{CH3}][BF$_4$]** (1.0 g, 4.81 mmol) and THF (40 mL) and cooled to -78 °C. Lithium bis(trimethylsilyl)amide (885 mg, 5.29 mmol) was dissolved in THF (20 mL) and added dropwise to the cooled reaction *via* cannula. The reaction mixture was stirred at -78 °C for 5 h before boron trifluoride etherate (0.71 mL, 5.77 mmol) was added dropwise. The temperature was maintained at -78 °C for a further 45 min before the reaction mixture was allowed to slowly warm to room temperature and stirred overnight. Volatiles were subsequently removed *in vacuo* to yield an orange-brown oil. The oil was dissolved in water (30 mL) and the product extract with dichloromethane (3 x 40 mL). The organic phase was dried with $MgSO_4$ and the solvent removed *in vacuo* to yield the product as an orange-yellow solid (709 mg, 78 %).

^{1}H NMR (400.2 MHz, $CDCl_3$, 298K): δ_H 7.32 (d, $^3J_{HH}$ = 1.9 Hz, 1H, NC*H*CH), 6.98 (d, $^3J_{HH}$ = 1.9 Hz, 1H, NC*H*CH), 5.13 (d, $^4J_{HH}$ = 2.63 Hz, 2H, NC*H$_2$*C), 3.94 (s, 3H, NC*H$_3$*), 2.58 (t, $^4J_{HH}$ = 2.63 Hz, 1H, CC*H*). **^{11}B{^{1}H} NMR** (128.4 MHz, $CDCl_3$, 298K): δ_B 0 (q, $^1J_{BF}$ = 35.7 Hz). **^{19}F{^{1}H} NMR** (376.5 MHz, $CDCl_3$, 298K): δ_F -139.8 (q, $^1J_{BF}$ = 35.7 Hz). **^{13}C{^{1}H} NMR** (100.6 MHz, $CDCl_3$, 298K): δ_C 122.34 (N*C*H), 120.11 (N*C*H), 76.44 (C*C*H), 75.63 (CH$_2$*C*CH), 38.92 (q, J_{CF} = 4.18 Hz, N*C*H$_2$C), 36.72 (q, J_{CF} = 2.89 Hz, N*C*H$_3$). **Elemental**

Microanalysis: calc. for $C_7H_8N_2BF_3$: C 44.73 %, H 4.29 %, N 14.90 %, found: C 43.72 %, H 4.28 %, N 14.57 %. **MS (ESI):** *m/z* calc. for $C_7H_8N_2BF_3Na$ ($[M+Na]^+$) 211.0625, meas. 211.0627 (100 %).

4.6 – Reaction of **[4.4][BF$_4$]** with Lithium bis(trimethylsilyl)amide

Lithium bis(trimethylsilyl)amide (0.20 g, 1.16 mmol) was dissolved in tetrahydrofuran (10 mL) and the resulting solution transferred to a stirred suspension of **[4.4][BF$_4$]** (0.50 g, 0.97 mmol) also in tetrahydrofuran (10 mL) at -78 °C. The reaction mixture was stirred at -78 °C for a further 1 h, with the initial brown suspension partially dissolving. The reaction mixture was then warmed to room temperature and stirred for a further 3 h, with all the solid dissolving and a dark brown solution resulting. Volatiles were removed *in vacuo* and the resulting light brown solid washed with hexane (20 mL) before extraction into diethyl ether (20 mL). The solvent was removed removed *in vacuo* yielding the product as a light brown solid (0.40 g). Based upon [NHC·Li(THF)][BF_4] 69 % yield.

^{1}H NMR (400.2 MHz, $CDCl_3$, 298 K): δ_H 8.13 (s, 1H, CC*H*NDipp), 7.20 (t, $^3J_{HH}$ = 7.8 Hz, 1H, Dipp *p*-C*H*), 7.09 (s, 1H, NC*H*), 7.04 (d, $^3J_{HH}$ = 7.8 Hz, 2H, Dipp *m*-C*H*), 6.73 (s, 2H, Mes *m*-C*H*), 6.09 (s, 1H, NC*H*), 5.40 (s, 2H, NCH_2), 2.37 (sept., $^3J_{HH}$ = 6.9 Hz, 2H, DippC*H*), 2.11 (s, 3H, Mes *p*-CH_3), 1.92 (s, 6H, Mes *o*-CH_3), 1.03 (m, 12H, DippCH(CH_3)$_2$). **^{13}C{^{1}H} NMR** (100.6 MHz, $CDCl_3$, 298K): δ_C 199.1 (N*C*N), 146.3 (Ar-C), 144.8, 137.8, 137.2, 135.3, 134.1, 130.8 (Mes *m-C*), 128.9 (C*C*HNDipp), 126.6 (Dipp *m-C*H), 123.9 (N*C*H), 121.2 (N*C*H), 119.8 (Dipp *p-C*H*)*, 45.2 (N*C*H_2), 28.7 (Dipp*C*H), 25.3 (DippCH(*C*H_3)$_2$), 21.0 (Mes *p-C*H_3), 17.0 (Mes *o-C*H_3).

4.7

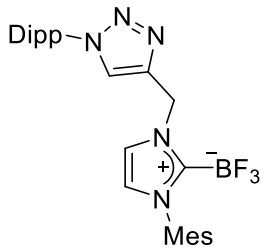

In a Schlenk tube, copper sulphate (0.20 g, 0.8 mmol) and sodium ascorbate (0.24 g, 1.2 mmol) were combined and made up to a combined 0.1 M solution with acetonitrile (20 mL). This mixture was stirred at 60 °C for 20 min, forming a yellow solution with undissolved blue solid. To this mixture was added **4.5^{Mes}** (0.23 g, 0.8 mmol), and the reaction mixture stirred at 60 °C for 1 h, producing an orange suspension. 1-Azido-2,6-diisopropylbenzene (0.16 g, 0.8 mmol) was added, and the reaction mixture stirred at 60 °C for 2 d, resulting in a darker orange suspension. The reaction mixture was then cooled to room temperature and filtered. Solvent was removed from the filtrate *in vacuo*, and the product was extracted into chloroform (100 mL) and repeatedly washed with water (3 x 100 mL). The organic layer was then dried over $MgSO_4$ before removal of the volatiles under *in vacuo* to yield a yellow solid. Yield: 0.18 g, 45 %. Crystals suitable for X-ray crystallography were grown *via* the slow evaporation of a toluene solution.

^{1}H NMR (500.3 MHz, $CDCl_3$, 298 K): δ_H 8.06 (s, 1H, CC*H*NDipp), 7.60 (d, $^{3}J_{HH}$ = 1.7 Hz, 1H, NC*H*), 7.52 (t, $^{3}J_{HH}$ = 7.9 Hz, 1H, Dipp *p*-C*H*), 7.30 (d, $^{3}J_{HH}$ = 7.9 Hz, 2H, Dipp *m*-C*H*), 6.98 (s, 2H, Mes *m*-C*H*), 6.91 (d, $^{3}J_{HH}$ = 1.7 Hz, 1H, NC*H*), 5.82 (s, 2H, NCH_2), 2.34 (s, 3H, Mes *p*-CH_3), 2.16 (sept., $^{3}J_{HH}$ = 6.8 Hz, 2H, DippC*H*), 1.97 (s, 6H, Mes *o*-CH_3), 1.14 (d, $^{3}J_{HH}$ = 6.8 Hz, 6H, DippCH(CH_3)$_2$), 1.09 (d, $^{3}J_{HH}$ = 6.8 Hz, 6H, DippCH(CH_3)$_2$). **^{11}B{^{1}H} NMR** (128.4 MHz, $CDCl_3$, 298 K): δ_B 0 (q, $^{1}J_{BF}$ = 34.7 Hz). **^{19}F{^{1}H} NMR** (376.5 MHz, $CDCl_3$, 298 K): δ_F -140.6 (q, $^{1}J_{BF}$ = 34.7 Hz). **^{13}C{^{1}H} NMR** (125.8 MHz, $CDCl_3$, 298 K): δ_C 145.9 (Dipp), 142.4 (CH_2*C*CH), 139.7 (Mes *p*-*C*CH_3), 134.4 (Mes *o*-*C*CH_3), 133.6, 132.9, 131.1

(Dipp *p*-*C*H), 129.1 (Mes *m*-*C*H), 127.5 (C*C*HNDipp), 124.0 (Dipp *m*-*C*H), 122.4 (N*C*H), 121.9 (N*C*H), 44.5 (q, J = 3.1 Hz, N*C*H_2), 28.6 (Dipp *C*H(CH_3)$_2$), 24.1 (Dipp CH(*C*H_3)$_2$), 21.3 (Mes *p*-*C*H_3), 17.2 (Mes *o*-*C*H_3). **Elemental Microanalysis:** calc. for $C_{27}H_{33}N_5BF_3$: C 65.46 %, H 6.71 %, N 14.14 %, found: C 65.28 %, H 6.8 %, N 13.98 %. **MS (ESI):** *m/z* calc. for $C_{27}H_{33}N_5BF_3Na$ ($[M+Na]^+$) 518.2676, meas. 518.2672 (100%).

General procedure for the synthesis of folic acid derivatives of the type 4.8^n

An adaptation of the synthesis reported by Ke *et al* was followed.[70] Folic acid (1 g, 2.27 mmol) and DCC (0.94 g, 4.53 mmol) were dissolved in dry DMSO (50 mL) under an inert atmosphere. Pyridine (10 mL) was added to the reaction mixture, which was stirred at room temperature for 1 h before addition of one equivalent of H_2N-[CH_2CH_2O]$_n$-$CH_2CH_2N_3$ (2.27 mmol) with the required chain length. The reaction mixture was stirred in the dark for a further 60 h. The resulting mixture was then filtered, under an inert atmosphere using a filter cannula, into a flask of vigorously stirring diethyl ether (200 mL) to produce a yellow precipitate. The precipitate was continuously agitated with slow stirring and most of the ether was decanted. The yellow solid was twice washed, to remove remaining DMSO, with a combination of acetone (60 mL) and ether (100 mL); stirring was maintained and the solvent decanted each time. Any remaining solvent was then removed *in vacuo* and the product obtained as a fine yellow powder.

4.8^2

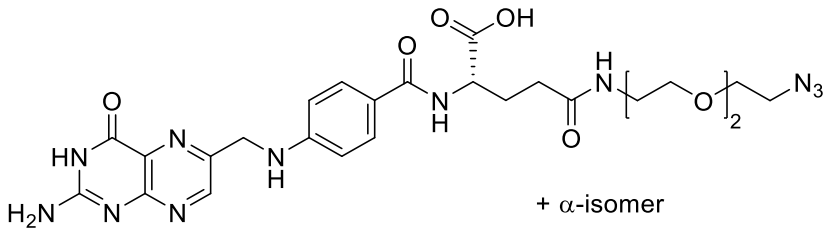

4.8^2 was prepared according to the general procedure described above. The reaction was conducted on a 1 g scale using: folic acid (1.0 g, 2.27 mmol), DCC (0.935 g, 4.53 mmol) and

H_2N-[CH_2CH_2O]$_2$-$CH_2CH_2N_3$ (0.4 g, 2.27 mmol). Yield: 1.02 g, 75 %. Spectroscopic characterisation was consistent with the literature.[70]

4.8^5

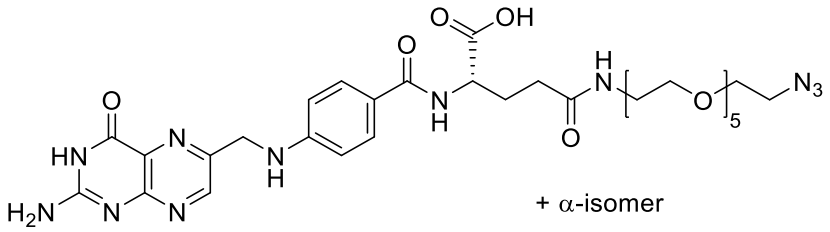

4.8^5 was prepared according to the general procedure described above. The reaction was conducted on a 1.3 g scale using: folic acid (1.3 g, 2.94 mmol), DCC (1.21 g, 5.88 mmol) and H_2N-[CH_2CH_2O]$_5$-$CH_2CH_2N_3$ (0.9 g, 2.94 mmol). Yield: 1.59 g, 74 %. Further purification can be achieved by column chromatography on neutral alumina, dry loaded, in ^{i}PrOH/H_2O + 1% [NH_4]OH (8:2 to 7:3).

^{1}H NMR (400 MHz, d6-DMSO, 298K): δ_H – 8.64 (s, 1H, pterin Ar*H*), 7.65 (m, 2H, Ph Ar*H*), 7.0 – 6.8 (br m, 2H, N*H*), 6.64 (m, 2H, Ar*H*), 4.48 (d, J_{HH} = 6.10 Hz, 2H, CH_2Ar), 4.39 – 4.22 (m, 1H, C*H*), 3.61 – 3.44 (m, 16H, OCH_2), 3.41 – 3.35 (m, 8H, OCH_2), 3.26 – 3.12 (m, 2H, PEG-CH_2), 2.25 (m, 2H, CH_2CO), 2.08 – 1.80 (m, 2H, OCCH$_2$CH_2). **^{13}C{^{1}H} NMR** (151.0, D_2O with NH_4OH (pH 9), 298K): δ_C 181.6 (*C*O), 178.6 (*C*O), 175.6 (*C*O), 174.5 (*C*O), 171.3, 170.2, 169.9 (*C*O), 169.1, 162.2, 162.1, 155.1 (Ar *C*), 151.2 (Ar *C*), 151.1 (Ar *C*), 151.0 (Ar *C*), 148.0, 147.9, 147.6 (Ar *C*H), 129.3 (Ar *C*H), 129.2 (Ar *C*H), 129.0, 128.0, 121.4, 120.8 (Ar *C*), 119.5, 115.1, 115.0, 112.6 (Ar *C*H), 112.5 (Ar *C*H), 69.6 – 69.4 (overlapping peaks, *C*H_2), 69.2 (*C*H_2), 68.9 (*C*H_2), 68.6 (*C*H_2), 55.2 (CH$_2$*C*(H)COOH), 55.0 (CH$_2$*C*(H)COOH), 50.1 (*C*H_2), 45.7 (Ar*C*H_2NH), 39.0 (*C*H_2), 38.9 (*C*H_2), 33.9 (*C*H_2CO), 32.6, 27.7 (*C*H_2CH$_2$CO). **MS (ESI)**: *m/z* calc. for $C_{31}H_{43}N_{11}O_{10}$ ([M+H]$^+$) 730.3267, meas. 730.3262 (100%).

4.9

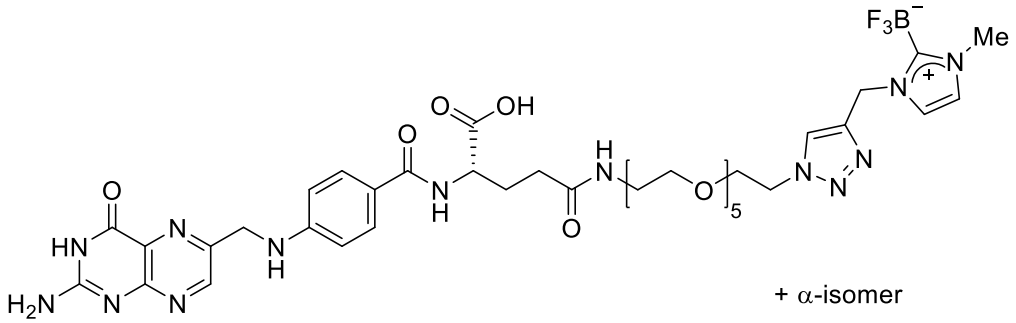

4.5^{CH3} (19.4 mg, 0.103 mmol), copper sulfate (6.4 mg, 0.026 mmol) and sodium ascorbate (15.3 mg, 0.077 mmol) were dissolved in methanol (1.5 mL). The reaction was stirred for 15 min before addition of a 0.1 M sodium hydroxide aqueous solution (1.5 mL) containing **4.8^{5}** (75 mg, 0.103 mmol). The reaction mixture was stirred for a further 2 h before volatiles were removed *in vacuo*. The remaining aqueous solution was adjusted to pH 2 with 0.1 M hydrochloric acid, leading to precipitation of the product. The suspension was centrifuged (6000 rpm, 2 min) and the supernatant decanted. The remaining solid was washed with water (1 mL), centrifuged again (6000 rpm, 2 min) and the supernatant removed. The residue was subsequently dried *in vacuo* to yield an orange powder. Yield: 79.5 mg, 84 %.

^{1}H NMR (400.2 MHz, d6-DMSO, 298 K): δ_H 8.64 (s, 1H, Pterin Ar*H*), 8.02 (s, 1H, Triazole Ar*H*), 7.65 (dd, J_{HH} = 8.8 Hz, 2H, Ph Ar*H*), 7.48 (d, J_{HH} = 3.3 Hz, 2H, Im Ar*H*), 6.98 – 6.76 (overlapping m, 2H, N*H*), 6.63 (dd, J_{HH} = 8.8 Hz, 2H, Ph Ar*H*), 5.46 (s, 2H, CH_2), 4.49 (m, 4H, ArCH_2NH, ArCH_2CH$_2$O), 4.39 – 4.23 (overlapping m, 1H, CH$_2$C(*H*)(COOH)NH), 3.79 (s, 3H, ImCH_3), 3.52 – 3.35 (overlapping m, 20H, CH_2O), 3.25 – 3.13 (overlapping m, 2H, CH_2O), 2.25 (m, 2H, CH$_2$CH_2CO), 2.09 – 1.80 (m, 2H, CH_2CH$_2$CO). **^{11}B{^{1}H} NMR** (128.4 MHz, d6-DMSO, 298 K): δ_B 0 (q, $^{1}J_{BF}$ = 36.1 Hz). **^{19}F{^{1}H} NMR** (376.5 MHz, d6-DMSO, 298 K): δ_F -135.8 (q, $^{1}J_{BF}$ = 36.1 Hz). **^{13}C{^{1}H} NMR**(100.6 MHz, d6-DMSO, 298 K): δ_C 174.1 (*C*O), 173.8 (*C*O), 171.8 (*C*O), 166.2 (*C*O), 160.6 (Ar *C*), 150.7 (Ar *C*), 141.9 (Tri *C*), 129.1, 129.0, 128.4 (Ar *C*), 124.4 (Tri *C*H), 123.4 (Im *C*H), 121.6 (Im *C*H), 121.4 (Ph *C*),

111.2 (Ph *C*H), 69.7 (*C*H_2), 69.6 (*C*H_2), 69.5 (*C*H_2), 69.1 (*C*H_2), 68.9 (*C*H_2), 68.6 (*C*H_2), 52.6 (CH_2*C(*H)COOH), 52.3 (CH_2*C(*H)COOH), 49.5 (Ar*C*H_2CH_2), 45.9 (Ar*C*H_2NH), 43.2 (*C*H_2), 38.5 (*C*H_2), 35.8 (N*C*H_3), 30.5 (CH_2*C*H_2CO), 27.1 (*C*H_2CH_2CO). **MS (ESI):** *m/z* calc. for $C_{38}H_{52}O_{10}N_{13}BF_3$ ($[M+H]^+$) 918.4006, meas. 918.3997 (100%)

4.8 References

[1] A. J. Arduengo, R. L. Harlow, M. Kline, *J. Am. Chem. Soc.* **1991**, *113*, 361–363.
[2] V. Nesterov, D. Reiter, P. Bag, P. Frisch, R. Holzner, A. Porzelt, S. Inoue, *Chem. Rev.* **2018**, *118*, 9678–9842.
[3] S. Díez-González, N. Marion, S. P. Nolan, *Chem. Rev.* **2009**, *109*, 3612–3676.
[4] P. L. Arnold, I. J. Casely, *Chem. Rev.* **2009**, *109*, 3599–3611.
[5] M. N. Hopkinson, C. Richter, M. Schedler, F. Glorius, *Nature* **2014**, *510*, 485–496.
[6] P. Bellotti, M. Koy, M. N. Hopkinson, F. Glorius, *Nat. Rev. Chem.* **2021**, *5*, 711–725.
[7] L. Benhamou, E. Chardon, G. Lavigne, S. Bellemin-Laponnaz, V. César, *Chem. Rev.* **2011**, *111*, 2705–2733.
[8] D. Bourissou, O. Guerret, F. P. Gabbaï, G. Bertrand, *Chem. Rev.* **2000**, *100*, 39–91.
[9] D. J. Nelson, S. P. Nolan, *Chem. Soc. Rev.* **2013**, *42*, 6723–6753.
[10] H. V. Huynh, *Chem. Rev.* **2018**, *118*, 9457–9492.
[11] R. Hoffmann, G. D. Zeiss, G. W. Van Dine, *J. Am. Chem. Soc.* **1968**, *90*, 1485–1499.
[12] V. Lavallo, Y. Canac, C. Präsang, B. Donnadieu, G. Bertrand, *Angew. Chemie Int. Ed.* **2005**, *44*, 5705–5709.
[13] D. Enders, K. Breuer, G. Raabe, J. Runsink, J. H. Teles, J.-P. Melder, K. Ebel, S. Brode, *Angew. Chemie Int. Ed. English* **1995**, *34*, 1021–1023.
[14] M. Melaimi, M. Soleilhavoup, G. Bertrand, *Angew. Chemie Int. Ed.* **2010**, *49*, 8810–8849.
[15] M. Der Su, S. Y. Chu, *Chem. Phys. Lett.* **1999**, *308*, 283–288.
[16] C. Boehme, G. Frenking, *J. Am. Chem. Soc.* **1996**, *118*, 2039–2046.
[17] C. Heinemann, T. Müller, Y. Apeloig, H. Schwarz, *J. Am. Chem. Soc.* **1996**, *118*, 2023–2038.
[18] A. J. Arduengo, H. V. R. Dias, R. L. Harlow, M. Kline, *J. Am. Chem. Soc.* **1992**, *114*, 5530–5534.
[19] M. K. Denk, K. Hatano, M. Ma, *Tetrahedron Lett.* **1999**, *40*, 2057–2060.
[20] A. Gómez-Suárez, D. J. Nelson, S. P. Nolan, *Chem. Commun.* **2017**, *53*, 2650–2660.
[21] A. J. Arduengo, J. R. Goerlich, W. J. Marshall, *J. Am. Chem. Soc.* **1995**, *117*, 11027–11028.
[22] F. Wang, L. jun Liu, W. Wang, S. Li, M. Shi, *Coord. Chem. Rev.* **2012**, *256*, 804–853.
[23] D. Enders, T. Balensiefer, *Acc. Chem. Res.* **2004**, *37*, 534–541.
[24] Xile Hu, Yongjun Tang, and Peter Gantzel, K. Meyer*, *Organometallics* **2003**, *22*, 612–614.
[25] N. M. Scott, R. Dorta, E. D. Stevens, A. Correa, L. Cavallo, S. P. Nolan, *J. Am. Chem. Soc.* **2005**, *127*, 3516–3526.
[26] H. Jacobsen, A. Correa, C. Costabile, L. Cavallo, *J. Organomet. Chem.* **2006**, *691*, 4350–4358.
[27] S. Fantasia, J. L. Petersen, H. Jacobsen, L. Cavallo, S. P. Nolan, *Organometallics* **2007**, *26*, 5880–5889.

[28] Matthew D. Sanderson, and Justin W. Kamplain, C. W. Bielawski*, *J. Am. Chem. Soc.* **2006**, *128*, 16514–16515.
[29] O. Back, M. Henry-Ellinger, C. D. Martin, D. Martin, G. Bertrand, *Angew. Chemie - Int. Ed.* **2013**, *52*, 2939–2943.
[30] A. Liske, K. Verlinden, H. Buhl, K. Schaper, C. Ganter, *Organometallics* **2013**, *32*, 5269–5272.
[31] S. V. C. Vummaleti, D. J. Nelson, A. Poater, A. Gómez-Suárez, D. B. Cordes, A. M. Z. Slawin, S. P. Nolan, L. Cavallo, *Chem. Sci.* **2015**, *6*, 1895–1904.
[32] A. J. Arduengo, F. Davidson, R. Krafczyk, W. J. Marshall, R. Schmutzler, *Monatshefte für Chemie* **2000**, *131*, 251–265.
[33] C. Tian, W. Nie, M. V. Borzov, P. Su, *Organometallics* **2012**, *31*, 1751–1760.
[34] K. Chansaenpak, M. Wang, Z. Wu, R. Zaman, Z. Li, F. P. Gabbaï, *Chem. Commun.* **2015**, *51*, 12439–12442.
[35] K. Chansaenpak, M. Wang, H. Wang, B. C. Giglio, F. P. Gabbaï, Z. Wu, Z. Li, *RSC Adv.* **2017**, *7*, 17748–17751.
[36] F. An, F. Nurili, H. Sayman, Z. Ozer, H. Cakiroglu, O. Aras, R. Ting, *J. Med. Chem.* **2020**, *63*, 12693–12706.
[37] S. Warsink, R. M. Drost, M. Lutz, A. L. Spek, C. J. Elsevier, *Organometallics* **2010**, *29*, 3109–3116.
[38] S. Ravula, N. E. Larm, Y. Liu, J. L. Atwood, S. N. Baker, G. A. Baker, *New J. Chem.* **2018**, *42*, 1979–1986.
[39] T. Lu, Z. Lu, Z.-X. Ma, Y. Zhang, R. P. Hsung, *Chem. Rev.* **2013**, *113*, 4862–4904.
[40] M. Iglesias, D. J. Beetstra, J. C. Knight, L. L. Ooi, A. Stasch, S. Coles, L. Male, M. B. Hursthouse, K. J. Cavell, A. Dervisi, I. A. Fallis, *Organometallics* **2008**, *27*, 3279–3289.
[41] J. P. Moerdyk, C. W. Bielawski, *J. Am. Chem. Soc.* **2012**, *134*, 6116–6119.
[42] W.-C. Shih, C.-H. Wang, Y.-T. Chang, G. P. A. Yap, T.-G. Ong, *Organometallics* **2009**, *28*, 1060–1067.
[43] P. L. Arnold, S. A. Mungur, A. J. Blake, C. Wilson, *Angew. Chemie Int. Ed.* **2003**, *42*, 5981–5984.
[44] R. Fränkel, C. Birg, U. Kernbach, T. Habereder, H. Nöth, W. P. Fehlhammer, *Angew. Chemie Int. Ed.* **2001**, *40*, 1907–1910.
[45] O. Spiegelstein, J. D. Eudy, R. H. Finnell, *Gene* **2000**, *258*, 117–125.
[46] A. C. Antony, *Annu. Rev. Nutr.* **1996**, *16*, 501–521.
[47] H. Elnakat, M. Ratnam, *Adv. Drug Deliv. Rev.* **2004**, *56*, 1067–1084.
[48] J. F. Ross, P. K. Chaudhuri, M. Ratnam, *Cancer* **1994**, *73*, 2432–2443.
[49] N. Parker, M. J. Turk, E. Westrick, J. D. Lewis, P. S. Low, C. P. Leamon, *Anal. Biochem.* **2005**, *338*, 284–293.
[50] W. Xia, A. R. Hilgenbrink, E. L. Matteson, M. B. Lockwood, J.-X. Cheng, P. S. Low, *Blood* **2009**, *113*, 438–446.
[51] D. M. S. H. Chandrupatla, C. F. M. Molthoff, A. A. Lammertsma, C. J. van der Laken, G. Jansen, *Drug Deliv. Transl. Res.* **2019**, *9*, 366–378.
[52] S. D. Boss, S. M. Ametamey, *Cancers (Basel).* **2020**, *12*, 1–20.
[53] M. Fernández, F. Javaid, V. Chudasama, *Chem. Sci.* **2018**, *9*, 790–810.
[54] C. Chen, J. Ke, X. Edward Zhou, W. Yi, J. S. Brunzelle, J. Li, E. L. Yong, H. E. Xu, K. Melcher, *Nature* **2013**, *500*, 486–489.
[55] S. D. Boss, T. Betzel, C. Müller, C. R. Fischer, S. Haller, J. Reber, V. Groehn, R. Schibli, S. M. Ametamey, *Bioconjug. Chem.* **2016**, *27*, 74–86.
[56] S. Quici, A. Casoni, F. Foschi, L. Armelao, G. Bottaro, R. Seraglia, C. Bolzati, N. Salvarese, D. Carpanese, A. Rosato, *J. Med. Chem.* **2015**, *58*, 2003–2014.

[57] A. H. Maurer, P. Elsinga, S. Fanti, B. Nguyen, W. J. G. Oyen, W. A. Weber, *J. Nucl. Med.* **2014**, *55*, 701–704.
[58] T. L. Ross, M. Honer, C. Müller, V. Groehn, R. Schibli, S. M. Ametamey, *J. Nucl. Med.* **2010**, *51*, 1756–1762.
[59] T. Betzel, C. Müller, V. Groehn, A. Müller, J. Reber, C. R. Fischer, S. D. Krämer, R. Schibli, S. M. Ametamey, *Bioconjug. Chem.* **2013**, *24*, 205–214.
[60] A. Bettio, M. Honer, C. Müller, M. Brühlmeier, U. Müller, R. Schibli, V. Groehn, A. P. Schubiger, S. M. Ametamey, *J. Nucl. Med.* **2006**, *47*, 1153–1160.
[61] C. R. Fischer, V. Groehn, J. Reber, R. Schibli, S. M. Ametamey, C. Müller, *Mol. Imaging Biol.* **2013**, *15*, 649–654.
[62] H. Schieferstein, T. Betzel, C. R. Fischer, T. L. Ross, *EJNMMI Res.* **2013**, *3*, 1–10.
[63] Y. Y. Gent, K. Weijers, C. F. Molthoff, A. D. Windhorst, M. C. Huisman, D. E. Smith, S. A. Kularatne, G. Jansen, P. S. Low, A. A. Lammertsma, C. J. van der Laken, *Arthritis Res. Ther.* **2013**, *15*, 1–11.
[64] C. R. Fischer, C. Müller, J. Reber, A. Müller, S. D. Krämer, S. M. Ametamey, R. Schibli, *Bioconjug. Chem.* **2012**, *23*, 805–813.
[65] Q. Chen, X. Meng, P. McQuade, D. Rubins, S.-A. Lin, Z. Zeng, H. Haley, P. Miller, D. González Trotter, P. S. Low, *Mol. Pharm.* **2016**, *13*, 1520–1527.
[66] Q. Chen, X. Meng, P. McQuade, D. Rubins, S.-A. Lin, Z. Zeng, H. Haley, P. Miller, D. González Trotter, P. S. Low, *Mol. Pharm.* **2017**, *14*, 4353–4361.
[67] N. J. F. Verweij, M. Yaqub, S. T. G. Bruijnen, S. Pieplenbosch, M. M. ter Wee, G. Jansen, Q. Chen, P. S. Low, A. D. Windhorst, A. A. Lammertsma, O. S. Hoekstra, A. E. Voskuyl, C. J. van der Laken, *Sci. Rep.* **2020**, *10*, 1–10.
[68] J. Milton Harris, N. E. Martin, M. Modi, *Clin. Pharmacokinet.* **2001**, *40*, 539–551.
[69] Z. Wu, X. Li, C. Hou, Y. Qian, *J. Chem. Eng. Data* **2010**, *55*, 3958–3961.
[70] M. R. Ke, S. L. Yeung, D. K. P. Ng, W. P. Fong, P. C. Lo, *J. Med. Chem.* **2013**, *56*, 8475–8483.
[71] L. N. Goswami, Z. H. Houston, S. J. Sarma, S. S. Jalisatgi, M. F. Hawthorne, *Org. Biomol. Chem.* **2013**, *11*, 1116–1126.
[72] M. Poe, *J. Biol. Chem.* **1977**, *252*, 3724–3728.

Chapter 5

N-Heterocyclic Carbene Stabilised Boranes for Fluoride Binding

5.1 Introduction

The development of the diverse range of radiofluorinated heteroatom tracers over the last 15 years has involved two main radiolabelling strategies: substitution and isotopic exchange (IE). Ideally, these labelling reactions efficiently incorporate [^{18}F]fluoride in mild, aqueous compatible conditions using a no carrier-added fluoride source to produce a product of high molar activity that requires minimal purification. The successful implementation of these characteristics in heteroatom-based tracer design has been instrumental to the successful labelling of challenging biomolecules such as peptides and antibodies.[1,2]

Substitution strategies have been used to mono- and tri-fluorinate boron precursors such as those shown in Scheme 5.1. Alkoxide and amino substituents have commonly been employed as the leaving groups for these reactions, with acidic conditions used to aid displacement *via* protonation.[3–6] Unlike the monofluorinated systems, the synthesis of [^{18}F]trifluoroborate groups often necessitates a high concentration of the fluoride source, with respect to the tracer precursor, to achieve the required three-fold fluoride binding. Whilst these [^{18}F]trifluoroborate groups have been synthesised with no carrier added fluoride sources, yields can often been improved by addition of a ^{19}F-source of fluoride to increase the concentration.[4] The reduction of molar activity by use of a carrier added fluoride source is mitigated however by the trifluorinated product achieving a molar activity approximately three-times that of the carrier added [^{18}F]fluoride source.[4]

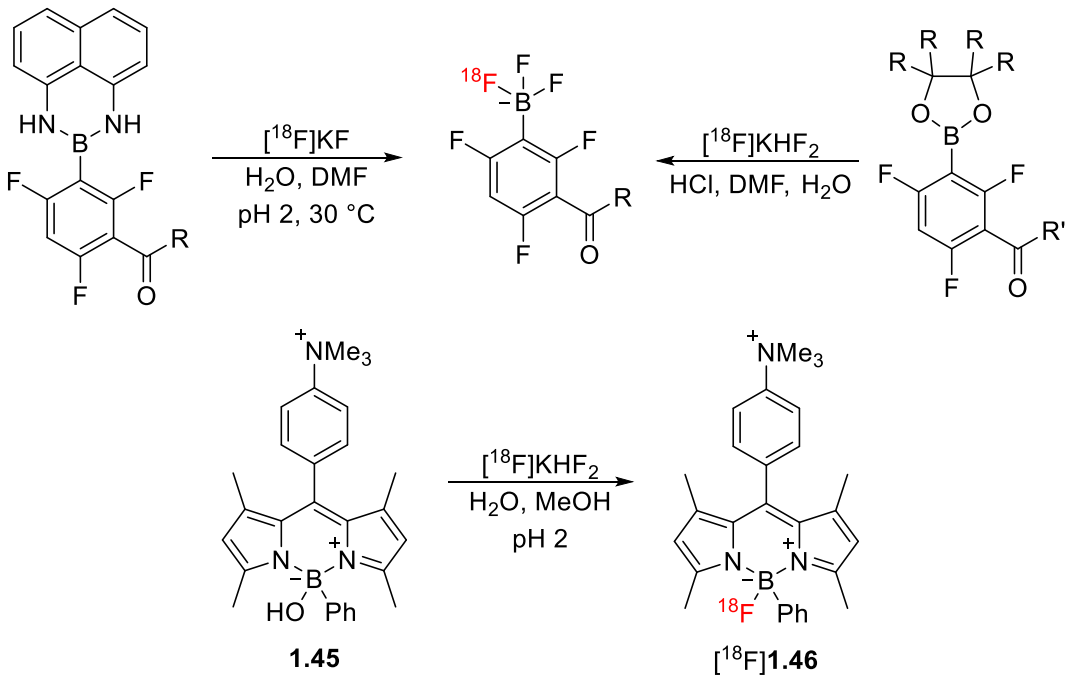

Scheme 5.1 – Substitution based radiolabelling reaction examples

Isotopic exchange is a simple, yet effective labelling method. The like-for-like exchange of a [^{19}F]fluoride ion for a [^{18}F]fluoride ion has several advantages as a method. Firstly, it exploits the requisite stability of the fluoroborate tracer by also utilising it as the precursor. A caveat to this however is that as the stability of fluoroborates increases, the B–F bonds become inherently less labile and therefore present a greater challenge to achieving sufficiently rapid exchange for effective labelling. Secondly, the identical nature of the starting material and product generally limits purification to the removal of unbound fluoride and avoids time-consuming HPLC. Finally, some compounds also tolerate water in the isotopic exchange reaction, although those of moderate tolerance can subsequently require additional purification steps to remove minor degradation products such as boronic acids.[7–9]

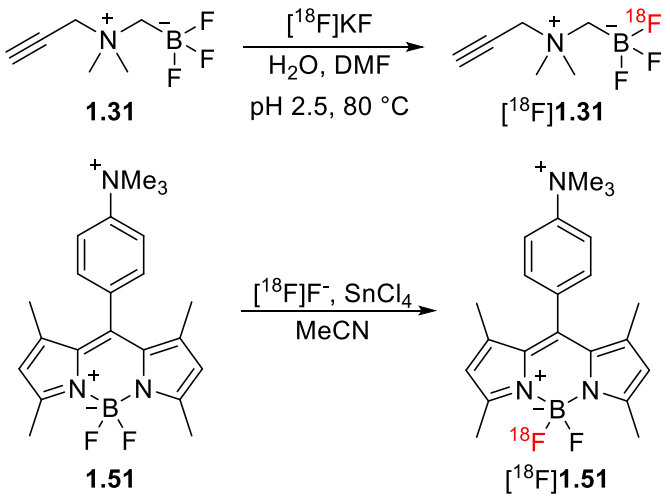

Scheme 5.2 – Examples of isotopic exchange reactions

High radiochemical yields and molar activities have been achieved with a variety of systems by conducting reactions at a low pH (pH ≤ 3), *i.e.* acid catalysed isotopic exchange (Scheme 5.2).[8–12] In a variation on this approach, Keliher *et al*. employed a Tf_2O/^{t}BuOH mixture for the *in situ* generation of triflic acid to initiate isotopic exchange with BODIPY derivatives.[13] Meanwhile, Liu *et al*. explored the addition of different Lewis acids to the labelling reaction of a cationic BODIPY derivative to labilise the robust B–F bonds for isotopic exchange after acidic conditions (pH 2) proved ineffective.[14] $SnCl_4$ proved to be the most effective of those explored and has subsequently been used as a Lewis acid promoter in isotopic exchange labelling reactions of other structures.[15–17] The amount of Lewis acid promoter required varies between systems: catalytic quantities are sufficient for labelling difluoro-dioxaborinin whilst NHC-BF_3 systems require a considerable excess for efficient labelling.

5.2 Aims

Current methods for ^{18}F-labelling carbene fluoroboranes are limited to Lewis acid promoted isotopic exchange (Scheme 5.3). These isotopic exchange labelling conditions are not universally applicable, however, with the promoter reagent $SnCl_4$ linked to the decomposition of conjugated biomolecules and reactions also requiring azeotropically dried

fluoride and solvents.[16,18] Hence, in order to fully exploit the potential of these highly stable carbene fluoroborane complexes, additional labelling strategies are sought. This chapter therefore reports on attempts to investigate substitution-based synthetic routes to these systems, and to explore how our second project objective of "rapid, efficient fluoride binding" may be achieved with this methodology. A substitution-based approach may also prove advantageous in other aspects, for example, by providing a water tolerant strategy or by producing higher molar activities given that the ^{18}F-products should be separable from unlabelled starting material.

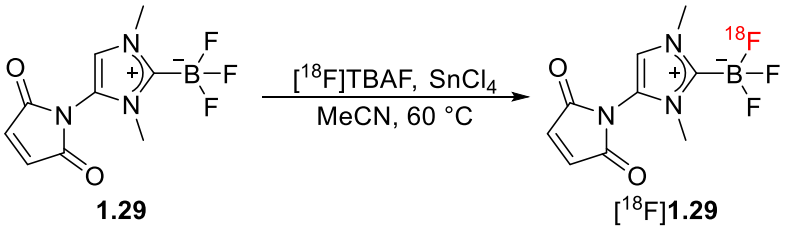

Scheme 5.3 – Isotopic exchange reaction of NHC-BF_3 compound

Previous reports of fluoride substitution at carbene bound boron centres have centred around carbene boranes (NHC-BH_3) in part due to the interest in using carbene boranes as hydrogen atom donors in radical chemistry.[19–21] Whilst the electrophilic source of fluorine "Selectfluor" can directly fluorinate these robust carbene boranes, nucleophilic routes have also been established which necessitate the generation of a reactive intermediate.[22–26] Triflic acid and iodine have both been used to activate the boranes, generating triflate and iodide derivatives which then readily undergo fluoride substitution, as illustrated in Scheme 5.4.[24,25] Currently, these intermediates limit fluoride incorporation to two ions and their sensitive nature has called for *in situ* syntheses.

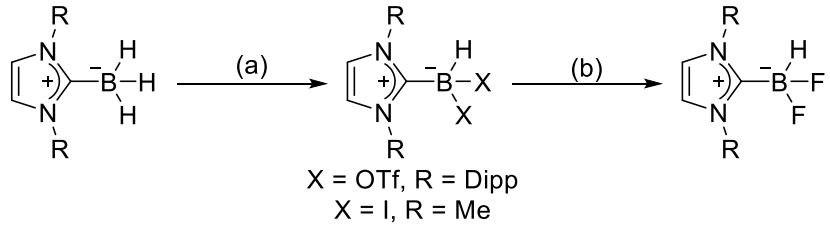

Scheme 5.4 – Synthesis of carbene stabilised difluoroborane. For X = OTf : (a) 2.3 eq TfOH, CH_2Cl_2 (b) 4 eq 1M TBAF in THF. For X = I: (a) 1 eq I_2 CH_2Cl_2 (b) 2 eq TBAF in THF.

The work described in this chapter consequently aims to expand the scope of available fluoride binding chemistry of carbene bound boranes in order to develop a versatile substitution-based strategy to carbene stabilised fluoroboranes. It is anticipated that with an appropriate choice of leaving groups, fluoride binding may be achieved in a timely manner without requiring the addition of reactive promoter reagents which may cause undesirable degradation. A selection of *N*-heterocyclic carbenes will also be utilised as stabilising groups in the expectation they will provide an additional handle with which to tune the fluoride binding, and stability, of the structures.

5.3 NHC-BBr_3 to NHC-BF_3

The *N*-heterocyclic carbene boron tribromide (NHC-BBr_3) adduct **5.1** was first employed as a simple system with which to investigate the nucleophilic fluoride substitution at a carbene borane framework featuring three leaving groups. **5.1** was isolated from a straightforward coordination reaction of the free carbene with boron tribromide in dichloromethane, previously reported by Aldridge and coworkers.[27]

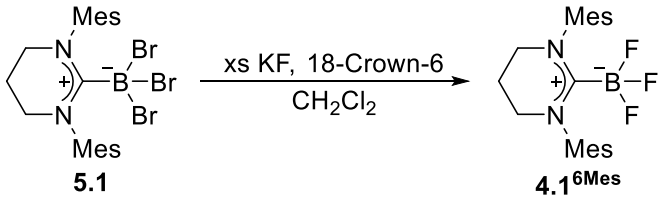

5.1 **4.1^{6Mes}**

Scheme 5.5 – Halide exchange reaction of NHC-BBr_3, **5.1**, with fluoride.

Fluoride uptake by **5.1** was assessed by combining the reagent with six equivalents of potassium fluoride and three equivalents of 18-crown-6 in dichloromethane (Scheme 5.5).

Following 15 minutes sonication, to aid fluoride solubility, the reaction was examined using multinuclear NMR spectroscopy. The ^{11}B NMR spectrum in Figure 5.1 indicates, by the absence of a singlet at -15 ppm, that **5.1** has been consumed and the trifluoroborate adduct **4.1^{6Mes}** has been formed as the major product with a dominant quartet ($^{1}J_{BF}$ = 37.4 Hz) at -1 ppm. This is further confirmed by the ^{19}F NMR spectrum where the corresponding 1:1:1:1 quartet is resolved at -140.9 ppm. Both spectra appear to contain small amounts of other products which are potentially mixed species containing both fluoride and bromide, but these can be removed upon washing the reaction mixture with water (whilst **4.1^{6Mes}** is stable). However, the ^{19}F NMR spectrum also features a prominent signal at -152.8 ppm associated with the $[BF_4]^-$ anion, hinting at the possibility for cleavage of the B–C bond under these conditions. This factor, together with the high moisture sensitivity of the tribromide adduct **5.1** motivated the search for more robust alternatives.

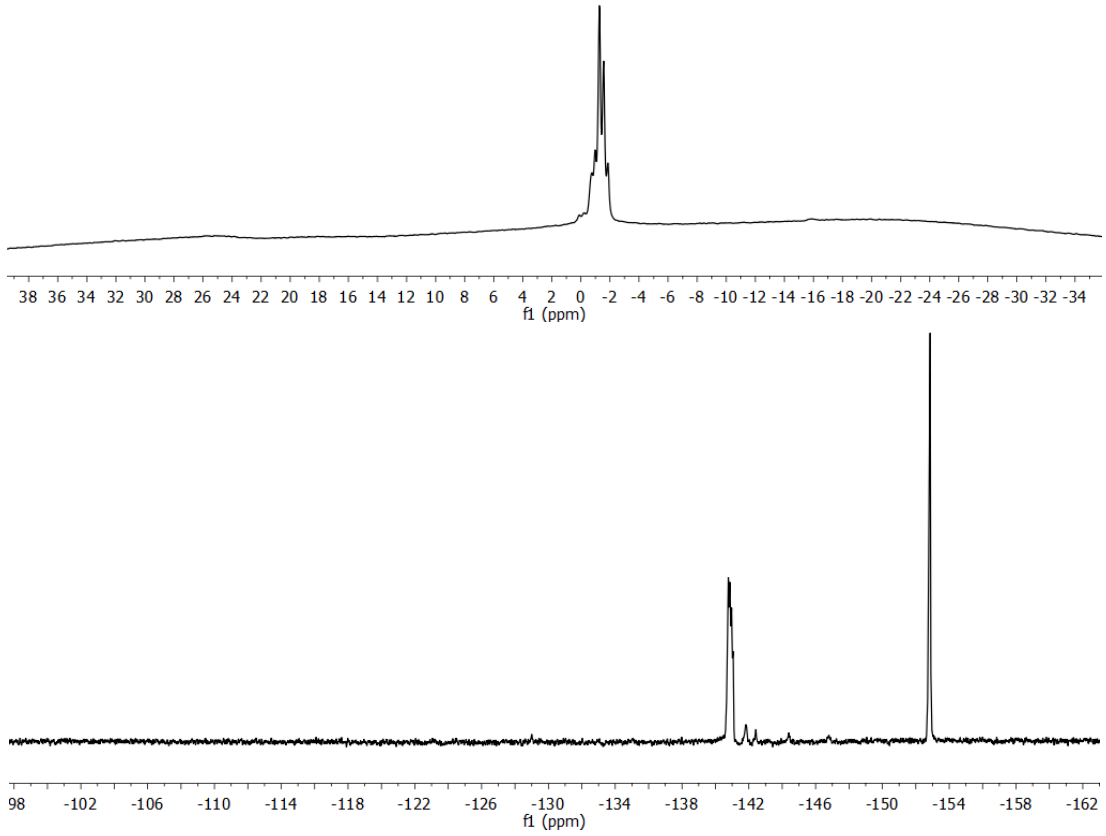

Figure 5.1 – ^{11}B NMR (top) and ^{19}F NMR (bottom) spectra for the fluoride substitution reaction of **5.1**.

5.4 *N*-Heterocyclic Carbene Catecholatoborenium Complexes and their Halide Bound Derivatives

Cationic boron compounds were considered attractive systems to investigate for rapid fluoride binding, with the electrostatic contribution of the positive charge strongly favouring coordination of the fluoride anion. Three-coordinate borenium systems further lend themselves to this purpose with the vacant *p*-orbital allowing facile coordination. NHC stabilised catecholatoborenium cations ([NHC-BCat]$^+$) were consequently targeted, with catechol utilised in the ligand framework to provide additional stabilisation of the boron centre through π-donation and the chelate effect, although its potential as a leaving group was also to be probed.

5.4.1 Synthesis

The borenium species **5.2^{SIMes}** and **5.2^{6Mes}** were consequently prepared in a facile two-step manner, by first combining the respective carbenes with bromocatecholborane before abstraction of the bromide with a suitable Lewis Acid such as $AlCl_3$. The successful synthesis of the respective [NHC-BCat]$^+$ cations was confirmed by the presence of a broad signal in the respective ^{11}B NMR spectra at *ca.* 26 ppm, in accord with previously reported examples.[28] The bromoborane intermediates in this synthetic pathway (**5.3** in Scheme 5.6) were also readily isolated, with the 1,3-bis(mesityl)imidazolylidene (IMes) and 1,3-bis(mesityl)imidazolinylidene (SIMes) complexes conveniently precipitating out of the hexane reaction medium. The ^{11}B NMR resonances of the series **5.3** are consistent with four-coordinate boron environments, appearing as singlets in the 6 – 11 ppm range. Syntheses of the corresponding borenium species **5.2** from the isolated precursors **5.3** was also found to improve purity compared to abstraction of the bromide ion *in situ*.

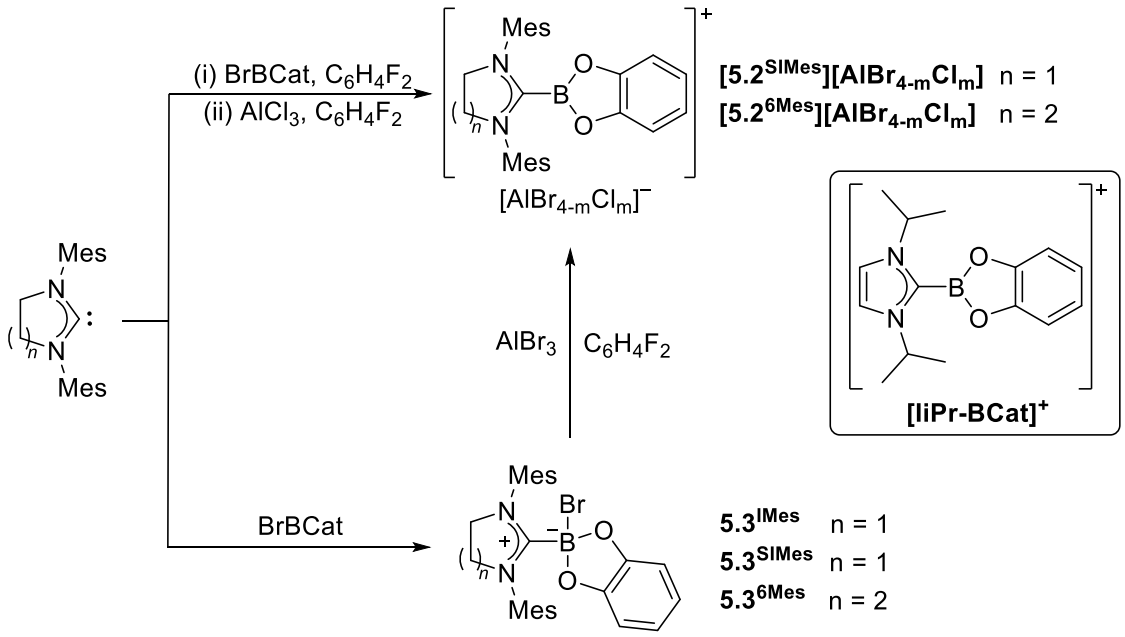

Scheme 5.6 – Synthesis of [NHC-BCat]$^+$ cations **5.2** and NHC-B(Br)Cat adducts **5.3**

5.4.2 Structural Characterisation of Borenium Complexes 5.2

[5.2^{SIMes}][AlBr$_4$] and **[5.2^{6Mes}][AlCl$_4$]** were crystallographically characterised allowing for structural comparison with the previously reported 1,3-bis(isopropyl)imidazolylidene complex **[(IiPr)-BCat]$^+$** (Scheme 5.6).[28] Inspection of the structural data in Table 5.1 reveals a distinct trend for the carbene series in which the carbon-boron bond lengths increase as the *p*-character of the carbene donor orbital increases. Hence, the structure of **5.2^{6Mes}** features the longest C–B bond of the three at 1.61(1) Å compared to 1.556(3) Å for the related imidazolylidene system.

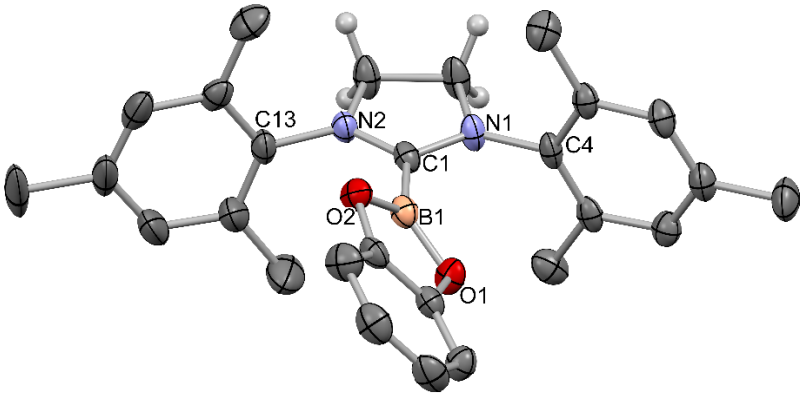

Figure 5.2 – Molecular structure of **[5.2^{SIMes}][AlBr$_4$]** showing one of two molecules in the asymmetric unit. Counteranion and selected hydrogens have been omitted for clarity. Thermal ellipsoids set at the 40 % probability level.

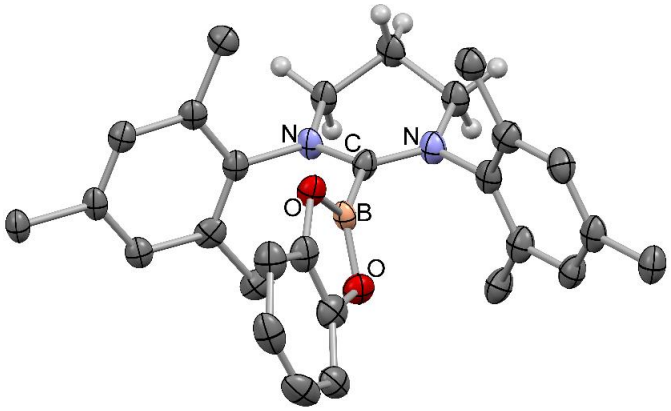

Figure 5.3 – Molecular structure of **[5.2^{6Mes}][AlCl$_4$]** showing one of two molecules in the asymmetric unit. Counteranion and selected hydrogens have been omitted for clarity. Thermal ellipsoids set at the 40 % probability level.

	[(IiPr)-BCat]$^+$ [28]	**[(SIMes)-BCat]$^+$ 5.2^{SIMes}**	**[(6Mes)-BCat]$^+$ 5.2^{6Mes}**
d(C–B)	1.556(3)	1.59(2) / 1.58(2)	1.61(1) / 1.61(1)
d(B–O)	1.377(2), 1.375(2)	1.36(2), 1.38(1) / 1.36(2), 1.37(1)	1.36(1), 1.37(1) / 1.36(1), 1.37(1)
d(C–N)	1.351(2), 1.354(2)	1.32(1), 1.33(1) / 1.32(1), 1.32(1)	1.31(1), 1.31(1) / 1.30(1), 1.34(1)
d(B---C$_{ipso}$)	—	3.05(2), 3.11(2) / 3.11(2), 3.01(2)	2.79(1), 2.78(1) / 2.79(1), 2.78(1)
∠(O–B–O)	113.0(1)	114(1) / 114(1)	113.9(7) / 113.9(7)
∠(C–B–O)	123.4(1), 123.6(2)	125(1), 121(1) / 122(1), 124(1)	123.3(7), 122.8(7) / 123.9(7), 122.1(7)
∠(N–C–N)	106.8(1)	111.5(9) / 111.8(9)	124.1(7) / 122.3(8)
∠(N–C–B–O)	-15.8(3)	-44(2) / -64(2)	82(1) / 74(1)

Table 5.1 – Selected bond lengths (Å) and angles (°) from the [NHC-BCat]$^+$ borenium structures.

The molecular structure of cation **5.2^{6Mes}**, shown in Figure 5.3, features a boron-arene interaction that has an apparent stabilising effect on the overall structure. This interaction is signalled by the close contact of the *ipso*-carbons of the flanking mesityl groups with the planar boron centre (2.79(1) Å and 2.78(1) Å), in addition to the alignment of the -BCat fragment with the vacant *p*-orbital of boron orientated towards the mesityl groups. This

interaction has previously been observed by Aldridge and co-workers in related 2,6-dimesitylpyridine-stabilised borenium complexes (featuring bromide or catecholate substituents at boron), as well as the $[(6Mes)\text{-}BBr_2]^+$ cation.[27] The authors described the interaction of the electron rich π-systems with the Lewis acidic boron centre as being primarily electrostatic in nature, given the long contact distances and lack of pyramidalization of the *ipso*-carbons.[27]

Additional stabilising interactions are not readily discernible in the **[5.2^{SIMes}][AlBr$_4$]** crystal structure. The wider angle defined by the flanking mesityl groups and a more rigid carbene backbone limit the arene approach to the boron centre to contact distances in the range 3.0 – 3.11 Å. While these contact distances are still within the van der Waals radii, they are considerably longer than those found in **5.2^{6Mes}** or the range previously reported for the 2,6-dimesitylpyridine structures (2.734 – 2.785 Å), suggesting that if an arene interaction is present it is likely to be very weak.[27] The -BCat group also does not favour a specific orientation, twisting 44(2) ° and 64(2) ° out of the plane of the carbene ring in the two molecules of the asymmetric unit. This contrasts the near perpendicular positioning of the -BCat group in the 6Mes structure (Table 5.1). Finally, unlike the related imidazolylidene stabilised borenium systems reported by Vidović and co-workers, the boron centre does not interact with the counteranion: the shortest boron bromine distance is 5.12(1) Å.[28,29] The high steric bulk of the mesityl groups likely inhibit a closer approach of the aluminium tetrabromide counteranion to the boron centre.

5.4.3 DFT Studies of Borenium Complexes 5.2

In order to shed further light on the impact of the different carbenes on the properties of the $[(NHC)\text{-}BCat]^+$ cations, DFT studies were undertaken. For comparison with the experimentally synthesised cations, the IMes derivative **5.2^{IMes}** was also optimised (Figure 5.4, top row). The resulting structures feature bond lengths and angles consistent with their

experimental equivalents (Table 5.2). Increasing proximity of the mesityl groups to the boron centre across the series is accompanied by an increase in the torsion angle between the planes of the carbene and -BCat groups. The three carbon backbone of the 6Mes carbene enables close approach of the mesityl groups to boron centre, which facilitates the boron-arene interaction and entails a perpendicular torsion angle between the -BCat and NHC planes. By contrast, the wide pocket defined by the flanking mesityl groups of the IMes system rules out any significant boron-arene interaction, and the corresponding NHC-BCat torsion angle is close to zero. The SIMes system resides between these extremes, with the flanking mesityl groups having a closer approach than in the IMes system and the torsion angle being at 60 °.

	5.2^{IMes}	**5.2^{SIMes}**	**5.2^{6Mes}**
d(B–C)	1.54969	1.57449	1.58454
d(B---C_{ipso})	3.11065 3.11059	3.00098 3.00103	2.76400 2.76144
∠(N–C–N)	106.460	112.737	123.132
∠(N–C–B–O)	2.57885	-60.10045	89.28937

Table 5.2 – Selected bond lengths (Å) and angles (°) from DFT optimised structures of the borenium cations.

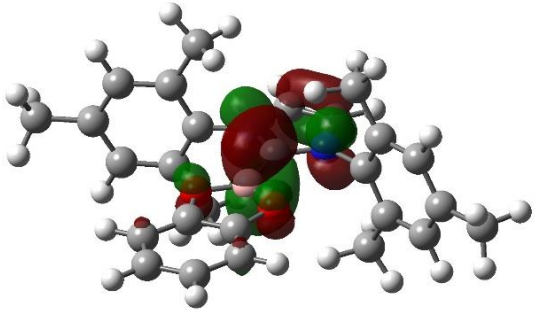

LUMO (-230.1 kJ mol^{-1})

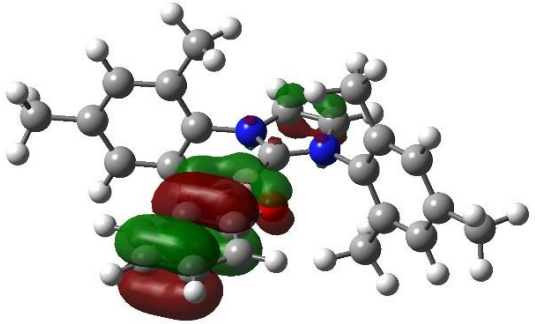

HOMO (-699.8 kJ mol^{-1})

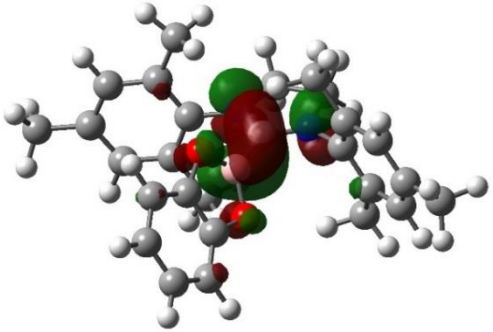

LUMO (-193.7 kJ mol^{-1})

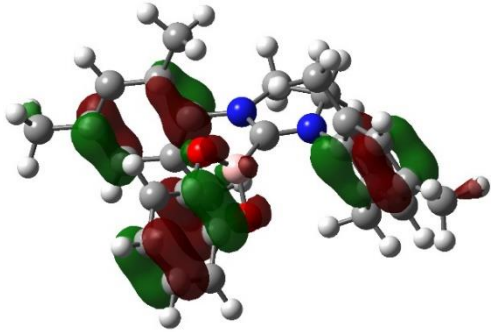

HOMO (-702.9 kJ mol^{-1})

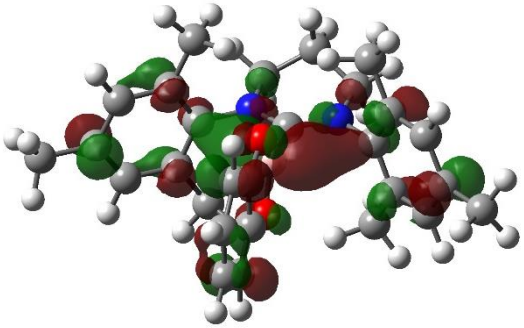

LUMO+1 (-110.3 kJ mol^{-1})

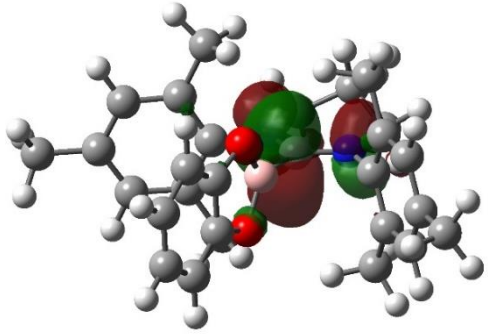

LUMO (-141.6 kJ mol^{-1})

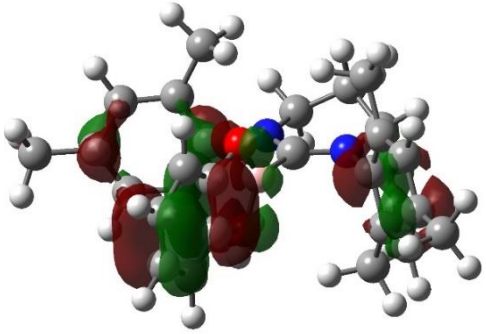

HOMO (-690.6 kJ mol^{-1})

Figure 5.4 – Frontier orbitals of **5.2^{IMes}** (top row), **5.2^{SIMes}** (middle) and **5.2^{6Mes}** (bottom) set at the iso-surface value of 0.04.

Whilst the HOMOs of the series are primarily comprised of the π-system of the -BCat moiety, the character and energy of the LUMO varies according to the carbene characteristics and functional group alignment of the borenium cation. For example, the LUMO of the **5.2^{6Mes}** cation is the highest in energy of the three and is composed of the carbene N–C–N π*-orbital. The p_{π}-orbital of the boron centre contributes to the LUMO+1, as part of a -BCat π*-orbital, having been destabilised in this case by the arene-interaction. By contrast, the LUMO of the **5.2^{IMes}** system features contributions from both the π*-orbital of the NHC and the π*-orbital of the -BCat moiety. The constructive overlap of the in-phase π*-orbitals is aided by the coplanar alignment of the groups and has a stabilising effect on the LUMO, as illustrated in Figure 5.5. As such, it is the lowest in energy of the three LUMOs at -230.1 kJ mol^{-1}. The resulting π-type orbital moreover resembles the respective SOMOs and HOMOs of related NHC-boryl radicals and anions.[30–33] Lastly, whilst the LUMO of the **5.2^{SIMes}** system is also comprised of in-phase NHC and -BCat π*-orbitals it does not experience the same extent of stabilisation as the LUMO of the **5.2^{IMes}** system (E = -193.7 kJ mol^{-1}). This is despite an expected better energy match between the two interacting π*-systems due to the N–C–N π*-orbital of the saturated NHC lying lower in energy than that of the unsaturated IMes carbene. The inferior stabilisation may be attributed to the twisted conformation of the structure, with its acute N–C–B–O torsion angle of 60 °, limiting the constructive overlap of the respective orbitals.

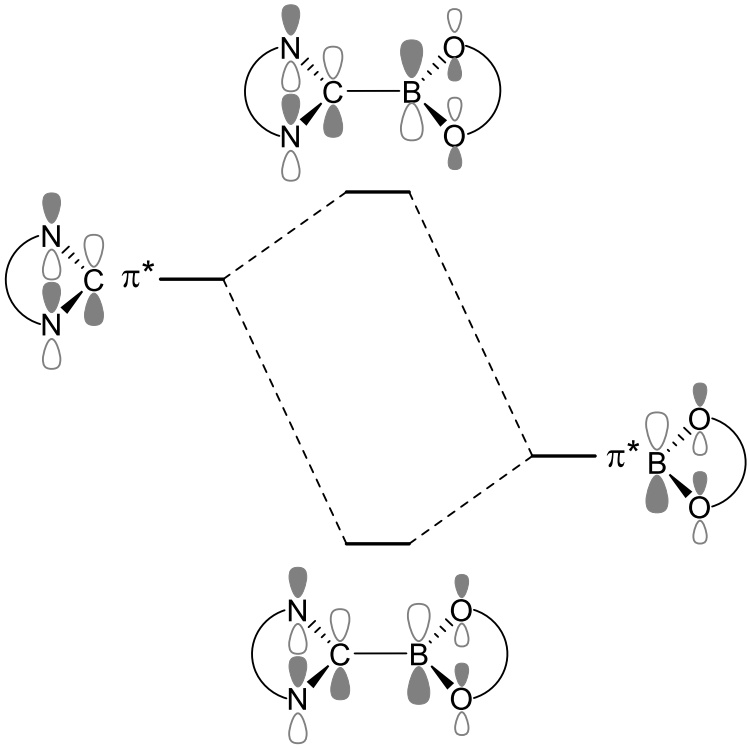

Figure 5.5 – Molecular orbital diagram depicting the interaction of π*-orbitals possible with the NHC and catecholborane groups.

5.4.4 Structural Characterisation of Bromoborane Complexes 5.3

As depicted in Figure 5.6, bromoborane compounds of the type **5.3** adopt a tetrahedral geometry at the boron centre with the B–Br bond positioned perpendicular to the plane of the carbene ring. Inspection of the structural data in Table 5.3 reveals some interesting differences between these structures. The C–B bond lengths feature the same trend as for the **5.2** series, increasing from 1.605(2) Å in **5.3^{IMes}** to 1.653(2) Å in **5.3^{6Mes}**. The increase in coordination number at boron leads to elongation of the C–B bonds compared to their respective borenium cations (*i.e.* 1.556(3) – 1.61(1) Å). Most noteworthy is the variation in B–Br bond lengths across the series and the concomitant change in boron pyramidalization. **5.3^{SIMes}** exhibits the shortest boron-bromide interaction (2.132(2) Å) and is pyramidalized at boron to the extent that the respective angles sum to 334.7 °. **5.3^{IMes}** meanwhile features a much longer B–Br bond (2.187(2) Å) and a more planar boron centre (338.9 °). The

corresponding values for **5.3^{6Mes}** fall between these limits at 2.151(2) Å and 336.7 ° respectively.

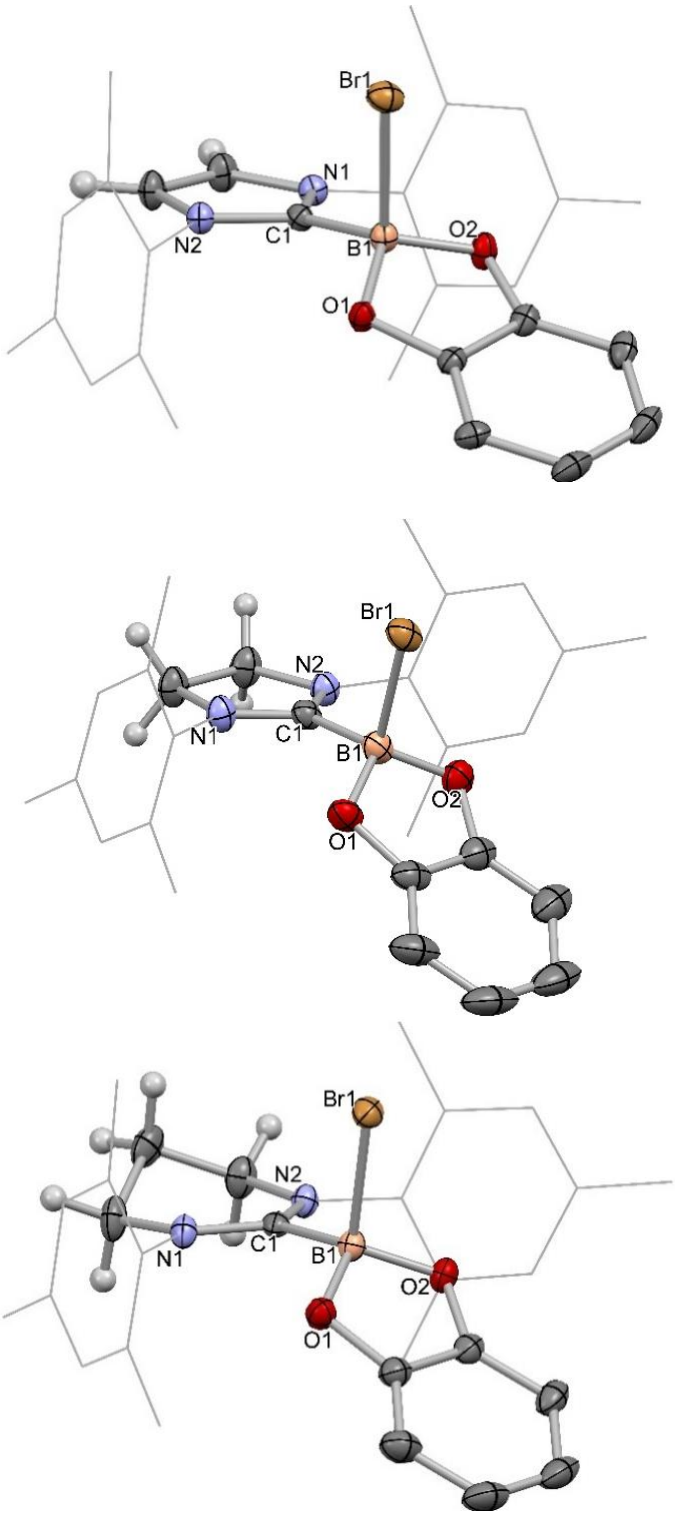

Figure 5.6 – Solid-state structures of **5.3^{IMes}** (top), **5.3^{SIMes}** (middle) and **5.3^{6Mes}** (bottom) as determined by X-ray crystallography. Thermal ellipsoids are set at 40 % probability level. Mesityl groups are represented as wireframe and most hydrogens have been omitted for clarity.

	IMes-B(Br)Cat **5.3^{IMes}**	**SIMes-B(Br)Cat** **5.3^{SIMes}**	**6Mes-B(Br)Cat** **5.3^{6Mes}**
d(C–B)	1.605(2)	1.627(2)	1.653(2)
d(B–Br)	2.187(2)	2.132(2)	2.151(2)
d(B–O)	1.439(2), 1.441(2)	1.453(2), 1.445(2)	1.448(2), 1.449(2)
d(C–N)	1.348(2), 1.351(2)	1.325(2), 1.326(2)	1.336(2), 1.335(2)
d(B---C_{ipso})	3.247(2), 3.178(2)	3.168(2), 3.159(2)	3.041(2), 3.005(2)
∠(O–B–O)	108.4(1)	107.5(1)	106.8(1)
∠(C–B–O)	114.5(1), 116.0(1)	113.2(1), 114.0(1)	114.8(1), 115.1(1)
Sum of Boron angles in NHC-BCat fragment	338.9	334.7	336.7
∠(N–C–N)	105.7(1)	110.2(1)	118.6(1)
∠(Br–B–O)	108.5(1), 106.3(1)	108.7(1), 109.0(1)	108.0(1), 107.5(1)
∠(C–B–Br)	102.41(9)	104.2(1)	104.2(1)
∠(N–C–B–Br)	98.9(1), -76.0(2)	-86.9(2), 96.1(2)	-87.9(2), 92.9(1)

Table 5.3 – Important bond lengths (Å) and angles (°) for **5.3** structures

The trend in the B–Br bond lengths appears to run counterintuitively to the LUMO energies of the corresponding borenium structures in Figure 5.4, which increase from **5.2^{IMes}** to **5.2^{6Mes}**. Indeed, where the planar **5.2^{IMes}** system features the lowest energy LUMO, it may be presumed to be the most Lewis acidic compound and its bromide complex consequently expected to feature the shortest B–Br bond, instead of the longest. However, it must be noted that the calculated LUMOs correspond to the ground-state structures of the borenium cations whose geometries are not generally reflected in the NHC-BCat fragments of the **5.3** bromide complexes (Figure 5.6). In particular, the three bromide complexes feature effectively coplanar alignments of the BCat and carbene fragments, whereas in the borenium structures the torsion angles between the two units vary significantly. This difference in geometry (and consequently coordination) is especially pronounced for the 6Mes bound systems. The

perpendicularly aligned structure of **5.2^{6Mes}** is stabilised by a boron-arene interaction meaning that it is the least Lewis acidic cation and features a high energy, carbene based LUMO. On the other hand, the NHC-BCat fragment in **5.3^{6Mes}** features a near coplanar alignment of the carbene and BCat groups, with a shorter B–Br bond than that found in **5.3^{IMes}**. This implies that if the structure of **5.2^{6Mes}** was also to be coplanar it would feature a lower energy LUMO than **5.2^{IMes}** and be a stronger Lewis Acid. With a coplanar alignment earlier noted to facilitate interactions between the boron centre and the carbene π-systems, the trend in coordination could be inferred to result from the differing π-characteristics of the saturated and unsaturated carbenes.

Interestingly, 6Mes-B(Br)Cat is found to spontaneously release bromide and generate the borenium salt **[5.2^{6Mes}]Br** in polar solvents such as dichloromethane, chloroform and acetonitrile. This dissociation is marked by a considerable downfield shift in the ^{11}B NMR signal from 11 ppm in d_6-benzene to *circa* 26 ppm in the more polar solvents. Spontaneous release of bromide is not observed for SIMes-B(Br)Cat or IMes-B(Br)Cat however, despite **5.3^{IMes}** notably featuring the longest B–Br bond of the series; these two adducts readily crystallise from boiling acetonitrile with retention of coordinated bromide. The facile bromide release by **5.3^{6Mes}** may therefore be attributed to the stabilising effect of the characteristic boron-arene interaction in the **5.2^{6Mes}** cation. The additional stabilisation provided by this interaction establishes the borenium salt as the more thermodynamically favourable compound in polar solvents where the salt is well solvated. Furthermore, comparison of the **5.3^{6Mes}** and **5.2^{6Mes}** structures highlights how the flexibility of the expanded ring carbene facilitates the boron-arene interaction. In particular, the heterocycles N–C–N angle substantially widens upon bromide dissociation from 118.6(1) ° in **5.3^{6Mes}** to 122.3(8) ° and 124.1(7) ° in the two molecules in the asymmetric unit of the borenium cation. This enables the distance between the boron centre and the *ipso*-carbons of the

flanking mesityls to decrease from 3.041(2) Å and 3.005(2) Å in the adduct to 2.79(1) Å and 2.78(1) Å in the cation.

5.4.5 Fluoride Binding

[5.2^{6Mes}][AlCl$_4$] demonstrates very fast uptake of fluoride, as expected. A CD_2Cl_2 solution of the borenium species was combined with six equivalents of potassium fluoride and three equivalents of 18-crown-6 and sonicated briefly to aid fluoride solubility. Monitoring the reaction after 15 minutes, the ^{1}H NMR and ^{11}B NMR spectra showed no signs of the starting material and the formation of one main product. The ^{11}B NMR spectrum is dominated by a doublet ($^1J_{BF}$ = 49.8 Hz) at 6 ppm whilst the ^{19}F NMR spectrum displays a corresponding 1:1:1:1 quartet at -135.9 ppm indicating that a single fluoride ion is taken up to form **5.4^{6Mes}** (Scheme 5.7). No sign of further fluoride uptake was observed, with minor signals in the spectra instead attributed to hydrolysis products such as protonated carbene and boric acid, likely resulting from adventitious moisture in the reaction.

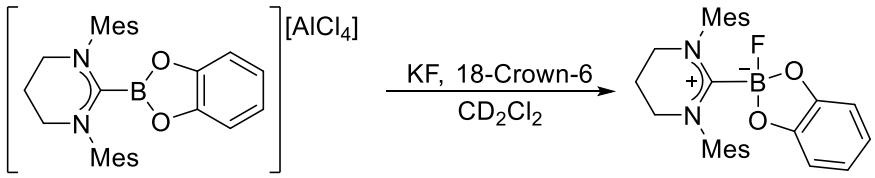

[5.2^{6Mes}][AlCl$_4$] **5.4^{6Mes}**

Scheme 5.7 – Fluoride binding reaction of **[5.2^{6Mes}][AlCl$_4$]**

Given the fluorophilicity of the tribromoborane **5.1**, fluoride uptake by bromoborane systems **5.3** was also examined. Each **5.3** derivative was taken up in acetonitrile with at least 1.5 equivalents of potassium fluoride and 18-crown-6 and stirred for several hours (Scheme 5.8). The reactions duly produced the respective monofluorinated compounds **5.4** as characterised by doublet signals in the ^{11}B NMR spectra at *ca.* 6 ppm. The ^{19}F NMR spectra exhibit the corresponding 1:1:1:1 quartets for **5.4^{IMes}** and **5.4^{SIMes}** at *circa* -143 ppm, marginally upfield from **5.4^{6Mes}**, and with coupling constants of *circa* 46 Hz. No sign of further fluoride substitution was observed upon monitoring reactions over an extended

period with a greater excess of fluoride, suggesting that systems of type **5.4** are not susceptible to displacement of the chelating catechol group.

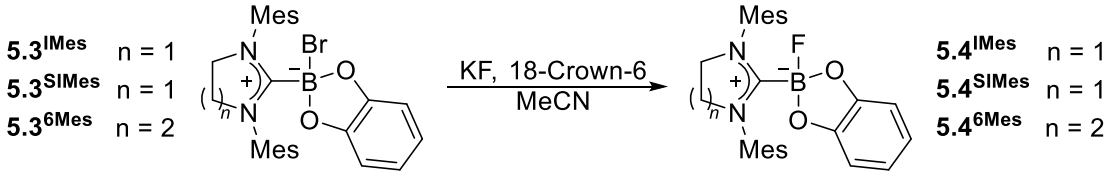

Scheme 5.8 – Fluoride binding of **5.3** series

Crystallographic characterisation of **5.4**$^{\mathbf{SIMes}}$ unambiguously confirmed the composition as NHC-B(F)Cat (Figure 5.7). The two distinct NHC-B(F)Cat molecules in the asymmetric unit each feature fluoride projected orthogonally to the plane of the carbene with B–F bond lengths of 1.393(3) Å and 1.406(3) Å, similar to that observed in other carbene-stabilised fluoroborane compounds. The B–C bonds of the two molecules are also of comparable length to NHC-BF_3 systems at 1.655(4) Å and 1.660(4) Å.

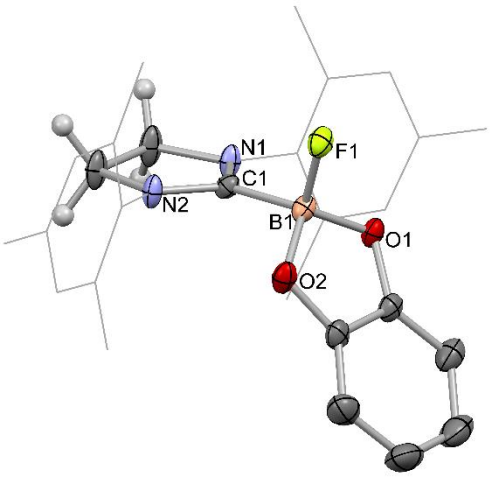

Figure 5.7 – Molecular structure of **5.4**$^{\mathbf{SIMes}}$ showing one of two molecules in the asymmetric unit. Thermal ellipsoids are set at the 40 % probability level. Mesityl groups are represented in wireframe format. Solvent molecule and most hydrogens have been omitted for clarity. Selected bond lengths (Å) and angles (°): B1–C1 1.660(4), B2–C28 1.655(4), B1–F1 1.393(3), B2–F2 1.406(3), N1–C1–B1–F1 96.4(3), N2–C1–B1–F1 -84.0(3), N3–C28–B2–F2 91.3(3), N4–C28–B2–F2 93.9(3).

The rate of fluoride uptake by the **5.3**$^{\mathbf{SIMes}}$ bromide adduct was subsequently investigated *via* NMR. A d_3-acetonitrile / difluorobenzene solution of **5.3**$^{\mathbf{SIMes}}$ was added to one equivalent of the soluble fluoride source tris(dimethylamino)sulfonium

difluorotrimethylsilicate (TASF). Significantly, the reaction reached completion within 5 minutes, *i.e.* before an NMR spectrum could be measured. This suggests that systems of the type **5.3** could provide a direct and timely route to **5.4**, that bypasses the need to synthesise the borenium salt without compromising on rate. Moreover, the coordinatively saturated structure of **5.3** offers greater potential for water resistance.

5.4.6 Moisture and Air Stability

The water stability of the **5.3**$^{\mathbf{SIMes}}$ was consequently tested by adding an excess of water to a dry d_3-acetonitrile solution. The compound was observed to rapidly decompose, with a ^{1}H NMR spectrum acquired five minutes after water addition showing no signs of the starting material. The ^{1}H NMR spectrum instead features signals consistent with the protonated carbene whilst the ^{11}B NMR is dominated by a broad resonance at 20 ppm suggesting boric acid has also been formed (Scheme 5.9).

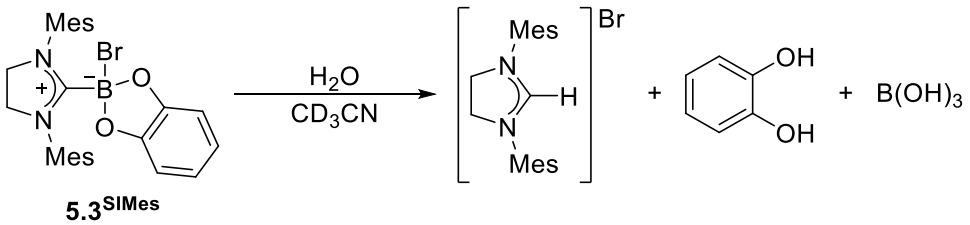

5.3$^{\mathbf{SIMes}}$

Scheme 5.9 – Hydrolysis reaction of **5.3**$^{\mathbf{SIMes}}$

The monofluoroborane **5.4** series by contrast is indefinitely air stable and is exceptionally robust to aqueous conditions. Testing the water stabilities of the series **5.4** was somewhat hindered by their poor solubility in predominantly aqueous solvent systems, but the compounds were sufficiently soluble in a 4:1 DMF-water mixture for solutions of 10 mM concentration to be made up and monitored *via* ^{19}F NMR spectroscopy. During the three-week period in which the samples were monitored, the spectra remained unchanged, and no sign of free fluoride was observed, indicating that the NHC-B(F)Cat systems are highly stable in the presence of water and are promising reagents for imaging purposes.

5.5 *N*-Heterocyclic Carbene Complexes of Catecholborane Derivatives

The previous section established a rapid, promoter-free, fluoride uptake pathway to water stable fluoroborane carbene compounds, **5.4**. However, whilst the four-coordinate bromide adducts **5.3** offer a direct route to **5.4**, they exhibit high sensitivity to air and moisture that is impractical for a late-stage labelling system. As a result, our attention turned to exploring alternative coordinatively-saturated derivatives of the type NHC-B(X)Cat that may exhibit greater stability in ambient conditions whilst still acting as a reactive precursor to fluoroborane complexes **5.4**.

Examination of the resonance forms of the NHC-B(X)Cat framework, illustrated in Scheme 5.10, reveals there is a significant amount of electron density at boron with, for example, the zwitterionic structure assigning a negative charge to the boron centre. The highly robust NHC-B(F)Cat structure of **5.4**, likely stabilises this electron density, in part, through the inductive withdrawing effect of the highly electronegative fluoride. We therefore resolved to explore other electron withdrawing groups as the X substituent, to investigate their effect on the stability and reactivity of the NHC-B(X)Cat framework. With this in mind, chloride and methoxide substituted compounds were targeted.

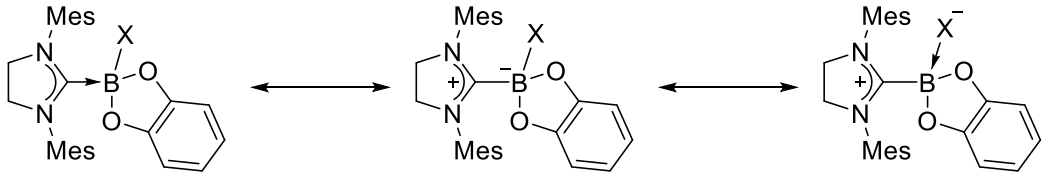

Scheme 5.10 – Resonance structures of an NHC-B(X)Cat framework

5.5.1 Synthesis and Characterisation

The chloride (**5.5**$^{\mathbf{SIMes}}$) and methoxide (**5.6**$^{\mathbf{SIMes}}$) adducts were synthesised by the same general procedure used to synthesise **5.3**$^{\mathbf{SIMes}}$. Accordingly, the compounds were isolated by precipitation from a mixture of the carbene and the respective catecholborane in hexane (Scheme 5.11). ^{11}B NMR characterisation reveals a singlet at 8 ppm for **5.5**$^{\mathbf{SIMes}}$ and 7 ppm

for **5.6**$^{\mathbf{SIMes}}$, slightly downfield of the bromide analogue. The methoxide adduct was found to be liable to degradation in solution however, hindering further purification and reactivity studies. Identifiable degradation products include the protonated carbene cation and the $BCat_2$ anion suggesting adventitious moisture was likely the cause. The apparent sensitivity of **5.6**$^{\mathbf{SIMes}}$ indicated it was unlikely to fulfil our aims of a bench-stable system and therefore was not pursued further.

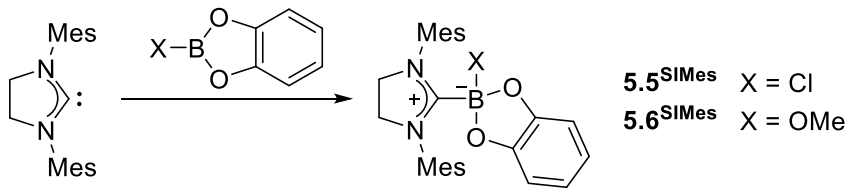

Scheme 5.11 – General reaction for the synthesis of NHC-B(X)Cat adducts

Recrystallisation of the chloride complex in acetonitrile yielded crystals suitable for X-ray crystallography. The two components in the resulting asymmetric unit closely resemble other NHC-B(X)Cat structures described in this chapter, with the B–Cl bond aligned perpendicular to the plane of the carbene ring (Figure 5.8). Further comparison of the imidazolinylidene bound halide series reveals typical haloborane trends, with significant data highlighted in Table 5.4. The B–C bonds of the two chloride structures average to 1.638 Å and reside between that of the bromide and fluoride complexes in length. This shortening of the B–C bond down the halide group is in accord with the typical increase in Lewis acidity of haloboranes down the group leading to a stronger association of the carbene. Concurrently, the geometry of the boron centre in the NHC-BCat fragment, *i.e.* the C-B-O_2 unit, becomes increasing planar down the group, suggesting weaker halide association that is consistent with the preference of boron for hard nucleophilic bases in accordance with HSAB theory.

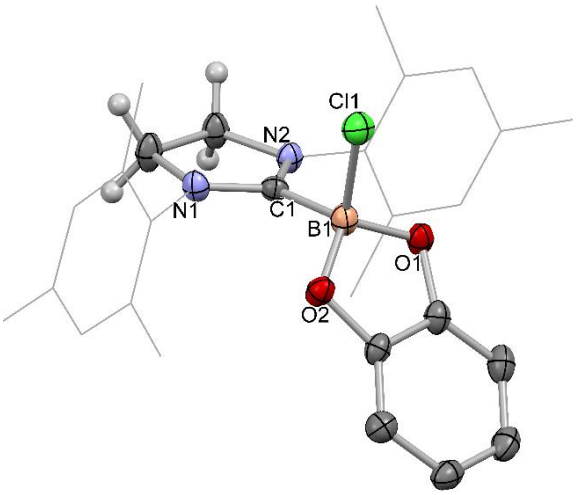

Figure 5.8 – Molecular structure of **5.5**$^{\mathbf{SIMes}}$ showing one of two molecules in the asymmetric unit. Thermal ellipsoids are set at 40 % probability level. Mesityl groups are represented as wireframe and most hydrogens have been omitted for clarity. Selected angles (°): N1–C1–B1–Cl1 -78.9(4), N2–C1–B1–Cl1 97.1(3), N3–C28–B2–Cl2 79.3(4), N4–C28–B2–Cl2 -96.7(3).

	SIMes-B(Br)Cat 5.3$^{\mathbf{SIMes}}$	**SIMes-B(Cl)Cat 5.5**$^{\mathbf{SIMes}}$	**SIMes-B(F)Cat 5.4**$^{\mathbf{SIMes}}$
d(C–B)	1.627(2)	1.634(5) / 1.641(5)	1.660(4) / 1.655(4)
d(B–O)	1.453(2), 1.445(2)	1.459(5), 1.460(5) / 1.457(5), 1.459(4)	1.472(3), 1.476(3) / 1.472(4), 1.474(4)
d(B–X)	2.132(2)	1.917(5) / 1.919(4)	1.393(3) / 1.406(3)
∠(O–B–O)	107.5(1)	106.9(3) / 107.2(3)	105.6(2) / 106.1(2)
∠(C–B–O)	113.2(1), 114.0(1)	112.7(3), 112.5(3) / 111.9(3), 113.5(3)	111.8(2), 109.7(2) / 109.8(2), 110.2(2)
Sum of Boron angles in NHC-BCat fragment	334.7	332.1 / 332.6	327.1 / 326.1
∠(O–B–X)	108.7(1), 109.0(1)	110.5(3), 111.3(3) / 110.7(2), 111.0(2)	111.0(2), 111.5(2) / 111.4(2), 111.2(2)
Sum of Boron angles in X-BCat fragment	325.2	328.7 / 328.9	328.1 / 328.7

Table 5.4 – Structural data for the halide series of NHC-B(X)Cat adducts. Bond lengths in Å and angles in °.

5.5.2 Fluoride Binding and Water Stability

The fluoride uptake and hydrolysis of **5.5**$^{\mathbf{SIMes}}$ was explored using similar conditions to that applied to **5.3**$^{\mathbf{SIMes}}$. Fluoride binding was assessed by adding 0.5 mL of a 0.04 M d_3-acetonitrile solution of **5.5**$^{\mathbf{SIMes}}$ to one equivalent of tris(dimethylamino)sulfonium difluorotrimethylsilicate (TASF). In the four-minute period between combining the reagents and acquisition of a ^{1}H NMR spectrum, the starting material was completely consumed and the ^{1}H NMR showed a clean conversion to **5.4**$^{\mathbf{SIMes}}$ had occurred. The water tolerance of **5.5**$^{\mathbf{SIMes}}$ was also explored in a similar manner by adding 50 μL of deionised water to 0.5 mL of the d_3-acetonitrile solution. As was observed for the bromide adduct, **5.5**$^{\mathbf{SIMes}}$ rapidly hydrolyses to its constituent parts within five minutes. Thus, the reactivity of the chloride system is essentially indistinguishable from that of **5.3**$^{\mathbf{SIMes}}$ under the applied conditions. With no discernible improvement in the water resilience of the NHC-B(X)Cat systems an alternative approach to a robust **5.4** precursor was sought.

5.6 *N*-Heterocyclic Carbene Stabilised Catecholatoboronium Complexes Featuring Different Donors

Four-coordinate boron cations are well established as exhibiting a high degree of air and moisture stability.[34] These so-called boronium species therefore present themselves as prime candidates in our search for bench-stable precursors to **5.4**, with the additional benefit of the positive charge introducing a Coulombic contribution to fluoride binding. Attention therefore turned to the use of a neutral donor group, L, as the leaving group in an [NHC-B(L)Cat]$^+$ boronium system. Furthermore, by considering the resonance forms of the structure in Scheme 5.12, it may be anticipated that by increasing the basicity of the donor group, the overall stability of the complex will increase as the donor can more readily stabilise the positive charge. This section will therefore describe the synthesis of a series of

[NHC-B(L)Cat]$^+$ compounds featuring systematic variation of the basicity of the L donor group and an investigation into the stability and fluoride binding by the boronium scaffolds.

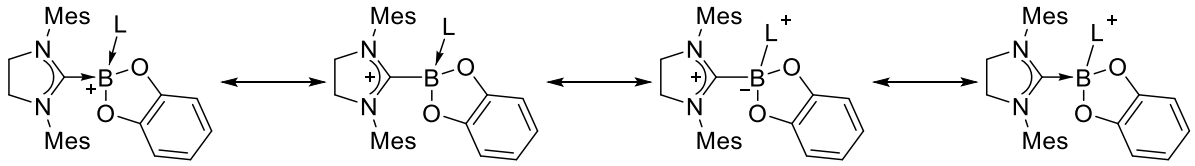

Scheme 5.12 – Resonance structures of [NHC-B(L)Cat]$^+$ boronium structures

5.6.1 Synthesis and Characterisation of Imidazolinylidene Complexes

A collection of boronium salts with *N*-heterocyclic molecules as the donor group L and SIMes as the stabilising carbene were consequently synthesised for comparison (Scheme 5.13). Compounds **5.7^{SIMes}** – **5.10^{SIMes}** were readily synthesised *via* simple substitution reactions of the labile bromide of **5.3^{SIMes}** with the respective donor group in acetonitrile. Substitution occurs cleanly and rapidly with the bromide displaced in a matter of minutes. One-to-one coordination was confirmed by the ratio of the donor and carbene signals in the ^{1}H NMR spectrum of the product, in addition to a slight downfield shift in the ^{1}H NMR signals of the methyl substituents of the donors in complexes **5.8^{SIMes}** – **5.10^{SIMes}**. The ^{11}B NMR data indicate that the boron environment has not experienced a significant change, with the signals appearing in the 5 – 7 ppm range, similar to the neutral precursor molecules.

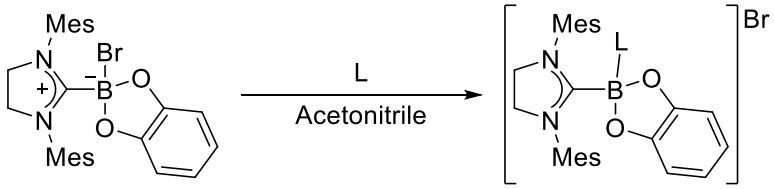

5.3^{SIMes}

Compound	L	pKa(LH) [35,36]
5.7^{SIMes}	Pyridine	5.23
5.8^{SIMes}	4-Methoxypyridine	6.58
5.9^{SIMes}	1-Methylimidazole	6.95
5.10^{SIMes}	4-Dimethylaminopyridine	9.60

Scheme 5.13 – General synthesis for [NHC-B(L)Cat]Br compounds **5.7^{SIMes} – 5.10^{SIMes}**. The table includes pKa values of the conjugate acid form of the L donor groups in aqueous solution.

Attempts to coordinate bulkier pyridine derivatives were less successful. Stirring **5.3^{SIMes}** with 2,6-dimethylpyridine resulted in multiple unidentified minor species, in addition to a significant amount of the bromide adduct remaining unreacted after several hours. This limited reactivity may be ascribed to the additional bulk of the pyridines *ortho*-methyl groups disfavouring coordination at boron on steric grounds, whilst also indicating the mesityl groups of the carbene are providing some degree of steric protection of the boron centre. The ^{1}H NMR spectra of **5.7^{SIMes}** – **5.10^{SIMes}** show no sign of steric congestion however, with the mesityl groups giving rise to two sharp alkyl singlets and one aromatic singlet indicating free rotation occurs in these compounds.

The crystallographic characterisation of **5.8^{SIMes}** – **5.10^{SIMes}** reveals striking structural similarities throughout the series despite the presence of different donors (Figure 5.9 – Figure 5.11, Table 5.5). The B–N bond lengths of the three compounds are equal within error at *circa* 1.57 Å, with the donor coordination also having induced the expected pyramidalization of the boron centres compared to the planar borenium cations. Additionally, the B–C bond lengths fall within a small range (1.652(4) – 1.665(5) Å); a range that is also noted to encompass the B–C bond of the fluoroborane **5.4^{SIMes}**. Finally, the L donor substituents of **5.8^{SIMes}** – **5.10^{SIMes}** appear to orientate to facilitate π-interactions between the flanking mesityl groups and the two aromatic substituents coordinated to boron.

	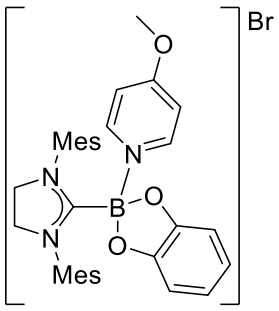 **5.8^{SIMes}**	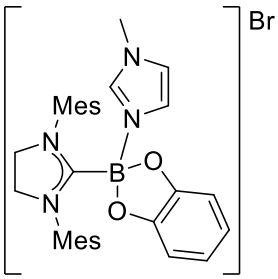 **5.9^{SIMes}**	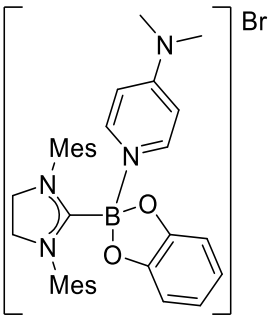 **5.10^{SIMes}**
d(C−B)	1.660(3)	1.652(4)	1.665(5)
d(B−N)	1.574(3)	1.577(5)	1.573(5)
d(B−O)	1.468(3), 1.472(2)	1.457(5), 1.468(4)	1.469(3), 1.470(4)
∠(O–B–O)	107.2(2)	107.9(3)	107.0(3)
∠(C–B–O)	109.1(2), 112.1(2)	108.3(2), 111.7(3)	107.6(2), 111.0(2)
Sum of Boron angles in NHC-BCat fragment	328.4	327.9	325.6

Table 5.5 – Selected bond lengths (Å) and angles (°) from the molecular structures of **5.8^{SIMes}**, **5.9^{SIMes}** and **5.10^{SIMes}**.

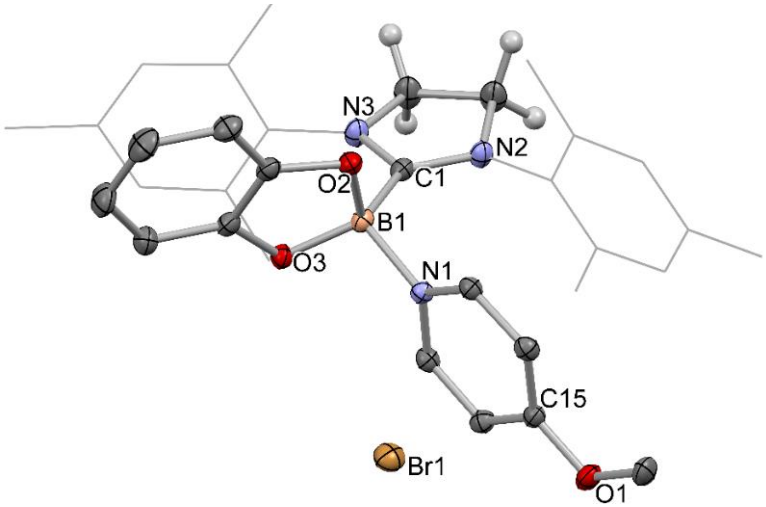

Figure 5.9 – Solid-state structure of **5.8^{SIMes}** as determined by X-ray crystallography. Thermal ellipsoids are set at the 40 % probability level. Mesityl groups are represented as wireframe and most hydrogens have been omitted for clarity. Selected additional bond lengths (Å): O1–C15 1.334(3), N2–C1 1.328(2), N3–C1 1.336(3).

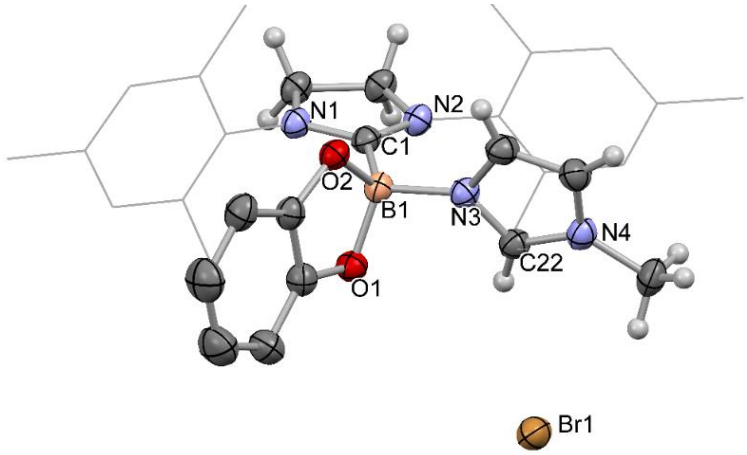

Figure 5.10 – Solid-state structure of **5.9**$^{\mathbf{SIMes}}$ as determined by X-ray crystallography. Thermal ellipsoids are set at the 40 % probability level. Mesityl groups are represented as wireframe and most hydrogens have been omitted for clarity. Selected additional bond lengths (Å): N3–C22 1.329(4), N4–C22 1.319(4), N4–C25 1.467(5), N1–C1 1.328(4), N2–C1 1.333(4).

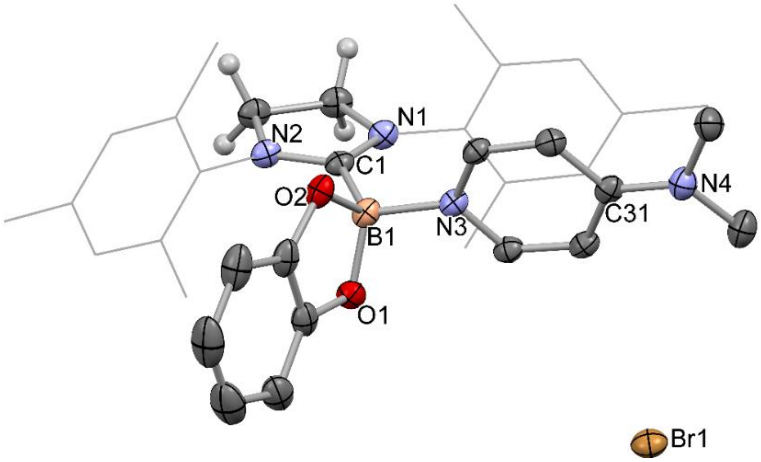

Figure 5.11 – Solid-state structure of **5.10**$^{\mathbf{SIMes}}$ as determined by X-ray crystallography. Thermal ellipsoids are set at the 40 % probability level. Mesityl groups are represented as wireframe and most hydrogens have been omitted for clarity. Selected additional bond lengths (Å): N4–C31 1.336(4), N1–C1 1.331(4), N2–C1 1.319(4).

Further inspection of compound **5.9**$^{\mathbf{SIMes}}$ (Figure 5.10) also suggests the positive charge of the complex is appreciably delocalised. In particular, the C22–N3 and C22-N4 bonds of the methylimidazole donor are noted to be nearly equal in length at 1.329(4) Å and 1.319(4) Å respectively. This feature contrasts with 'free' imidazoles, such as 1-benzylimidazole where the equivalent bonds are of more different length (1.326(3) Å and 1.351(2) Å).[37] The C–N bonds of the donor group thus more closely resemble the partial double bonds of an imidazolium cation, with its increased delocalisation; in 1,3-di(methyl)imidazolium chloride, for example, the C–N bonds are 1.323(2) Å and 1.335(2) Å in length.[38] This observation

suggests **5.9**$^{\mathbf{SIMes}}$ features an appreciable contribution from the resonance structures, in Scheme 5.12, where positive charge is taken on by the donor molecule.

5.6.2 Fluoride Binding in Dry Conditions

To assess the fluoride binding capabilities of the boronium species **5.7**$^{\mathbf{SIMes}}$ – **5.10**$^{\mathbf{SIMes}}$ NMR studies were undertaken with one-to-one binding conditions. Accordingly, a 0.04 M d_3-acetonitrile solution of each compound was made up and 0.5 mL added to approximately one equivalent of the soluble fluoride source tris(dimethylamino)sulfonium difluorotrimethylsilicate in a J-Youngs NMR tube. As anticipated, all four compounds cleanly generate the mono-fluorinated species **5.4**$^{\mathbf{SIMes}}$, as shown by the appearance of the characteristic ^{11}B NMR doublet and ^{19}F NMR quartet. Fluoride binding is also evident in the ^{1}H NMR spectrum of each reaction mixture by an upfield shift in the carbene backbone singlet to 4.05 ppm for the fluoroborane. Consequently, the well separated starting material and product resonances provide a useful handle with which to monitor the reactions.

The reaction timescales varied significantly between the boronium complexes. Pyridine complex **5.7** demonstrated the fastest fluoride uptake, fully converting to **5.4**$^{\mathbf{SIMes}}$ within four minutes, *i.e.* before the reaction could be monitored *via* NMR. On the other hand, the DMAP complex **5.10**$^{\mathbf{SIMes}}$ takes four weeks to achieve 65 % conversion to the fluoroborane product. The slower reactions of compounds **5.8**$^{\mathbf{SIMes}}$ – **5.10**$^{\mathbf{SIMes}}$ were monitored over an extended period with the resulting temporal plots included in Figure 5.12. To achieve 50 % conversion takes **5.8**$^{\mathbf{SIMes}}$ 17 minutes, **5.9**$^{\mathbf{SIMes}}$ 23.5 hours and **5.10**$^{\mathbf{SIMes}}$ 15.6 days. The subsequent half-lives also become progressively longer in each case, as demonstrated in the plot for compound **5.8**$^{\mathbf{SIMes}}$ (top left of Figure 5.12) where having passed 50 % conversion in 17 minutes it takes a further 27 minutes to reach 75 % and then an additional 38 minutes to reach 87.5 %; these changes are inconsistent with a first or second order reaction.

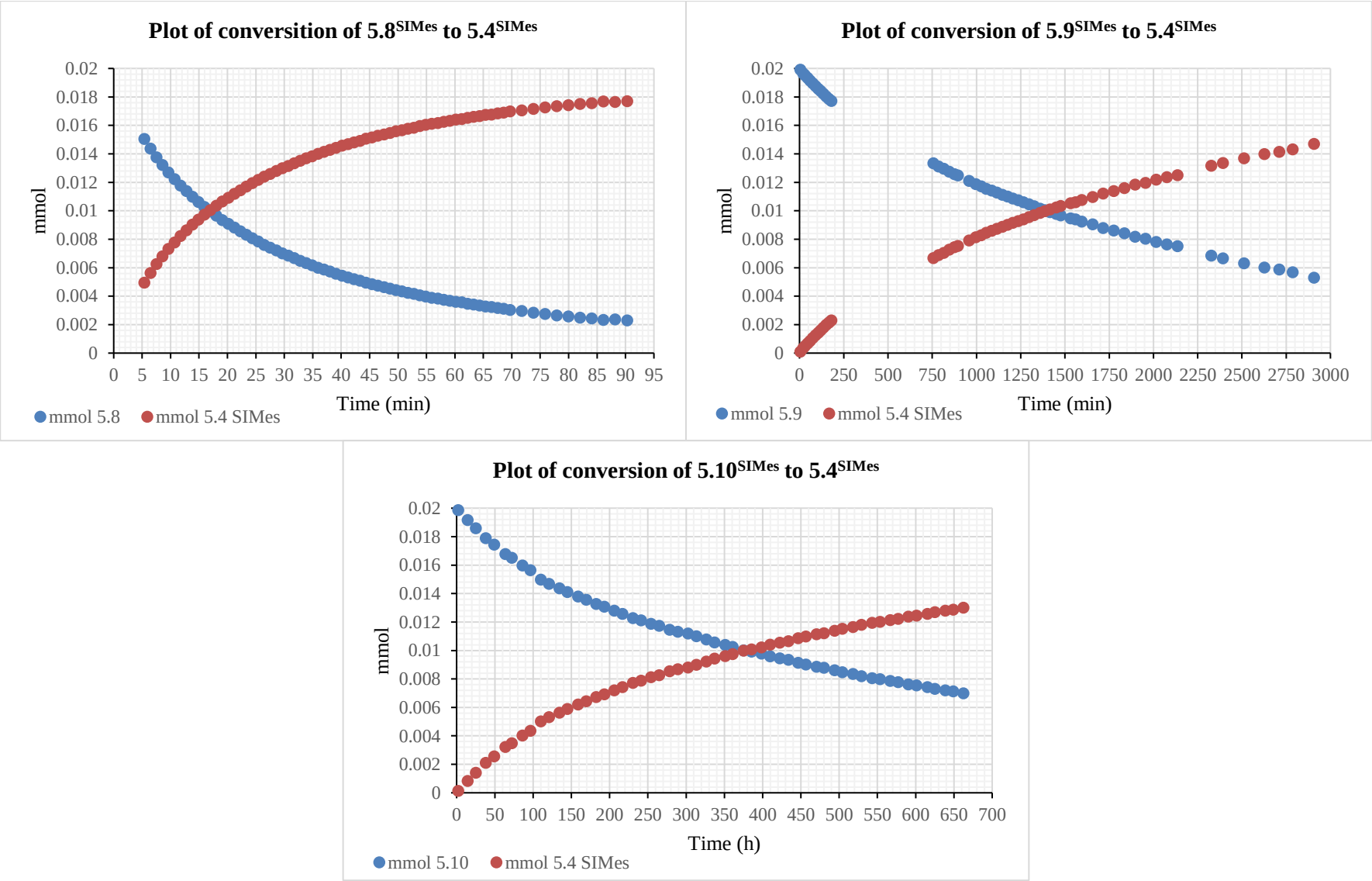

Figure 5.12 – Plots for the fluoride substitution reactions of **5.8**^{SIMes} (top left), **5.9**^{SIMes} (top right) and **5.10**^{SIMes} (bottom left) showing change in molar quantities against time in minutes or hour.

The substantial variation in the rate of fluoride uptake, with the different donor substituents, suggests the substitutions are occurring *via* a dissociative mechanism where breaking the B–N bond is the rate determining step of the reaction. The intermediate in the reaction is therefore the three coordinate borenium cation **5.2**$^{\mathbf{SIMes}}$. In addition to rapidly binding fluoride to form **5.4**$^{\mathbf{SIMes}}$, the intermediate **5.2**$^{\mathbf{SIMes}}$ can also rebind the dissociated donor resulting in an equilibrium between the four coordinate boronium starting material and the three coordinate borenium intermediate (Scheme 5.14). As the reaction progresses and the donor group increases in concentration, the reverse reaction of the equilibrium has a retarding effect on the rate and thereby elongates the half-lives. Moreover, the marked decrease in the rate through the series, from **5.7**$^{\mathbf{SIMes}}$ to **5.10**$^{\mathbf{SIMes}}$, indicates the activation energy for donor dissociation increases as the basicity of the donor increases. This relationship is the result of the more basic donors exerting a greater stabilising effect on the [NHC-B(L)Cat]$^+$ cation with respect to the unbound [NHC-BCat]$^+$ cation. Consequently, the energy gap between the starting material and the reaction intermediate is greater and the activation energy increases.

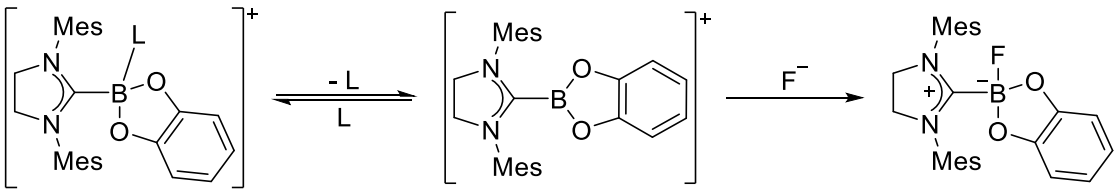

Scheme 5.14 – Mechanism for fluoride uptake by [NHC-B(L)Cat]$^+$ boroniums.

5.6.3 Water and Air Stability

To examine the aqueous stabilities of complexes **5.7**$^{\mathbf{SIMes}}$ – **5.10**$^{\mathbf{SIMes}}$, 50 μL of water was added to 0.5 mL of the 0.04 M compound stock solutions for a 10:1 acetonitrile-water solution. Subsequent monitoring of the reactions *via* ^{1}H NMR showed hydrolysis was occurring for all four compounds to again produce the protonated carbene with no observable intermediates. Boric acid and the [$BCat_2$]$^-$ anion were observed in the ^{11}B NMR spectra. As for fluoride substitution, the rate of hydrolysis slows from minutes to weeks as

the donor group increases in basicity: **5.7** was completely hydrolysed within six minutes whilst 10 % of **5.10^{SIMes}** remains in solution four weeks after the addition of water. The *pseudo*-first order conditions of the reactions, arising from the addition of excess water, enabled rate constants to be established when the reactions were slow enough to be monitored (Figure 5.13 and Table 5.6). Accordingly, the half-lives for **5.8^{SIMes}**, **5.9^{SIMes}** and **5.10^{SIMes}** were determined to be 8.5 minutes, 11.3 hours and 8.5 days respectively, demonstrating a significant improvement in water resilience compared to previous compounds in this chapter.

Compound	**Rate constant, k_{obs} (s^{-1})**	**Half life, $t_{1/2}$ (min)**
5.8^{SIMes}	1.367×10^{-03}	8.5
5.9^{SIMes}	1.702×10^{-05}	6.79×10^{2}
5.10^{SIMes}	9.428×10^{-07}	1.23×10^{4}

Table 5.6 – Hydrolysis rate constants and half lives.

The strong parallels between the trends in hydrolysis and fluoride substitution indicates hydrolysis is also occurring *via* a dissociative mechanism. Following donor dissociation, the borenium intermediate is attacked by water and likely forms a boronic acid species such as NHC-B(OH)Cat (Scheme 5.15). Subsequent carbene protonation and B–C bond cleavage leads to the complete degradation of the molecule. The donor dependence indicates the donor dissociation is still the rate determining step of the reaction, with the subsequent hydrolysis steps occurring rapidly in the aqueous conditions.

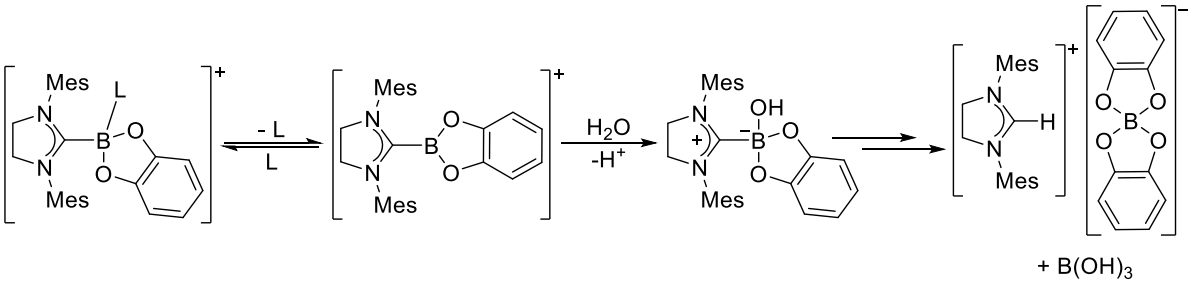

Scheme 5.15 – Hydrolysis reaction of [NHC-B(L)Cat]$^{+}$ boronium structures.

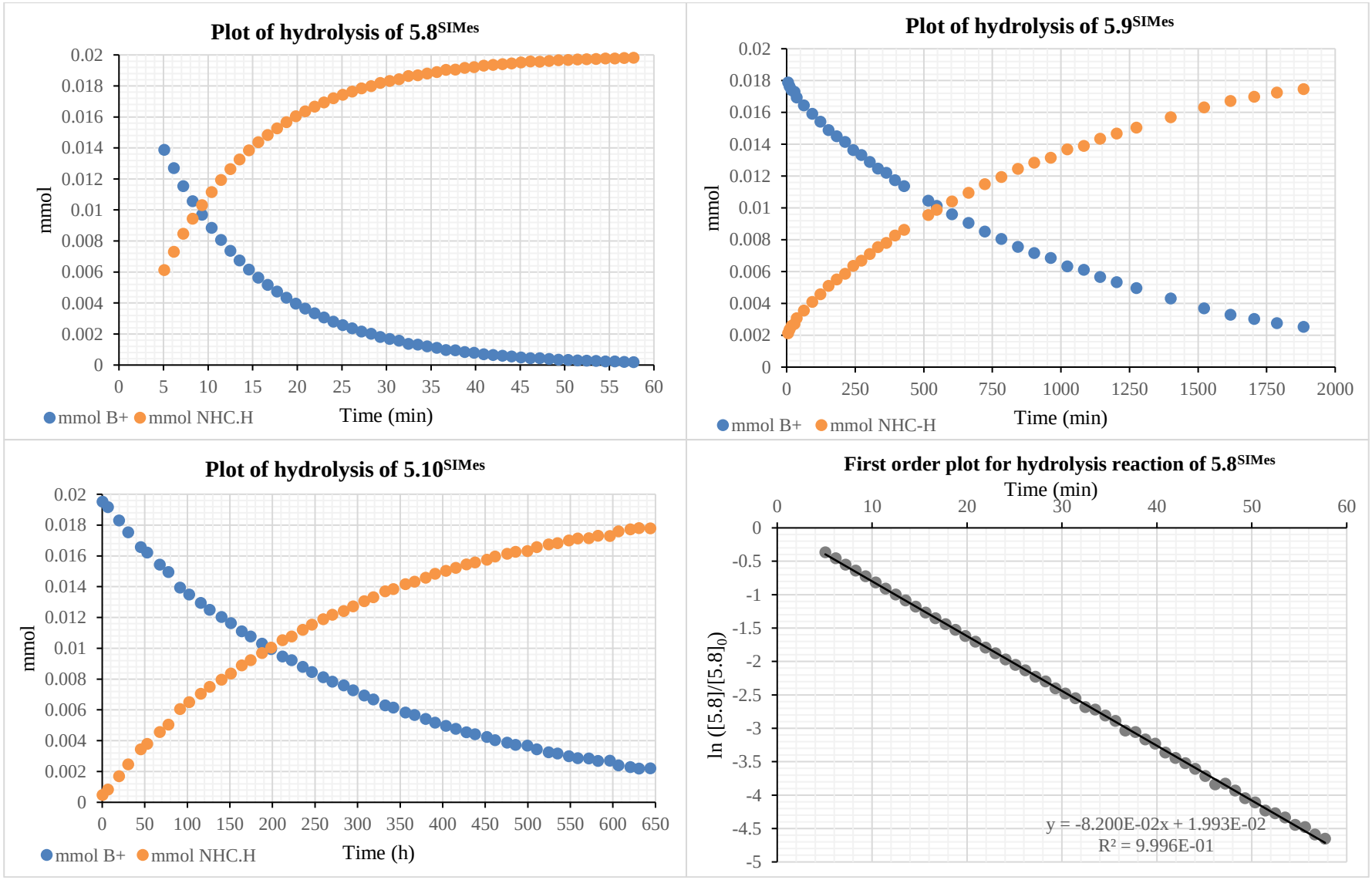

Figure 5.13 – Plots for the hydrolysis reactions of **5.8** (top left), **5.9** (top right) and **5.10** (bottom left) showing change in molar quantities against time in minutes or hours. First order plot for **5.8** (bottom right).

The two most robust complexes, **5.9**$^{\mathbf{SIMes}}$ and **5.10**$^{\mathbf{SIMes}}$, are stable solids in air for six days with no apparent signs of degradation by ^{1}H NMR spectroscopy. By contrast, the pyridine and 4-methoxypyridine complexes degraded quickly. ^{1}H NMR spectra of samples of **5.7**$^{\mathbf{SIMes}}$ and **5.8**$^{\mathbf{SIMes}}$ which were exposed to air as solids for less than 90 minutes before being taken into dry, degassed $CDCl_3$ showed primarily protonated carbene and shifted donor signals consistent with the unbound L donors. The degradation of these solids upon exposure to air may be associated with their sensitivity to moisture.

5.6.4 Fluoride Binding at Elevated Temperatures

Despite the exceptional stability of **5.9**$^{\mathbf{SIMes}}$ and **5.10**$^{\mathbf{SIMes}}$, their potential application for radiofluorination is hampered by their slow rates of fluoride uptake at room temperature which are incompatible with the time constraints imposed by fluorine-18. Consequently, the one-to-one binding reactions were investigated across an elevated temperature range of 50 – 70 °C to explore the effect of temperature on the rate. The same conditions as in section 5.6.2 were applied with timing beginning upon insertion of the NMR tube into the preheated NMR machine, approximately one minute after the reagents were combined. As expected, the elevated temperatures lead to a marked increase in the rate of fluoride uptake for both compounds (Table 5.7). The time taken to reach 50 % consumption of **5.10**$^{\mathbf{SIMes}}$ declines from over two weeks at room temperature to six hours at 50 °C and then to 16 minutes at 70 °C. **5.9**$^{\mathbf{SIMes}}$ meanwhile takes less than 30 minutes to reach 50 % conversion at temperatures of 50 °C and above, with the half-life approximately halving for every 5 °C increase. Most notably however **5.9**$^{\mathbf{SIMes}}$ reaches 97 % conversion in 20 minutes at 65 °C and 12 minutes at 70 °C, timescales that are promising for radiofluorination. **5.10**$^{\mathbf{SIMes}}$ on the other hand still takes 90 minutes to reach 93 % conversion at the highest temperature explored, suggesting further investigation is required to find alternative fluoride binding conditions where **5.10**$^{\mathbf{SIMes}}$ may usefully be applied.

Temperature	Time for 50% of reagent to be consumed	
	5.9^{SIMes}	**5.10**^{SIMes}
Room Temp	23.5 h	15.6 d
50 °C	25 min	360 min
55 °C	13 min	170 min
60 °C	~ 7 min	76 min
65 °C	< 5 min	27 min
70 °C	< 3 min	16 min

Table 5.7 – Time taken for 50 % consumption of **5.9** and **5.10**^{SIMes} in one-to-one fluoride binding reactions at different temperatures

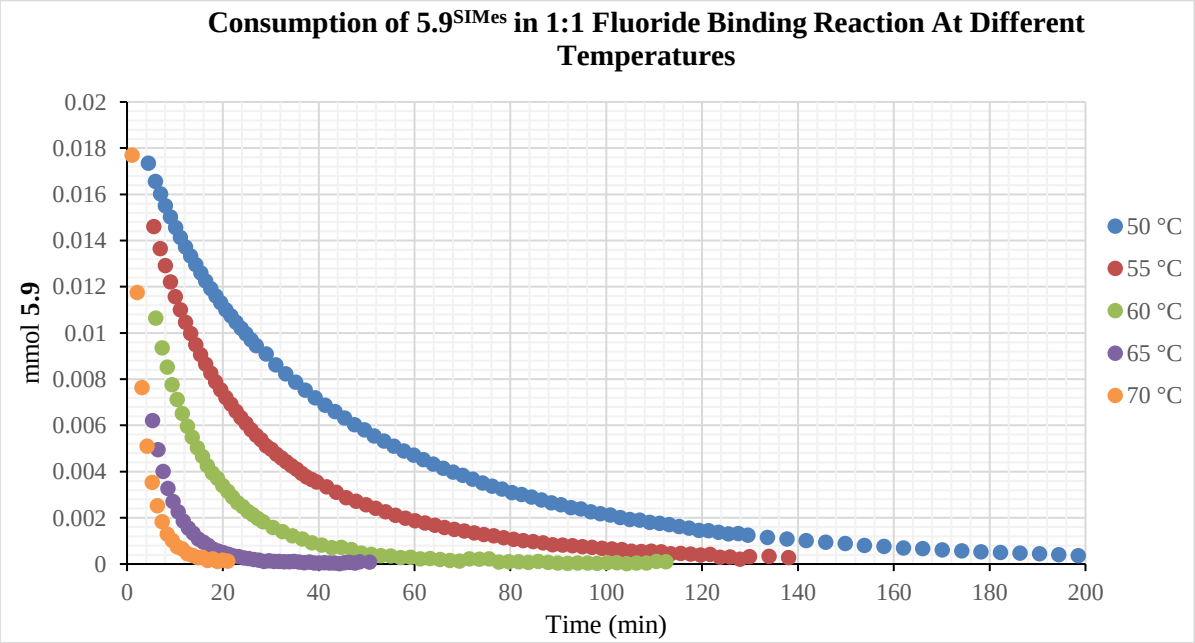

Figure 5.14 – Consumption of **5.9**^{SIMes} against time (min) in one-to-one reactions with fluoride across a 50 – 70 °C temperature range.

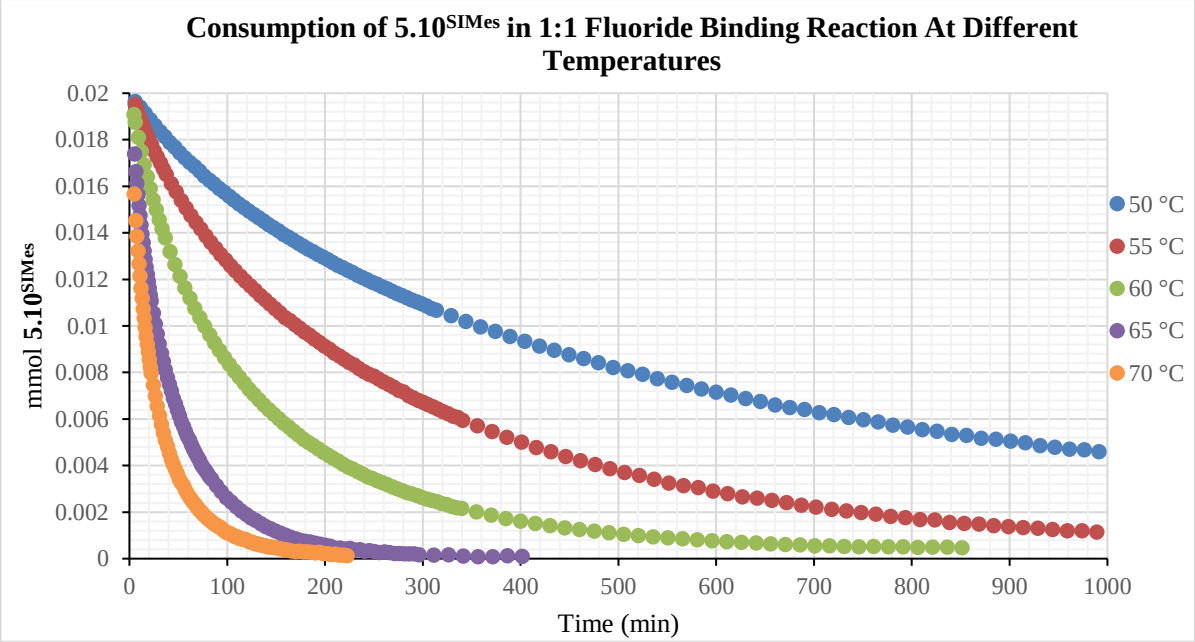

Figure 5.15 – Consumption of **5.10**^{SIMes} against time (min) in one-to-one reactions with fluoride across a 50 – 70 °C temperature range.

To further investigate the mechanism of fluoride substitution, the reactions with **5.9**^{SIMes} were repeated over the same temperature range with an excess of fluoride used for *pseudo*-first order conditions. From the resulting first order plots, rate constants (k_{obs}) were established for each temperature and half-lives calculated (Table 5.8). The half-lives noted in Table 5.8, are shorter than the time taken to reach 50 % conversion for the one-to-one binding reactions in Table 5.7 because the *pseudo*-first order conditions disfavour the reverse direction of the pre-equilibrium that otherwise retards the rate. With the k_{obs} values for the five temperatures in hand, an Eyring plot was used to establish the enthalpy of activation (131 kJ mol^{-1}) and entropy of activation (98 J K^{-1} mol^{-1}) for the reaction. The large entropy of activation is consistent with the dissociative mechanism and the accompanying increase in disorder at the transition state. Additionally, an Arrhenius plot of natural log of k_{obs} against 1/T yielded an estimated activation energy of 134 kJ mol^{-1}, accounting for the slow reaction at room temperature.

Temperature (°C)	Rate Constant, k_{obs} (s^{-1})	Half-life, $t_{1/2}$ (min)
50	5.289×10^{-4}	21.8
55	1.096×10^{-3}	10.5
60	2.093×10^{-3}	5.5
65	5.585×10^{-3}	2.1
70	8.901×10^{-3}	1.3

Table 5.8 – Rate constants (s^{-1}) and half-lives (s) from the reactions of **5.9^{SIMes}** with an excess of fluoride across a 50 – 70 °C temperature range.

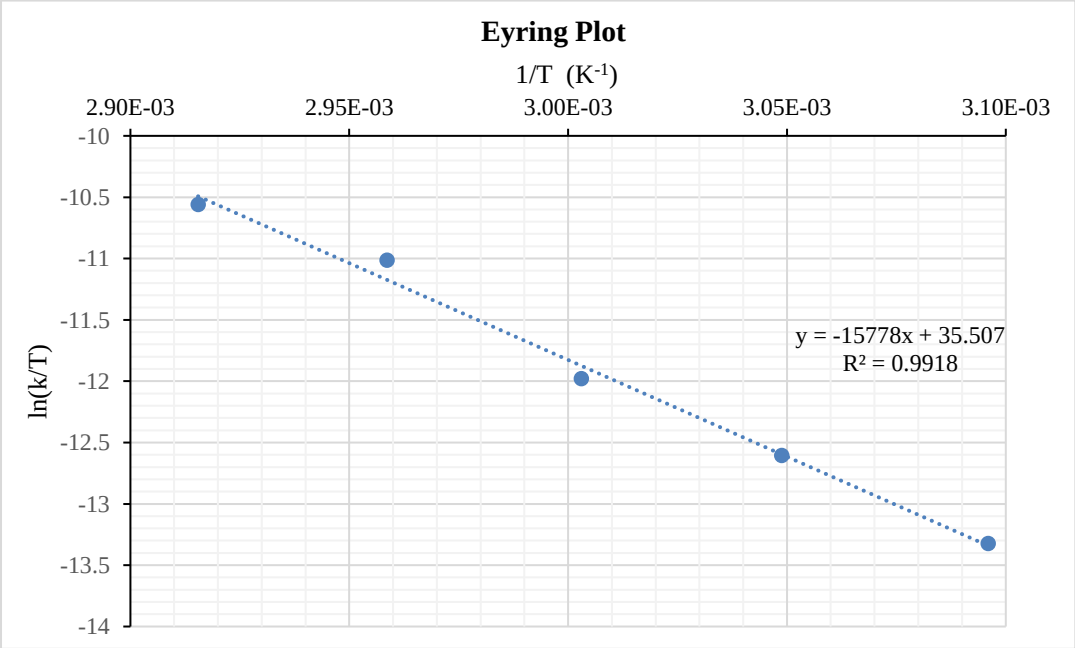

Figure 5.16 – Eyring plot from *pseudo*-first order reactions of **5.9^{SIMes}** with fluoride across a 50 – 70 °C temperature range.

5.6.5 Fluoride Binding in Wet Conditions

A preliminary investigation of fluoride uptake in wet conditions was also undertaken due to the interest in obviating azeotropic drying from [^{18}F]fluoride preparation procedures. Reactions were consequently conducted using controlled quantities of water to explore the competition between fluoride binding and hydrolysis. Accordingly, the methylimidazole bound boronium salt, **5.9^{SIMes}**, was combined with seven equivalents of the hydrated tetrabutylammonium fluoride salt in d_3-acetonitrile and the reaction monitored by multinuclear NMR. Several B–F coupled species were observed to form over the course of

five days. The desired NHC-B(F)Cat derivative **5.4^{SIMes}** is identified as a minor product of the reaction, marked by its characteristic doublet signal at 6 ppm ($^{1}J_{BF}$ = 46 Hz) in the ^{11}B NMRs of Figure 5.17. The prominent quartet in the ^{11}B NMRs at 0 ppm ($^{1}J_{BF}$ = 16.4 Hz) and the corresponding ^{19}F NMR signal at -143.6 ppm are however consistent with the formation of $[BF_3(OH)]^-$ as the major product of the reaction. Two further B–F coupled species are also observed in Figure 5.17 as a doublet at 8 ppm ($^{1}J_{BF}$ = 30.9 Hz) and a triplet at 2 ppm ($^{1}J_{BF}$ = 31.3 Hz) with the corresponding ^{19}F NMR quartets arising at -134.6 ppm and -136.5 ppm respectively. Although the exact composition of these monofluorinated and difluorinated boron species is currently unknown, they are presumed to be intermediates in the stepwise formation of $[BF_3(OH)]^-$. Overall, the mixture of products and dominant formation of the $[BF_3(OH)]^-$ anion are consistent with the excess water greatly inhibiting the formation of **5.4^{SIMes}**. This result likely stems from water out-competing fluoride to coordinate with the borenium reaction intermediate and subsequently leading to extensive degradation of the carbene borane scaffold.

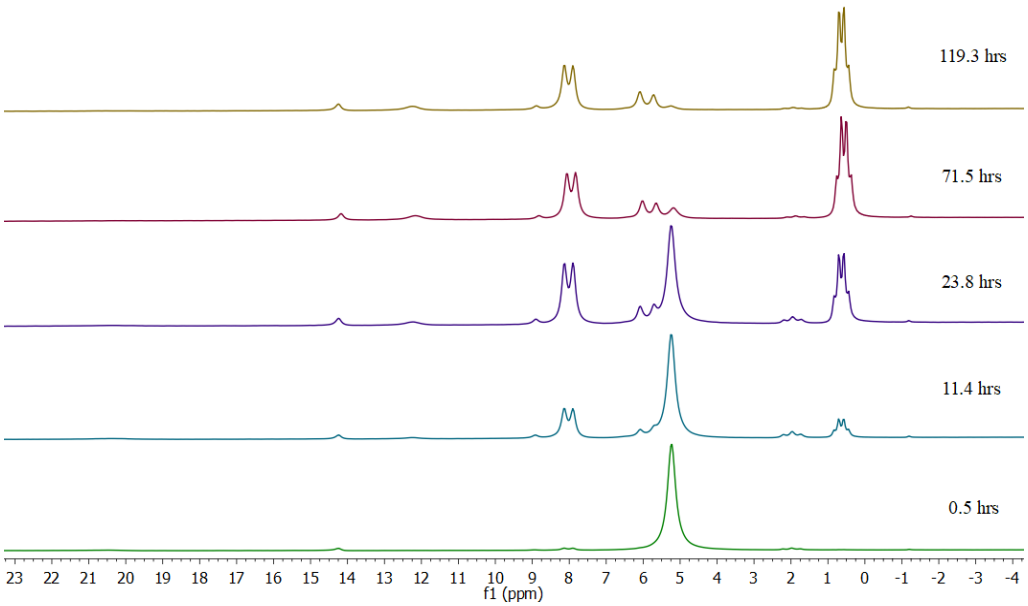

Figure 5.17 – ^{11}B NMRs of the wet fluoride binding reaction with **5.9^{SIMes}** over time

5.7 *N*-Heterocyclic Carbene Catecholatoboronium Complexes Featuring Different Carbenes

The carbene group offers another point of modification through which the reactivity of these [NHC-B(L)Cat]$^+$ cations might be tuned. The previous section established that the rate of fluoride uptake and hydrolysis with the [SIMes-B(L)Cat]$^+$ cations is a reflection of the donor stabilisation of the four coordinate boronium species with respect to the three coordinate [SIMes-BCat]$^+$ borenium cation that constitutes the reaction intermediate in a process occurring *via* a dissociative mechanism. As discussed in Section 5.4, the [NHC-BCat]$^+$ **5.2** series exhibits notable differences in character and stabilisation depending on the characteristics of the coordinated NHC. It was therefore hypothesised that the different carbenes would also impact the reactivity of [NHC-B(L)Cat]$^+$ systems and the dissociative loss of the L donor. Of the SIMes boronium series, the **5.10^{SIMes}** DMAP complex was observed to be the most robust, as well as the slowest to bind fluoride. A range of related [NHC-B(DMAP)Cat]$^+$ complexes was therefore investigated, as it was anticipated they might exhibit the most noticeable differences in reactivity as a function of the NHC.

5.7.1 Synthesis and Characterisation

The IMes and 6Mes derivatives of **5.10** were synthesised using the same synthetic route described for the SIMes boronium salts, *i.e.* the respective bromide adduct **5.3** was combined with dimethylaminopyridine in acetonitrile for a simple substitution reaction. Complexation was confirmed in the ^{1}H NMR spectra by an upfield shift of the aromatic resonances of the DMAP unit as well as a downfield shift of the -NMe_2 signal compared to the free ligand. The ^{11}B NMR singlets are also in the expected four-coordinate region at 6 ppm.

Crystallographic characterisation of the two complexes allows for structural comparison with the SIMes derivative, **5.10^{SIMes}** (Figure 5.18, Figure 5.19, and Table 5.9).

The boron-carbene bond lengths increase from 1.638(4) Å in **5.10^{IMes}** to 1.695(2) Å in **5.10^{6Mes}**, consistent with the trends reported for other structures in this chapter. The B–N bonds are again noted to be remarkably similar, falling across a limited range of 1.571(4) – 1.583(2) Å, which also encompasses the B–N bonds of **5.8** and **5.9**. The pyramidalization of the boron centre upon DMAP coordination does show some variation with angles totalling 327.3 °, 325.6 ° and 332.4 ° for **5.10^{IMes}**, **5.10^{SIMes}** and **5.10^{6Mes}** respectively. When the uncertainty of the constituent angles has been accounted for **5.10^{IMes}** and **5.10^{SIMes}** can be considered to be comparable. The greater planarity of the **5.10^{6Mes}** boron centre in Figure 5.19 is also accompanied by an alternative orientation of the boron substituents, compared to the other **5.10** boronium structures: the B–N bond lies perpendicular to the plane of the carbene and the catecholate group is aligned face-to-face with the plane of the NHC. This alternative arrangement is presumably the result of the smaller binding pocket of the expanded ring carbene preventing the π-stacking of the aromatic rings observed for the other **5.10** boroniums. The increased planarity of the boron centre may therefore be the result of the interaction between the NHC and BCat π-systems.

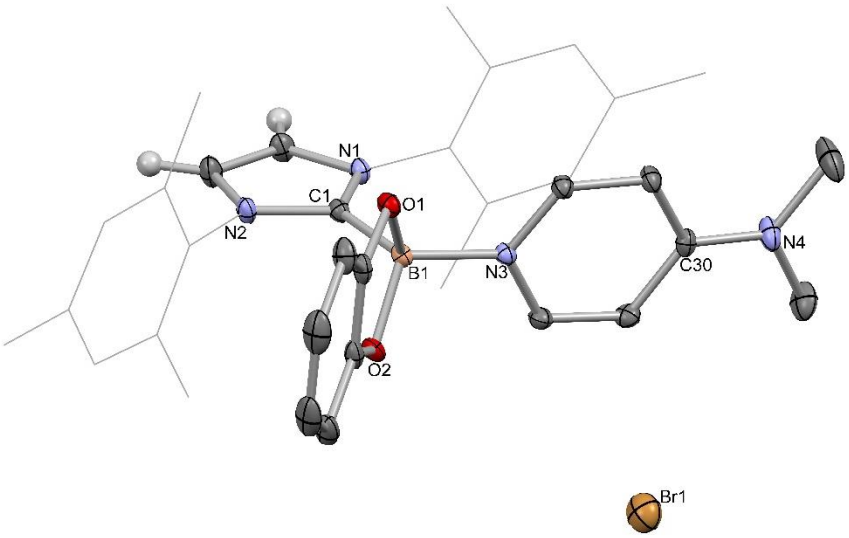

Figure 5.18 – Molecular structure of **5.10^{IMes}**. Thermal ellipsoids are set at 40 % probability level. Mesityl groups are represented as wireframe. Solvent molecule and most hydrogens have been omitted for clarity.

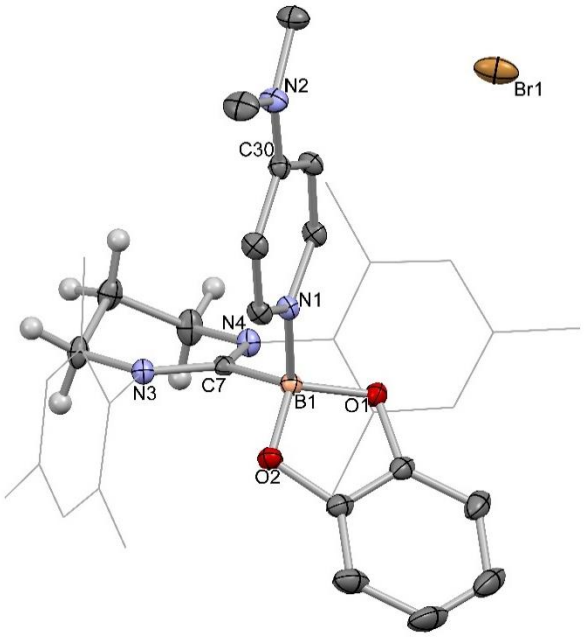

Figure 5.19 – Molecular structure of **5.10^{6Mes}**. Thermal ellipsoids are set at 40 % probability level. Mesityl groups are represented as wireframe. Solvent molecule and most hydrogens have been omitted for clarity.

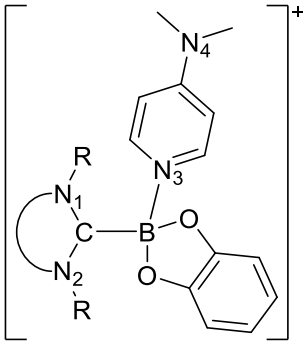	**5.10^{IMes}**	**5.10^{SIMes}**	**5.10^{6Mes}**
d(C–B)	1.638(4)	1.665(5)	1.695(2)
d(B–N3)	1.571(4)	1.573(5)	1.583(2)
d(B–O)	1.473(3), 1.471(4)	1.469(3), 1.470(4)	1.464(2), 1.461(2)
d(B---C$_{ipso}$)	3.092(6), 3.292(4)	3.118(4), 3.374(4)	3.092(2), 2.973(2)
∠(O–B–O)	106.9(2)	110.1(2)	118.3(1)
∠(C–B–O)	109.8(2), 110.6(2)	107.6(2), 111.0(2)	112.5(1), 113.1(1)
Sum of Boron angles in NHC-BCat fragment	327.3	325.6	332.4

Table 5.9 – Structural bond lengths (Å) and angles (°) for **5.10** complexes.

5.7.2 Fluoride Binding and Water Stability

With the **5.10** series in hand, one to one fluoride binding and hydrolysis reactions were investigated using the procedures described in sections 5.6.2 and 5.6.3. The characteristic B—F coupled signals in the ^{11}B and ^{19}F NMRs confirmed **5.10^{IMes}** and **5.10^{6Mes}** yield the expected monofluorinated **5.4** products upon addition of fluoride, whilst the ^{1}H and ^{11}B NMR spectra of the hydrolysis reaction mixtures confirmed that the compounds again decompose to the protonated carbene and boric acid species. The reactions were slow enough to be monitored by NMR, with the carbene backbone resonances again providing useful handles with which to monitor the reactions. Fluoride uptake by the two new compounds was found to be significantly faster than by **5.10^{SIMes}**, with **5.10^{IMes}** and **5.10^{6Mes}** reaching 50 % consumption in 1.7 days and 5 minutes respectively. Hydrolysis is likewise accelerated with the half-lives established as 14.6 hours for **5.10^{IMes}** and 3.1 minutes for **5.10^{6Mes}**. The sensitivity of **5.10^{6Mes}** also extends to benchtop conditions, with the compound degrading quickly in air; no starting material is observed in the ^{1}H NMR spectra of a solid sample that had been exposed to air for an hour before being dissolved in dry $CDCl_3$. By contrast, no sign of degradation is observed in a ^{1}H NMR of **5.10^{IMes}** after 6 days exposed to air.

	Fluoride Binding 50 % consumption of 5.10	**Hydrolysis Half-life $t_{1/2}$**
5.10^{IMes}	1.7 d	14.6 h
5.10^{SIMes}	15.6 d	8.5 d
5.10^{6Mes}	5 min	3.1 min

Table 5.10 – Timescales for reactions with the **5.10** complexes

The variation in the reaction rates of the **5.10** series implies that the energy barrier to DMAP dissociation is greatest for **5.10^{SIMes}** and lowest for **5.10^{6Mes}**. This trend may be attributed to a diminishing energy difference between the dissociated reaction intermediates and the **5.10** starting material, leading to a concomitant lowering of the activation energy

required for dissociation. Hence, the particularly rapid reactions with **5.10**$^{\mathbf{6Mes}}$ stem from the energetic accessibility of the highly stabilised **5.2**$^{\mathbf{6Mes}}$ cation that forms as an intermediate. This accessibility is especially apparent upon consideration of the respective energies of the DFT optimised structures in Figure 5.20, where the energy difference between **5.10**$^{\mathbf{6Mes}}$ and its dissociated intermediates is nearly half that observed for the SIMes system. This is presumably a testament to the additional stabilisation provided by the arene-boron interaction in **5.2**$^{\mathbf{6Mes}}$. Meanwhile, the marginally lower energy difference of the IMes system, compared to the SIMes system, suggests the IMes system also offers a lower energy pathway to DMAP dissociation, consistent with the experimental results. This energy difference is minimal, however, underscoring the comparative similarity of the two five membered ring carbene systems.

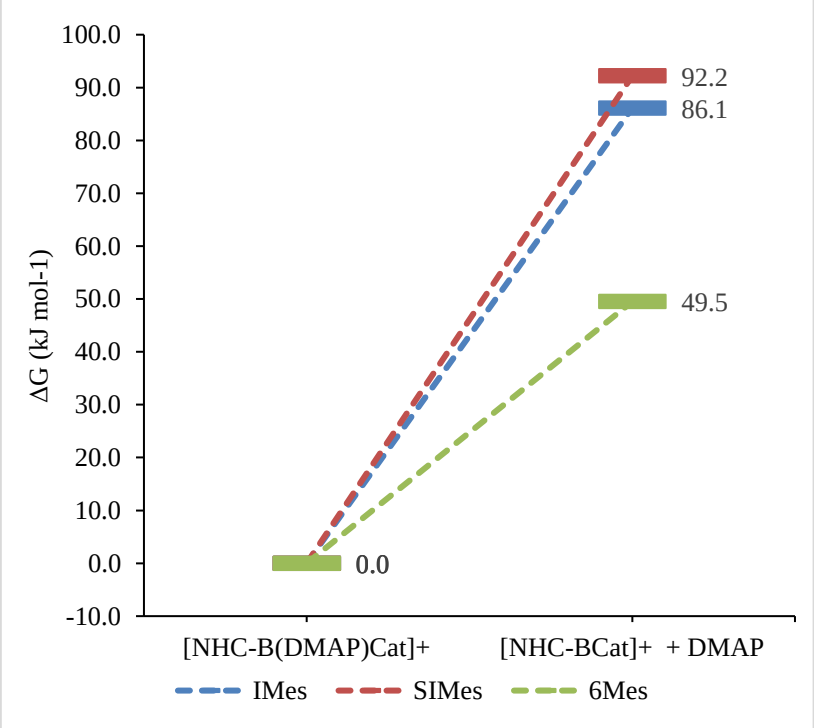

Figure 5.20 – Energy profile of the dissociation of DMAP from the **5.10** cations to form the respective **5.2** cation.

5.8 Conclusions

The synthesis and characterisation of a new library of NHC stabilised boranes, based upon an NHC-BCat scaffold, has been described. The three NHC-B(F)Cat systems, differentiated by their carbene donors, all exhibit excellent water stability and are indefinitely air stable. This made them attractive reagents to explore further for PET imaging purposes with the generic stability, irrespective of carbene, also offering favourable flexibility for development. Moreover, the fluoroborane adducts may be synthesised from robust, coordinatively saturated precursors *via* promoter-free fluoride substitution reactions and, unlike substitution-based synthesise for trifluoroborate compounds, these compounds do not require a significant excess of fluoride to drive the reactions to the product, thereby minimising the need for a carrier added source of [^{18}F]fluoride.

Reactions of these NHC stabilised boranes occur *via* a dissociative mechanism. The rate of reaction with fluoride or water therefore varies considerably with the identity of the leaving group and characteristics of the [NHC-BCat]$^{+}$ borenium that constitutes the reaction intermediate. Investigation of the X-ray structures of the borenium cations showed that the different carbene characteristics could significantly impact the geometry of the cation. Most notably, the X-ray crystal structure of **5.2^{6Mes}** reveals a stabilising boron-arene interaction, that arises due to the small binding pocket and flexibility of the 6Mes carbene.

Bromide and chloride dissociation from the neutral adducts occurs readily, leading to rapid substitution reactions. Bromide dissociation was even observed to occur spontaneously from **5.3^{6Mes}**, in solvents of suitable polarity, due to the thermodynamic favourability of the arene-stabilised **5.2^{6Mes}** borenium cation. Whilst the rapid uptake of fluoride by these systems is highly favourable, the similarly rapid degradation in air and moisture makes these highly sensitive compounds ill-suited to their desired, practical application.

The reactivity of positively charged boronium structures featuring neutral, basic leaving groups can readily be tuned by utilising a leaving group of the appropriate basicity. The more basic donors exert a greater stabilising effect on the boronium system, with respect to the borenium reaction intermediate, thereby increasing the activation energy required for dissociation. Consequently, the pyridine complex **5.7**$^{\mathbf{SIMes}}$ reacts with fluoride and water in a matter of minutes whilst the DMAP complex **5.10**$^{\mathbf{SIMes}}$ reacts over several weeks. The air stable DMAP complex **5.10**$^{\mathbf{SIMes}}$ appears to be moderately over-stabilised, with the comparatively slow fluoride uptake likely impractical for application. By comparison, the slightly less basic methylimidazole donor of **5.9**$^{\mathbf{SIMes}}$ achieves a balance, conferring sufficient stability to the compound to render it air stable whilst also remaining sufficiently labile that high fluoride uptake may be achieved in a one-to-one binding reaction over 20 minutes at temperatures over 60 °C. The range of bases so far investigated is of course not exhaustive, with plenty of scope for further development.

The reactivity of the boronium cations was also demonstrated to be tunable by the choice of carbene donor group, further emphasising the versatility of this approach. This is primarily the result of the different characteristics of the carbenes influencing the stabilisation of the borenium reaction intermediate, with respect to the boronium cation, and consequently the activation energy required to access it as part of the dissociative mechanism. In particular, the 6Mes carbene was found to produce a DMAP complex that reacts with fluoride and water significantly faster than the SIMes equivalent due to the formation of the arene-stabilised **5.2**$^{\mathbf{6Mes}}$ borenium species. Notably, the air stable IMes complex **5.10**$^{\mathbf{IMes}}$ also reacts more quickly than the over-stabilised SIMes derivative with reaction timescales more comparable to the methylimidazole complex **5.9**$^{\mathbf{SIMes}}$. It is therefore anticipated that at elevated temperatures **5.10**$^{\mathbf{IMes}}$, like **5.9**$^{\mathbf{SIMes}}$, would bind fluoride on a timescale compatible with radiofluorination; further work is needed to confirm this.

Furthermore, the full scope of the IMes-BCat scaffold is yet to be explored, with alternative, less basic donors offering opportunities for faster fluoride binding and optimisation of stability.

Future work would endeavour to verify the potential of these systems by conducting ^{18}F-fluorination experiments. Of the compounds described in this chapter, the SIMes methylimidazole complex and the IMes DMAP complex stand out as exhibiting the most promising fluoride binding and bench stability characteristics for this work.

5.9 Experimental

[5.2^{SIMes}][AlBr$_4$] – [(SIMes)-BCat][AlBr$_4$]

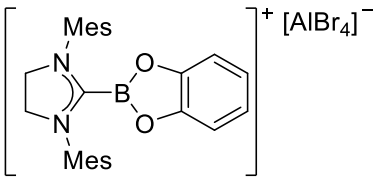

Aluminium tribromide (79 mg, 0.297 mmol) was dissolved in difluorobenzene (3 mL) and added dropwise to a stirred suspension of **5.3^{SIMes}** (150 mg, 0.297 mmol) in difluorobenzene (5 mL). The solid rapidly dissolves from the reaction to produce a pale pink solution. After 1 h the volatiles were removed *in vacuo* to yield a pure pink powder. Yield: 182 mg, 79 %. Crystals suitable for X-ray diffraction were obtained by layering a difluorobenzene solution with hexanes.

Spectroscopic Data: ^{1}H NMR (500.3 MHz, $CDCl_3$, 298 K): δ_H 7.16 (m, 4H, Cat C*H*), 6.97 (s, 4H, Mes *m*-C*H*), 4.71 (s, 4H, NCH_2), 2.44 (s, 12H, Mes *o*-CH_3), 2.27 (s, 6H, Mes *p*-CH_3). **^{11}B{^{1}H} NMR** (128.4 MHz, $CDCl_3$, 298 K): δ_B 26 (br s). **^{13}C{^{1}H} NMR** (125.8 MHz, $CDCl_3$, 298 K): δ_C 146.6 (Cat *C*O), 141.6 (Mes *p*-*C*CH$_3$), 135.3 (Mes *o*-*C*CH$_3$), 130.6 (Mes *m*-*C*H), 129.9 (Mes *C*N), 125.0 (Cat *C*H), 113.9 (Cat *C*H), 53.7 (NCH$_2$), 21.3 (Mes *p*-*C*H$_3$),

18.0 (Mes *o*-*C*CH_3). **Elemental Microanalysis**: calc. for $C_{27}H_{30}N_2O_2BAlBr_4$: C 42.01 %, H 3.92 %, N 3.63 %; meas. C 42.20 %, H 4.08 %, N 3.65 %.

[5.2^{6Mes}][AlBr$_4$] – [(6Mes)-BCat][AlBr$_4$]

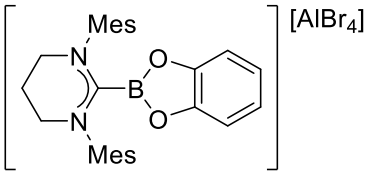

Aluminium tribromide (77 mg, 0.289 mmol) was dissolved in difluorobenzene (5 mL) and added dropwise to a bright yellow solution of **5.3^{6Mes}** (150 mg, 0.289 mmol) in difluorobenzene (5 mL) turning the solution bright orange-red. The reaction was stirred for 30 min before the solvent was removed under reduced pressure. The remaining residue was washed with minimal benzene (2 x 2.5 mL) to yield an off white solid. Yield: 161 mg, 71 %.

Spectroscopic Data: ^{1}H NMR (500.3 MHz, $CDCl_3$, 298 K): δ_H 7.02 (s, 4H, Cat C*H*), 6.85 (s, 4H, Mes *m*-C*H*), 3.96 (t, $^3J_{HH}$ = 5.5 Hz, 4H, NC$H_2$$CH_2$), 2.74 (quin, $^3J_{HH}$ = 5.5 Hz, 2H, NCH_2CH_2), 2.43 (s, 12H, Mes *o*-CH_3), 2.14 (s, 6H, Mes *p*-CH_3). **^{11}B{^{1}H} NMR** (128.4 MHz, $CDCl_3$, 298 K): δ_B 26 (br s). **^{13}C{^{1}H} NMR** (125.8 MHz, $CDCl_3$, 298 K): δ_C 146.1 (Cat *C*O), 141.5 (Mes *p*-*C*CH_3), 135.6 (Mes N*C*), 135.4 (Mes *o*-*C*CH_3), 130.4 (Mes *m*-*C*H), 124.4 (Cat *C*H), 113.2 (Cat *C*H), 47.7 (N*C*$H_2$$CH_2$), 21.2 (Mes *p*-*C*$H_3$), 19.6 ($NCH_2$*C*$H_2$), 18.0 (Mes *o*-*C*$CH_3$). **Elemental Microanalysis**: calc. for $C_{28}H_{32}N_2O_2BAlBr_4$: C 42.79 %, H 4.10 %, N 3.56 %; meas. C 42.69 %, H 4.08 %, N 3.58 %.

[5.2^{6Mes}][AlCl$_4$] – [(6Mes)-BCat][AlCl$_4$]

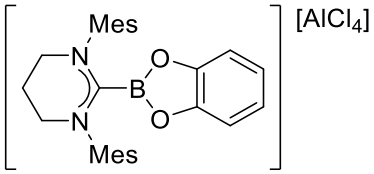

A difluorobenzene (10 mL) solution of bromocatecholborane (323 mg, 1.63 mmol) was added dropwise to a solution of 6Mes carbene (474 mg, 1.48 mmol) in difluorobenzene (5 mL). After 1 h, a solution of aluminium trichloride (296 mg, 2.22 mmol) dissolved in difluorobenzene (10 mL) was added to the reaction. The reaction was subsequently stirred overnight before the volatiles were removed *in vacuo* and the residue washed with hexane to yield a brown powder. The solid was recrystallised from a concentrated difluorobenzene solution layered with hexanes yielding crystals suitable for X-ray diffraction. Yield: 225 mg, 25 %.

Spectroscopic Data: ^{1}H NMR (400.2 MHz, CD_2Cl_2, 298 K): δ_H 7.07 – 6.99 (overlapping m, 4H, Cat C*H*), 6.89 (s, 4H, Mes *m*-C*H*), 3.88 (t, $^3J_{HH}$ = 5.7 Hz, 4H, NCH_2CH$_2$), 2.67 (quin, $^3J_{HH}$ = 5.7 Hz, 2H, NCH$_2$CH_2), 2.43 (s, 12H, Mes *o*-CH_3), 2.15 (s, 6H, Mes *p*-CH_3). **^{11}B{^{1}H} NMR** (128.4 MHz, $CDCl_3$, 298 K): δ_B 26 (br s).

5.3^{IMes} – IMes-B(Br)Cat

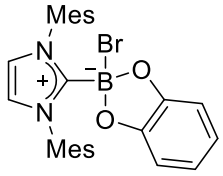

Bromocatecholborane (653 mg, 3.28 mmol) was dissolved in 20 mL hexane and added to a stirred suspension of IMes carbene (1.0 g, 3.28 mmol) in hexane (40 mL) leading to rapid formation of a fine white suspension. The reaction was stirred for a further 20 min before the solid was filtered and washed with hexane (20 mL). The solid was then dried *in vacuo* to

yield a pure white powder (1.59 g, 96 %). Crystals suitable for X-ray diffraction were obtained from a hot solution of acetonitrile that was subsequently cooled to -25 °C.

Spectroscopic Data: ^{1}H NMR (500.3 MHz, CD_3CN, 298 K): δ_H 7.40 (s, 2H, NC*H*), 7.10 (s, 4H, Mes *m*-C*H*), 6.66 (m, 2H, Cat C*H*), 6.48 (m, 2H, Cat C*H*), 2.41 (s, 6H, Mes *p*-CH_3), 2.09 (s, 12H, Mes *o*-CH_3). **^{11}B{^{1}H} NMR** (128.4 MHz, CD_3CN, 298 K): δ_B 6 (s). **^{13}C{^{1}H} NMR** (125.8 MHz, CD_3CN, 298 K): δ_C 150.5 (Cat *C*O), 141.0 (Mes *p*-*C*CH_3), 136.3 (Mes), 134.4 (Mes), 129.7 (Mes *m*-*C*H), 125.0 (N*C*H), 121.0 (Cat *C*H), 110.8 (Cat *C*H), 21.2 (Mes *p*-*C*H_3), 18.2 (Mes *o*-*C*H_3). **Elemental Microanalysis**: calc. for $C_{29}H_{31}BBrN_3O_2$: C 63.99 %, H 5.74 %, N 7.72 %; meas. C 63.94 %, H 5.61 %, N 7.72 %.

5.3^{SIMes} – SIMes-B(Br)Cat

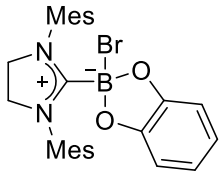

A Schlenk tube was charged with 400 mg (1.31 mmol) of SIMes carbene and hexane (20 mL) added to form a suspension. In a separate Schlenk tube, bromocatecholborane (285 mg, 1.44 mmol) was dissolved in hexane (20 mL) before slow addition to the carbene suspension. A fine white precipitate rapidly formed. The reaction was stirred for a further 30 min before stirring was turned off, and the suspension was allowed to settle. The reaction was subsequently filtered and the solid washed with hexane (15 mL) of before drying *in vacuo*. The white solid was then recrystallised from a hot acetonitrile solution cooled to -25 °C yielding colourless crystals. Yield: 575 mg, 87 %. Crystals suitable for X-ray diffraction were obtained by slow evaporation of a difluorobenzene solution.

Spectroscopic Data: ^{1}H NMR (400 MHz, CD_3CN, 298 K): δ_H 7.02 (s, 4H, Mes *m*-C*H*), 6.63 (m, 2H, Cat C*H*), 6.41 (m, 2H, Cat C*H*), 4.21 (s, 4H, NCH_2), 2.31 (s, 6H, Mes *p*-CH_3), 2.31 (s, 12H, Mes *o*-CH_3). **^{11}B{^{1}H} NMR** (128.4 MHz, CD_3CN, 298 K): δ_B 8 (s). **^{13}C{^{1}H}**

NMR (125.8 MHz, CD_3CN, 298 K): δ_C 150.4 (Cat *C*O), 139.9 (Mes *p*-*C*CH_3), 137.1 (Mes N*C*), 134.5 (Mes *o*-*C*CH_3), 130.0 (Mes *m*-*C*H), 120.8 (Cat *C*H), 110.6 (Cat *C*H), 51.9 (NCH_2), 21.1 (Mes *p*-*C*H_3), 18.5 (Mes *o*-*C*H_3). **Elemental Microanalysis**: calc. for $C_{33}H_{34}N_2O_2BBrF_2$: C 64.00 %, H 5.53 %, N 4.52 %; meas. C 63.74 %, H 5.67 %, N 4.65 %.

5.3^{6Mes} – 6Mes-B(Br)Cat

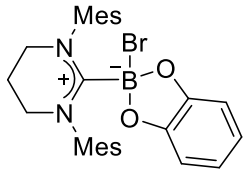

1.2 g (3.74 mmol) of freshly isolated 6Mes carbene was dissolved in toluene (20 mL). A toluene solution (15 mL) of bromocatecholborane (0.74 g, 3.74 mmol) was slowly added to the reaction and left to stir for 30 min. The volatiles were subsequently removed to yield an off-white solid. Yield: 1.82 g, 94 %. Crystals suitable for X-ray diffraction were obtained by slow evaporation from a difluorobenzene solution.

Spectroscopic Data: ^{1}H NMR (400.2 MHz, C_6D_6, 298 K): δ_H 6.75 (br s, 4H, Mes *m*-C*H*), 6.57 (overlapping m, 4H, Cat C*H*), 2.90 (br s, 4H, NC*H*$_2$CH_2), 2.31 (s, 12H, Mes *p*-C*H*$_3$), 2.10 (s, 6H, Mes *o*-C*H*$_3$), 1.41 (quin, $^3J_{HH}$ = 5.5 Hz, 2H, NCH$_2$C*H*$_2$). **^{11}B{^{1}H} NMR** (128.4 MHz, C_6D_6, 298 K): δ_B 11 (br s). **^{13}C{^{1}H} NMR** (125.8 MHz, C_6D_6, 298 K): δ_C 150.1 (Cat *C*O), 140.5 (Mes), 138.3 (Mes *p*-*C*CH_3), 135.2 (Mes), 129.6 (Mes *m*-*C*H), 120.3 (Cat *C*H), 110.5 (Cat *C*H), 40.1 (N*C*$H_2C H_2$), 21.1 (Mes *p*-*C*H_3), 20.0 (NCH$_2$*C*H_2), 19.1 (Mes *o*-*C*H_3).

5.4^{IMes} – IMes-B(F)Cat

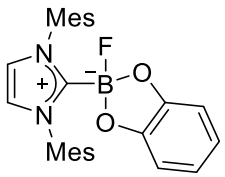

Potassium fluoride (28 mg, 0.477 mmol) and 18-crown-6 (95 mg, 0.358 mmol) were stirred in acetonitrile (20 mL) before addition to a stirred solution of **5.3^{IMes}** (120 mg, 0.238 mmol)

in acetonitrile (15 mL). The reaction was stirred for 24 h before volatiles were removed *in vacuo*. The white residue was taken up in dichloromethane (20 mL) and washed with water (3 x 15 mL) before drying with magnesium sulfate. The organic phase was then concentrated to a minimum and an excess of hexane added. The resulting solid was isolated by filtration. Yield: 63 mg, 60 %.

Spectroscopic Data: **^{1}H NMR** (400.2 MHz, $CDCl_3$, 298 K): δ_H 7.07 (s, 2H, NC*H*), 6.86 (s, 4H, Mes *m*-C*H*), 6.36 (m, 2H, Cat C*H*), 6.23 (m, 2H, Cat C*H*), 2.27 (s, 6H, Mes *p*-CH_3), 2.09 (s, 12H, Mes *o*-CH_3). **^{11}B{^{1}H} NMR** (128.4 MHz, $CDCl_3$, 298 K): δ_B 6 (d, $^{1}J_{BF}$ = 45.8 Hz). **^{19}F{^{1}H} NMR** (376.5 MHz, $CDCl_3$, 298 K): δ_F -142.8 (q, $^{1}J_{BF}$ = 45.8 Hz). **^{13}C{^{1}H} NMR** (100.6 MHz, $CDCl_3$, 298 K): δ_C 151.2 (Cat *C*O), 139.7 (Mes *p*-*C*CH_3), 134.6 (Mes *o*-*C*CH_3), 133.7 (Mes N*C*), 129.0 (Mes *m*-*C*H), 122.8 (N*C*H), 117.8 (Cat *C*H), 108.6 (Cat *C*H), 21.2 (Mes *p*-*C*H_3), 17.4 (Mes *o*-*C*H_3). **MS (ESI):** *m/z* calc. for $C_{27}H_{28}O_2N_2B$ ($[M\text{-}F]^+$) 423.2240 , meas. 423.2240 (100 %).

5.4^{SIMes} – SIMes-B(F)Cat

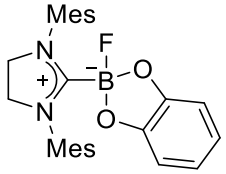

Potassium fluoride (95 mg, 1.63 mmol) and 18-crown-6 (431 mg, 1.63 mmol) were stirred in acetonitrile (25 mL) for 5 min before the solution was cannula transferred to a flask containing **5.3^{SIMes}** (500 mg, 1.63 mmol). The reaction was stirred for a further 4 h before volatiles were removed *in vacuo*. The residue was subsequently washed with water (5 mL) and hexane (15 mL) before drying *in vacuo* to yield a white solid. Yield: 467 mg, 64 %. Crystals suitable for X-ray diffraction were obtained by slow diffusion of hexane into a concentrated THF solution of the product.

Spectroscopic Data: **^{1}H NMR** (400.2 MHz, $CDCl_3$, 298 K): δ_H 6.82 (s, 4H, Mes *m*-C*H*), 6.36 (m, 2H, Cat C*H*), 6.19 (m, 2H, Cat C*H*), 4.00 (s, 4H, NCH_2), 2.29 (s, 12H, Mes *o*-CH_3), 2.24 (s, 6H, Mes *p*-CH_3). **^{11}B{^{1}H} NMR** (128.4 MHz, $CDCl_3$, 298 K): δ_B 6 (d, $^{1}J_{BF}$ = 46.4 Hz). **^{19}F{^{1}H} NMR** (376.5 MHz, $CDCl_3$, 298 K): δ_F -143.2 (q, $^{1}J_{BF}$ = 46.4 Hz). **^{13}C{^{1}H} NMR** (100.6 MHz, $CDCl_3$, 298 K): δ_C 151.1 (Cat *C*O), 138.7 (Mes *p*-*C*CH_3), 135.3 (Mes *o*-*C*CH_3), 133.7 (Mes N*C*), 129.2 (Mes *m*-*C*H), 117.9 (Cat *C*H), 108.7 (Cat *C*H), 51.0 (N*C*H_2), 21.1 (Mes *p*-*C*H_3), 17.6 (Mes *o*-*C*H_3). **Elemental Microanalysis**: calc. for $C_{27}H_{30}N_2O_2BF$: C 72.98 %, H 6.81 %, N 6.30 %; meas. C 73.10 %, H 6.81 %, N 6.27 %. **MS (ESI):** *m/z* calc. for $C_{27}H_{30}O_2N_2BFNa$ ([M+Na]$^{+}$) 467.2279 , meas. 467.2270 (100 %).

5.4^{6Mes} – 6Mes-B(F)Cat

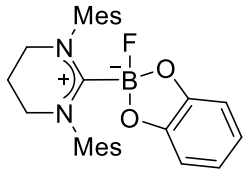

Potassium fluoride (29 mg, 0.501 mmol) and 18-crown-6 (99 mg, 0.376 mmol) were stirred in acetonitrile (20 mL) before addition to a stirred solution of **5.3^{6Mes}** (130 mg, 0.250 mmol) in acetonitrile (10 mL). The reaction was stirred for 24 h before volatiles were removed *in vacuo*. The white residue was taken up in dichloromethane (20 mL), washed with water (3 x 15 mL) before drying with magnesium sulfate. The organic phase was then concentrated to a minimum and an excess of hexane added. The resulting fine needles were isolated by filtration. Yield: 64 mg, 56 %.

Spectroscopic Data: **^{1}H NMR** (400.2 MHz, $CDCl_3$, 298 K): δ_H 6.82 (s, 4H, Mes *m*-C*H*), 6.36 (m, 2H, Cat C*H*), 6.17 (m, 2H, Cat C*H*), 3.50 (t, $^{3}J_{HH}$ = 5.9 Hz, 4H, NCH_2CH_2), 2.34 (overlapping m, 2H, NCH_2CH_2), 2.29 (s, 12H, Mes *o*-CH_3), 2.23 (s, 6H, Mes *p*-CH_3). **^{11}B{^{1}H} NMR** (128.4 MHz, $CDCl_3$, 298 K): δ_B 6 (d, $^{1}J_{BF}$ = 49.8 Hz). **^{19}F{^{1}H} NMR** (376.5 MHz, $CDCl_3$, 298 K): δ_F -135.9 (q, $^{1}J_{BF}$ = 49.8 Hz). **^{13}C{^{1}H} NMR** (100.6 MHz, $CDCl_3$, 298

K): δ_C 151.0 (Cat *C*O), 140.9 (Mes), 137.7 (Mes *p*-*C*CH_3), 134.2 (Mes), 129.6 (Mes *m*-*C*H), 117.6 (Cat *C*H), 108.7 (Cat *C*H), 48.8 (N*C*H_2*C*H_2), 21.1 (Mes *p*-*C*H_3), 20.9 (NCH_2*C*H_2), 17.9 (Mes *o*-*C*H_3). **MS (ESI):** *m/z* calc. for $C_{28}H_{32}O_2N_2B$ ($[M-F]^+$) 439.2553, meas. 439.2555 (100 %).

5.5^{SIMes} – SIMes-B(Cl)Cat

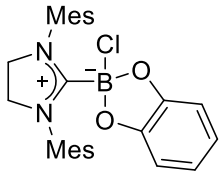

A flame-dried Schlenk tube was charged with SIMes (500 mg, 1.63 mmol) and hexane (30 mL) then added. In a separate Schlenk tube *B*-chlorocatecholborane (252 mg, 1.63 mmol) was dissolved in hexane (15 mL) and added dropwise to the carbene suspension. The reaction mixture, which rapidly forms a white precipitate, was stirred for 1 h before the precipitate was allowed to settle and filtered. The solid is washed with hexane (15 mL) and dried *in vacuo*. The resulting white powder was recrystallised from a concentrated solution in hot acetonitrile that was subsequently cooled to -25 °C, yielding colourless block crystals suitable for X-ray crystallography. Yield: 481 mg, 80 %.

Spectroscopic Data: ^{1}H NMR (400.2 MHz, CD_3CN, 298 K): δ_H 7.01 (s, 4H, Mes *m*-C*H*), 6.54 (m, 2H, Cat C*H*), 6.31 (m, 2H, Cat C*H*), 4.08 (s, 4H, NCH_2), 2.34 (s, 6H, Mes *p*-CH_3), 2.28 (s, 12H, Mes *o*-CH_3). **^{11}B{^{1}H} NMR** (128.4 MHz, CD_3CN, 298 K): δ_B 8 (s). **^{13}C{^{1}H} NMR** (125.8 MHz, CD_3CN, 298 K): δ_C 151.4 (Cat *C*O), 139.7 (Mes *p*-*C*CH_3), 137.1 (Mes *o*-*C*CH_3), 134.9 (Mes N*C*), 130.0 (Mes *C*H), 120.1 (Cat *C*H), 109.9 (Cat *C*H), 51.9 (N*C*H_2), 21.2 (Mes *p*-*C*H_3), 18.2 (Mes *o*-*C*H_3). **Elemental microanalysis**: calc. $C_{29}H_{33}N_3O_2BCl$: C 69.41 %, H 6.63 %, N 8.37 %; meas. C 69.42 %, H 6.75 %, N 8.47 %.

5.6^{SIMes} – SIMes-B(OMe)Cat

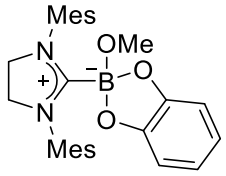

B-methoxycatecholborane (2.87 mL, 0.5 M in hexane, 1.44 mmol) was added to a suspension of SIMes carbene (400 mg, 1.30 mmol) in hexane (15 mL). The reaction was stirred for 1 h before the white precipitate was allowed to settle and the reaction mixture filtered. The solid was washed with hexane (5 mL) and then dried *in vacuo* to yield a white powder of reasonable purity. Yield: 363 mg, 61 %.

Spectroscopic Data: ^{1}H NMR (500.3 MHz, C_6D_6, 298 K): δ_H 6.67 (s, 4H, Mes *m*-C*H*), 6.67 (m, 2H, Cat C*H*), 6.58 (m, 2H, Cat C*H*), 3.13 (s, 3H, OCH_3), 3.00 (s, 4H, NCH_2), 2.25 (s, 12H, Mes *o*-CH_3), 2.12 (s, 6H, Mes *p*-CH_3). **^{11}B{^{1}H} NMR** (128.4 MHz, C_6D_6, 298 K): δ_B 7 (s). **^{13}C{^{1}H} NMR** (125.7 MHz, C_6D_6, 298 K): δ_C 153.8 (Cat *C*O), 138.1 (Mes *p*-*C*CH_3), 135.8 (Mes), 135.2 (Mes), 129.3 (Mes *m*-*C*H), 117.9 (Cat *C*H), 108.5 (Cat *C*H), 50.3 (NCH_2), 47.8 (O*C*H_3), 21.1 (Mes *p*-*C*H_3), 17.9 (Mes *o*-*C*H_3).

General procedure for the synthesis of [NHC-B(L)Cat]Br compounds 5.7 – 5.10

A flame-dried Schlenk tube was charged with one equivalent of **5.3** and the solid suspended in acetonitrile. One equivalent of the donor reagent was then added to the stirred reaction mixture, leading to rapid dissolution of the suspended solid. The reaction mixture was stirred for a further 30 min before the volatiles were removed *in vacuo* to afford the product as a white solid.

5.7^{SIMes} – [SIMes-B(Py)Cat]Br

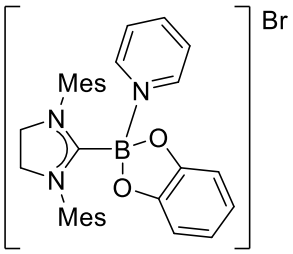

5.7^{SIMes} was prepared according to the general procedure by suspending **5.3^{SIMes}** (750 mg, 1.48 mmol) in acetonitrile (20 mL) and adding neat pyridine (0.12 mL, 1.48 mmol). Yield: 736 mg, 85 %. Further purification can be achieved by recrystallisation from dichloromethane and Et_2O.

Spectroscopic Data: ^{1}H NMR (400.2 MHz, $CDCl_3$, 298 K): δ_H 8.23 (tt, $^{3}J_{HH}$ = 7.71 Hz, 1.51 Hz, 1H, Py *p*-C*H*), 8.17 (d, $^{3}J_{HH}$ = 5.23 Hz, 2H, Py *o*-C*H*), 7.61 (m, 2H, Py *m*-C*H*), 6.73 (s, 4H, Mes *m*-C*H*), 6.51 (m, 2H, Cat C*H*), 6.33 (m, 2H, Cat C*H*), 4.39 (s, 4H, NCH_2), 2.27 (s, 12H, Mes *o*-CH_3), 2.21 (s, 6H, Mes *p*-CH_3). **^{11}B{^{1}H} NMR** (128.4 MHz, $CDCl_3$, 298 K): δ_B 7 (s). **^{13}C{^{1}H} NMR** (125.8 MHz, $CDCl_3$, 298 K): δ_C 149.1 (Cat *C*O), 144.5 (Py *p*-*C*H), 142.5 (Py *o*-*C*H), 139.8 (Mes *p*-*C*CH_3), 135.4 (Mes), 132.4 (Mes), 129.6 (Mes *m*-*C*H), 126.6 (Py *m*-*C*H), 120.6 (Cat *C*H), 110.1 (Cat *C*H), 52.5 (N*C*H_2), 21.1 (Mes *p*-*C*H_3), 18.1 (Mes *o*-*C*H_3). **Elemental Microanalysis**: calc. for $C_{33}H_{37}N_3O_2Cl_2BBr$: C 59.22 %, H 5.57 %, N 6.28 %; meas. C 59.53 %, H 5.67 %, N 5.94 %.

5.8^{SIMes} – [SIMes-B(PyOMe)Cat]Br

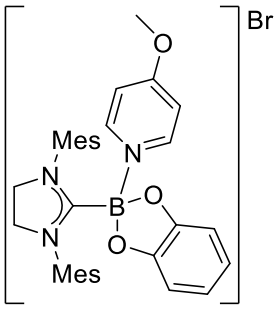

Following the general procedure, **5.8^{SIMes}** was prepared from **5.3^{SIMes}** (150 mg, 0.317 mmol) suspended in acetonitrile (10 mL) and neat 4-methoxypyridine (32 μL, 0.317 mmol). Yield: 108 mg, 55 %. Crystals suitable for X-ray crystallography were obtained by recrystallisation from dichloromethane and Et_2O.

Spectroscopic Data: ^{1}H NMR (500.3 MHz, $CDCl_3$, 298 K): δ_H 7.95 (d, $^{3}J_{HH}$ = 7.4 Hz, 2H, Py C*H*), 7.05 (d, $^{3}J_{HH}$ = 7.4 Hz, 2H, Py C*H*), 6.71 (s, 4H, Mes *m*-C*H*), 6.45 (m, 2H, Cat C*H*), 6.28 (m, 2H, Cat C*H*), 4.28 (s, 4H, NCH_2), 4.05 (s, 3H, OCH_3), 2.25 (s, 12H, Mes *o*-CH_3), 2.18 (s, 6H, Mes *p*-CH_3). **^{11}B{^{1}H} NMR** (128.4 MHz, $CDCl_3$, 298 K): δ_B 6 (s). **^{13}C{^{1}H} NMR** (125.7 MHz, $CDCl_3$, 298 K): δ_C 170.6 (Py *C*O), 149.3 (Cat *C*O), 143.8 (Py *C*H), 139.6 (Mes *p*-*C*CH_3), 135.2 (Mes *o*-*C*CH_3), 132.4 (Mes *i*-*C*), 129.6 (Mes *m*-*C*H), 119.8 (Cat *C*H), 112.2 (Py *C*H), 109.9 (Cat *C*H), 58.4 (Py O*C*H_3), 52.2 (N*C*H_2), 21.0 (Mes *p*-*C*H_3), 18.1 (*o*-*C*H_3). **Elemental Microanalysis**: calc. for $C_{33}H_{37}N_3O_3BBr$: C 64.51 %, H 6.07 %, N 6.84 %; meas. C 64.57 %, H 6.22 %, N 6.84 %. **MS (ESI)**: *m/z* calc. for $C_{33}H_{37}O_3N_3B$ ([M]+) 534.2926, meas. 534.2922 (100 %).

5.9^{SIMes} – [SIMes-B($C_4H_6N_2$)Cat]Br

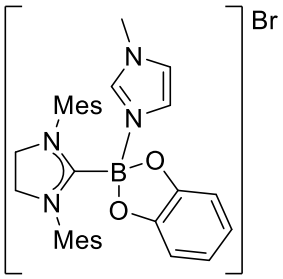

Following the general procedure, **5.9** was synthesised by suspending **5.3^{SIMes}** (500 mg, 0.99 mmol) in acetonitrile (20 mL) and adding neat 1-methylimidazole (83 μL, 1.04 mmol). Yield: 462 mg, 79 %. Crystals suitable for X-ray crystallography were obtained from a dichloromethane solution layered with hexanes.

Spectroscopic Data: ^{1}H NMR (400.2 MHz, $CDCl_3$, 298 K): δ_H 7.32 (t, $^3J_{HH}$ = 1.7 Hz, 1H, NC*H*CH), 7.05 (br s, 1H, NC*H*C), 6.72 (s, 4H, Mes *m*-C*H*), 6.70 (t, $^3J_{HH}$ = 1.7 Hz, 1H, NC*H*CH), 6.37 (m, 2H, Cat C*H*), 6.17 (m, 2H, Cat C*H*), 4.17 (s, 4H, NCH_2), 3.57 (s, 3H, NCH_3), 2.16 (s, 18H, Mes CH_3). **^{11}B{^{1}H} NMR** (128.4 MHz, $CDCl_3$, 298 K): δ_B 5 (s). **^{13}C{^{1}H} NMR** (100.6 MHz, $CDCl_3$, 298 K): δ_C 149.5 (Cat *C*O), 139.2 (Mes), 135.1, 134.9, 132.5, 129.2 (Mes *m*-*C*H), 123.4 (Im N*C*HCH), 120.9 (Im N*C*HCH), 119.3 (Cat *C*H), 109.5 (Cat *C*H), 51.8 (NCH_2), 35.7 (Im NCH_3), 20.9 (Mes *p*-CH_3), 17.67 (Mes *o*-CH_3). **Elemental Microanalysis**: calc. for $C_{31}H_{36}BBrN_4O_2$: C 63.39 %, H 6.18 %, N 9.54 %; meas. C 63.28 %, H 6.23 %, N 9.54 %.

5.10^{SIMes} – [SIMes-B(DMAP)Cat]Br

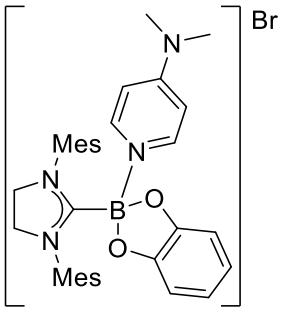

5.10^{SIMes} was prepared according to the general procedure by suspending **5.3^{SIMes}** (750 mg, 1.48 mmol) in acetonitrile (25 mL) and adding a solution of dimethylaminopyridine (181 mg, 1.48 mmol) dissolved in acetonitrile (10 mL). Yield: 761 mg, 82 %. If required, further purification can be achieved by recrystallisation with dichloromethane and hexane. Colourless crystals suitable for X-ray diffraction were grown from a dichloromethane solution layered with hexanes**.**

Spectroscopic Data: ^{1}H NMR (500.3 MHz, $CDCl_3$, 298 K): δ_H 7.46 (d, $^{3}J_{HH}$ = 7.7 Hz, 2H, DMAP C*H*), 6.71 (s, 4H, Mes *m*-C*H*), 6.44 (m, 2H, Cat C*H*), 6.32 (d, $^{3}J_{HH}$ = 7.7 Hz, 2H, DMAP C*H*), 6.26 (m, 2H, Cat C*H*), 4.26 (s, 4H, NCH_2), 3.10 (s, 6H, N(CH_3)$_2$), 2.22 (s, 12H, Mes *o*-CH_3), 2.17 (s, 6H, Mes *p*-CH_3). **^{11}B{^{1}H} NMR** (128.4 MHz, $CDCl_3$, 298 K): δ_B 6 (s). **^{13}C{^{1}H} NMR** (125.8 MHz, $CDCl_3$, 298 K): δ_C 156.2 (DMAP *p*-*C*N(CH$_3$)$_2$), 149.7 (Cat *C*O), 140.6 (DMAP *C*H), 139.2 (Mes *p*-*C*CH$_3$), 135.3 (Mes N*C*), 132.8 (Mes *o*-*C*CH$_3$), 129.5 (Mes *m*-*C*H), 119.5 (Cat *C*H), 109.7 (Cat *C*H), 106.5 (DMAP *C*H), 52.2 (N*C*H$_2$), 40.3 (DMAP N(*C*H$_3$)$_2$), 21.0 (Mes *p*-*C*H$_3$), 18.0 (Mes *o*-*C*H$_3$). **Elemental Microanalysis**: calc. (for $C_{34}H_{40}BBrN_4O_2$) C 65.09 %, H 6.43 %, N 8.93 %; meas. C 65.09 %, H 6.43 %, N 8.89 %. **MS (ESI):** *m/z* calc. for $C_{34}H_{40}O_2N_4B$ ([M]+) 547.3243, meas. 547.3229 (100 %).

5.10^{IMes} – [IMes-B(DMAP)Cat]Br

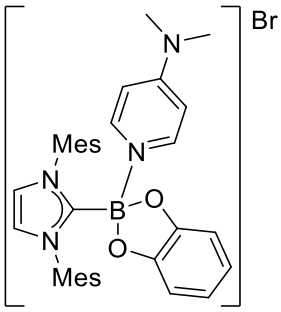

Following the general procedure, **5.10^{IMes}** was synthesised by suspending **5.3^{IMes}** (1.0 g, 1.99 mmol) in acetonitrile (30 mL) and adding a solution of dimethylaminopyridine (243 mg, 1.99 mmol) in acetonitrile (15 mL). The product was subsequently washed with dry ethyl acetate. Yield: 1.02 g, 82 %. Colourless crystals suitable for X-ray crystallography were obtained *via* dichloromethane/hexane layering.

Spectroscopic Data: ^{1}H NMR (500.3 MHz, $CDCl_3$, 298 K): δ_H 7.60 (d, $^3J_{HH}$ = 7.6 Hz, 2H, DMAP C*H*), 7.40 (s, 2H, NC*H*), 6.80 (s, 4H, Mes *m*-C*H*), 6.46 (m, 2H, Cat C*H*), 6.44 (d, $^3J_{HH}$ = 7.7 Hz, 2H, DMAP C*H*), 6.30 (m, 2H, Cat C*H*), 3.15 (s, 6H, N(CH_3)$_2$), 2.23 (s, 6H, Mes *p*-CH_3), 2.01 (s, 12H, Mes *o*-CH_3). **^{11}B{^{1}H} NMR** (128.4 MHz, $CDCl_3$, 298 K): δ_B 6 (s). **^{13}C{^{1}H} NMR** (125.8 MHz, $CDCl_3$, 298 K): δ_C 156.4 (DMAP *C*N(CH_3)$_2$), 149.9 (Cat *C*O), 140.5, 140.3, 134.5 (Mes), 132.7 (Mes), 129.4 (Mes *m*-*C*H), 125.1 (N*C*H), 119.5 (Cat *C*H), 109.7 (Cat *C*H), 106.8 (DMAP *C*H), 40.4 (DMAP N(*C*H_3)$_2$), 21.2 (Mes *p*-*C*H_3), 17.6 (Mes *o*-*C*H_3). **Elemental Microanalysis**: calc. for $C_{35}H_{40}N_4O_2BBrCl_2$: C 59.18 %, H 5.68 %, N 7.89 %; meas. C 60.09 %, H 5.78 %, N 8.02 %.

5.10^{6Mes} – [6Mes-B(DMAP)Cat]Br

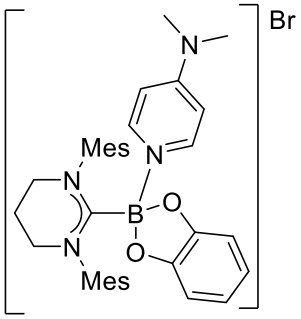

Following the general procedure, **5.10^{6Mes}** was synthesised by dissolving **5.3^{6Mes}** (800 mg, 1.54 mmol) in acetonitrile (10 mL) and adding a solution of dimethylaminopyridine (188 mg, 1.54 mmol) dissolved in acetonitrile (5 mL). After the volatiles were removed *in vacuo*, the product was obtained as an off-white solid. Yield: 774 mg, 78 %. Crystals suitable for X-ray crystallography were obtained from a concentrated fluorobenzene solution.

Spectroscopic Data: ^{1}H NMR (500.3 MHz, $CDCl_3$, 298 K): δ_H 7.29 (d, $^3J_{HH}$ = 7.7 Hz, 2H, DMAP C*H*), 6.72 (s, 4H, Mes *m*-C*H*), 6.44 (m, 2H, Cat C*H*), 6.32 (d, $^3J_{HH}$ = 7.7 Hz, 2H, DMAP C*H*), 6.22 (m, 2H, Cat C*H*), 3.66 (t, $^3J_{HH}$ = 5.8 Hz, 4H, NC*H*$_2$CH$_2$), 3.11 (s, 6H, N(C*H*$_3$)$_2$), 2.48 (quin, $^3J_{HH}$ = 5.8 Hz, 2H, NCH$_2$C*H*$_2$), 2.23 (s, 12H, Mes *p*-C*H*$_3$), 2.19 (s, 6H, Mes *o*-C*H*$_3$). **^{11}B{^{1}H} NMR** (128.4 MHz, $CDCl_3$, 298 K): δ_B 6 (s). **^{13}C{^{1}H} NMR** (125.8 MHz, $CDCl_3$, 298 K): δ_C 155.9 (DMAP *p*-*C*N(CH$_3$)$_2$), 149.4 (Cat *C*O), 141.0 (DMAP *o*-*C*H), 139.8 (Mes *o*-*C*CH$_3$), 138.4 (Mes *p*-*C*CH$_3$), 134.4 (Mes N*C*), 129.7 (Mes *m*-*C*H), 119.5 (Cat *C*H), 109.8 (Cat *C*H), 106.4 (DMAP *m*-*C*H), 50.6 (N*C*H$_2$CH$_2$), 40.2 (DMAP N(*C*H$_3$)$_2$), 21.0 (Mes *p*-*C*H$_3$), 20.6 (NCH$_2$*C*H$_2$), 18.5 (Mes *o*-*C*H$_3$).

5.10 References

[1] V. Bernard-Gauthier, J. J. Bailey, Z. Liu, B. Wängler, C. Wängler, K. Jurkschat, D. M. Perrin, R. Schirrmacher, *Bioconjug. Chem.* **2016**, *27*, 267–279.

[2] E. A. Rodriguez, Y. Wang, J. L. Crisp, D. R. Vera, R. Y. Tsien, R. Ting, *Bioconjug. Chem.* **2016**, *27*, 1390–1399.

[3] R. Ting, C. Harwig, U. Auf Dem Keller, S. McCormick, P. Austin, C. M. Overall, M. J. Adam, T. J. Ruth, D. M. Perrin, *J. Am. Chem. Soc.* **2008**, *130*, 12045–12055.

[4] Z. Liu, Y. Li, J. Lozada, P. Schaffer, M. J. Adam, T. J. Ruth, D. M. Perrin, *Angew.*

Chemie - Int. Ed. **2013**, *52*, 2303–2307.
[5] Z. Li, T.-P. Lin, S. Liu, C.-W. Huang, T. W. Hudnall, F. P. Gabbaï, P. S. Conti, *Chem. Commun.* **2011**, *47*, 9324.
[6] J. A. Hendricks, E. J. Keliher, D. Wan, S. A. Hilderbrand, R. Weissleder, R. Mazitschek, *Angew. Chemie - Int. Ed.* **2012**, *51*, 4603–4606.
[7] Z. Liu, N. Hundal-Jabal, M. Wong, D. Yapp, K. S. Lin, F. Bénard, D. M. Perrin, *Medchemcomm* **2014**, *5*, 171–179.
[8] Z. Li, K. Chansaenpak, S. Liu, C. R. Wade, P. S. Conti, F. P. Gabbaï, *Medchemcomm* **2012**, *3*, 1305.
[9] Z. Liu, M. Pourghiasian, M. A. Radtke, J. Lau, J. Pan, G. M. Dias, D. Yapp, K. S. Lin, F. Bénard, D. M. Perrin, *Angew. Chemie - Int. Ed.* **2014**, *53*, 11876–11880.
[10] M. Jauregui-Osoro, K. Sunassee, A. J. Weeks, D. J. Berry, R. L. Paul, M. Cleij, J. P. Banga, M. J. O'Doherty, P. K. Marsden, S. E. M. Clarke, J. R. Ballinger, I. Szanda, S. Y. Cheng, P. J. Blower, *Eur. J. Nucl. Med. Mol. Imaging* **2010**, *37*, 2108–2116.
[11] M. Anbar, S. Guttmann, *J. Phys. Chem.* **1960**, *64*, 1896–1899.
[12] Z. Liu, Y. Li, J. Lozada, J. Pan, K.-S. Lin, P. Schaffer, D. M. Perrin, *J. Label. Compd. Radiopharm.* **2012**, *55*, 491–496.
[13] E. J. Keliher, J. A. Klubnick, T. Reiner, R. Mazitschek, R. Weissleder, *ChemMedChem* **2014**, *9*, 1368–1373.
[14] S. Liu, T. P. Lin, D. Li, L. Leamer, H. Shan, Z. Li, F. P. Gabbaï, P. S. Conti, *Theranostics* **2013**, *3*, 181–189.
[15] K. Chansaenpak, M. Wang, Z. Wu, R. Zaman, Z. Li, F. P. Gabbaï, *Chem. Commun.* **2015**, *51*, 12439–12442.
[16] K. Chansaenpak, M. Wang, H. Wang, B. C. Giglio, F. P. Gabbaï, Z. Wu, Z. Li, *RSC Adv.* **2017**, *7*, 17748–17751.
[17] F. An, F. Nurili, H. Sayman, Z. Ozer, H. Cakiroglu, O. Aras, R. Ting, *J. Med. Chem.* **2020**, *63*, 12693–12706.
[18] S. Liu, D. Li, Z. Zhang, G. K. Surya Prakash, P. S. Conti, Z. Li, *Chem. Commun.* **2014**, *50*, 7371–7373.
[19] S. H. Ueng, M. M. Brahmi, É. Derat, L. Fensterbank, E. Lacôte, M. Malacria, D. P. Curran, *J. Am. Chem. Soc.* **2008**, *130*, 10082–10083.
[20] S. H. Ueng, A. Solovyev, X. Yuan, S. J. Geib, L. Fensterbank, E. Lacôte, M. Malacria, M. Newcomb, J. C. Walton, D. P. Curran, *J. Am. Chem. Soc.* **2009**, *131*, 11256–11262.
[21] T. Taniguchi, *Chem. Soc. Rev.* **2021**, *50*, 8995–9021.
[22] S. Nerkar, D. P. Curran, *Org. Lett.* **2015**, *17*, 3394–3397.
[23] D. A. Bolt, S. J. Geib, D. P. Curran, *Tetrahedron* **2018**, *74*, 6961–6965.
[24] A. Solovyev, Q. Chu, S. J. Geib, L. Fensterbank, M. Malacria, E. Lacôte, D. P. Curran, *J. Am. Chem. Soc.* **2010**, *132*, 15072–15080.
[25] D. Subervie, B. Graff, S. Nerkar, D. P. Curran, J. Lalevée, E. Lacôte, *Angew. Chemie - Int. Ed.* **2018**, *57*, 10251–10256.
[26] M. M. Brahmi, M. Malacria, D. P. Curran, L. Fensterbank, E. Lacôte, *Synlett* **2013**, *24*, 1260–1262.
[27] H. B. Mansaray, A. D. L. Rowe, N. Phillips, J. Niemeyer, M. Kelly, D. A. Addy, J. I. Bates, S. Aldridge, *Chem. Commun.* **2011**, *47*, 12295–12297.
[28] D. C. H. Do, S. Muthaiah, R. Ganguly, D. Vidović, *Organometallics* **2014**, *33*, 4165–4168.
[29] S. Muthaiah, D. C. H. Do, R. Ganguly, D. Vidović, *Organometallics* **2013**, *32*, 6718–6724.
[30] T. Matsumoto, F. P. Gabbaï, *Organometallics* **2009**, *28*, 4252–4253.

[31] H. Braunschweig, C. W. Chiu, K. Radacki, T. Kupfer, *Angew. Chemie Int. Ed.* **2010**, *49*, 2041–2044.
[32] J. C. Walton, M. M. Brahmi, L. Fensterbank, E. Lacôte, M. Malacria, Q. Chu, S. H. Ueng, A. Solovyev, D. P. Curran, *J. Am. Chem. Soc.* **2010**, *132*, 2350–2358.
[33] J. C. Walton, M. M. Brahmi, J. Monot, L. Fensterbank, M. Malacria, D. P. Curran, E. Lacôte, *J. Am. Chem. Soc.* **2011**, *133*, 10312–10321.
[34] W. E. Piers, S. C. Bourke, K. D. Conroy, *Angew. Chemie - Int. Ed.* **2005**, *44*, 5016–5036.
[35] W. M. Haynes, Ed. , in *CRC Handb. Chem. Physics, 95th Ed.*, CRC Press LLC, **2014**, pp. 5-94–103.
[36] I. Kaljurand, A. Kütt, L. Sooväli, T. Rodima, V. Mäemets, I. Leito, I. A. Koppel, *J. Org. Chem.* **2005**, *70*, 1019–1028.
[37] D. J. Nielsen, C. Pettinari, B. W. Skelton, A. H. White, *Acta Crystallogr. Sect. C Cryst. Struct. Commun.* **2004**, *60*, o542–o544.
[38] A. J. Arduengo, H. V. R. Dias, R. L. Harlow, M. Kline, *J. Am. Chem. Soc.* **1992**, *114*, 5530–5534.

Chapter 6

Conclusions and Outlook

6.1 Conclusions and Further Work

This project has explored the synthesis and stability of fluoroborane compounds with a view to the design of [^{18}F]fluoroborane based radiotracers for PET imaging. To suit imaging applications prospective fluoroborane compounds are required to be robust to *in vivo* conditions, readily fluorinated *via* a kinetically facile route and suited to a variety of bioconjugation methods. Hence, this study has explored three fundamental aspects of fluoroborane design: aqueous stability, efficiency of fluoride uptake and versatility for bioconjugation.

Initial work focused on investigating boronic ester functionalised 1,8-diboryl-naphthalene systems to establish if they could be employed as robust fluoride receptors by exploiting the thermodynamic advantages of the chelate effect. Bis-boronic acids and esters were found to be challenging targets, with synthetic efforts frustrated by oxide inhabiting the binding pocket and the resulting B–O–B anhydride bridge inhibiting fluoride chelation. An unsymmetrical 1,8-diboryl-naphthalene system with a single catecholborane ester group was readily accessible on the other hand and demonstrated to be a capable fluoride receptor. However, experimental and quantum chemical studies revealed the fluoride chelate to be the kinetic product of the coordination reaction, with a thermodynamically driven rearrangement positioning a catechol-oxygen in the binding pocket and fluoride in a terminal position. Consequently, it was concluded that the B–O–B anhydride bridge is a thermodynamic sink for these 1,8-diboryl-naphthalene systems and presents a shortcoming for aqueous applications.

Attention subsequently turned to *N*-heterocyclic carbene stabilised fluoroborane systems. Imidazolylidene adducts of boron trifluoride had previously been demonstrated to be stable *in vivo* and described as "essentially immortal" in aqueous solution.[1,2] Our work sought to develop these systems further, to introduce a greater range of bioconjugation routes and to overcome the limitations of the Lewis acid promoted isotopic exchange labelling methodology.

The modular design of NHC's presented multiple opportunities for introducing groups suitable for bioconjugation. The generic water stability of NHC-BF_3 systems with different carbene backbones was thus first established, to confirm that modifications to the carbene donor character would not significantly impact robustness. The triazolylidene adduct was an exception to this trend, with the observed protodeboronation attributed to the endocyclic backbone nitrogen interacting with water and promoting B–C bond cleavage. NHC-BF_3 adducts functionalised at the nitrogen were also obtained *via* a straightforward and effective synthetic route. The facile *N*-alkylation of readily available imidazoles, along with the formation of a lithium-carbene intermediate complex, are integral features of this versatile and functional group tolerant route. It is envisioned this synthetic strategy may be readily applied in the future to synthesise a library of NHC-BF_3 compounds functionalised with groups such as carboxylic acids and amines for bioconjugation and thereby reveal the full utility of this approach.

Alkyne appended NHC-BF_3 compounds were demonstrated to be compatible with CuAAC chemistry conditions enabling conjugation with a folic acid derivative. Future work will seek to develop these systems further to verify the PET imaging potential of the alkyne appended NHC-BF_3 as a prosthetic group and its folic acid derivative as a radiotracer. As such, the isotopic exchange labelling of both these systems will be explored with typical Lewis acid promoter reagents. Some synthetic flexibility is also possible for this work due to

the noted speed of the click reaction, thus offering the possibility of bioconjugation as the final step post-labelling should Lewis acid-mediated degradation of the folate moiety prove problematic. Finally, *in vivo* studies will be used to evaluate the biodistribution of the [^{18}F]folic acid derivative and to establish the *in vivo* stability of the NHC-BF_3 group.

A systematic study of NHC stabilised boron centres and their fluoride binding properties produced a swift, promoter-free fluorination pathway for these systems as an alternative to Lewis acid promoted fluoride exchange. Carbene stabilised catecholato-borenium complexes were investigated for this purpose, along with a family of four-coordinate derivates featuring additional anionic or neutral donor groups. Methodical changes to the donor and carbene characteristics demonstrated how the fluoride uptake and hydrolytic stability of the four-coordinate scaffolds could be tuned, with the cationic boronium species exhibiting the greatest scope for optimisation. It was concluded that this tuning of reactivity originates from the comparative stabilisation of the starting material and the intermediate species controlling the activation energy of the dissociative rate determining step of the substitution. Whilst the carbene characteristics primarily influence the energy of the three-coordinate borenium reaction intermediate, the donor group controls the stabilisation of the boronium complexes with respect to this intermediate. As a result, careful donor choice, based upon pKa, can be used to achieve a workable compromise between kinetically facile fluoride uptake at elevated temperatures and the stability of the boronium precursor to hydrolysis. Thus, the methyl-imidazole bound, bench-stable compound **5.9^{SIMes}** was demonstrated to achieve fluoride uptake in a timescale feasible for radiofluorination at temperatures of 60 °C and above. Following the development of a suitable work-up procedure, future work would seek to verify the applicability of this approach by examining fluoride uptake by the boronium complexes in ^{18}F-labelling conditions; the methylimidazole complex **5.9^{SIMes}** and the DMAP complex **5.10^{IMes}** would be the candidates of choice for this

initial work. Finally, in order to progress these systems towards PET imaging applications, future work will also need to combine these scaffolds with carbenes functionalised for bioconjugation. It is envisioned that, with careful consideration of the reaction conditions to avoid undesired coordination by the base or the solvent, the methodology developed in this thesis for the synthesis of functionalised NHC-BF_3 compounds may be utilised.

6.2 Outlook Beyond Fluoride

Due to the central aims of this project, the reactivity studies in this thesis focused on fluoride coordination chemistry, however, the identified characteristics of the NHC stabilised catecholborane derivatives would suggest they merit a broader investigation of their reactivity. In particular, the ability of the bench-stable boronium complexes to react *via* a dissociative mechanism and generate a Lewis acidic borenium centre *in situ* may prove to be of synthetic use.

The vacant coordination site and highly electrophilic nature of borenium species have previously been demonstrated to activate covalent bonds and facilitate organic transformations such as hydrogenation, hydroboration and hydrosilylation.[3–5] These transformations have been reported to occur using both stoichiometric and catalytic quantities, with carbene stabilised borenium compounds in particular proving to be effective catalysts.[6–8] Consequently, screening the activity of our borenium species in the presence of, for example, hydrogen may reveal new avenues of reactivity. Moreover, the apparent differences in the Lewis acidity of the NHC-BCat borenium compounds when different carbene donors are used could prove useful in adapting the Lewis acidic properties of the system for the required reactivity. The steric shielding of the boron centre in these reagents, as highlighted by the failure of sterically encumbered bases such as lutidine to coordinate, furthermore, indicates these borenium centres could be well suited to engage in Frustrated

Lewis Pair type reactivity; although conversely this steric bulk may also *limit* reactivity at the boron centre.[9]

6.3 References

[1] K. Chansaenpak, M. Wang, Z. Wu, R. Zaman, Z. Li, F. P. Gabbaï, *Chem. Commun.* **2015**, *51*, 12439–12442.

[2] K. Chansaenpak, M. Wang, H. Wang, B. C. Giglio, F. P. Gabbaï, Z. Wu, Z. Li, *RSC Adv.* **2017**, *7*, 17748–17751.

[3] X. Tan, H. Wang, *Chem. Soc. Rev.* **2022**, *51*, 2583–2600.

[4] T. S. De Vries, A. Prokofjevs, E. Vedejs, *Chem. Rev.* **2012**, *112*, 4246–4282.

[5] P. Eisenberger, C. M. Crudden, *Dalt. Trans.* **2017**, *46*, 4874–4887.

[6] J. M. Farrell, J. A. Hatnean, D. W. Stephan, *J. Am. Chem. Soc.* **2012**, *134*, 15728–15731.

[7] P. Eisenberger, B. P. Bestvater, E. C. Keske, C. M. Crudden, *Angew. Chemie Int. Ed.* **2015**, *54*, 2467–2471.

[8] A. Prokofjevs, A. Boussonnière, L. Li, H. Bonin, E. Lacôte, D. P. Curran, E. Vedejs, *J. Am. Chem. Soc.* **2012**, *134*, 12281–12288.

[9] J. M. Farrell, R. T. Posaratnanathan, D. W. Stephan, *Chem. Sci.* **2015**, *6*, 2010–2015.